

**Design and Development of a Dual Flow System  
For Fluid Delivery in Grinding Application**

**Vijay Kumar. Tipparthi**

*A thesis submitted in partial fulfilment of the requirements  
of Liverpool John Moores University for the degree of Doctor of  
Philosophy*

*This research programme was carried out in collaboration with  
Rolls Royce Plc.*

**January - 2017**



**A collaborative project between  
Rolls Royce Plc and Liverpool John Moores University**

**This project was partly funded by Rolls Royce,  
Partly funded by Liverpool John Moores University  
and mainly financed by the Author of this work.**

# ABSTRACT

The main aim of this research work is investigate into coolant delivery system in order to develop a radically new generation of parametric multi-purpose nozzle system, which incorporate a dual/triple flow coupled system to deliver a low volume, low pressure fluid for both conventional and MQL coolant applications in grinding process with step-up pressure. The investigation aimed to show through design, simulation and experimental study the possibility of a step change in the amount of cutting fluid used in grinding by combining positive aspects of MQL and conventional nozzles, to come up with high performance universal nozzle and draw its characteristics via measurement in terms of jet velocity, trends of coherence length, and fluid flow patterns.

To achieve this, aim a new concept termed '*Nested Nozzles*' was designed and implemented giving birth to a new approach to fluid delivery that is "*Dual/Triple Fluid Configurable Delivery*". It is demonstrated here for the first time that by nesting a nozzle in the cavity of another one can step up the inlet pressure by a factor, thus eliminating the need of high pressure supply. The nested nozzle acts as a flow conditioner creating a laminar flow; also in addition the flow through this nested nozzle accelerates the primary flow, thus inducing a stepping effect in the velocity. Besides flow conditioning, pressure and velocity step-up effect, the nested nozzle offers the supply of one or two fluids either alone or in combination. This, together with the main nozzle allows for dual/triple fluid delivery and their combination

The relationship between the flows and the pressures in the main and nested nozzles was investigated and an optimized design emerged with a modular configurable multi-purpose nozzle. Here with a single nozzle one could apply conventional flood cooling with reduced fluid requirement, MQL or multiple fluid deliveries. The nozzle exit aperture can be flexibly configured based on the application need from 0.3 mm up to 0.7 mm.

A wide range of simulations was undertaken in *SolidWorks CFD* and *ANSYS CFX* software packages. Air, oil, water and their mixtures were used as cooling media. The results revealed the flow behaviour intra-nozzle and externally where the fluid exited the nozzle aperture. The jet coherency length was estimated from these simulations along with velocity profiles. An attempt was made in simulating Wheel-Nozzle-Workpiece subsystem to show the interaction of the three elements.

A test rig was set up using a surface grinding machine, which was modified and instrumented with 3-axis digital readout, data acquisition system with LabVIEW software and sensors with Pitot tube. The results of the measurement reveal fundamentally new behaviour of the fluid that has not recorded earlier. In a three-layered measurement across nozzle aperture and along the stream, it was found that the fluid velocity after exiting the nozzle increased from top layer to bottom layer, however decreased monotonically down the stream. A conical core of fluid keeping original exit velocity was observed in the centre of the jet. These two key findings gave an indication as to where to position the workpiece (grinding contact zone) and the orientation of the nozzle relative to the cutting zone. It is therefore suggested that the bottom third of the jet be directed into the contact zone whilst the top two thirds be aimed at the wheel.

As this work has only answered some questions in fluid application, it has conversely opened numerous questions yet to be investigated, therefore, recommendations for further studies are given along with some initial ideas and directions.

# ACKNOWLEDGEMENT

My immense gratitude go to Rolls Royce Plc and Liverpool John Moores University for their financial support to this work, which allowed me to complete my studies, owing to the financial difficulties I have had at various stages of this project.

I would like to thank heart fully to my director of studies, **Dr. Andre D L Batako** for his invaluable guidance and help throughout the course of this project. Thanks are due not only for his help during my university time, also for the numerous hours spent on technical ideas and his continuous assessment of my progress, and for his efforts both in practical help and theoretical guidance that were fundamental to the successful completion of the project.

Gratitude is also presented to Dr. Xun Chen whose invaluable assistance and encouragement throughout this project has been vital to the author.

I would also like to thank the technical staff without whom, no experimental work could have been accomplished; particular thanks go to Mr. Peter Moran, Mr. Paul Wright, and Mr. Mick Noord for their constant encouragement, and support throughout my time at AMTReL.

Special thanks to Miss. Roja Shalini. Boorada for her great and valuable support and boundless encouragement throughout this project.

Finally, I would like to thank my family who has provided the much needed emotional support and guidance throughout the course of this endeavour.



*This Thesis is dedicated to my Father **Tipparthi.Rammurthy**  
(Supervisor in Jig Boring Section in Hindustan Machine Tools,  
H.M.T, India)*

*First and foremost, I have to thank my parents for their endless love,  
Support and Encouragement throughout my life and giving me  
strength to reach for the stars and chase my dreams*



# CONTENTS

<b>ABSTRACT .....</b>	<b>I</b>
<b>ACKNOWLEDGEMENT .....</b>	<b>III</b>
<b>CONTENTS .....</b>	<b>V</b>
<b>NOMENCLATURE .....</b>	<b>XI</b>
<b>ACRONYMS AND ABBREVIATIONS .....</b>	<b>XV</b>
<b>LIST OF FIGURES.....</b>	<b>XVI</b>
<b>LIST OF TABLES.....</b>	<b>XX</b>
<b>Chapter-1 INTRODUCTION .....</b>	<b>1-1</b>
1. Grinding of Metals .....	1-1
2. Problem Statement .....	1-1
3. Lubrication .....	1-3
4. Importance of Nozzle Systems for Grinding Fluid Application .....	1-4
5. Scope of this Investigation .....	1-5
6. Project Aim and Research Objectives .....	1-5
7. Thesis Structure .....	1-6
<b>Chapter-2 BACKGROUND TO GRINDING PROCESS.....</b>	<b>2-1</b>
2.1 Introduction .....	2-1
2.2 Grinding process.....	2-1
2.3 Types of grinding process .....	2-2
2.3.1 Surface Grinding Process .....	2-3
2.3.2 Cylindrical Grinding Process .....	2-4
2.3.3 Centreless Grinding.....	2-4
2.4 Grinding Mechanisms .....	2-5
2.4.1 Geometric Contact Length .....	2-6
2.4.2 Kinematic Contact Length: .....	2-9
2.4.3 Real Contact Length.....	2-9
2.4.4 Equivalent Chip Thickness.....	2-12
2.4.5 Material Removal Rate.....	2-13
2.5 Grinding Process Parameters.....	2-13
2.5.1 Forces and Power .....	2-14

2.5.2 Grinding Ratio (G-Ratio) .....	2-15
2.5.3 Infeed-Rate .....	2-16
2.5.4 Wheel Speed.....	2-16
2.5.5 Work Speed .....	2-16
2.6 Abrasive Grinding Wheels .....	2-16
2.6.1 Natural Abrasives .....	2-18
2.6.2 Synthetic Abrasives.....	2-18
2.6.3 Super-Abrasives .....	2-20
2.7. Grinding Wheel Bonds.....	2-20
2.7.1 Grinding wheel marking Systems .....	2-22
2.7.2 Wheel wear and Dressing.....	2-24
2.7.3 Bond and Grain Fracture .....	2-26
2.8 Advanced Technologies in Grinding Process .....	2-27
2.8.1 Vibration Assisted Grinding.....	2-28
2.9 Thermal Effects on Grinding Contact Zone .....	2-28
2.10 Temperature Distribution in Grinding.....	2-30
2.11 Thermal Damage & Grinding Energy Dissipation.....	2-30
<b>Chapter-3 Coolants and Lubricants Used in Grinding Process.....</b>	<b>3-1</b>
3.1 Coolant Application in Grinding.....	3-1
3. 2 Grinding Contact Zone .....	3-2
3.3 Functions and Role of Coolants in Grinding Application .....	3-4
3.3.1 Oil-based coolants .....	3-6
3.3.2 Water-based Coolants.....	3-7
3.3.3 Additives .....	3-8
3.3.4 Advantages of Grinding Fluids .....	3-8
3.4 Fluid Treatment .....	3-9
3.5 Cooling Mechanisms in Grinding .....	3-9
3.6 Coolant Flowrate .....	3-10
3.7 Grinding Nozzle .....	3-11
3.8 Nozzle Design Guidelines .....	3-13
3.8.1 Types of Nozzles .....	3-15
3.8.2 Shoe Nozzles .....	3-17
3.8.3 Nozzles for High-Speed Grinding.....	3-17

3.8.4 Coherent Jet Nozzle.....	3-21
3.9 Position of Grinding Fluid Nozzles.....	3-22
3.10 Useful Flow .....	3-23
3.11 Air Barrier Effect on Grinding Wheel.....	3-25
<b>Chapter 4 MQL in Grinding Applications.....</b>	<b>4-1</b>
4.1 Introduction .....	4-1
4.2 Background to MQL .....	4-2
4.3 Cost Benefits of ‘MQL’ Application.....	4-6
4.4 Working Principle of MQL System .....	4-8
4.5 Classification of MQL system.....	4-10
4.5.1 Internal method.....	4-11
4.5.2 External method .....	4-11
4.5.3 Types of MQL Nozzles .....	4-12
4.6 Lubricants Used in MQL.....	4-14
4.7 Benefits of MQL in Grinding.....	4-15
4.8 Lubrication Mechanism in Grinding Process .....	4-15
4.9 Application of ‘MQL’ in Various Processes .....	4-17
4.9.1 MQL in Milling.....	4-17
4.9.2 MQL in Drilling .....	4-19
4.9.3 MQL in Turning .....	4-20
4.10 Comparison of MQL with Conventional Coolant Systems.....	4-21
4.11 Utilization of MQL with Water in CBN Grinding.....	4-22
4.12 Investigation of Flow Behaviour in MQL for Modification of Nozzle Design .....	4-23
<b>Chapter-5 Nozzle Initial Simulation Using CFD .....</b>	<b>5-1</b>
5.1 Flow Straightener Designs .....	5-1
5.2 Geometry of the Models.....	5-3
5.2.1 Primary Nozzle Design (Main Nozzle).....	5-4
5.2.2 Secondary Nozzle Design (Nested Nozzle) .....	5-4
5.3 Fluid Flow in the Nested Nozzle.....	5-5
5.4 Initial investigation into Minimum Quantity Lubrication (MQL) Nozzle.....	5-7
5.5 Nested Nozzle Design (Flow Conditioners).....	5-9
5.6 Diffuser as Pressure Cone .....	5-11
5.7 Design of Pressure Cone as a Nested Nozzle.....	5-15

5.8 Nozzle Cavity Design.....	5-16
5.9 Basic Studies of Internal Fluid Flows .....	5-17
5.9.1 Problems with Existing Nozzles.....	5-17
5.9.2 Effect of Internal Cavity Profiles .....	5-18
5.9.3. Good Performance of Modified Nozzle Designs .....	5-20
5.10 Preliminary Simulation Work .....	5-21
5.10.1 Initial Nozzle Simulation.....	5-22
5.10.2 Model of the Nozzle with Hydrofoil (Nested Nozzle) .....	5-24
5.10.3 Fluid Flow in Main Nozzle No-Nested .....	5-25
5.10.4 Nozzle with Pressure Cone (No-Hydrofoil).....	5-26
5.10.5 Nozzle Simulation with Hydrofoil (No-Cone).....	5-27
5.10.6 Nozzle Simulation with Pressure Cone and Nested Nozzle.....	5-28
5.10.8 Nozzle Simulation for MQL.....	5-29
5.10.9 Nozzle with Hydrofoil and Curved-Shape cone.....	5-30
5.10.10 Full Design Iterations .....	5-30
5.11 Types of Internal Nozzle Cavity profiles .....	5-32
5.12 (Set-1) Study of Conical-Shape Nested Nozzle .....	5-33
5.13 (Set-2) Conical-Shape Nozzle with Dolphin-Tail Exit .....	5-35
5.14 (Set-3) Nozzle with Egg-Shaped Pressure Cone (Nested Nozzle).....	5-36
5.15 (Set-4) Nozzle with Pressure Cone (Dual Flow)-Flat Exit.....	5-38
5.16 (Set-5) Nozzle with 1-mm Gap between Cone and Main Nozzle (Dual Flow) .....	5-40
5.17 (Set-6) Nozzle with Pressure Cone (Dual Flow)-Flat Exit.....	5-41
5.19 (Set-8) Nozzle with Cone Dolphin-Tail Exit (Dual Flow).....	5-44
5.20 (Set-9) Nozzle with Cone Dove-Tail Exit (Dual Flow) .....	5-45
5.21 (Set-10) A Novel Modular Adaptable Universal Nozzles.....	5-48
5.22 Nozzle with flow rate 80 litres per min (Flow Ratio 2/6 may be use 1/3) .....	5-51
5.23 Nozzle Simulation with Air Flow for MQL (Single Phase).....	5-53
5.24 Nozzle with Air Simulation - Velocity Vs Pressure.....	5-55
<b>Chapter-6 Investigation into the Performance of Final Nozzle .....</b>	<b>6-1</b>
6.1 Introduction .....	6-1
6.2 Background of ‘CFD’ .....	6-1
6.3 Overview of <i>ANSYS CFX</i> .....	6-2
6.3.1 Turbulence Models.....	6-3

6.3.2 Shear Stress Transport Model (SST).....	6-3
6.3.3 ANSYS CFX Turbulence Near-Wall Treatment.....	6-4
6.4 Multiphase Fluid Flow Models .....	6-4
6.4.1 Multiphase Flow Regimes .....	6-6
6.4.2 Method of Choosing Appropriate Multiphase Model .....	6-6
6.4.3 Volume of Fluid (VOF) Model .....	6-8
6.5 Performance & Characterization of Final Nozzle .....	6-9
6.5.1 Geometry Creation of the Model.....	6-10
6.5.2 Meshing .....	6-11
6.6 Nozzle Simulation Results .....	6-15
6.6.1 Nozzle No-Cone (Flow Rate 10-Litre/min-Single Phase Flow) .....	6-15
6.6.2 Nozzle Velocity Plot No-Cone at 10-Litre/min-Single Phase Flow .....	6-18
6.6.3 Nozzle Exit Velocity Profile .....	6-19
6.6.4 Pressure Plot (10-Litre/min-Single Phase Flow).....	6-20
6.6.5 Plain Nozzle without Cone at 5-Litre/min-Single phase Flow) .....	6-21
6.6.6 Nozzle Velocity Plot across length (5 Litre/min Single Phase Flow).....	6-22
6.6.7 Nozzle Exit Velocity Profile Plot (5 Litre/min Single Phase Flow) .....	6-23
6.7 Nozzle with Cone at Flow Rate (10-Litre/min-Single Phase Flow) .....	6-23
6.7.1 Nozzle Velocity Plot with Cone (10-Litre/min-Single Phase Flow).....	6-25
6.7.2 Nozzle Pressure Plot with Cone (10-Litre/min-Single Phase Flow).....	6-26
6.8 Nozzle with Cone at Flow Rate 5-Litre/min-Single Phase Flow).....	6-28
6.8.1 Nozzle Velocity Plot with Cone (5-Litre/min-Single Phase Flow).....	6-29
6.8.2 Nozzle Exit Velocity Profile with Cone (5-Litre/min-Single Phase Flow).....	6-30
6.9 Nozzle with No-Cone (Single Phase) with Various Flow Rates .....	6-31
6.9.1 Nozzle Exit Velocity Profile Plot with various Flow Rates (No-Cone).....	6-33
6.9.2 Comparison of Nozzle Simulation Results .....	6-34
6.10 Nozzle Jet Coherence Length Determination from Fluid Jet Break Up.....	6-35
6.11 MQL Nozzle Simulation with Cone (Air & Oil Multi-Phase Flow).....	6-40
6.11.1 MQL Nozzle Velocity Plot (Main Inlet 4-Bar, Nested Flow 100 ml/hr) .....	6-44
6.11.2 MQL Nozzle Velocity Plot (Main Inlet 6-Bar, Nested Flow 100 ml/hr.) .....	6-45
<b>Chapter-7 Experimental Methods and Techniques .....</b>	<b>7-1</b>
7.1 Introduction .....	7-1
7.2 Experimental Methods and Apparatus .....	7-1

7.3 Fluid Pressure Measurement .....	7-2
7.4 Pressure Transducer .....	7-4
7.5 Measurement Technique .....	7-5
7.6 Nozzle Inspection Test Rig .....	7-6
7.7 Nozzle Positioning System.....	7-7
7.8 Fluid Delivery System for Nozzle.....	7-8
7.9 Pitot Tube Measurement System to Determine Jet Coherency .....	7-10
7.10 Nozzle Test with Coolant.....	7-12
7.11 Nozzle Test with Air for ‘MQL’ .....	7-14
7.12 LabVIEW Data Acquisition .....	7-16
<b>Chapter-8 Experimental Procedure and Results .....</b>	<b>8-1</b>
8.1 Nozzle Flow Tests .....	8-1
8.2 Nozzle & Pitot tube Measurement System.....	8-3
8.2.1 Nozzle with Pressure cone .....	8-5
8.3 Nozzle with Cone Air Jet Velocity Profiles .....	8-7
8.4 Nozzle with Pressure Cone Velocity Surface plot (1-Bar Air Pressure).....	8-10
8.5 Nozzle with Pressure Cone (Input Supply 3-Bar Velocity Surface Plot) Results.....	8-12
8.6 Nozzle with Pressure Cone (Input 6-Bar Velocity Surface Plot) Results .....	8-14
8.7 Performance of Nozzle without Cone and With-Pressure Cone .....	8-16
8.8 Nozzle with Cone (Flowrate 10-L/min water) .....	8-18
8.9 Multi-layer Surface Plot (Nozzle with Cone 10 L/min Flowrate).....	8-20
8.10 Multi-layer Plot nozzle with cone Exit Opening 0.4 mm.....	8-24
8.11 Nozzle Coherence Length Tests.....	8-25
8.12 Verification and Comparison of Simulation Results.....	8-27
8.13 Comparative studies of MQL Nozzle performance .....	8-28
<b>Chapter-9 Discussion .....</b>	<b>9-1</b>
9.1 Development of the Nozzle Design.....	9-2
9.2 Development of the Simulation.....	9-3
9.3 Limitations of the Simulation.....	9-4
9.4 Experimental Methods .....	9-5
<b>Chapter-10 Conclusions and Recommendations of Future Works .....</b>	<b>10-1</b>
10.1 Conclusion.....	10-1
10.2 Recommendations of Future Works.....	10-3

<b>Appendix-1 Optimisation of Nozzle Exits .....</b>	<b>A1-1</b>
<b>Appendix-2 Refining of Nozzles .....</b>	<b>A2-1</b>
<b>Appendix-3 MQL System and Equipments .....</b>	<b>A3-1</b>
<b>Appendix-4 LabVIEW Program.....</b>	<b>A4-1</b>
<b>Appendix-5 Nozzle External Jet 3-D Surface Plots .....</b>	<b>A5-1</b>
<b>References .....</b>	<b>R-1</b>
<b>Bibliography.....</b>	<b>B-1</b>

## NOMENCLATURE

Symbol	Meaning	Units
$a$	Applied Depth of Cut	mm
$a_e$	Real/Actual Depth of Cut	mm
$V_s$	Wheel Surface Speed	m/sec
$V_w$	Work Surface Speed	m/sec
$d$	Wheel Infeed rate	m/sec
$P$	Pressure	Pascal (Pa)/ N/m <sup>2</sup>
$V$	Velocity	m/sec
$\rho$	Fluid Density	kg/m <sup>3</sup>
$Q$	Volumetric Flow rate	m <sup>3</sup> /sec
$V_j$	Jet Velocity	m/sec
$lg$	Geometric Contact Length	m
$ds$	Wheel Diameter	m
$\theta_s$	Contact Arc Angle	Degrees
$d_e$	Effective Wheel Diameter	m
$d_w$	Workpiece Diameter	m
$d_s$	Wheel Diameter	m
$t_{gc}$	Grain Contact Time	--
$l_k$	Kinematic Contact length	m
$l_e$	Real Contact Length	m
$L_w$	Workpiece Length	m
$R_r$	Roughness Factor	--

$a^*$	Effective 'Contact Radius' of a Rough Surface	m
$a_0$	Contact Radius for smooth Surfaces	m
$K_s$	Wheel Thermal Conductivity	W/(m-K)
$K_w$	Workpiece Thermal Conductivity	W/(m-K)
$h_{eq}$	Equivalent chip thickness	m
$Q_w$	Volumetric Material Removal Rate	m <sup>3</sup> /sec
$b_w$	Contact/Workpiece Width	m
P	Grinding Power	W
$F_t$	Tangential force	N
$F_n$	Normal force	N
$F_a$	Axial force	N
$\mu$	Wheel Dynamic Viscosity	Kg/ (m.s)
$\mu$	Friction Co-efficient/Force ratio	---
$a_d$	Dressing Depth of Cut	m
$f_d$	Dressing Feed Per Revolution	m/min
$R_t$	Height of the Groove	m
$b_d$	Width of the Dressing Tool	m
$\Delta s$	Volume of wheel wear	mm <sup>3</sup>
$\Delta w$	Volume of metal removed	mm <sup>3</sup>
$D_j$	Diameter of the Jet	mm
$l$	Length of Exit	mm
$d$	Outlet of the Nozzle	mm
$D$	Diameter of the Supply	mm

$\frac{3}{4} D$	Length of Concave Profile Angle	mm
$1.5 D$	Concave angle	mm
$d_{jet}$	Diameter of the Jet	mm
$P_p$	Pumped Pressure	N/m <sup>2</sup>
$C_v$	Velocity Co-efficient	---
$C_a$	Contraction Co-efficient	---
$C_d$	Orifice Discharge Co-efficient	---
$L_{slot}$	Length of Exit	mm
$h_{slot}$	Height of Exit	mm
$V_{slot}$	Velocity of Jet	m/sec
$w_{slot}$	Width of the Exit	mm
U	Velocity of Fluid	m/sec
D	Diameter of Nozzle	mm
$M'_{slot}$	Momentum of Supplied Fluid	kg.(m/sec)
$h_{jet}$	Jet Thickness	mm
$\nu$	Kinematic Viscosity	m <sup>2</sup> /sec
$M'_{air}$	Momentum of Air boundary Layer	m <sup>2</sup> /sec
$\rho_{slot}$	Air density	kg/m <sup>3</sup>
$h_{air}$	Air boundary layer thickness	mm
$\beta$	Nozzle direction in relation to feed direction	m/min
$d$	Distance from nozzle tip to cutting zone	mm
h	Height	m

## ACRONYMS AND ABBREVIATIONS

GERI	General Engineering Research Institute
EPA	Environmental Protection Agency/Authority
NDG	Near Dry Grinding
MQL	Minimum Quantity Lubrication
CNC	Computer Numerically Controlled Machine
HEDG	High Efficiency Deep Grinding
NDM	Near Dry Machining (No Coolant)
WET	Conventional Flood Cooling
CBN	Cubic Boron Nitride (CBN)
SiC	Silicon Carbide
Al <sub>2</sub> O <sub>3</sub>	Aluminium Oxide
HEDG	High Efficiency Deep Grinding
L/min	Litres per minute
CLSM	Con focal laser scanning microscopy
DOC	Depth of Cut
CVD	Chemical Vapour Deposition Coating
LDA	Laser Doppler Anemometry

# LIST OF FIGURES

Figure 2.1: Types of Grinding Process.....	2-2
Figure 2.2: Types of Surface Grinding Processes .....	2-3
Figure 2.3: Grinding Mechanisms.....	2-5
Figure 2.4: Geometric Contact Length ' $l_g$ '.....	2-6
Figure 2.5: (a) Geometric Contact Length (b) Real Depth of Cut .....	2-11
Figure 2.6: 3-Grinding Force Components .....	2-14
Figure 2.7: Types of Abrasive Wheels.....	2-17
Figure 2.8: Conventional Grinding Wheels Standard Marking System.....	2-23
Figure 2.9: Wheel Surface; a) Plated CBN; b) Single Point Dressing.....	2-25
Figure 2.10: Bond and grain fracture .....	2-26
Figure 3.1: 4-Regions of fluid flow process beneath grinding wheel .....	3-3
Figure 3.2: Role of process fluid in grinding .....	3-4
Figure 3.3: Classification of Grinding Coolants .....	3-6
Figure 3.4: Internal Nozzle Cavity Design.....	3-14
Figure 3.5: Round Swivel, Spot Jet, Flat Headed and Click-fit nozzles .....	3-15
Figure 3.6: Coherent jet, Spot jet and Wedge shaped nozzles .....	3-16
Figure 3.7: (a) Simple Orifice; (b) Webster Orifice Nozzle.....	3-18
Figure 3.8: Typical Exits of the Nozzle Chamber.....	3-20
Figure 3.9: Positioning of Fluid Supply tangentially to the Wheel.....	3-22
Figure 3.10: Useful Collection System (Jones and Shipman Dominator) .....	3-24
Figure 3.11: Air Barrier Effect .....	3-25
Figure 3.12: Air Flow Through and Around a Grinding Wheel .....	3-26
Figure 3.13: (a) Air Flow Field Using Scrapers for Better Wetting.....	3-27
Figure 3.14: Boundary layer effect reversed airflow opposing the fluid .....	3-28
Figure 3.15: Coolant passing through the grinding zone .....	3-28
Figure 4.1: Example of Fluid Costs in Manufacturing.....	4-7
Figure 4.2: Steidle Lubrimat L-50 MQL System .....	4-8
Figure 4.3: Principle of Operation of Lubrimat L-50 MQL System .....	4-9
Figure 4.4: MQL Systems, (a) Internal (b) External Mixing .....	4-11
Figure 4.5: Types of MQL Nozzles.....	4-12
Figure 4.6: System of centrifugal oil mist supply into a small-sized grinding wheel .....	4-13
Figure 4.7: (a) MQL System Setup (b) Lubrication Mechanism in MQL .....	4-16
Figure 4.8: (a) Schematic View of Nozzle Position.....	4-18
Figure 4.9: (a) Internal; (b) External MQL in Drilling.....	4-19
Figure 4.10: Schematic Representation of targeted MQF application in machining .....	4-21
Figure 4.11: (b) Velocity Vector and Vol. Fraction Contour of Air-Fluid Mixture.....	4-24
Figure 5.1: Various Types of Flow Straighteners (AMTReL).....	5-2
Figure 5.2: Simple Grid-Flow Straightener in a Taper Nozzle .....	5-3



Figure 5.3: Nozzle Components .....	5-4
Figure 5.4: Hydrofoil (Flow Conditioner).....	5-5
Figure 5.5: Flow profile in nested nozzle with rectangular and circular exit.....	5-6
Figure 5.6: MQL Flow in Nozzle with 3-Core Inlets.....	5-8
Figure 5.7: Transformation of Pressure Cone Design .....	5-11
Figure 5.8: Effect of pressure cones in a diffuser, pressure profile.....	5-12
Figure 5.9: Flows over Cylindrical Vs Elliptical/ Egg Shape Cone.....	5-14
Figure 5.10: Egg-Shape Pressure Cone Velocity Streamlines .....	5-15
Figure 5.11: Nozzle exit configurations .....	5-16
Figure 5.12: Turbulence, Recirculation and Stagnations in Nozzle Cavity .....	5-18
Figure 5.13: Improved and Modified Nozzle Designs .....	5-20
Figure 5.14: Nozzle with Hydrofoil Circular Exit .....	5-22
Figure 5.15: Nozzle with Hydrofoil Rectangular Exit .....	5-23
Figure 5.16: Internal View of Nozzle Components .....	5-24
Figure 5.17: Plain Nozzle Flow Streamlines (Flow Trajectories) .....	5-25
Figure 5.18: Flow Trajectories of Nozzle with Cone .....	5-26
Figure 5.19: Velocity Streamline of Nozzle with Hydrofoil.....	5-27
Figure 5.20: Assembly Model.....	5-28
Figure 5.21: Dual flow system with hydrofoil and Pressure Cone .....	5-28
Figure 5.22: Flow Profile with Air as Fluid for MQL.....	5-29
Figure 5.23: Turbulence near Hydrofoil.....	5-30
Figure 5.24: Nozzle Exit and Cavity Profiles.....	5-32
Figure 5.25: Conical-Shape Nested Nozzle with Triangular Exit.....	5-34
Figure 5.26: Performance of Dolphin tail Profile with 100 litres/min (30/70 l/min).....	5-35
Figure 5.27: Other Nozzle Exit Profiles .....	5-37
Figure 5.28: Simulation Setup.....	5-38
Figure 5.29: Design-1 (30/90 l/min) with 5-mm gap between cone and main nozzle.....	5-39
Figure 5.30: Design-2 (120-l/min) with 1-mm gap between the cone and main nozzle.....	5-40
Figure 5.31: Nozzle with Flat Exit of 1-mm gap between the cone and main nozzle .....	5-41
Figure 5.32: Nozzle with Modified Exit (30/50 litre/min-Single Phase Flow).....	5-43
Figure 5.33: Performance of Dolphin-Tail Exit 100 litres/min (Flow ratio 30/70) .....	5-44
Figure 5.34: Pressure Developments with cone and without cone.....	5-46
Figure 5.35: Dove-Tail Nozzles with Cone.....	5-47
Figure 5.36: Geometry of Actual Nozzle Model.....	5-48
Figure 5.37: Vertical and horizontal cross cuts .....	5-49
Figure 5.38: Velocity Field in Cross-section of Dovetail profile.....	5-50
Figure 5.39: Velocity Graph across the Nozzle Length .....	5-51
Figure 5.40: Dove-Tail Nozzle Exit Velocity Profile .....	5-52
Figure 5.41: Simulation with Air at 50, 25, 13 and 4 bars .....	5-54
Figure 5.42: Nozzle Air Pressure Vs Velocity .....	5-55
Figure 6.1: Example of typical Flow Patterns for Flow in Horizontal Pipes .....	6-5
Figure 6.2: Final Nozzle Model Design .....	6-10
Figure 6.3: Mesh formation and Regions of interest.....	6-11

Figure 6.4: Mesh Statistics .....	6-12
Figure 6.5: Mesh Improvement using layers of Inflation mesh .....	6-13
Figure 6.6: Example of Nozzle Domain Setup.....	6-14
Figure 6.7: Nozzle with Dove-Tail Exit No-Cone (Flowrate 10 L/min).....	6-15
Figure 6.8: Turbulence and Eddy Cut-plots .....	6-17
Figure 6.9: Water Superficial Velocity across Length of Nozzle (mm) .....	6-18
Figure 6.10: Nozzle Exit Velocity Profile (Flow Rate 10 l/min No-Cone) .....	6-19
Figure 6.11: Pressure Plot across Length of Nozzle (mm).....	6-20
Figure 6.12: Velocity Profiles of Nozzle Exit.....	6-21
Figure 6.13: Nozzle without Cone (Flow rate 5 Litre/min Single Phase Flow).....	6-22
Figure 6.14: Nozzle Exit Velocity Profile No-Cone .....	6-23
Figure 6.15: Nozzle Velocity Exit Profiles .....	6-24
Figure 6.16: Velocity across Nozzle length .....	6-25
Figure 6.17: Pressure Plot across Nozzle length .....	6-26
Figure 6.18: Jet velocity Profile across Nozzle Width (With-Cone) .....	6-27
Figure 6.19: Velocity Profiles of Nozzle Exit.....	6-28
Figure 6.20: Velocity plot across Nozzle length .....	6-29
Figure 6.21: Nozzle Jet Velocity Profile (With-Cone).....	6-30
Figure 6.22: Velocity Profile for Nozzle with No-Cone Flow rate 40 & 50 litre/min .....	6-31
Figure 6.23: Velocity Profile for Nozzle with No-Cone Flow rate 60 to 120 litre/min .....	6-32
Figure 6.24: Velocity profile in the centre line across the nozzle exit.....	6-33
Figure 6.25: Nozzle Exit Velocity Vs Various Flow rate .....	6-35
Figure 6.26: Schematic for the definition of Nozzle Jet Coherence Length .....	6-36
Figure 6.27: Velocity Contour Plots Drawn on Horizontal and Vertical Planes .....	6-37
Figure 6.28: Cut planes where jet velocities were recorded.....	6-38
Figure 6.29: Velocity profile in the centre line across the nozzle exit up to 200 mm.....	6-39
Figure 6.30: MQL Nozzle Configuration.....	6-40
Figure 6.31: MQL Nozzle Simulation for Air & Oil Multi-Phase Flow.....	6-41
Figure 6.32: Multiphase Nozzle Simulation.....	6-42
Figure 6.33: MQL Air Exit Jet Velocity .....	6-44
Figure 6.34: MQL Air Exit Jet Velocity across Nozzle Length (6-bar).....	6-45
Figure 6.35: MQL Air Exit Jet Velocity .....	6-45
Figure 6.36: MQL Nozzle Convergence Plot.....	6-46
Figure 7.1: Pitot tube Pressure Measurement in Dynamic Fluid System.....	7-3
Figure 7.2: Working Principle of Pressure Transducers (NI National Instruments).....	7-4
Figure 7.3: Nozzle Inspection Test Rig.....	7-6
Figure 7.4: Nozzle Positioning System with Rotary Mechanism .....	7-8
Figure 7.5: Coolant Supply System.....	7-9
Figure 7.6: (a) Pitot tube System (b) Sensor probe directed to nozzle exit.....	7-10
Figure 7.7: Nozzle Jet Measurement System .....	7-11
Figure 7.8: Pitot tube Motion through the Nozzle Exit Fluid Stream .....	7-12
Figure 7.9: Sliding System Fixed on Machine Head.....	7-13
Figure 7.10: MQL Nozzle Experimental Setup for Testing .....	7-14
Figure 7.11: Sampling of a MQL Spray Droplets on Paper .....	7-15

Figure 7.12: Signal Acquired across Nozzle Exit (a) Raw Signal and (b) Filtered Signal ... 7-16

Figure 8.1: (a) Distance between Layers.....	8-3
Figure 8.2: Close View of Nozzle Exit with 3-Layers.....	8-4
Figure 8.3: Measurement System.....	8-5
Figure 8.4: Velocity Profiles of Nozzle with Cone.....	8-7
Figure 8.5: Velocity Surface Plot (1-6 Bars) on Nozzle Exit.....	8-8
Figure 8.6: Surface plot of Increasing Air Velocity.....	8-8
Figure 8.7: Graph- Input Supply (Bars) Vs Output Air Velocity (m/sec).....	8-9
Figure 8.8: Graph- Input & Output Air Pressure in Bars.....	8-9
Figure 8.9: Nozzle with Cone Middle Layer Surface Plot-(Input 1-Bar).....	8-10
Figure 8.10: Nozzle with Cone Multi-Layer Surface Plot (Input 1-Bar).....	8-11
Figure 8.11: Nozzle with Cone Middle Layer Surface Plot (Input 3-Bar).....	8-12
Figure 8.12: Nozzle with Cone Multi-Layer Surface Plot (Input 3-Bar).....	8-13
Figure 8.13: Nozzle with Cone Velocity Surface Plot (Input 6-Bar).....	8-14
Figure 8.14: Multi-Layer Velocity Surface Plot (Input 6-Bars).....	8-15
Figure 8.15: Nozzle without Cone.....	8-16
Figure 8.16: Jet Velocity Profile of Nozzle without Cone at 10-L/min.....	8-17
Figure 8.17: Multi-Layer Velocity Surface Plot (No-Cone Flowrate 10-L/min).....	8-18
Figure 8.18: Nozzle with Cone Middle Layer Surface Plot.....	8-19
Figure 8.19: Multi-Layer Surface Plot (Nozzle with Cone 10 L/min).....	8-20
Figure 8.20: (a) Velocity Profile (b) Visualization of 3-Layers in Vertical Direction.....	8-21
Figure 8.21: Nozzle with Cone aperture (a) 0.4 and (b) 0.5 mm.....	8-22
Figure 8.22: Multi-Layer-Nozzle with Cone Exit Opening 0.4 mm.....	8-24
Figure 8.23: Coherence Length of Nozzle with for 6 bar air pressure.....	8-25
Figure 8.24: Coherence length of Nozzle with Cone for 10 L/min (water).....	8-26
Figure 8.25: Jet Velocity Profiles for 5-l/min with/out cone.....	8-27
Figure 8.26: Jet Velocity Profiles of Flowrate 10-L/min with cone & without Cone.....	8-28
Figure 8.27: MQL Nozzle with Cone (6-Bar & 4-Bar, Nested flow 100 ml/hr).....	8-29
Figure 8.28: 1-Bar Air Nozzle with Cone Experimental Vs Simulation.....	8-30
Figure 8.29: 3-Bar Air Nozzle with Cone Experimental Vs Simulation.....	8-30
Figure 9.2: Workpiece in wrong position.....	9-7
Figure 9.3: Workpiece in good position.....	9-7
Figure 9.4: Position of Nozzle Exit Bottom Layer Targeted to Contact Zone.....	9-8
Figure 9.5: Close View of 3-Layers Matching to Targeted Contact Zone.....	9-9
Figure 9.6 Triple-Layer Velocity Profiles in Vertical and Horizontal Planes.....	9-10

# LIST OF TABLES

<b>Table 2.1:</b> Types of Abrasives.....	2-18
<b>Table 2.2:</b> Typical Hardness Values of Abrasive Grain Materials at Ambient Temp.....	2-19
<b>Table 2.3:</b> Bond Types of Various Abrasives .....	2-20
<b>Table 5.1:</b> Nozzle Input Parameters.....	5-24
<b>Table 5.2:</b> Nozzle Input Parameters .....	5-25
<b>Table 5.3:</b> Comparative Results with Water.....	5-29
<b>Table 5.4:</b> (Set-1) CFD Input Parameters.....	5-34
<b>Table 5.5:</b> (Set-2) CFD Input Parameters.....	5-35
<b>Table 5.6:</b> (Set-3) CFD Input Parameters.....	5-36
<b>Table 5.7:</b> (Set-4) CFD Input Parameters.....	5-38
<b>Table 5.8:</b> (Set-6) CFD Input Parameters.....	5-41
<b>Table 5.9:</b> (Set-8) CFD Input Parameters.....	5-44
<b>Table 5.10:</b> (Set-9) CFD Input Parameters.....	5-46
<b>Table 5.11:</b> (Set-10) CFD Input Parameters.....	5-48
<b>Table 6.1:</b> Mesh Criteria for Nozzle.....	6-13
<b>Table 6.2:</b> Pre-Processing Physics Definition .....	6-14
<b>Table 6.3:</b> Comparative Results of Various Flowrates and Nozzle Exit velocities.....	6-34
<b>Table 8.1:</b> Air pressure reading for Nozzle with Pressure Cone.....	8-6
<b>Table A-4.1:</b> Specification of Differential Pressure Gauge.....	A4-1

**CHAPTER-1**  
**INTRODUCTION**

## Chapter-1 INTRODUCTION

### 1. Grinding of Metals

Grinding is a metal cutting process primarily used to remove the excess metal and it is also used as a finishing operation that removes relatively small quantities of the metal. Grinding is performed by means of bonded abrasive particles rigidly mounted on a rotating wheel. Grinding wheel is a multipoint cutting tool whereas each abrasive particles acts as single point cutting tool. The grinding process is used for extremely high surface finish quality and accuracy of the shape and dimensions. The life of the grinding wheel is also very important. Grinding of very hard material leads to the increase in the temperature during the grinding process. High temperature causes damages to the workpiece as well as to the grinding wheel. To reduce these undesired effects of grinding process the coolant is provided during cutting process. This helps in extending the life of the grinding wheel, improving process performance and workpiece quality. Currently the usage of coolants in the industries for machining processes is increasing due to increased demands in production rates and this causes more investment in the coolant fluids with subsequent impact on environment.

### 2. Problem Statement

The use of cutting fluids for machining process has a great impact on the metal working environment, and it is becoming more and more significant matter for the legislation due to environmental impact. However, for these reasons a strong emphasis is being placed on the development of alternative way to find environmentally friendly technology “Go green”. All these factors have led to research centres and universities to focus their efforts on researching other solution to the production processes, creating new technologies to reduce or avoid the production of environmentally aggressive residues. Considering the use of coolants in machining processes, the two main

important aspects are the ecological and economic issues of using conventional wet grinding, which both are of high interest to the manufacturing industries. On the other hand, persistent attempts to completely avoid cutting fluids, in many cases cooling is still essential for the economically feasible service life of cutting tools and the required accuracy and surface qualities. This is particularly true when the workpiece requires tight tolerances, high dimensional and shape. (Silva *et al*, 2005).

Current legislation on health and safety and impact on environment put pressure on manufacturing industries to energy efficient, environmental friendly. This implies cutting down the resource used and pollutant injected into the environment. The UK regulations under the ‘Waste framework directive’ (91/156/EEC amending 75/442/EEC on waste) (<https://www.gov.uk/topic/environmental-management/waste>) incorporating discharges of industrial wastes metal working fluids, have become more stringent. These now require industries to take any and all measures necessary to ensure the safe collection and disposal of waste coolants and oils as far as possible, give priority to the processing of waste streams. On the other side, the cost of the coolant materials, filtering, rising cost of coolant waste disposal (£26 to dispose of 200 litres of used coolant), as well as maintenance and repair of coolant systems are high, and they encompass a share of about 16.9% of overall production costs. “*This is higher than tool cost*”. This statistic shows that the efficient use of coolant can be an effective cost saving tool as well as being environmentally responsible. Further to this, 10% of the UK total oil sales for 1999 (approximately 1,000,000 tons a year) was attributed to metalworking as an industry. For example, a 5% reduction in machining coolant would save approximately 7,200 tons a year with the associated relevant impact on the environment. Conventional grinding, whilst a vital manufacturing process, is clearly not environmentally friendly.

Other important negative aspects on the working environment are the potential health problems for the machinist, risk of explosive coolant, waste disposal of non-organic coolant materials, water contamination for cleaning the workpiece, as well as coolant

waste disposal contaminated with abrasive particles & debris and other related activities causes some important ecological problems. (Najiha, 2016)

Within manufacturing, certain niche sectors have arisen to accommodate the demands of minimal fluid usage. Minimum Quantity Lubrication (MQL) is a prime example of the attempts to advance coolant delivery, consumption and efficacy. Both dry machining and MQL have specialised fields of application and lead to the focus of this investigation. It is between MQL and conventional coolant delivery where the relevance of useful flow is most significant. The main aim is to create a bridge between the specialist area of absolute minimal fluid application and the common industrial approach of ‘more is better’. This should allow some of the benefits of MQL to be exploited by the wider industry. In order to achieve this kind of advance, the entire grinding process needs to be considered. The process parameters, such as wheel speed, workpiece speed, fluid delivery method, flow rates and pressure, and depth of cut must be fused in a system in order to advance fluid application efficiency in grinding (Jackson, 2008).

In the case of machining process in particular the volume used can reach up to 120 litres per minute at 60-80 bars. However, with the current climate change and the economic pressures, manufacturing industries cannot continue this practice of “*The more the better*”. Therefore, there is a big demand in reducing the amount of coolant use in the manufacturing industries. The key to a successful reduction in coolant is the “*Nozzle design and optimization*” by focusing on this concept and developing a novel nozzle model that could lead to a large reduction in the coolant, with the notion of “*The less the better*”.

### **3. Lubrication**

The coolant has a great effect in grinding processes; the role of the coolant in grinding process can be categorized into cooling and lubrication in the contact zone, chip transportation, grinding wheel cleaning and corrosion reduction. Among these duties,



the cooling and lubrication role are accomplished by reduction of heat generation through lubrication effect by providing a lubricating film and thus lowering the friction, as well as reducing the heat transferred to the workpiece and tool through cooling effect. Higher material removal rates along with high surface quality are main goals in grinding processes but these two factors are often in opposition, increasing one of them often means reducing the other. The reason for this is in the nature of grinding process. Increased material removal rate generally causes higher heat generation due to higher energy flux in the contact zone. Higher heat generation often causes higher wheel wear, and thermal damages or quality issues.

#### **4. Importance of Nozzle Systems for Grinding Fluid Application**

The design of a nozzle is very broad topic in grinding technology used to achieve the highest possible cooling and lubrication effect to wheel and workpiece. The coherent jet nozzle developed by Webster et al. which helps to reduce the air barrier and to achieve a coolant jet velocity better matched with grinding wheel speed (Webster, 2002). A concave internal profile of the jet nozzle provides a best longer coherent jet and better enrichment of the coolant in the grinding contact zone. Coherency is better achieved with large contraction ratios and a smooth internal surface (Webster, 1995). Jet coherence can be improved for all types of nozzles by incorporating flow conditioning tubes or plates that direct the flow within the nozzle (Brinksmeier et al, 1999).

The area of fluid application is very wide, however improvement to the nozzle design for delivery systems is constrained by limited understanding of nozzle internal flow, nozzle positioning and system requirements for optimal fluid delivery. A principal function of fluid is to improve lubrication subsequently reducing the risk of thermal damage and improving the process performance. Grinding fluid is delivered at a particular flow rate and pressure, so an understanding of these parameters may help in reducing the consumption of the coolants. However, exceeding the optimal delivery conditions result in excess energy consumption and environmental cost. Research is required to establish the required delivery parameters for achievement of optimal fluid

delivery at needed velocity and pressure to provide the best results in a range of applications (Baines-Jones, 2003).

There is no simple principle that states the flow requirement for satisfactory grinding performance. Low removal rate grinding can often be satisfactorily conducted with low grinding fluid flow. High removal rate grinding requires higher flow rates to remove grinding heat and swarf. Increasing flow reduces bulk temperatures but when combined with high jet speed nozzles create heat within the coolant. This heat has to be eliminated through a heat exchanger. High-speed, high removal rate grinding requires useful flow to be maximised. Increasing flow does not necessarily increase useful flow. It is usually recommended for high-speed grinding that jet velocity should be equal to wheel speed for maximum useful flow although some results give indication that lower jet speeds may employed (Rowe, 2014).

## **5. Scope of this Investigation**

This project is an attempt to solve the above-mentioned problem by investigating into a new generation of nozzle system with the intent to reduce the volume of cutting fluids used in grinding applications. The system to be designed will use small amount of fluid, which is delivered at the low pressure. This will be achieved through an optimization process at the design stage using 3D solid modelling and simulation. The main aim is to design a parametric multi-purpose nozzle system that can be used for both conventional and MQL application. The system could be scaled and extended to other manufacturing processes. This project involves fundamental knowledge of design, principle of mechanical engineering and fluid dynamics, and will progress through series of steps i.e. CAD modelling, Simulation, Manufacturing and Experimentation.

## **6. Project Aim and Research Objectives**

The main aim of this project is investigate into coolant flow delivery system in order to develop a radically new generation of nozzles which incorporate a dual coupled flow



system to deliver a low volume, low pressure flow for both conventional and MQL systems.

- Review of existing nozzles for flood delivery and MQL systems and their applications.
- Research and develop of a set of CAD models of new generation of low volume high-pressure nozzles for conventional cutting fluids.
- CFD simulations and optimization of nozzles CAD models using *Solidworks*.
- Research and develop of a new generation of MQL nozzles for grinding.
- CFX simulations and optimization of CAD models of the MQL nozzles.
- Performance characterisation of selected nozzle for MQL using *ANSYS CFX*
- Manufacture of novel modular adaptable nozzle prototype.
- Tests for performance characterisation
  - Data acquisition, MATLAB and LabVIEW.
  - Flow profile and jet velocity measurements.

## 7. Thesis Structure

The root of this thesis is in the initial studies and optimised nozzle design and fluid delivery analysis. Throughout, references to the grinding nozzle, MQL nozzle, optimisation of the nozzle simulation work and design methods will be maintained. This will achieve the documentation of comprehensive and traceable requirements throughout then experimental procedures.

Chapter 2: This chapter presents the background to grinding process and previous relevant research works. The review starts by covering the grinding process in general then focus on the grinding types and technologies. Review on existing nozzles, design techniques and effect of grinding wheel nozzle positioning.

Chapter-3: The review on coolants and lubricants used in grinding process and fluid flow through the contact zone. Classification, role of lubricants and reduction of coolant



in grinding processes. Also presents the problems associated with the grinding fluids and its applications. System designs for improved lubrication & cooling, optimisation of fluid delivery systems for effective cooling in the grinding process.

Chapter 4: Reviews introduction and background to MQL in grinding process, advantages and disadvantages of MQL, types of MQL nozzles and its applications in grinding is presented.

Chapter-5: Presents an overview of set of CAD models and design techniques for this work. Development of nested nozzles and concept of pressure cone were presented. Initial nozzle simulation work along with nozzle design techniques is identified. It also presents fundamental studies concerned with contained fluid flows and a proposed ANSYS CFX solution is developed. This area of work also contains detailed analysis of internal fluid flows using ANSYS CFX tool and the nozzle optimisation techniques.

Chapter-6: This chapter describes the refining of the simulation for nozzle manufacture, along with fluid flows and proposed CFX solution is developed by using ANSYS CFX tool. This section of work also contains a detailed analysis of simulations of internal fluid flows are illustrated.

Chapter-7: Describes the equipment and sensors used in the testing stages of all main and ancillary apparatus are described both in how it was used and the calibration procedure employed and the experimental study that was predominantly based on a purpose modified Jacobson surface-grinding machine. Also, it discusses the experimental test designed to evaluate the performance of the nozzle with different nozzle phases (MQL & Conventional type). The nozzle flow testing of the system is identified with reference to the previous experimental work carried out on finding the jet velocity profiles and jet coherency of differing nozzle system.

Chapter-8: Seeks to explain the experimental process used in this thesis. A full layout of all the experiments carried out during this project is presented. Using MATLAB tool



building 3-D surface plots allowed describing in detail the information relevant to each individual test.

Chapter-9: Presents a comprehensive discussion of all the work undertaken. All the experimental and development work that was undertaken is discussed together nozzle design, simulation work and experimental tests findings to propose a new novel optimised nozzle design for coolant delivery systems for increased performance in grinding application.

Chapter-10: Provides conclusions from the research work. Conclusions are given with concise insight into the developments of this work and what it can offer here a vision for future developments in this field is given by suggesting several projects for the continuation of the work started within this project.



## **Chapter-2**

### **Background to Grinding Process**

## Chapter-2 BACKGROUND TO GRINDING PROCESS

### 2.1 Introduction

Grinding is a finishing process used in wide variety of applications with components of high-required tolerances. However, in grinding high temperature generated during machining which leads to thermal damage to the workpiece, also induces micro cracks and tensile stresses on ground surface and this is one of the most significant aspect in this process. This damage can be minimising by a proper application of coolant delivery to the grinding contact zone. The purpose of this section is to cover some fundamentals of grinding process and its types, grinding mechanisms, abrasive wheels and process parameters, as well as to give an insight into the previous researchers work in area of fluid application to reduce temperature effects in grinding.

### 2.2 Grinding process

Grinding is one of the most major material removal process in manufacturing, which utilises five main elements are (a) hard abrasive grit particles are bonded rigidly to form a round shape disk called grinding wheel, (b) workpiece, (c) fluid, (d) atmosphere and (e) grinding swarf. These elements are crucial in grinding process; the abrasive hard material rubs against the metal part surface and removes very tiny pieces of material. The grinding machine supports the workpiece and position in proper adjustment in relation to the wheel which is precisely and accurately balanced to rotate at very higher speeds. The main characteristic of grinding is that the components produced will have high precision (tight tolerances) and high surface finish quality (low roughness). The rubbing action of these abrasive particles between grinding wheel and workpiece generates high heat flux so that the cutting area needs flooding coolant to reduce high temperatures and distortion, and also the damage of risk to the specimen. Compare to other machining processes, grinding is more expensive and requires a high-energy input

per volume of material removed. Some of the aspects of grinding are large contact area between the workpiece and the tool and there is a high friction between abrasives and surface of the workpiece, this leads to an increase of problems in supplying coolant to the grinding zone or contact arc, thus resulting in a high risk of thermal damage to the workpiece as well as loading and wear of the grinding wheel. The total expenditure of the machining costs in industrial countries is nearly about 20-25% (Malkin, 1989). The work presented by Tonshoff (2002), deals with various elements and approaches in process monitoring during grinding; different sensing techniques were introduced to measure the relevant quantities subsequent control action initiated in order to close the process control loop.

### 2.3 Types of grinding process

In grinding processes various types of machines are used but all the machines will generally remove material essentially in the same way by the use of grinding wheel. The grinding machines involve typically the way of specimen being supported and ground and depend on the type of surface that has to be ground. As shown in Fig.2.1 there are three main types of grinding namely:

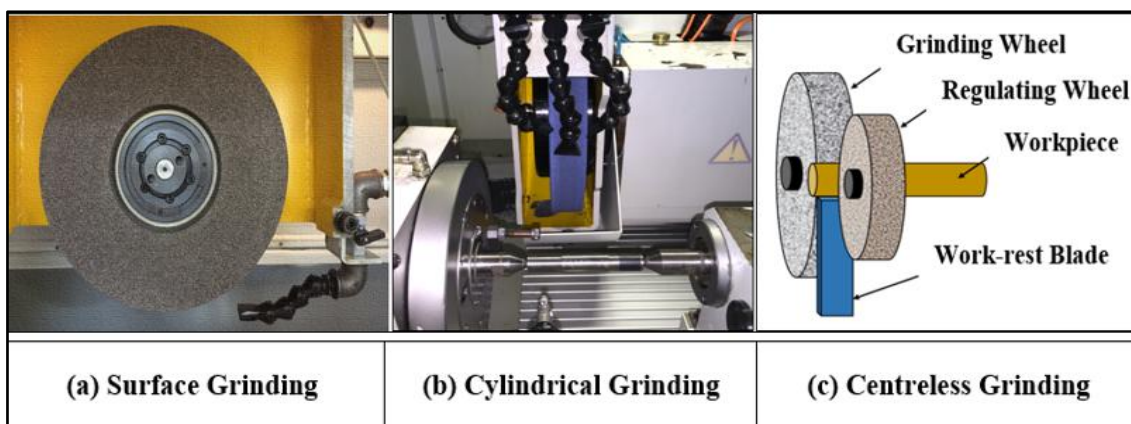


Figure 2.1: Types of Grinding Process

1. Surface Grinding.
2. Cylindrical Grinding.

- Centred grinding
  - Internal grinding
3. Centreless Grinding.
- Thru-feed grinding
  - Plunge or form grinding

### 2.3.1 Surface Grinding Process

In surface grinding the grinding wheel rotates at higher speeds whilst the workpiece reciprocates linearly under the wheel where some amount of material is removed to form a flat surface finish.

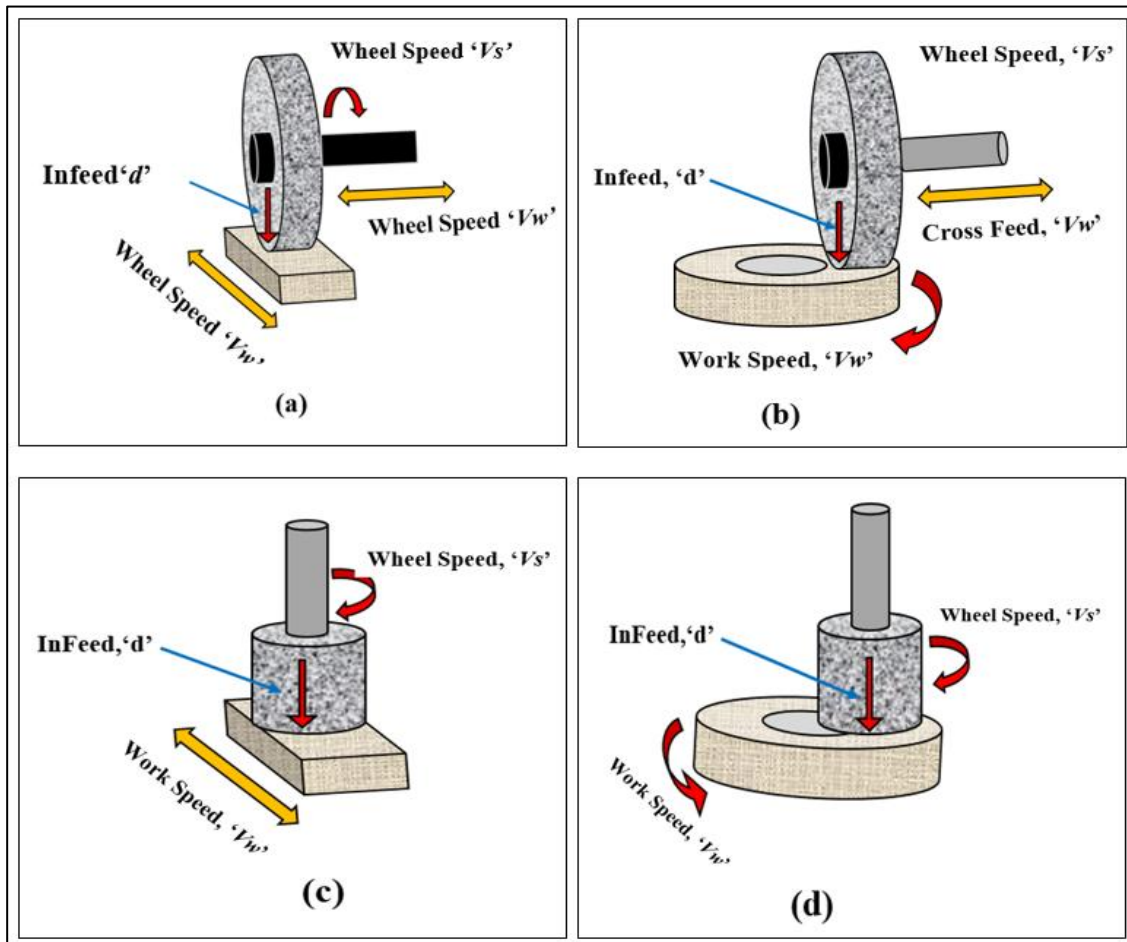


Figure 2.2: Types of Surface Grinding Processes

Work is most magnetically attached to the worktable, and mostly surface grinding machine uses horizontal spindle which can be moved and adjusts up and down to allow edge or face of the wheel to contact area. The edge of the grinding wheel, moves at a speed of  $V_s$ , the workpiece moves at a speed of  $V_w$ , and the depth of cut  $a_e$ , is removed such that a flat surface is created. The types of surface grinding are shown on above Fig.2.2: (a) Horizontal spindle with reciprocating worktable (b) Horizontal spindle with rotating worktable (c) Vertical spindle with reciprocating worktable (d) vertical spindle with rotating worktable.

### 2.3.2 Cylindrical Grinding Process

In cylindrical grinding both the wheel and the work part rotate relative to each other with a single line contact as depicted in above Fig.2.1 (b). This process is used to grind cylindrical parts, the variations of cylindrical grinding are centred, internal and centreless grinding.

- In Centred grinding the part is mainly shaped form outside surface which must rotate about its axis. Depending of the movement of the wheel this is divided into traverse or plunge mode grinding.
- Internal Cylindrical Grinding: in internal cylindrical grinding a small wheel grinds the inside diameter of the specimen. The workpiece is held in a rotating chuck in the headstock and the wheel rotates at very high rotational speed. In this operation, the workpiece rotates and grinding wheel reciprocates.

### 2.3.3 Centreless Grinding

In centreless grinding, the workpiece rotates between a grinding wheel and a regulating drive wheel. The workpiece is supported from below by a fixed work-rest blade or fixing the part on a spindle axis whilst being ground, as illustrated and described in the Fig.2.1 (c). In centreless grinding this involves another two basic modes of grinding are “Thru-Feed” and “In-Feed” or “Plunge” mode.

## 2.4 Grinding Mechanisms

In grinding process involves three main mechanisms, which are:

- Sliding/Rubbing action
- Ploughing
- Chip formation

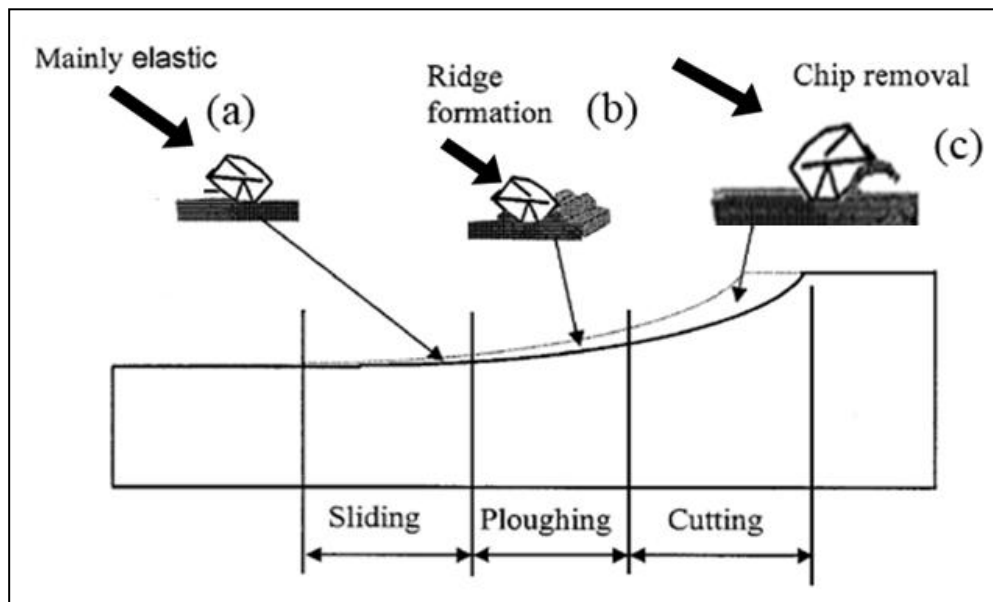


**Figure 2.3: Grinding Mechanisms**

(Adapted from Rowe *et al*, 2003)

(Rubbing, Ploughing and cutting as grain penetration increases in the arc of constant)

When the grinding wheel grains cuts deeply into the workpiece material normal and tangential forces are generated between the wheel and the workpiece; these forces causes the abrasive grains penetrates into the workpiece. (Rowe, 2014; Qi, 1997) In the first phase of mechanism the interaction between the grit cutting point and the workpiece, induces elastic deformation on the workpiece surface, leading to rubbing. Figure 2.3 (a) illustrates the cutting point on grain area where rubbing occurs just before the ploughing stage. In the second mechanism, by increasing the grain penetration into the workpiece surface, plastic deformation occurs due to large rake angle of the grain,

and this mechanism is called ploughing, which produces a side flow to form ridges as well as piled up material in front grain is illustrated in below Fig.2.3 (b). This second mechanism continues up to the point where plastic deformation reaches to a critical value along with sufficient grain penetration into workpiece so that the chip is formed and the cutting process takes place. In this last mechanism material removal and chip formation occurs as depicted in Fig.2.3 (c). The sliding and ploughing led to extremely high heat generation in grinding (Tawakoli, 2008). The depth of cut is affected by the shape & sharpness of the grit cutting edge, grit orientation, its rake angle, the coefficient of friction and the applied force on the workpiece.

#### 2.4.1 Geometric Contact Length

The geometric contact length ' $l_g$ ' is determined from the analysis of the contact geometry between a wheel and workpiece. In the surface grinding process, the wheel has diameter ' $d_s$ ' and rotates with a wheel speed ' $V_s$ ', whereas the workpiece moves with a speed of ' $V_w$ '.

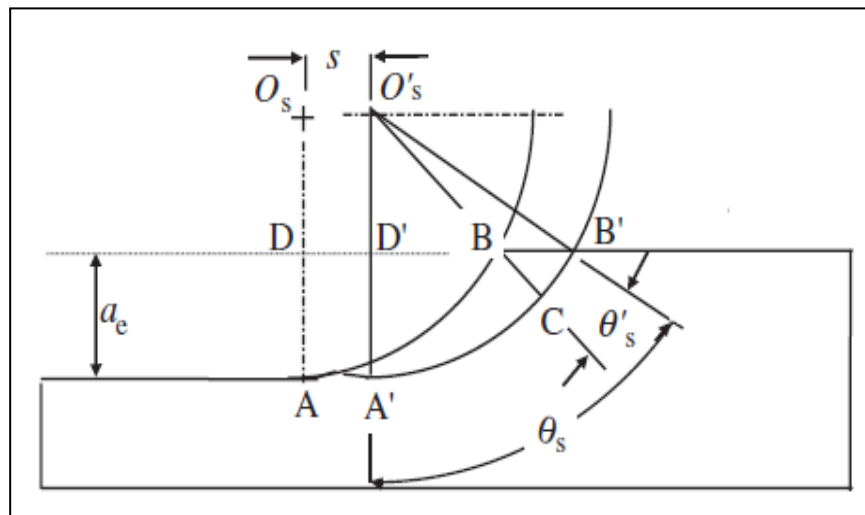


**Figure 2.4: Geometric Contact Length ' $l_g$ '**

(Marinescu *et al*, (2004))

A layer of material of a thickness equivalent to the DOC, ' $a$ ' is removed. For the purpose of calculation ' $a_e$ ', the real DOC, should be used instead of the applied DOC ' $a$ '.

The length of uncut chip is equal to the length of contact between the wheel and the workpiece, with reference to Marinescu *et al*, (2004) the geometric contact length is defined as the arc length  $AB = A'B'$ .

As shown in above Fig.2.4: For surface grinding the geometric contact length is:

$$l_g = \frac{d_s}{2} \cdot \theta_s \quad (2.1)$$

Where;

$l_g$  = Geometric contact length

$d_s$  = Wheel diameter

$\theta_s$  = Contact arc angle.

However,  $l_g$  is usually evaluated from the chord length AB rather than the arc length, so that

$$l_g = \sqrt{DB^2 + AD^2} \quad (2.2)$$

These two expressions give the same result if  $\theta_s$  is small, and DB can be found from the principle of intersecting chords.

$$DB = \sqrt{(d_s - a_e) a_e} \quad (2.3)$$

If  $a_e/d_s$  is small generally, for surface and cylindrical grinding processes, the following form can be used:

$$l_g = \sqrt{a_e \cdot d_s} \quad (2.4)$$

More generally, for both surface and cylindrical grinding processes

$$l_g = \sqrt{a_e \cdot d_e} \quad (2.5)$$

Where;  $d_e$  is the effective wheel diameter is given as the sum of the curvatures of the wheel and the workpiece (Marinescu *et al*, 2004)

$$\frac{1}{d_e} = \frac{1}{d_s} \pm \frac{1}{d_w} \quad (2.6)$$

The effective diameter is used because the contact length depends on the relative curvature of the wheel and the machined surface. The effective diameter is an inverse measure of relative curvature. Contact length has a particular significance for the concentration of energy and forces in the contact zone and for rubbing wear of the abrasive grains. The real contact length can be much larger than the geometric contact length.

If  $a_e = 0.1 d_s$ , which is extremely large depth of cut for most grinding operations, the error in the simplified expression for  $l_g$  is about 1%. This expression is a very good approximation even when the depth of cut is large. It was assumed that the arc of contact was circular and it's a good approximation in conventional grinding operations, if the grinding wheel is remains circular. If the grain speed  $V_s$ , is higher the work speed,  $V_w$ , a cutting edge coming into contact with workpiece at point B follows a path very close to being circular and exists at point A. In conventional grinding operations, grain speed is approximately two orders of magnitude greater than the workspeed, that is,  $V_s/V_w \approx 100$ . Clearly, the deviation from circularity is small. (Marinescu *et al*, 2004).

Qi, (1995; 1997) investigated to measure the contact length with an insulated contact electrical sensor inserting into the workpiece. A voltage was supplied to the sensor during the grinding wheel passes over the sensor; contact signal was recorded with the earthed workpiece. The duration of the signal wave gives a measure of the contact length and it was found that the magnitude of real contact length is up to three times that of geometric contact length under the large depth of cuts and high-speed ratio. Geometrical contact length can be used to represent the real contact length without loss of accuracy.

### 2.4.2 Kinematic Contact Length:

At higher workspeeds, the contact length as derived by geometry is increased. When the wheel centre,  $O_s$ , has moved forward a distance,  $S$  to  $O'_s$ , shown in above Fig.2.4, a succeeding cutting edge comes into contact with the workpiece at  $B'$  sweeping out the path  $B'A'$ . It may be seen that the cutting edge exists from the workpiece at a point halfway between  $A$  and  $A'$ . In other words, the cutting edge is in contact for an extra angular rotation  $\theta'_s$  so that the total arc contact on the wheel is  $\theta_s\theta'_s$ . The relative horizontal speed between the wheel and the workpiece is  $V_s \pm V_w$ , where the (+ sign) is for up-grinding and the (- sign) is for down-grinding. The extra distance travelled by the grain is  $s/2$ . Therefore, grain contact time is  $t_{gc} = \left(l_g + \frac{s}{2}\right) \cdot \left(\frac{1}{V_s}\right)$ . The kinematic contact length is given by distance travelled at the relative speed  $V_s \pm V_w$  during grain contact time,  $t_{gc}$ :

$$l_k = \left(1 \pm \frac{V_w}{V_s}\right) \left(l_g + \frac{s}{2}\right) \quad (2.7)$$

The contact length is slightly increased for up-grinding and slightly reduced for down-grinding. At higher workspeeds, the uncut chip shape is shorter and fatter for down-grinding than for up-grinding. Also the shock loading on the grains is greater. This has the implication of a greater tendency for grain fracture in down-grinding and less tendency to dull, if speed ratio is sufficiently large. Therefore, it is assumed that  $l_k = l_g$  (Marinescu *et al*, 2004).

### 2.4.3 Real Contact Length

The wheel penetration into the workpiece results in area of contact where the cutting action occurs. The length of the grinding contact zone is the length of abrasive grains in contact with workpiece material. The intensity of energy flux into the workpiece surface depends on the contact length between the wheel and workpiece material. The contact length is a significant determinant of the maximum temperature of the workpiece surface, the nature of the surface stresses and grinding wheel wear. Deflections in



contact zone results in elastic and plastic behaviour of both wheel and workpiece, and it increases contact area and number of grains. Real contact length varies from geometric length due to deformations.

The contact length is influenced by many factors that are kinematic roughness of the workpiece, uncut chips thickness, time of contact between abrasive grains with the workpiece material, the number of active and wear of the grains, temperature and wear of the grains. The temperature distribution into the workpiece material is a function of real contact length. The key parameter is errors in contact region leads to difficult to predict the temperature in the grinding process (Rowe *et al*, 1993).

Considering any measurement in the grinding contact zone it is a function that necessary to analyse a geometry of the contact zone. The contact zone region is the product of the contactwheel width,  $b_w$  and the geometric contact length,  $l_g$ . The contact width will remain constant unless the wheel is changed. However, the contact length is highly dependant on the type of material and grind being used.

The below Fig.2.5 Illustrates the scaled stiff geometry of grind, an estimate can be attempted of expected contact length . The nature of the wheel and workpiece contact zone in grinding has a strong impact on the high generated temperature. Also has effect on surface integrity and force as well as wheel wear in grinding Zhou *et al*, (1992). However, Qi, (1995) showed that the geometrical contact length is always an underestimate of the actual contact length achieved when grinding sometimes by a factor of 3. The real contact length ( $l_e$ ) according to Qi *et al*, (1997) is dependant on the wheel roughness, normal force, depth of cut and mechanical properties of the grinding wheel. The deformation of both the wheel and the workpiece causes a lengthening effect of the contact zone. It is important that more realistic value of real contact length is used when considering the length of any grinding contact zone. This becomes apparent in the analysis of thermal model for the calculation of the grinding temperature (Morgan *et al*, 1998).

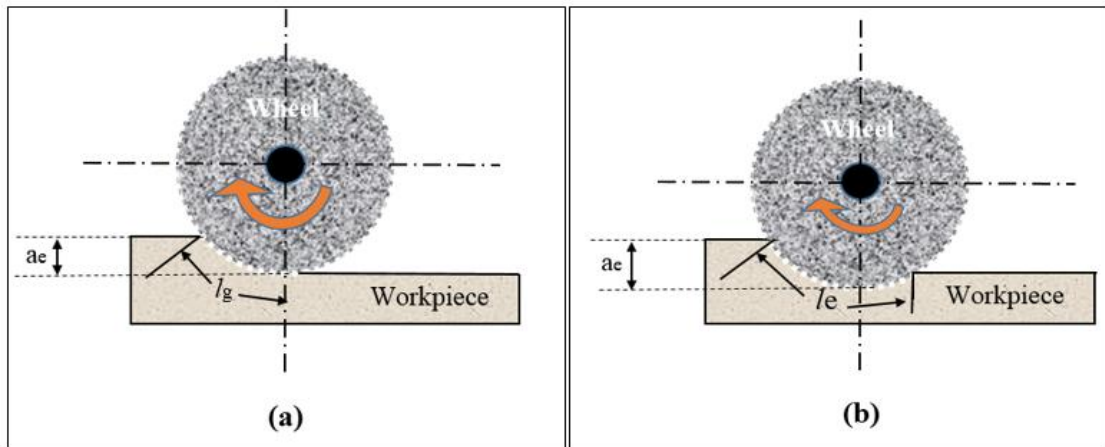


**Figure 2.5: (a) Geometric Contact Length (b) Real Depth of Cut**

These considerations lead Qi to the following equations defining the real, contact length based on roughness parameters, equations (2.8) and a second equation utilising a contact area approach, equation (2.9)

$$l_e = [R_r \cdot 8 \cdot F_n (K_s + K_w) d_s + a \cdot d_s]^{0.5} \quad (2.8)$$

$$\text{And } l_e = \left[ R_A \cdot \left( \frac{R_p}{c} \right)^2 \cdot \left( \frac{F'_n}{H_v} \right) + a \cdot d_s \right]^{0.5} \quad (2.9)$$

Where,  $R_r = a^*/a_0 =$  Roughness Factor,  $a^*$  = the effective 'Contact radius' of a rough surface defined  $a_0 =$  the contact radius for smooth surfaces.

Qi *et al*, (1997) proposed a new technique for the grinding contact length using applied power source methods. The contact length is divided into two, that a maximum contact length and a local contact length. The results showed that maximum contact length is about 22-50% longer than the local one. Previously the contact length was measured in various methods using thermocouple technique but, the advanced and latest improvements in current experiment gave the better results. Gu, (1988) in his experiment used a thinner thermal junction to form a thermocouple more sensitive than that relevant for average temperature measurements, in this mode the contact length

measured approximately appeared to be 25-30% longer than those measured by the previous conventional thermocouple techniques.

#### 2.4.4 Equivalent Chip Thickness

The equivalent chip thickness may be defined as the thickness of a continuous layer of material removed at a volumetric rate per unit width (Marinescu *et al*, 2004; Malkin, 1989). The equivalent chip thickness ( $h_{eq}$ ) is considered as another way of measuring the efficiency of the process. It actually represents the thickness of the chip that leaves the wheel after grinding. This value is proportional to the workspeed ( $V_w$ ) and real depth of cut ( $a_e$ ) and inversely proportional to the wheel speed  $V_s$ . The description of this factor is given by the following equation:

$$h_{eq} = \frac{Q'_w}{V_s} = \frac{V_w \cdot a_e}{V_s} \quad (2.10)$$

Where;  $V_w$  = Workpiece Speed (m/sec)

$V_s$  = Linear Wheel Speed (m/sec)

$a_e$  = Actual Depth of Cut (mm)

The experimental results of grinding are often expressed in terms of equivalent chip thickness as it can be related to other grinding parameters. There is a relation between  $h_{eq}$  and forces, surface quality and wheel life. However, it can be seen that two identical values of  $h_{eq}$  may be obtained for very different grinding conditions and therefore care is needed in its use and interpretation of the results. A new chip thickness model has been validated experimentally by incorporating the fracture toughness of abrasive and workpiece to assess the performance of super abrasive grinding of alumina ceramics and also compared to the surface roughness obtained with existing and proposed chip thickness models (Somasundaram, 2013).



### 2.4.5 Material Removal Rate

The material removal in grinding is an important factor for applications in industry as it describes the performance of a wheel or the whole process. Increasing higher wheel speeds automatically increase efficiency. Increasing wheel speed, without changing other grinding conditions will reduce efficiency and not increase removal rate. To maximize the removal rate, need to increase feed rate and mainly to reduce specific energy, increase removal rate and maintain workpiece quality this will achieve by considering the effect of changing one parameter at a time. The material removal rate  $Q$  is given as: (Rowe, 2014).

$$\text{Material removal rate: } Q = a_e * b_w * V_w \quad (2.11)$$

Where:  $a_e$  is the actual (real) depth of cut in (mm)

$b_w$  = workpiece width in (mm)

$V_w$  = workpiece speed (m/sec)

The specific removal rate  $Q'$  is defined as the removal rate per unit grinding contact width and allows the results to be presented in a generic way. The units are in  $\text{mm}^3/\text{mm}/\text{s}$ .

$$Q' = a_e V_w \quad (2.12)$$

### 2.5 Grinding Process Parameters

The grinding process parameters are significant in machining; the rate of material removal rate depends upon the process variables, such as wheel parameters, speeds, machine and coolant.



### 2.5.1 Forces and Power

Forces are developed between the wheel and the workpiece owing to the grinding action. In the grinding wheel running with no load power ' $P_{NL}$ ' is dissipated in the spindle bearings and the motor windings. When grinding fluid switched on an additional power ' $P_f$ ' is dissipated by the fluid drag on the wheel. When the contact is made between the grinding wheel and workpiece, depth of cut builds up and hence spindles max power.

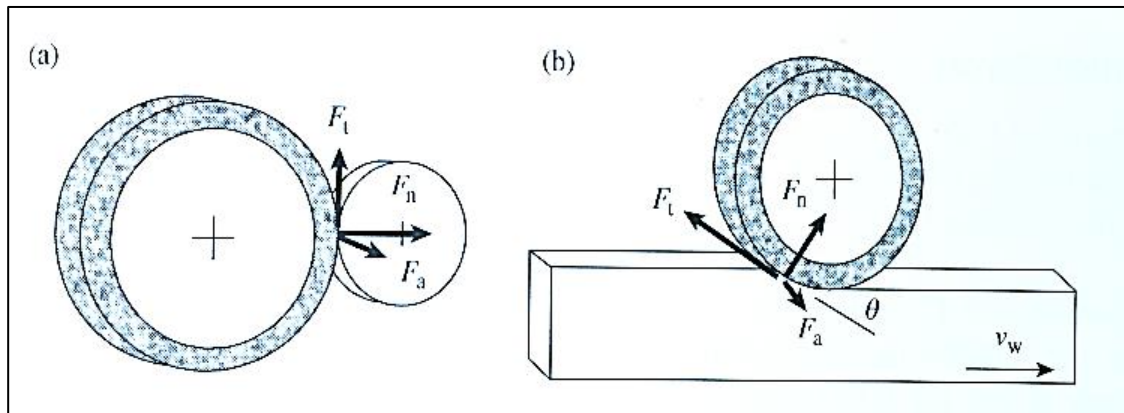


**Figure 2.6: 3-Grinding Force Components**

**(a) Small Depth of Cut (b) Large Depth of Cut**

(Rowe, 2014)

Subtracting no-load power and fluid drag power from the max power one can identify the net grinding power ' $P$ '. Grinding power can also be identified by measuring grinding forces, these resolved into three components, tangential force ' $F_t$ ', normal force ' $F_n$ ' and axial force ' $F_a$ ' as illustrated in Fig 2.6 for two grinding situations. In Fig 2.6 (a) the tangential force ' $F_t$ ' is the vertical force ' $F_v$ ' and the normal force ' $F_n$ ' is the horizontal force measured perpendicular to the contact point. The total grinding power is given by:

$$P = F_t(V_S \pm V_{ft}) + F_n * V_{fn} + F_a * V_{fa} \approx F_t V_S \quad (2.13)$$

The (+ sign) implies up-cut grinding where workpiece motion opposes the grinding wheel motion and (- sign) implies down-cut grinding workpiece motion assists the grinding wheel motion.

### 2.5.2 Grinding Ratio (G-Ratio)

Grinding force ratio is a parameter that gives indirect information about the efficiency of grinding. Force ratio is defined as the volume of material removed per unit volume of wheel wears. However, G ratio increases with less wheel wear and /or higher metal removal. The higher it is, the better the grinding conditions, especially in terms of longer wheel life. The wheel life is an economic issue in order to achieve low costs with high quality output they are various parameters which affect the wheel life is

- High grinding forces and high power
- Poor surface integrity
- Lack of dimensional accuracy
- Surface burn and damage to high temperatures
- Poor dressing and truing operations

$$\text{G-Ratio} \quad G = \Delta w / \Delta s \quad (2.14)$$

Where;  $\Delta w$  = Volume of metal removed ( $\text{mm}^3$ )

$\Delta s$  = Volume of wheel wear ( $\text{mm}^3$ )

$$\text{Co-efficient of grinding; } \mu = Ft / Fn \quad (2.15)$$

$Ft$  = Tangential force

$Fn$  = Normal force

This coefficient will vary from 0.2 in case of low stock removal such as grinding hard steel to 0.8 when the material removal stock is high such as grinding soft steel or grey cast iron. However, this coefficient is affected by the use of coolant as it changes the hydrodynamic pressure created by high wheel speeds and this effect is very obvious with viscosity straight oils (Marinescu *et al*, 2007; 2013)

### **2.5.3 Infeed-Rate**

Increasing feed rate, with other constant speeds, increases forces, roughness and reduces redress life, specific energy. The process becomes more efficient until excessive infeed rate leads to high wheel wear, a low grinding ratio and rapid wheel breakdown.

### **2.5.4 Wheel Speed**

Increasing wheel speed has the opposite effect. Increasing wheel speeds with other speeds constant, reduces grinding forces, roughness and increases redress life and specific energy, thus reduces process efficiency. The purpose of increasing wheel speeds is to allow infeed rate to be increased, thus increases production rate while maintaining quality levels and process efficiency.

### **2.5.5 Work Speed**

Increasing work speed, at constant removal rate, has a relatively small effect on the process within the stable range. High work speeds increase the probability of chatter so there is a maximum work speed limit, which is for a particular workpiece diameter. At low work speeds, the probability of thermal damage to the workpiece increases. The burn boundary can be moved outwards by using a sharper abrasive to reduce the specific energy.

## **2.6 Abrasive Grinding Wheels**

An abrasive wheel is a basically high precision tool composed of an abrasive grains rigidly bonded together by a bonding material. The process of using abrasive grits is to remove material at higher cutting speeds and shallow depths of penetration. The particles may be (a) free or (b) bonded in resin on a belt called coated product (c) close packed into wheels. Abrasives processes are categorized into four groups (a) grinding (b) honing (c) lapping and (d) polishing. Grinding and honing employ bonded within the abrasive tool, whereas lapping and polishing employ free abrasive particles, often suspended in a liquid or wax medium.





**Figure 2.7: Types of Abrasive Wheels**

The quality and surface finish of the component depends on the type of wheel used and grinding conditions. The grinding wheel is characterized by:

- The abrasive grains
- The bond that rigidly supports the grains while cutting
- Fillers to promote the metal removing action
- Grit size
- Grade
- Structure

The combination of first two components in the abrasives gives a definite characteristic known as structure (pores). In order to provide chip clearance, air spaces or voids must be left between adjacent grains. Considering a bond, an abrasive product is suitable for the operation it has to perform; all of its components have to be taken into account. In general, there are two types of abrasives are employed ‘Natural’ and ‘Synthetic’:

Natural	Synthetic
Diamond	Aluminum Oxide wheel ( $Al_2O_3$ )
Sandstone	Silicon Carbide (SiC)
Garnet	Zirconia alumina
Flint	Cubic boron nitride (CBN)
Corundum	( $Al_2O_3$ ) and magnetite ( $Fe_3O_4$ )
Emery	Super abrasives (Diamond and CBN)

**Table 2.1: Types of Abrasives**

(Rowe, 2014)

**2.6.1 Natural Abrasives**

Natural abrasives are not much in use due to their lack of durability to withstand high grinding pressures, except diamond abrasives. Emery abrasives are no longer used in making grinding wheels but it is often preferred for use as a coated abrasive cloth and paper as well as many buffing compositions. Diamond is classified as both natural and synthetic abrasive. Natural stones that are unsuitable for gems are entitled as borts (grade of diamond). Next, they are crushed down into a series of sizes for abrasive use. Diamonds have the highest hardness and require a unique bond, which is more specialized than that of conventional grinding wheels.

**2.6.2 Synthetic Abrasives**

These are artificial abrasives that are mostly used in industry covering almost all the needs for grinding wheels. The most important property of an abrasive is hardness and it is retained at high temperatures. The hardness of the abrasives is substantially reduced at typical contact temperatures between a grain and a workpiece at 1000 C, the hardness of the most abrasives is halved by contact temperatures. Table 2.2 gives knoop hardness



<b>Super-Abrasive Material</b>	<b>Typical knoop Hardness value (kg/mm<sup>2</sup>)</b>
Diamond	7000
Cubic boron nitride (CBN)	4700
Boron carbide	2800
<b>Conventional Abrasives</b>	
Silicon carbide	2500
Aluminium oxide (Al <sub>2</sub> O <sub>3</sub> )	2000
Cemented carbides	1400-1800
Quartz	800
Hardness steel	740
Glass	300-500

**Table 2.2: Typical Hardness Values of Abrasive Grain Materials at Ambient Temperature**

Aluminium oxide (Al<sub>2</sub>O<sub>3</sub>) these are artificial abrasives and related to conventional synthetic abrasive, commonly used, and allow accurate control over the form and physical characteristics of the abrasive grain. These are softest of this group and are used to grind ferrous materials and high strength alloys.

Another type of wheel used are Silicon Carbide (SiC) grinding wheels, slightly harder than Aluminium Oxide wheels, but are not as tough. SiC wheels are generally used to grind non-ferrous materials such as aluminium, brass, and stainless steels, as well as some brittle materials such as cast iron and ceramics. But it has less impact resistance than aluminium. The Zirconium alumina is used for rough grinding metals and particularly ferrous metals as it has the highest resistance of all the conventional abrasives (Rowe, 2014).

### 2.6.3 Super-Abrasives

Cubic boron nitride (CBN) is a man-made abrasive CBN wheels are the second hardest known to man. These CBN wheels are used for grinding much harder materials such as hardened tool steels, and aerospace alloys. Compared to diamond abrasives it is impact resistant, heat resistant and chemically less active. Diamond has the highest hardness of all the abrasives and Diamond grinding wheels are produced naturally or synthetically. Diamond grinding wheels are used to grind hard ferrous materials, abrasive materials such as ceramics, cemented carbides, and glass (Murphy, 2007). Diamond and cubic boron nitride (CBN) wheels belong to this group of abrasives, and is used to grind carbides, ceramics, glass and other materials. It is such as steels and alloys.

### 2.7. Grinding Wheel Bonds

The wheel bond types fall into main three classes:

- Organic and Resin Bond
- Vitrified Bond
- Metal Bond.

Conventional Abrasive wheels	Super Abrasive Wheels
Resinoid	Resinoid
Shellac	
Oxychloride	Metal
Rubber	-----
Silicate	-----
Vitrified	Vitrified

**Table 2.3: Bond Types of Various Abrasives**

The grains of these abrasives are held together to form the disk shape of the wheel. The bond must be strong enough to withstand high grinding force pressures, centrifugal forces and temperatures without disintegrating, whilst resisting chemical action by the cutting fluids. There are different types of bonds for conventional abrasives and for super-abrasive wheels which are depicted in the table below. Super-abrasive wheels also use vitrified and resinoid bonds (Malkin & Guo, 2008).

Mostly half of the wheels used in industry are vitrified but the trend towards higher wheel speeds has led to some replacements by resinoid wheels, especially for heavy-duty grinding. The use of vitrified wheels was restricted for peripheral speeds about 30 m/s owing to limitations of its strength, although advanced methods come for wheel reinforcement now make it possible to use of highest speeds over 120-200 m/s with glass derivative.

**Vitrified wheels:** are made with the combination of clay and feldspar, and a frit generally used for alumina wheels.

**Resin –bonded wheels:** are made with mixture of abrasive grains with phenolic thermosetting resins and plasticizers, moulding to shape and baking at 150 -200°C the bond hardness is verified by controlling the amount of plasticizers and by adding fillers. Rubber bonds consist of vulcanized natural or synthetic rubber. These wheels are popular for finishing bearings and cutting tools.

**Silicate-bonded wheels:** are manufactured by mixing sodium silicate with abrasive, tamping in a mould, drying and baking.

**Shellac-Bonded Wheels:** Is the natural organic material, which is rarely used nowadays as a bond material. These wheels can be manufactured by mixing abrasive grain with shellac under pressure in heated moulds. These wheels are used mainly for fine finishing of mill-rolls, camshafts and cutlery.

Another less common type of bond is *oxychloride* which is cold-setting cement from

mixture of magnesium oxide and an aqueous solution of magnesium chloride. This wheel was popular a long ago it is used for only disk grinding and it is susceptible to chemical attack by fluids so it is mostly used for dry grinding. Some of the higher end abrasive processes can be used to produce extremely fine surface finishes, to 0.025 (Murphy, 2007)

**Coated abrasives:** The abrasive grit may be bonded to a paper, fabric or metal surface with a water-soluble or water-resistive adhesive. The grit is spaced in a controlled manner and is often deposited electrostatically to align its sharp edges perpendicular to the baking surface.

### 2.7.1 Grinding wheel marking Systems

For a selection of abrasive wheel composition, it is convenient to refer to the standard marking systems of grinding wheels. The wheel's specification defines the following parameters:

- Type of abrasive
- abrasive grain size
- wheel hardness
- wheel structure
- bond type
- Manufacturer identification code

A standard grit number is defined in terms of grain sizes corresponding to five such sieves. For example, grit number 46 involves grains caught on sieves number 30, 40, 45, 50 and 60 using a standard sample size and sieve-shaking procedure. Fig.2.8 illustrates an example of marking system. The standard marking system for conventional wheels' aluminium oxide and silicon carbide includes symbol A and C that indicates whether the abrasive material is aluminium or silicon carbide. There are many types of synthetic aluminium oxide plus two common types of silicon carbide with different chemical compositions and structural characteristics, which in turn, affect their physical and mechanical properties.



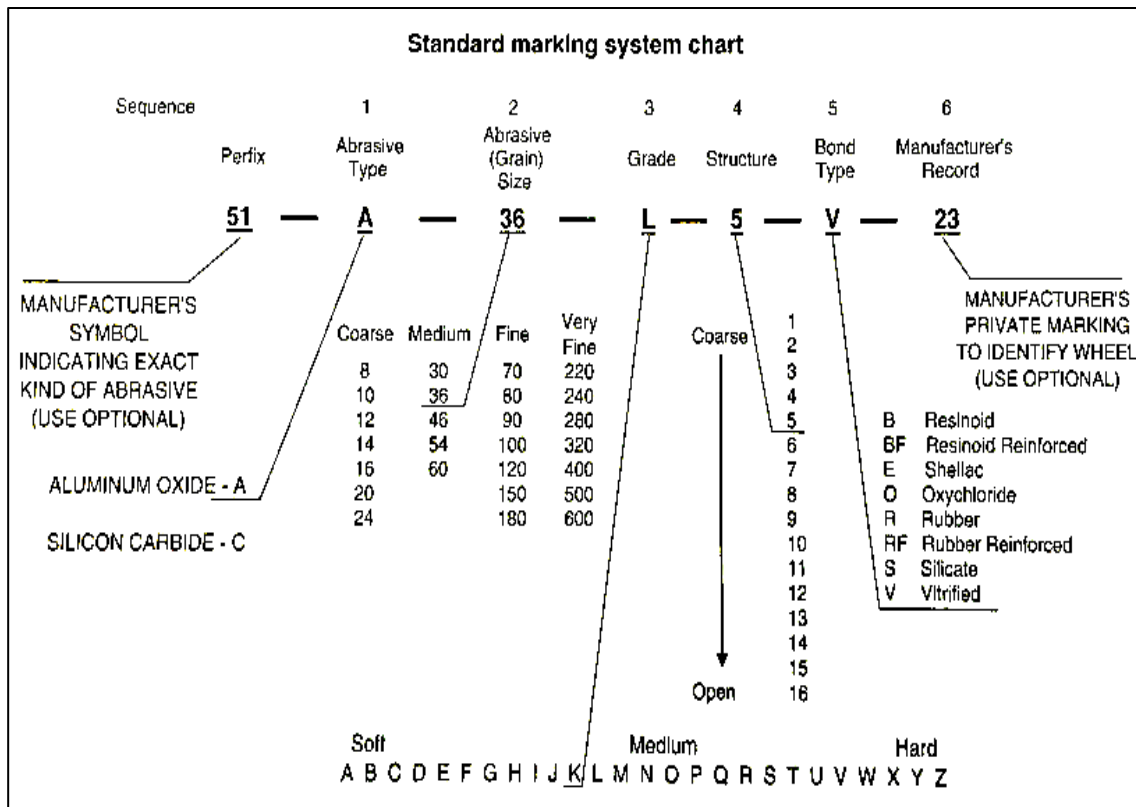


**Figure 2.8: Conventional Grinding Wheels Standard Marking System**

(Malkin & Guo, 2008)

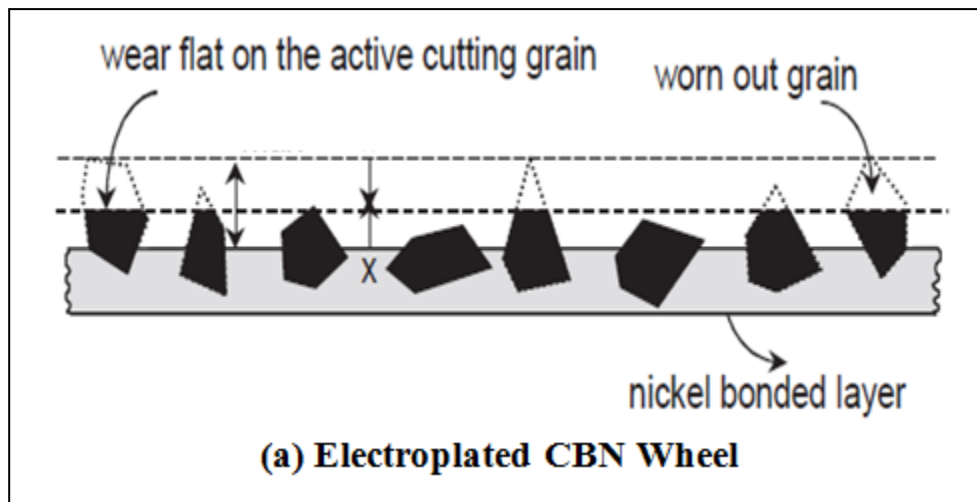
A manufacturer prefix in the form of letter or number usually appears to the left of the abrasive letter to indicate the particular type of alumina or silica carbide used. The symbol to the right of the abrasive grain type indicates the abrasive grain size by a grit number, which is related to the mesh number for the screen used to sort the grains. Larger number indicates a smaller grain size.

Sieving (screening), is generally used for sizing of conventional abrasive grains coarser than 240 grit size, and sedimentation method is used with finer grits (micro grits). The sieving method consists of from coarser aperture sieves first through progressively finer meshes. The mesh number increases down the stock. Normally the aperture size decreases by a factor of square root (2) between adjacent sieves in stack of standard sieves.

### 2.7.2 Wheel wear and Dressing

The wheel wear rate effect is depending on many factors such as grain type, grain cleavage, grain dissolution or due to chemical reactions, grinding conditions and process type, coolant type, machine stiffness, operator experience and many other variables including dressing conditions.

The other main reasons for rapid wheel wear may include soft wheel, improperly balanced wheel, machine vibration, excessive DOC, higher workspeeds, inadequate fluid delivery to the wheel. The wheel durability is defined by the dressing interval and varies due to its independence on the operating factors influencing workpiece surface finish, geometry and quality. Generally, wheel wear also causes change in wheel speed, increasing speed at a constant removal rate, reduces forces on the grains and therefore reduces its self-sharpening ability of the wheel. Wheel wear due to dressing which can result often much higher than due to grinding, therefore during dressing it is important to remove only small layer of abrasive to avoid its needless wheel and dresser usage. It can be clear that dressing is the one of the most influential aspects of the grinding process (Chen and Rowe, 1995; Chen et al, 1996).



(a) Electroplated CBN Wheel

(Malkin and Guo, 2007)

The dressing and truing is performed on all conventional wheels before grinding. Vitrified and other type of bonded wheels are always dressed and trued before grinding is to be performed, this is one of the most vital operation for wheel life. After certain time of operation, the cutting edges of the wheel become dull and flat and rub against the material workpiece instead of cutting.

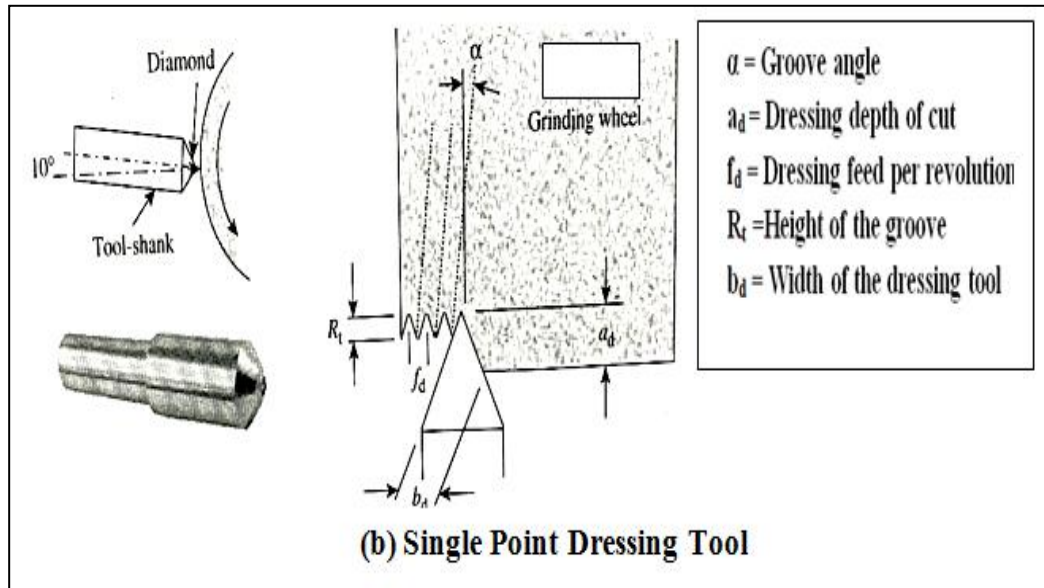


**Figure 2.9: Wheel Surface; a) Plated CBN; b) Single Point Dressing**

(Rowe, 2014)

In truing, if any material stuck or clogs will clean off and to develop new cutting grit points on the surface of the wheel. This is also used in order to correct the eccentricity of the wheel shape. Truing and dressing in case of super-abrasives are different, and in some types of super-abrasives wheels, no dressing is required i.e. metal bond.

The above Fig 2.9 (a) Illustrates the surface of a metal plated wheel and a (b) single point diamond set in a tool-shank, the point showed is very sharp and the included angle is much larger as in the actual tool shown and dressing is often rounded. The tool holder allows the tool-shank to be set at a drag angle of the order of  $10^\circ$  and tool-shank must be rigidly mounted in a tool holder. The dressing tool is traversed across the surface of

the wheel to generate the required form and cutting surface. The coolant must be supplied before commencing the dress pass to keep the diamond cool. If no coolant is supplied during pass this may leads to damage of the diamond due to thermal shock. The effects of diamond may be mitigated by rotating the diamond about 90° axes at frequent intervals (Rowe, 2014).

### 2.7.3 Bond and Grain Fracture

Grinding wheel grain fracture is much more likely to occur by mechanically induced tensile stresses within the abrasive grains than by mechanically induced compressive stresses.

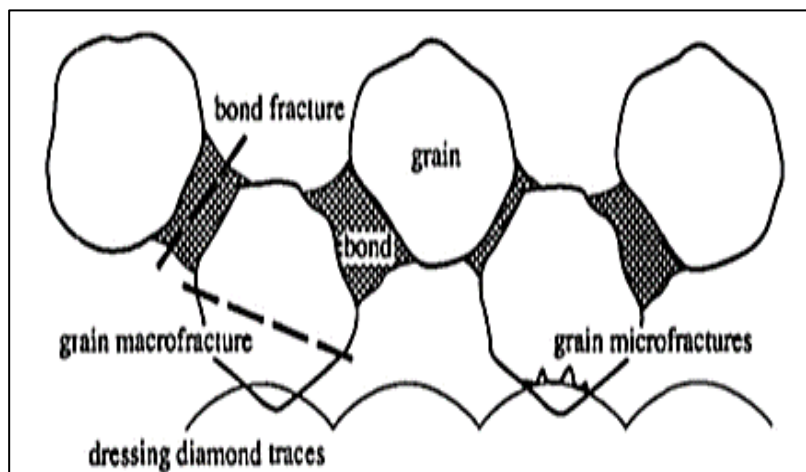


**Figure 2.10: Bond and grain fracture**

(Chen & Rowe, 1995)

The good performance of the wheel while grinding under different conditions is the level of tensile stress induced in grains. High tensile stresses lead to grain fracture, when a grain breaks off but the rest of the grain remains bonded in the grinding wheel. The edges of the (broken) fractured grain area become new sharp cutting edges on the grinding wheel. This allows the grinding wheel self-sharpening, a unique property of a cutting tool. Fig 2.10 depicts bond fracture occurs when the individual grains are pulled out of the bonding material. Bond fracture usually occurs because the grain has become dull due to attritious wear and the resulting cutting force is excessive. Sharp grains cut

more efficiently with lower cutting forces; hence, they remain attached in the bond structure (Chen & Rowe 1995).

## 2.8 Advanced Technologies in Grinding Process

One of the latest techniques in special micro manufacturing is abrasive grits grown from seeds. Another high speed grinding of (305.5 m/s) using synthesised man made abrasives such as cubic boron nitride (CBN wheels) special bonding materials (Badger, 2004).

Another development is High efficiency deep grinding (HEDG) a new advanced grinding method which operates high depths of cuts, high speeds and with consequent high material removal rates exceeding 1200-2000 mm<sup>3</sup>/mm/s. In creep-feed grinding operation replaces separate milling and finish grinding operations saving time and money. These new improved developments make possible of high accuracy production rates without damage to the components with high thermal effects. This process requires effective coolant delivery and high power.

In HEDG temperatures are relatively low despite the high material removal rates, (Rowe *et al* 2003; Batako *et al*, 2005) Several methods have been employed to measure the temperature during HEDG process such as optical method, fibre optics method and thermocouple method some methods have accurately proved compare to predict and measures values but this process needs more research.

The development of creep-feed grinding into HEDG process high performance vitrified wheels was employed on a machining centre. The process is termed 'VIPER' was developed by Rolls Royce in collaboration with Tyrolit and Makino. This 20 years method of grinds is applied mainly in nickel alloy turbine blades and achieved high removal rates of up to 80-200 mm<sup>3</sup>/mm/s, which is extremely fast for hard materials. The aluminium oxide grinding wheels employed are 120-200 mm diameter and are dressed only once just prior to the finishing cuts. Another modern method is 'peel grinding' this method achieves flexible grinding operations with variety of diameters, grooves, thrust faces and forms using one setup. Peel grinding is often compared with

hard turning where a tool is traversed along a hardened workpiece following an appropriate form (Rowe, *et al*, 2003).

### **2.8.1 Vibration Assisted Grinding**

It was shown that costs were lower, even allowing for a more expensive grinding machine of 63 KW at Liverpool John Moores University (LJMU) for high speed grinding Optimos segmented grinding wheel were employed containing Altos high-porosity and high aspect ratio sintered alumina grain and permit grinding speeds up to 140 m/sec (Tsiakoumis, 2011, 2012; and Batako, 2012, 2015) have developed a new low frequency oscillating stages which showed that the application of vibration to grinding process leads to higher removal rates, lower cutting force, better surface finish and longer wheel life with high G-ratio compared to conventional grinding.

### **2.9 Thermal Effects on Grinding Contact Zone**

In grinding extremely high temperatures are generated during machining process these are due to the high material removal rate, rake angles, ploughing and rubbing of the abrasive particles against the work surface. But normally these high temperatures and friction are common. The heat generated in the grinding process is transferred to the work piece, wheel and coolant. Kuriyagawa, (2002) measured the temperature distribution in grinding contact zone between the wheel and specimen in creep feed grinding using a system of thermocouples. Normally grinding employs a higher unit grinding force and grinding speed than cutting processes and therefore involves a significantly higher energy. Approximately about 80% of the thermal heat is transferred into workpiece while in conventional machining operations most of the heat generated is removed by the chips. This induced high temperatures influences on property of grinding grits; decrease the service life of the grinding wheel. To minimise the temperature in the grinding arc and to improve the quality of the workpiece, life of the cutting tool and machining, different cooling lubrication technologies are applied in the grinding process.

### ***Needs of Coolant***

In grinding, flood-cooling is the most common lubrication method, which requires about 60 L/min of flowrate. The fluid flow can cool and lubricate the wheel and workpiece and flush out the debris. Flood cooling in grinding showed better workpiece surface quality than dry grinding. The rotation of grinding wheel at a higher speeds tend to forms a layers of air barrier on the surface of the wheel, which makes difficult for the fluid to enter into the gap between grinding wheel and workpiece interface. Therefore, the effective flow rate between grinding wheel and workpiece interface is only about 5% - 40%. Moreover, in the grinding process, leakage, or overflow of the grinding fluid may cause significant damage to the health of workers and water contamination. Mineral oils are used as a lubricating fluid and have excellent lubrication properties, but its low cooling property and high cost limit its application in machining.

To protect environment and reduce costs, “*dry grinding*” is adopted because it is significantly more advantageous but it consumes more energy than any other processes, more heat gathers in grinding zone. Only 10% of heat is removed by the grinding wheel and chips in the grinding process. The gathered heat which leads to high temperature and without lubrication and cooling effect of the grinding fluid, effects the grinding wheel wears seriously, and the workpiece accuracy and surface integrity deteriorate.

The grinding wheel must meet the requirements of this process and should have high hardness, toughness and wear resistance. These specific conditions required by dry grinding limit its wide application in grinding applications (Wang, 2016). High surface temperatures cause several damaging effects, which primarily include surface burn and cracking. Burn marks appear as discoloration on the surface. These burn marks are an immediate sign of metallurgical damage beneath the surface. An extreme case of thermal damage is the sight of surface cracks. The cracks in grinding appear perpendicular to the rotation of the grinding wheel (Murphy, 2007).



### 2.10 Temperature Distribution in Grinding

Temperature distribution in grinding is crucial for investigation of thermal softening effects in material and thermal damages on the workpiece surface. Many models have been introduced and developed by the researchers. A model for energy partition was developed by Guo and Malkin for shallow grinding based on sliding, ploughing energy where 55% of the energy is chip formation which goes into workpiece. (Tahvilian, 2013) studied, heat generation distribution in robotic grinding operation based on local chip thickness and friction effect over the corresponding contact zone at the workpiece interface. The calculation of the chip thickness is based on a wear model of the grinding wheel in accordance with an impact-cutting behaviour, observed with high-speed camera.

Temperature distribution in the workpiece was simulated with 3-D transient thermal finite element (FE) code. Tahvilian, (2013) found that energy partition ratio in flexible robotic grinding is small than in conventional grinding. Kim *et al*, (1997) estimated heat flux distribution and energy partition to the workpiece for creep-feed grinding. An inverse heat transfer analysis was applied to calculate the heat flux and cooling distributions on the workpiece surface. The diverse thermal effects generated in high efficiency deep grinding (HEDG), it is found that steady state conditions are achieved for sufficient workpiece length and high speeds. (Jin, 2002) developed a new thermal model of circular arc contact with transient analysis.

### 2.11 Thermal Damage & Grinding Energy Dissipation

One of the main limitations to increase removal rates during grinding process is thermal damage to the workpiece surface, evidenced by the appearance of tempered colours on the surface, softening and re-hardening of the surface material. With burn the grinding forces and rate of wheel wear alter and consequently wheel life may reduce (Rowe *et al*, 1988).

Grinding energy is dissipated from the grinding zone in a number of ways, i.e.

- The heat conducted away by the grinding wheel.
- The heat conducted away by the workpiece.
- The heat carried away by the chips.
- The heat dissipated into the coolant by means of convection.
- The kinetic energy imparted to the chips.
- The energy required for generating a new surface.
- The residual energy imparted to the ground surface.

### **2.12 Summary**

This literature review has given a good insight into the background of grinding process and previous relevant research works. The review covered all the grinding process in general then focuses on the grinding types and technologies. Review on existing grinding mechanisms, contact length measurements, design techniques and effect of grinding wheel wear, which helped in designing the optimised nozzle for the grinding process. Effects of thermal problems in contact region during grinding. Precautions to be taken particularly during grinding in order to avoid any high heat generation, grain fracture, high impact forces, and uneven material removal rates and wheel clogging problems were highlighted. Considering some of these issues a high jet nozzle needs to be developed.

Finally a basic discussion about the abrasive wheels was provided with grade system. Grinding wheel abrasive and grain bond materials were also discussed and how wheel composition influenced performance. Wheel wear, grain fracture, truing and dressing were also discussed.

## **Chapter-3**

### **Coolants and Lubricants Used in Grinding Process**

## Chapter-3 Coolants and Lubricants Used in Grinding Process

### 3.1 Coolant Application in Grinding

Fluid is applied in grinding process to aid lubrication, to remove swarf and for bulk cooling. Lubrication reduces frictional forces and subsequently reduces abrasive wear and the generation of heat, leading to improved surface quality and productivity. The correct application of fluid has been the subject of significant recent research effort. A key parameter for establishing the efficiency of fluid delivery in the contact region is useful flow. This term is generally regarded as a measure of the flow that passes through the grinding contact zone. (Jackson *et al*, 2005) A grinding coolant is used for two purposes, first to reduce thermal energy build-up by convective cooling and minimise the friction generated heat by lubricating the cutting interface. The second is used to reduce wheel wear and process efficiency.

The life of the grinding wheel is also very important, when grinding of very hard materials like hardened steels, high temperature resistant steels, sintered aluminium oxide and sintered carbides, which leads to increase in the temperature during the grinding process. High temperature causes thermal damages to workpiece as well as to the grinding wheel, which leads to the poor surface quality of the component, inadequate removal rates and high wheel wear. To reduce these undesired effects of the grinding process the coolant is provided during the metal cutting process. Coolants are used to flush out the chip during the machining process, this helps in extending the life of the grinding wheel. Therefore, the application of coolant in grinding is necessary and high importance. Currently the usage of these coolants in the industries for machining processes is increased and this causes more investment in the coolant fluids. The fluid application in grinding process is very wide however, improvement to the nozzle design for delivery systems is constrained by limited understanding of nozzle internal flow,

nozzle positioning and system requirements for optimal fluid delivery. A principal function of fluid is to improve lubrication subsequently reducing the risk of thermal damage and improving the process performance. Grinding fluid is delivered at a particular flow rate and pressure, so an understanding of these parameters may help in reducing the consumption of the coolants. However, exceeding the optimal delivery conditions result in excess energy consumption and environmental cost. Research is required to establish the required delivery parameters for achievement of optimal fluid delivery at needed velocity and pressure to provide the best results in a range of applications. (Morgan *et al*, 2008)

Chang, (1997) investigated the depth of fluid penetration into the grinding wheel and flow rate through the grinding contact zone and the useful flow, to ground a porous workpiece by replacing the grinding wheel with a porous layered solid disk to observe the hydrodynamic and the pressure of the fluid agents.

Nguyen, (2005) has developed two analytical models to provide a physical understanding of the mechanisms of coolant penetration into the grinding contact zone. Using segmented and conventional wheels and it is concluded that coolant minimisation is possible using the segmented wheel and the efficiency depends on the wheel speed and method of coolant supply.

### **3. 2 Grinding Contact Zone**

The process fluid does not assure high workpiece quality and grinding process efficiency, it is known however that cutting fluids lowers the temperatures mainly by minimizing the friction between the wheel and workpiece. Lubrication depends on fluid entering the contact region between the wheel and the workpiece. It does not mean that a bulk volume of fluid has to be used, however lubrication may be ineffective if no fluid enters the contact zone at all (Marinescu *et al*, 2004). In order to achieve possible adequate cooling and lubrication a proper nozzle arrangement is required.



For better understanding of the fluid flow process pass through the grinding contact zone, the whole process can be divided into 4-regions: (1) the mixing zone, (2) the entrance zone, (3) the grinding zone and, (4) the open zone as shown in Fig.3.1 Hryniewicz, (1998). The entrance zone is the region where the rotating wheel drags the fluid ejected from nozzle into grinding zone. The grinding zone is the region where the rotating wheel makes contact with the workpiece. Almost all the heat is generated in this zone. The open zone is the region where the fluid is separated from the wheel due to centrifugal force. The mixing zone is the region where the recirculation fluid mixed with the freshly ejected fluid before going into the entrance zone.

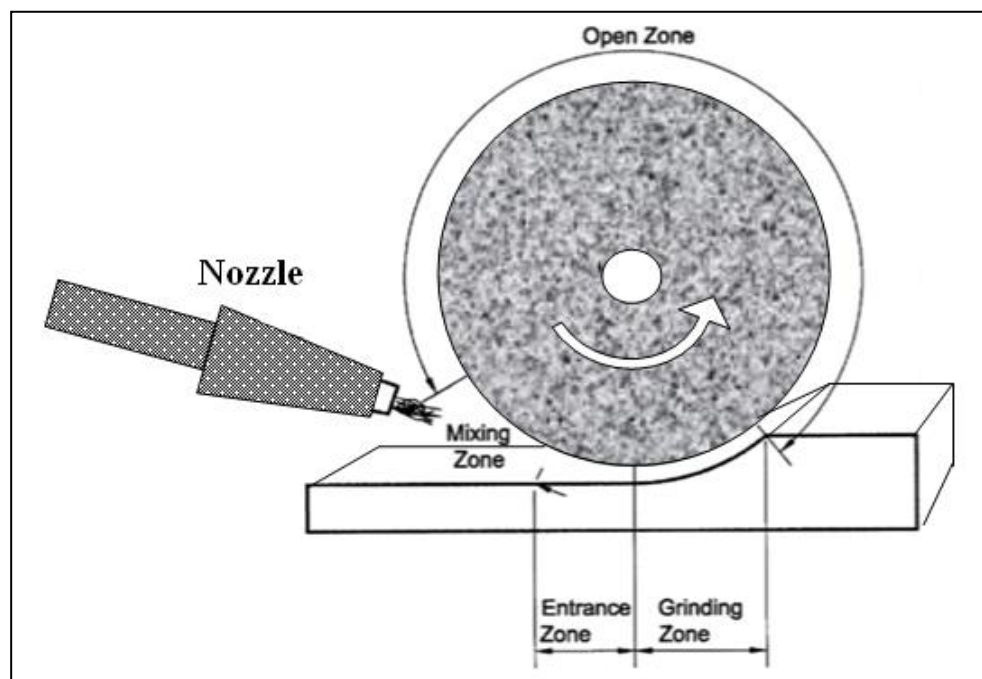


**Figure 3.1: 4-Regions of fluid flow process beneath grinding wheel**

(Adapted from Hryniewicz, 1998)

The porosity of the wheel serves as the transportation of the fluid from entrance zone into the grinding zone. The coolant from the supply nozzle jet first filled the pores along the wheel, and then the coolant is transport within the pores into the grinding zone, the

coolant is rejected off the wheel after it leaving the grinding zone due to centrifugal force and later enters the open zone.

In order to calculate the useful flow rate passed the grinding zone, several methods had been used to observe the process. Schumack (1991) analyzed the process by assuming the condition where fluid flow between a non-porous and smooth grinding wheel, and a flat work piece surface. However, this method only applicable to theoretical analysis as grinding wheels is not smooth but porous. Guo and Malkin (1992) considered the ram pressure of the jet ejected out of the nozzle as the agent to fill the wheel pores; the fluid is then forced through the grinding zone.

### 3.3 Functions and Role of Coolants in Grinding Application

Howes, (1990); Brinksmeier, (1999); Marinescu et al, (2004) summarised the functions of cutting fluid as follows. Grinding process generates excessive heat energy in the grinding contact zone. This thermal energy must be reduced or removed to prevent from high residual stresses, high local temperatures and phase transformations, so, the role of coolant is necessary to cool and lubricate the workpiece and the wheel during grinding.

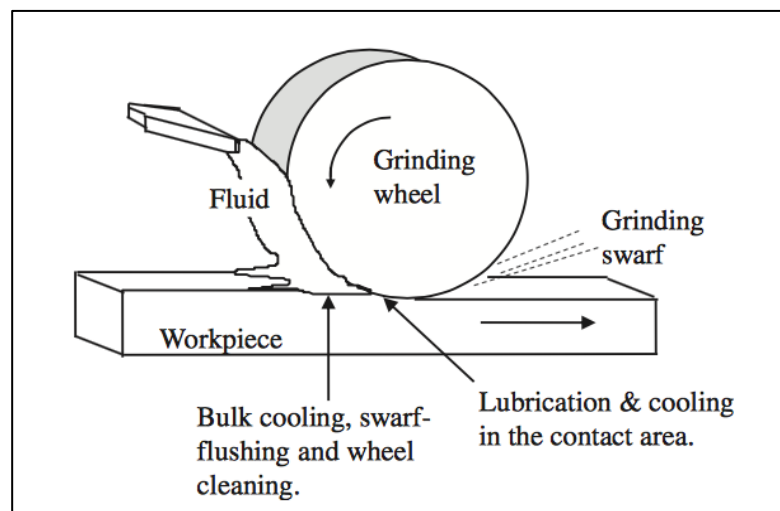


**Figure 3.2: Role of process fluid in grinding**

(Marinescu *et al*, 2004)

- Mechanical lubrication of the abrasive contacts
- Chemo-physical lubrication of the abrasive contacts
- Cooling in the contact area, particularly in Creep feed grinding
- Bulk cooling outside the contact area
- Flushing or transport of the debris away from the abrasive process
- Transport of abrasives to a loose abrasive process
- Entrapment of abrasive dust and metal process vapours

The requirements of the modern high speed abrasive processes need careful planning to obtain the benefits of optimal lubrication, cooling and wheel cleaning. Large flow-rates and high-energy consumption is the priced matter paid to achieve a satisfactory fluid delivery. Fig.3.2 illustrates a single flood nozzle may not be sufficient to satisfy the various functions expected of the process fluid. A medium flow-rate nozzle with a medium pressure head, for example, 4-bar may be used to supply fluid to the contact area. Another 100-bar, high-pressure nozzle may be used continuously or discontinuously as a cleaning jet to force fluid at high velocity into pores of the wheel. The main aim is to remove loose and weakened grits from cutting surface. The high-pressure jet also removes loose swarf from the wheel surface and this slows down the rate of wheel loading. (Marinescu *et al*, 2004)

Most grinding fluids can be categorized either as straight or neat oils or as soluble oils. Straight oils are mineral-oil-based fluids with additions of fatty materials for lubrication and wettability, and usually sulphur and /or chlorine for added wear reduction. Soluble oils are water-based fluids containing oil emulsions and numerous other ingredients which may include fatty materials, sops, sulphur, and chloride for lubrication, surfactants for wetting and detergency and to prevent foaming, rust inhibitors, and germicides. (Malkin, 2008)

Cooling and lubrication requirements differ in every application and mainly depend on grinding conditions. Every coolant consists of a basic fluid, to which are added other

products such as anti-wear, anti-corrosion or emulsifying agent. Coolants are divided according to DIN 51385 into three major categories water-based and oil-based or oil-in-water emulsion or with a neat mineral oil or neat synthetic oil. But the main groups of cutting fluids are divided into two categories as illustrated in Fig.3.3. (Brinksmeier, 1999)

- Oil-based coolants
- Water-based Coolants.

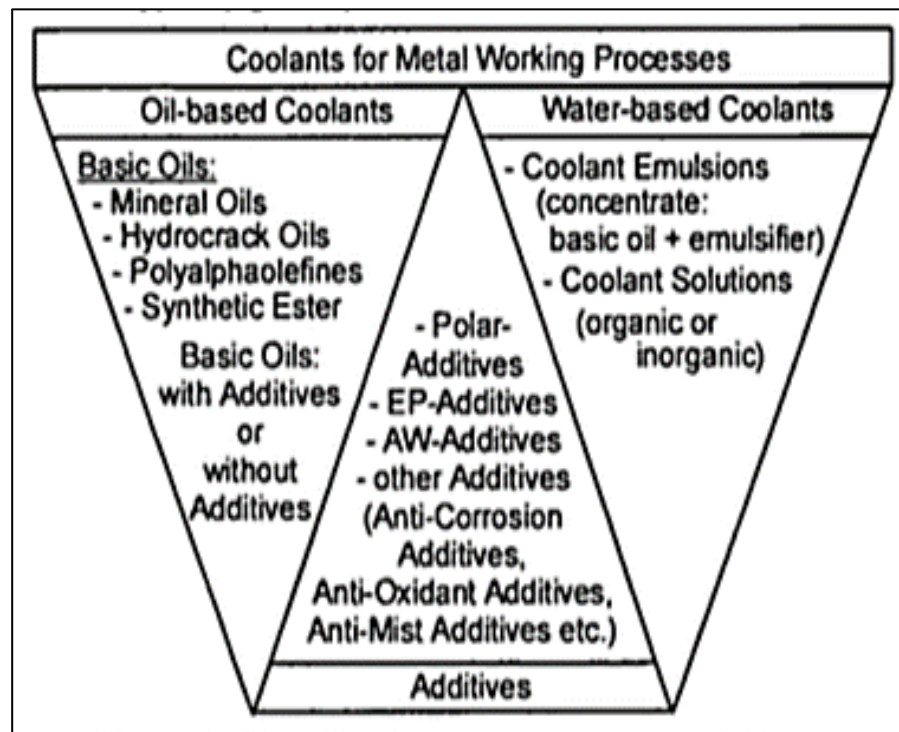


Figure 3.3: Classification of Grinding Coolants

(Brinksmeier, 1999)

### 3.3.1 Oil-based coolants

In order to reduce friction and temperatures during machining processes it is necessary to create separation films (consisting of coolant and specific additives) between solid

surface of the tool and workpiece. Emulsion oils are often known as soluble oils, which contain 50-80% of mineral oils in concentrate. Oil-based coolants consist of about 80-95% of basic oil and they are divided into four types (Brinksmeier, 1999).

- The basic oils without additives.
- The basic oils with chemically active additives.
- The basic oils with surface-active additives.

The basic oils with chemically active additives that stable adsorption layers.

*The commonly used basic oils are:*

- Mineral oil: natural C-H bonds, must be free of harmful aromatic compounds by refining
- Hydrocrack oils: partly synthetic, low content of aromatic compounds, improved mineral oil.
- Polyalphaolefins: fully synthetic oil with branched hydrocarbons, thermally stable.
- Synthetic ester: fully synthetic oil of fatty ester acids, thermally stable, biologically decomposable, useable as basic oil and as additive.

These types of Oil-based coolants normally provide high corrosion resistance and lubrication effect in comparison to water-based coolants. Also, low viscosity oils have a better crack penetration ability compare to higher viscosity oils. Higher viscosity oils adhere more strongly and produce less oil mist. (Brinksmeier, 1999)

### **3.3.2 Water-based Coolants**

These coolants contain about 20-70% of the basic mineral oil. They are used for high cooling effects and washing capabilities. Water-based coolants consist of inorganic or organic substances and water and very seldom contain mineral oils. High chemical stability and transparency are further advantages in high cooling efficiency and washing away capability. Their main disadvantage is the susceptibility to leakage and

microorganisms leading to high maintenance costs. Also, the water and oil phases must be separated before disposal. Common oil concentrations in emulsions for grinding operations are between 2 and 15%. Water-based coolants contain up to 20 components in which, each of the components can themselves be multi component mixtures. (Brinksmeier, 1999)

### 3.3.3 Additives

Additives are added to basic fluids to broadly optimize particular types of production process; each one is aimed at improving specific coolant properties. Additives can be divided into three main groups:

- Enhancers of physical coolant characteristics.
- Enhancers of chemical and physical coolant characteristics.
- Other additives.

During metallic solid body frictional contact, certain additives form highly stable compounds either due to their charge polarity or due to chemical reactions at the metal surface. These reactions take place within defined temperatures ranges, so the process temperature is an important influencing factor in the effectiveness of the additive.

Polar active substances (synthetic ester, fatty acids), extreme-pressure additives (sulphur carrier), anti-wear additives (phosphorous compounds) and others (anti-corrosion additives, anti-mist additives, anti-oxidants, and emulsifiers) are all employed as additives. (Brinksmeier, 1999)

### 3.3.4 Advantages of Grinding Fluids

1. Large reduction in the thermal damage to the workpiece.
2. Reduced wheel wear.
3. Less loading of work material.
4. Reduced dressing frequency.
5. Higher removal rates and better surface quality.



### 3.4 Fluid Treatment

The fluid treatment is important in application of grinding fluids for many reasons. In the closed system, the machine and components need to be protected from corrosion. This requires the addition of rust inhibitors to the fluid. The swarf generated in the process must be separated out and recycled or sent for disposal. This requires a filtration system. Lubrication properties can be improved by addition of oily compounds or other synthetic compounds designed for the particular grinding wheel and workpiece material combination. Bacteria and fungi build up in a closed system, so bactericides and fungicides must be added. Foaming must be prevented requiring a foam suppressant. Even a well-designed coolant system, it may be necessary to completely change the coolant mixture on a weekly basis. Water quantity needs to be controlled for use of emulsions. Hard water may undermine the resulting properties of the fluid. A pH value of 6-7 is recommended and deionization may be required for grinding high-tuff materials (Rowe, 2014).

### 3.5 Cooling Mechanisms in Grinding

The main characteristic of the grinding process is the relatively large contact area between the wheel and workpiece in comparison with other machining processes. The heat generated during the grinding process is critical to the workpiece quality, and there is a high risk of thermal damage. The fluid accomplishes this by reducing the amount of friction in the grinding contact zone through its lubrication properties. Also, it reduces heat by converting some energy into the fluid instead of the workpiece. When the cutting fluid is colder, the heat transfer is more effective. If the chips are not taken out from the grinding zone, it reduces the life of the grinding wheel and dulls the wheel, and only ploughing and rubbing occur. If this clogging happens continuously to the wheel, the forces and internal energy input would greatly increase and the heat imparted to the workpiece will be more. The cutting fluid in the grinding zone initially undergoes nucleating boiling. This process enhances the rate of heat transfer between the workpiece and the fluid. Further

increase of heat the fluid will turn into film boiling where a vapour is developed between the workpiece and the fluid. The vapour acts as an insulator and prevents heat transfer to the fluid. As a result, the temperature of the workpiece suddenly increases and leading to burn of the material. For effective way of cooling it is very important that the workpiece temperature does not reach or exceed the fluid's film boiling temperature as the critical burnout limit. The point where the heat is generated at the grinding wheel is called as critical burn out point. The heat generated at this point should be controlled to prevent the damage of the workpiece (Irani, 2005).

### 3.6 Coolant Flow rate

Coolant flow rate is the significant factor in the machining process. Using of high-pressure flow and high spindle power tends to accelerate the fluid through the contact zone leading to high surface finish quality. Brinksmeier *et al* (1999) proposed an effective supply of coolant flow rate, shape and dimensions of nozzle geometry for the conventional flood cooling aimed and focussed to better understand the role of coolant in the complex fluid mechanics of the machining process. Excessive amount of working fluids are used in the industry. Okuyama *et al* (1993) studied the effect of coolant supply depending on various parameters such as nozzle output flow rate. They proposed a new method for measuring the heat transfer coefficient in the vicinity of the wheel-workpiece close to contact area. Thus they describes the influence of variations in different parameters, they explained that increasing the fluid velocity can guide to a digressive incline of the coefficient of heat transfer and provide a lower cooling efficiency, due to geometrical limitations of the flow rate though the grinding arc.

Brinksmeier *et al* (1999) and Klocke *et al*, (2000) analysed the hydrodynamic effects in the grinding contact zone. They showed that the force directed perpendicular to the grinding contact, increases with increasing coolant flow rates at constant geometry of the fluid nozzle.



The useful flow rate is a cutting fluid, which goes through the grinding zone and affects the mechanism of the grinding; therefore, the key target is to increase this useful flow. A research based on Guo and Malkin, (1992) concludes that the flow rate is equal to the amount of fluid retained in the grinding wheel from the point of application to the grinding wheel accelerate the coolant speed to force it through the wheel contact zone. High volumes of cutting fluid is generally used in the conventional fluid delivery in which some amount of cutting fluid is considered as the useful flow rate. This has opened the gates for the research on delivering the minimum cutting fluids which effect grinding conditions. It is known as (MQL) minimum quantity lubrication.

### **3.7 Grinding Nozzle**

The delivery of the grinding fluid to the contact zone is generally achieved via a nozzle. The nozzle geometry influences the fluid velocity and flow pattern on exit from the nozzle orifice. It is important to the efficiency of the process and to the performance of the operation that the fluid is delivered in a manner that ensures the desired jet velocity has adequate coverage of the contact zone.

The delivery of a coolant jet via nozzle has two advantages, one is that the cutting fluid can be delivered with a high velocity to penetrate into the air boundary layer or pores of the wheel and the second; it is used to clean the wheel by removing loose chips from the grinding wheel pores. The main purpose of the nozzle is to direct the fluid to the grinding contact zone and to increase the velocity of the process fluid by restricting the cross-sectional area of the jet stream. A well-designed turbulent flow nozzle converts approximately half the pressure energy into kinetic energy than a laminar flow nozzle. Laminar flow nozzle has the advantage that the jet stream coherence and velocity will be maintained for a greater distance than a turbulent flow nozzle. Laminar flow can only be achieved with Reynolds number less than 2,000. This implies low jet velocities compared with peripheral wheel velocity.

The works of Alberdi, (2011) showed the influence of nozzle design and development of velocity pressure fields using CFD simulation for optimization of fluid application in grinding contact zone. Also grinding improvements in wheel life and surface finish was obtained by using new designed nozzle.

A coherent jet from a Rouse profiled nozzle showed very little dispersion with mineral oil, where the Reynolds number of the jet was much lower than that with water at the same pressure. For this reason, nozzles designed to be coherent with water have even better jet quality with oil.

Alberto, (2013) studied two approaches aiming at the optimisation of fluid application in grinding. The first was influence of nozzle design on the development of velocity and pressure fields is studied using CFD and the second was to correlate the effect of tool geometry developed on grinding process conditions.

Gviniashvili, (2003) used wheel, jet velocity and power required for fluid acceleration to determine a suitable fluid passage value nozzle outlet delivery gap to achieve a required fluid film thickness in the grinding work zone. Yumusak, (2012) worked on the development of an efficient and reliable rocket nozzles design tool and methods depending on the accuracy of the fluid flow models

Webster, (1995) suggested that coolant plays an important role in grinding process for long contact arc in creep feed grinding process. The objective of his study was to develop a new range of nozzle, which gives high improved jet coherency over existing commercial nozzles to minimise 'misdirected flow' before passing through the contact zone. It was stated by Brinksmeier, (1999) that the workpiece quality depends on proper supply of coolant and any misdirected flow will lead to thermal damage to the workpiece and grinding wheel wear. Also found that the main characteristic of grinding process compare to other is the relatively large contact arc between the work piece and grinding wheel.



### 3.8 Nozzle Design Guidelines

A successful delivery of the grinding fluid to the contact zone is very much dependent on nozzle design, nozzle position and the fluid flow. The nozzle geometry influences the profile of jet velocity and flow pattern at the exit from the nozzle orifice. It is important to the efficiency of the process and to the performance of the operation that the fluid is delivered in a manner that ensures the desired jet velocity has adequate coverage of the contact zone. Often, assumptions about adequate coverage are based on visual inspections of the jet coherence, (Morgan *et al*, 2008).

The cooling effects of the grinding fluids can be maximised by good nozzle design. The lengths of pipe within a flow system must be adequately selected to attenuate the effect of elbows and transitions along the fluid path. The shape and size of the aperture affects the profile of the jet and its coherency. The following guidelines must be observed when designing an efficient nozzle for grinding application (Jackson, 2008).

- Coolant delivery is affected by the nozzle design. In particular nozzle geometry, smooth surface finish, nozzle fillets, break-edges and size of opening are very important.
- Matching the speed of the fluid jet with the wheel peripheral speed is desired but recent finding suggested that this is not always the best. An optimum jet speed should be in the region of 0.6~0.8 ( $V_j = 0.6 V_s$ ) of wheel speed, (Jackson, 2008).
- The coolant delivery systems should be designed with attention to changes in the shape and size of hoses, pipes, and connectors. Important are nozzles, nozzle positions, flow rate settings, pump capacity, flow conditioners, large diameter straight pipes, and flexible hoses. Increasing nozzle distance tends to reduce the cooling performance of the grinding fluid especially with nozzle designs that produce low coherence jet streams.
- There may be no need for profiled nozzles since a large single coherent nozzle or several smaller coherent jets can be utilized.

- If expensive rectangular nozzles must be used, an aspect ratio of 5–8 (width ( $W_{\text{slot}}$ )/height ( $h_{\text{slot}}$ ) see Fig.3.8 (b) is recommended.
- The most suitable way of producing a coolant jet that serves its purpose is to use coherent nozzles, which maintain a coherent jet over a given distance. Coherent nozzles use an internal geometry see Fig.3.4 (a) Rouse coherent nozzle that gives low dispersion, therefore minimum entrained air within the jet. A definition of coherent length is the distance from the nozzle exit up to a dispersion of two to three times the exit diameter.
- The nozzle should have sharp exit edges.
- The nozzle should have high concentration ratio from inlet to outlet.
- Elbows and changes in the pipes diameter should be avoided.
- A straight pipe placed between a flow conditioner and nozzle is needed to encourage a uniform-velocity flow condition. (Irani, 2005)

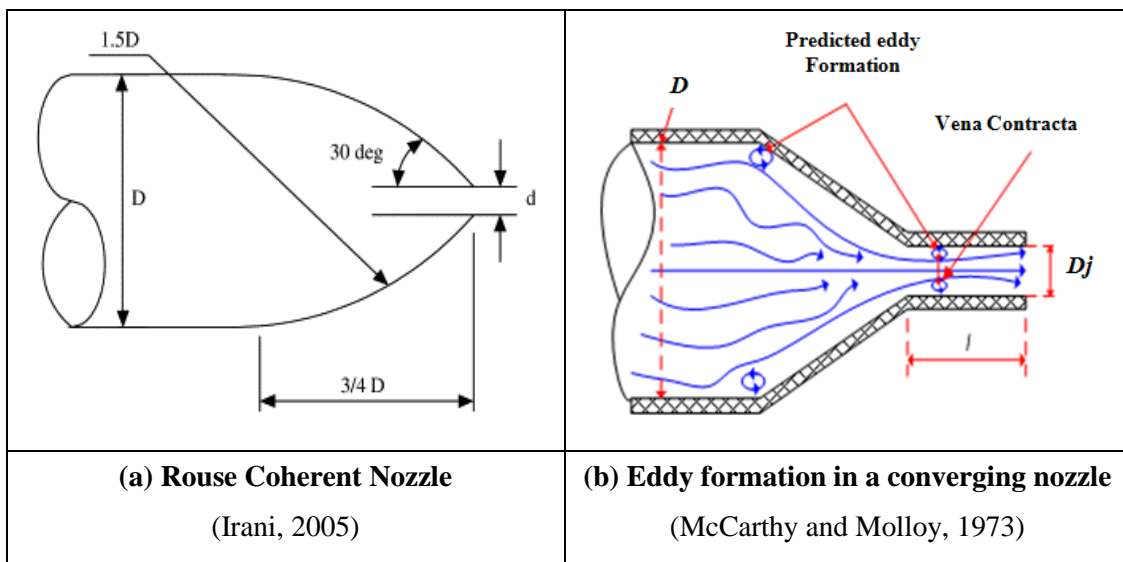


**Figure 3.4: Internal Nozzle Cavity Design**

$D$  = Diameter of the inlet,  $D_j$  = Diameter of the jet;  $l$  - length of exit, ' $d$ ' = Outlet of the nozzle,  $D$  = Diameter of the supply;  $\frac{3}{4} D$  = Length of Concave profile angle,  $30^\circ$  = Angle between edge of exit to profile,  $1.5D$  = concave angle.

A common problem with orifice nozzles is the ‘vena contracta’ effect as shown in Fig.3.4 (b). This is where the fluid adheres to the edges of the opening, consequently reducing the size of the opening. In a typical orifice, this effect reduces the size of the outlet to 60 - 80 per cent of its physical size. As the fluid flows from a large region into a smaller region, the sudden change in section leads to eddy formation and secondary flow appears causing the jet to disperse. Fig.3.4 (a) is the ‘Rouse coherent nozzle’ with key dimensional relationships that allow achieving a uniform flow within the nozzle itself and a coherent jet at the exit.

### 3.8.1 Types of Nozzles



**Figure 3.5: Round Swivel, Spot Jet, Flat Headed and Click-fit nozzles**

(Coolant grind.technologies.com)

There exists a wide range of nozzles used for various engineering applications such as fire fighting, agricultural irrigation, and metal machining processes some of the commonly used grinding coolant nozzles are presented in Fig.3.5 and Fig.3.6.

- Convergent nozzle: is a type of nozzle where it's cross sectional area continuously drops towards the exit. It is generally used for non-compressible liquids.
- Divergent nozzle: is a type of nozzle where it's cross sectional area continuously increases from start towards the end.
- Convergent-divergent nozzle: is a type of nozzle where from the start; the area of the nozzle first decreases and then increases from the point where it diverges.

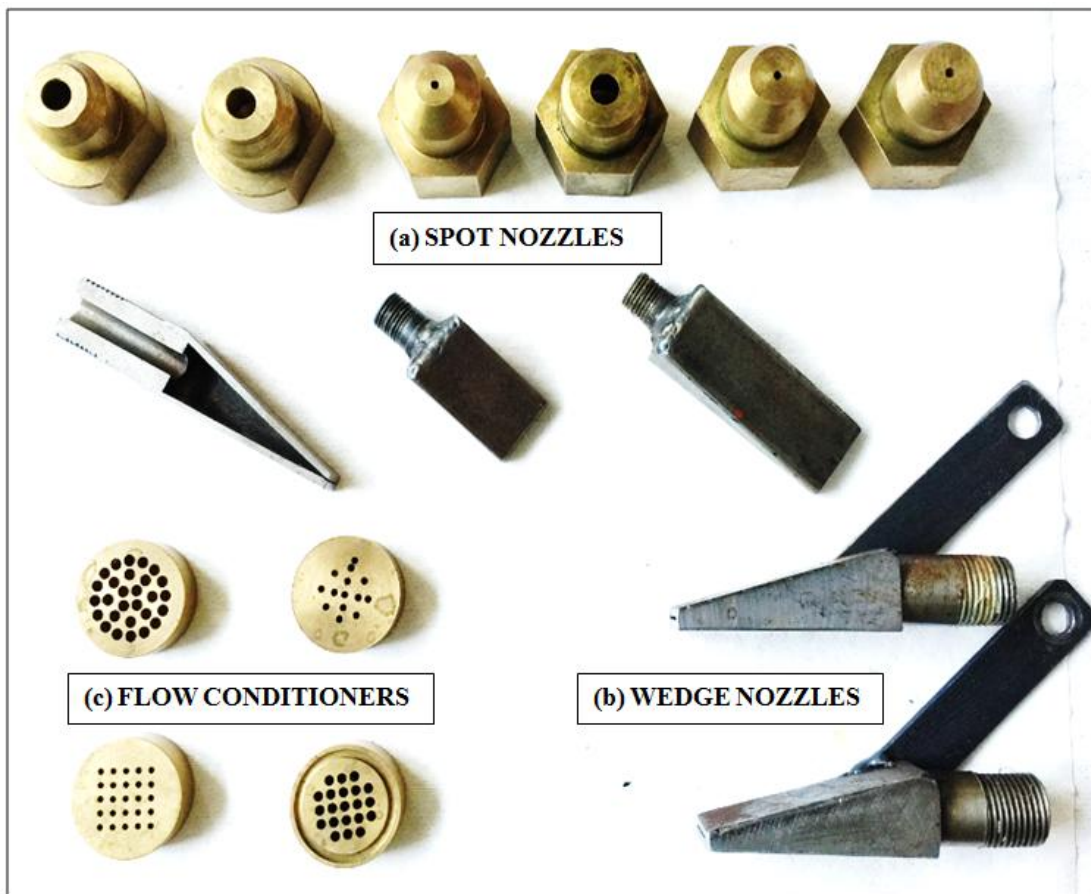


Figure 3.6: Coherent jet, Spot jet and Wedge shaped nozzles

### 3.8.2 Shoe Nozzles

Shoe nozzles are used for a low-pressure method of applying cutting fluid to the grinding process. Shoe nozzle is the best method for applying the cutting fluid to the wheel periphery. The system works by the fluid entering a manifold and then propelled to the wheel speed in the shoe and carried into the cutting arc. One of the major reasons of using shoe nozzles is very effective and able to maximize the amount of cutting fluid passing through the grinding zone, the normal forces, temperatures and friction will likely to be reduced; this result has been confirmed by Klocke *et al*, (2000). Other way of using shoe nozzle is that it acts as an air scraper that directs the layer of turbulent air following the wheel's periphery, away from the grinding wheel Gviniashvili, (2003). But in this process an additional spindle power is required to accelerate the fluid up to the wheel speed.

### 3.8.3 Nozzles for High-Speed Grinding

The main key factor is to direct the cutting fluid to the optimal position to accomplish maximum fluid flow penetration into the grinding interface. The pressure energy of the fluid upstream of the nozzle is converted partly into kinetic energy and partly into heat energy within nozzle. Delivery of cutting fluid jet nozzle have two advantages first, the fluid can be delivered with enough high velocity to penetrate the boundary layer of air, and second, if applied at very high velocity, it may be used to clean the wheel mechanically by removing loose metal from the pores (Marinescu *et al*, 2004). However laminar flow nozzles have the benefit that the jet stream maintains the coherency for a longer length which means that the turbulent nozzles must be positioned as close to the grinding contacts as possible. For Reynolds numbers of less than 2,000, laminar flow is produced; implying lower jet velocities compared with peripheral wheel velocity. The Reynolds number ( $Re$ ) is given by:

$$Re = \frac{\rho V_{jet} d_{jet}}{\eta} \quad (3.1)$$

Where ' $\rho$ ' is the density of the fluid, ' $V_{jet}$ ' is the velocity of the jet, ' $d_{jet}$ ' is the diameter of the jet and ' $\eta$ ' is the viscosity of the fluid. For an example to match a peripheral speed of 100 m/s with a 1mm nozzle, using water, the Reynolds number is expressed as:

$$R_e = \frac{1,000 \times 100 \times 0.001}{0.001} = 100,000 \quad (3.2)$$

In this case, it is clear to understand that the nozzle must be designed using turbulent flow equations. A turbulent nozzle is an orifice of short length (L) to diameter ratio (d), preferably less than 0.25 shown in Fig.3.7 (a). The ideal designs for a turbulent nozzle are a smooth convergent nozzle with a smooth orifice. Another design uses a concave convergent section with a convex convergent exit. The smooth chamfer or smooth flat face avoids jet stream interference (Rowe *et al* 2004).

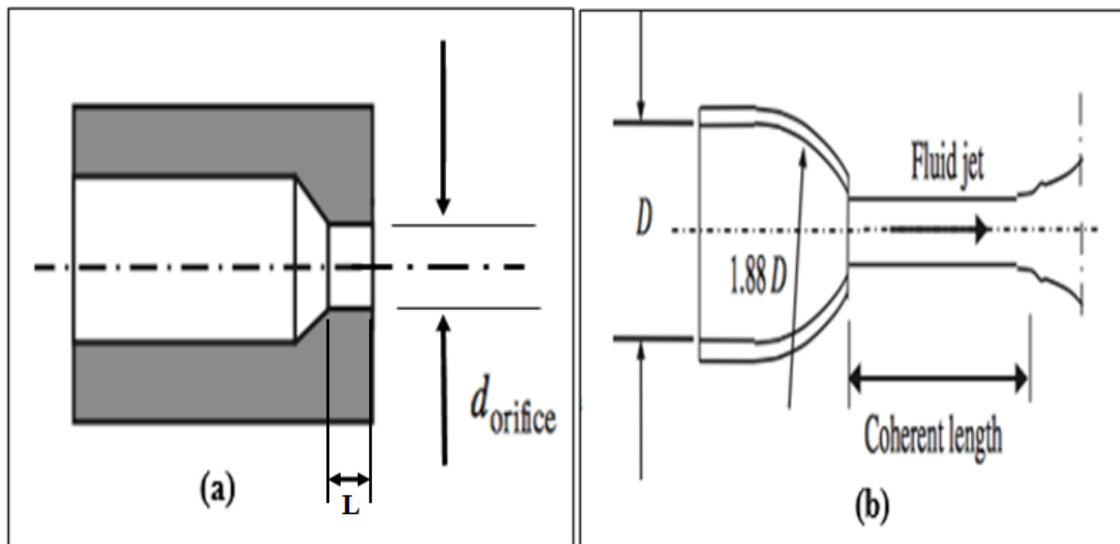


**Figure 3.7: (a) Simple Orifice; (b) Webster Orifice Nozzle**

(Marinescu *et al*, 2004).

Fig 3.7 (a) The simple orifice nozzle has a small length to diameter ratio and produces turbulent flow with vena contracta in the jet stream close to the exit. Fig 3.7 (b) A Webster nozzles with convergent internal sections that smooth flow through the orifice

and gives a longer coherent length Equations that aimed for this type of nozzle design are:

$$P_p = \frac{l \times V^2 \text{ Orifice}}{2 C_v^2} \quad (3.3)$$

Where  $P_p$  is a pumped pressure available at nozzle inlet and  $C_v$  is a velocity coefficient (typically  $0.95 < C_v < 0.98$ ).

The flow rate  $Q_f$  is given as:

$$Q_f = C_a \frac{\pi \times d_{\text{orifice}}^2 \times V_{\text{orifice}}}{4} \quad (3.4)$$

Where  $C_a$  is a contraction coefficient (typically 0.63)

Furthermore, the flow rate expands to:

$$Q_f = C_d \frac{\pi \times d_{\text{orifice}}^2}{4} \sqrt{2 \frac{P_p}{l}} \quad (3.5)$$

Where  $C_d = \text{Orifice discharge coefficient} = C_a \times C_v$ .

$C_d$  varies with Re, typically  $0.3 < C_d < 0.56$  for  $\text{Re} = 10^2$  and  $\text{Re} = 10^6$  respectively.

For wider grinding contacts instead of orifice nozzle the slot nozzle Fig.3.8 (b) is used. As of slot nozzle allows a coolant flow in the form of flat smooth jet in to the grinding contact (Marinescu *et al*, 2004).

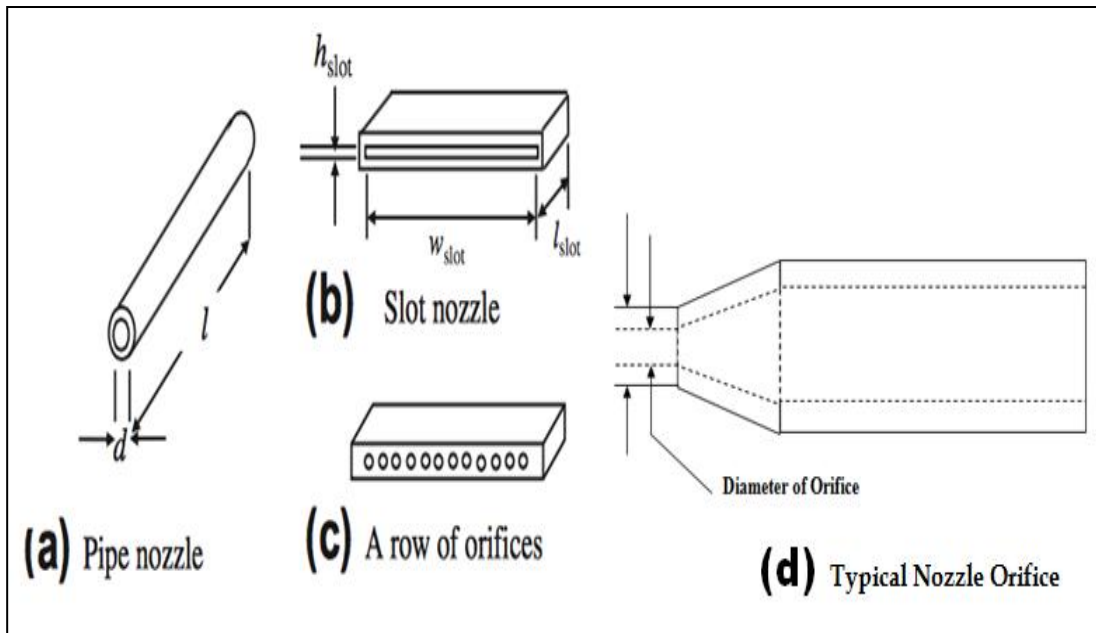


**Figure 3.8: Typical Exits of the Nozzle Chamber**

(Marinescu *et al*, 2004)

Based on slot nozzles there are three principle key points:

- Due to narrow slot thickness and length of pre-slot chamber achieves a laminar flow with high flow rates without much difficulty.
- Easy to design for laminar or turbulent flows.
- A large chamber within the supply pipe and the slot, which allows the flow to get smooth path.

Equations aimed for this type of nozzle design are:

$$R_e = \frac{\rho h_{slot} V_{slot}}{\eta} \quad (3.6)$$

$$P_p = \frac{12\eta l_{slot} V_{slot}}{h_{slot}^2} + \rho V_{slot}^2 \quad (3.7)$$

Where; ' $P_p$ ' is pumped pressure available at nozzle inlet.

The flow rate is given by:

$$Q_f = V_{slot} h_{slot} w_{slot} \quad (3.8)$$

In his research, Rowe (2001) exposed the three significant design considerations based on geometrical shapes of the slot nozzles to obtain an optimal fluid flow:

- Width of slot should be at least 20 times the height for laminar flow.
- Length of slot should be as short as possible for turbulent flow.
- Smooth concave converging section, as in orifice case, gives turbulent flow.

Webster, Cui and Mindek (1995) carried out research into the effects of coherent jet and dispersed jet coolant fluid at the exit of the nozzle. They concluded by using the measurement system of grinding temperature that, the temperature was minimised with the coherent jet nozzle in contrast to the dispersed nozzle jet.

#### 3.8.4 Coherent Jet Nozzle

Many researchers investigated into finding the most suitable coherent jet nozzles, which produces a jet in a desirable way to maintain its shape over a given distance. However, in the grinding environment, until the Research work of Webster, Cui and Mindek (1995) there is little or no useful effort on coherent jets. To reduce the temperature in the grinding contact the focus was to supply the maximum amount of fluid into that area, thus supply seems to be reasonable to assume through the use of coherent jet will be more convenient than applying it with a non-coherent jet supplied from a conventional nozzle. One useful advantage of coherent jet is that firing the coolant from a distance allows for placement of the nozzle at a longer distance from the grinding area to reducing the amount of equipment in closed complex workpieces.

### 3.9 Position of Grinding Fluid Nozzles

The positioning of nozzle plays significant role in grinding process to improve the coolant delivery into the grinding contact zone. The grinding wheel drags the fluid and draws it into the contact arc area where it is necessary. The common approach of nozzle position for coolant delivery is tangential to the grinding wheel. Fig.3.9 illustrates that the tangential supply of fluid flow takes and accelerate the coolant in a straight line toward the contact zone. The work of Ebbrell *et al* (2000) noticed that the coolant delivery via a tangential jet, tend to increase the side leakage. By raising the nozzle slightly (12 mm from the horizontal), reduce the side leakage as negligible quantity.

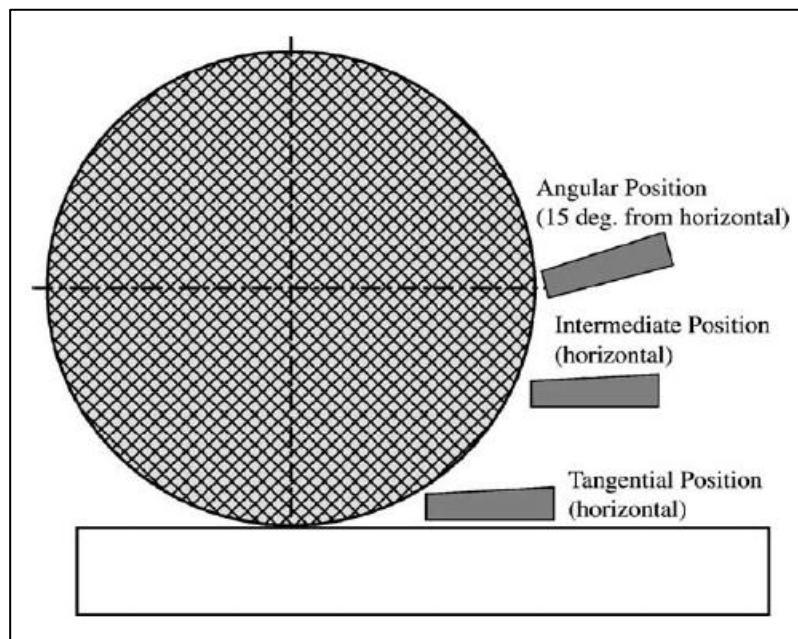


**Figure 3.9: Positioning of Fluid Supply tangentially to the Wheel**

(Ebbrell, 2000)

Campbell (1995) found, for example, nozzle is positioned with a combined of high nozzle velocity and small angle, relatively above the workpiece, deflect the coolant off the wheel and away from the grinding contact area. He also concluded that, it is not easy to maintain or develop the highly coherent jet, that consist of: allowing for good

conditions, symmetry, entry length, smooth geometry and that matches the jet speed to the grinding wheel speed as described by Webster *et al* (1995).

It is necessary to aim the correct possible angle, where it can be achieving the best grinding performance through cooling, lubrication and cleaning. Campbell (1995) ran an experiment to find the correct nozzle angle using a straight oil coolant and a rectangular cross-section coolant nozzle. In distinct intervals increments of 5°, Campbell observed the variations in primary nozzle angle between 5° and 30°. By measuring the hydrodynamic pressures with the use of pressure sensors, finally he found that the best nozzle angle of considering all conditions was 5° from the horizontal.

### 3.10 Useful Flow

The many researches in the past justify the term in a particular need for a parameter such as 'Useful Flow'. Brinksmeier *et al*, (1999) stated that "Further investigations in the fields of fluid dynamics processes in supply nozzles and in the grinding zone are the key to optimisation of cooling and lubrication during grinding". From this study, many researches now adopt the term 'useful flow'. Chang, (1994); Rowe, (2004) and Gviniashvili, (2005) all investigated into this 'useful flow' and came up their own work. Morgan *et al*, (2008) investigated the quantity of fluid required for grinding process and method of fluid application they suggested that supply flow rate needs four times the achievable 'useful' flow rate. Improved system design allows 'actual' useful flow rate to approach 'achievable' useful flow rate and is dependent on wheel porosity and wheel speed whereas actual useful flow rate depends on nozzle position, design, flow rate and velocity.

Jackson *et al* (2005), work focuses on the measurable for this to improving the fluid application system. Although the basis of the term of useful flow rate was exclusively on the volume of fluid flow passing through the grinding contact zone.



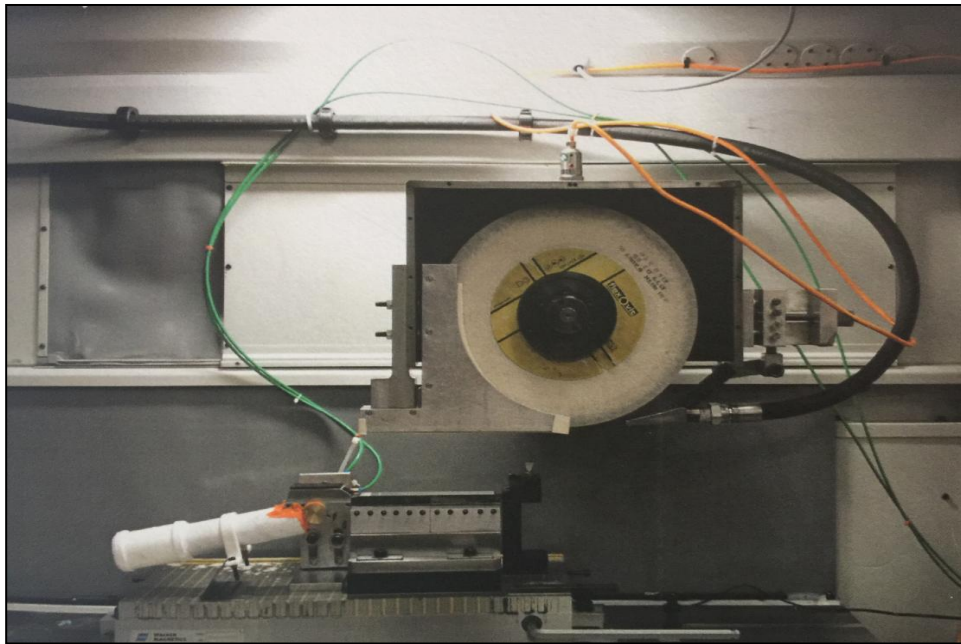


**Figure 3.10: Useful Collection System (Jones and Shipman Dominator)**

(Jackson *et al*, 2005)

On the other hand, this term generally use the amount of fluid delivered through the coolant nozzle, but it embraces the complete volume of porosity of the wheel, wheel speed, and jet velocity and nozzle position. For advance focus the term, useful flow defines as ‘optimal useful flow’ achieved by useful collection system illustrated in Fig.3.10. There are six major benefits from the understanding of optimal useful flow rate:

- Reducing the overall cost to the process in a manufacturing.
- Reducing the environmental impact of the fluid.
- Improving the efficiency of overall process performance.
- The convenient flow: The amount of coolant physically able to pass through the grinding contact zone.
- The useful flow: A combination of the convenient flow and additional fluid flow adjustments such as flow through the wheel and higher pressure in contact zone.

- The optimal useful flow: the amount of coolant that passes through the contact zone functioning as an effective lubricant and providing sufficient local cooling' this is most useful to industry and gives users to a particular minimum amount applicable (Jackson *et al*, 2005).

### 3.11 Air Barrier Effect on Grinding Wheel

Air barrier effect is a phenomenon where a boundary layer of air develops around a rotating grinding wheel see Fig.3.11 (a) Han and Li (2013) developed theoretical model of airflow field, and Ebbrell *et al* (1999) and Wu Hui (2009) carried out some experimental investigations by using Laser-Doppler-Anemometer (LDA) see Fig.3.11 (b) techniques to look the air barrier of coolant flow briefly entering in to the contact zone for advanced effects of the air barrier.

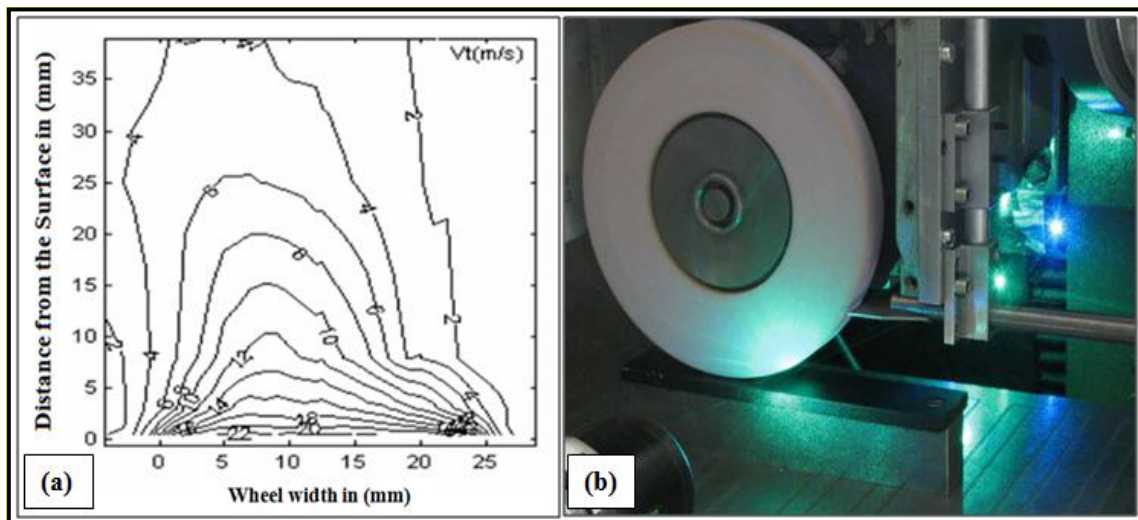


**Figure 3.11: Air Barrier Effect**

**(a) Air Tangential Velocity ( $V_t$ ) Contour (Wheel Speed = 30 m/s) (Han and Li, 2013) (b) LDA Setup with Smoke Generator (Wu, 2009)**

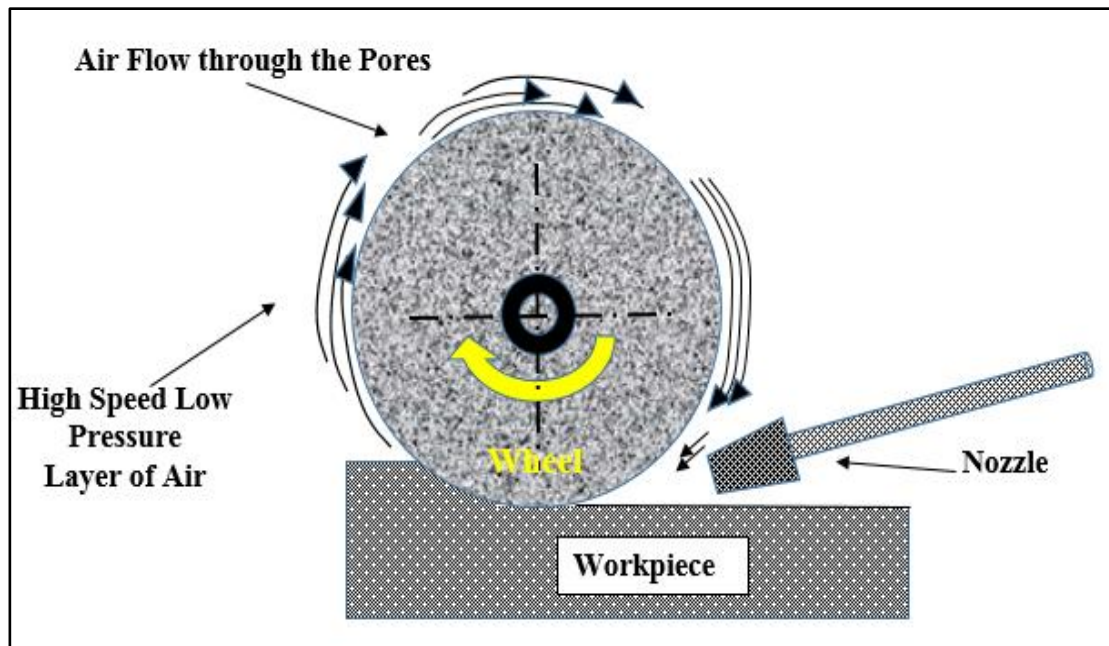


**Figure 3.12: Air Flow Through and Around a Grinding Wheel**

The need for high fluid velocities to penetrate the air boundary layer make the application of water based cutting fluids much more difficult in terms of a coherent jet. This is due to low velocity and corresponding high Reynolds number, which is greater than 2300, will result in turbulent flow. Reynolds number for a jet of fluid is derived is shown in equation (3.1).

The application of neat oil is easier owing to its higher viscosity but in the environmental concerns is leading it to be phased out in favour of water based fluids.

Research by Inasaki, (1998) stated that the air barrier influence is extremely important especially in high-speed grinding processes; the formation of air barrier is due to two major airflows around the wheel surface are:

- Air flow in the circumferential direction (dragged through with surface roughness).
- Air spouting normal to the wheel surface.

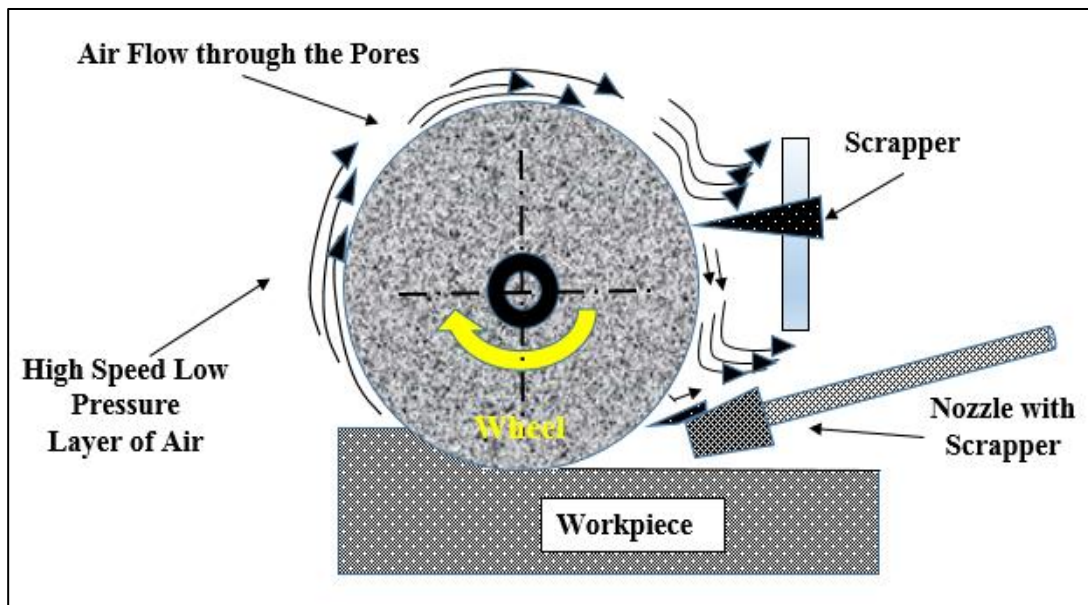


**Figure 3.13: (a) Air Flow Field Using Scrapers for Better Wetting**

Bijoy, (2011), Shibata (1982) investigated on airflow field using baffles for stiff air layer formation. For the better wetting ‘scrapers’ are useful. The significance use of the scrapers is that, they reduce the thickness of the air at the wheel circumference, effectively reducing the ‘air barrier’.

Ebbrell, (2000) was found that no cutting fluid passed beneath the grinding wheel between 0 and 80  $\mu\text{m}$  minimum gap (The wheel is 0.08 mm above the workpiece surface rotating at 33.5 m/sec). This is mainly due to a significant portion of the air boundary layer reversing as it approaches the minimum gap. The direction of this reversed air flow opposes the flow of cutting fluid and has enough momentum to hold the cutting fluid back from entering the grinding contact zone, where it can be seen the workpiece surface on the exit side of the wheel remains dry. The below Fig.3.14 illustrates that the fluid is forced to remain at the entrance zone by the boundary layer effect and coolant become ‘stagnant’ it means no coolant can penetrate effectively to cool the workpiece. When the gap is more than 80  $\mu\text{m}$ , (The wheel is 1 mm above the workpiece surface rotating at 33.5 m/sec) momentum of the reversed airflow is reduced.

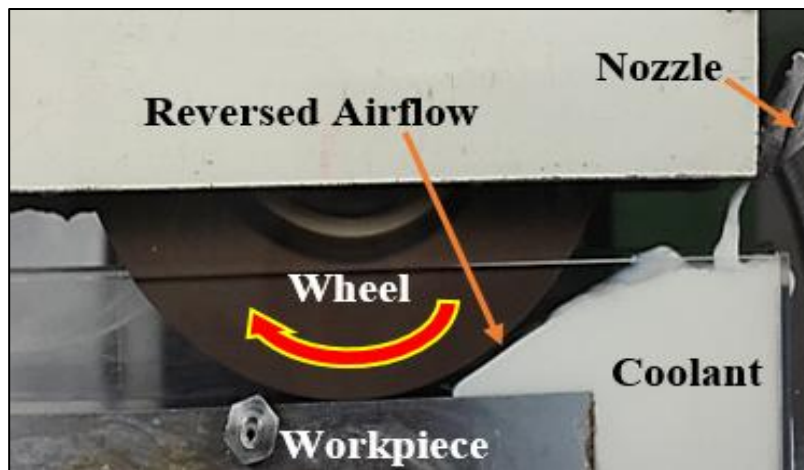


**Figure 3.14: Boundary layer effect reversed airflow opposing the fluid**

(Ebbrell, 1999)

Hence, the fluid is able to overcome the boundary layer effect and pass through the contact zone. This situation is due to the minimum gap has sufficient space to allow the air pass beneath the wheel rather than being reversed Fig.3.15 illustrates that a combination layer of air and coolant passed through the thickness between grinding wheel and workpiece.

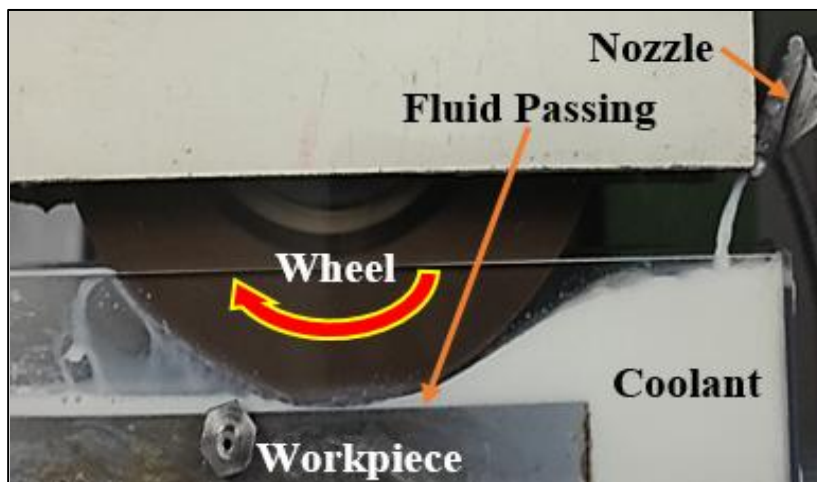


**Figure 3.15: Coolant passing through the grinding zone**

(Ebbrell, 1999)

In conclusion, lubrication efficiency and useful flow rate are dependent on the minimum gap. If the minimum gap is insufficient, then the useful flow rate is limited.

Marinescu *et al*, (2004) stated that when coolant penetrates the air barrier to remove the heat in the grinding contact area, therefore the momentum of supplied coolant must be equal or exceed the momentum of the air barrier. The rate of momentum of the fluid is given by

$$M'_f = \rho_f h_{jet} v_{jet}^2 \quad (3.9)$$

Where:  $\rho_f$  = Fluid density,  $h_{jet}$  = Jet thickness and  $v_{jet}^2$  = Jet speed

The rate of momentum of an air boundary layer of thickness  $h_{air}$ , generated by the wheel is given by

$$M'_{air} = \rho_{air} h_{air} V_s^2 \quad (3.10)$$

Where:  $\rho_{air}$  = Air density,  $h_{air}$  = Air boundary layer thickness and  $V_s^2$  = Wheel speed

These two equations allow an approximation of the minimum jet speed that will be required to penetrate the air barrier, as shown in equation (3.12). This is assuming the jet profile used will supply the entire length of the grinding zone contact inlet.

$$v_{jet} = V_s \sqrt{\frac{\rho_{air} \cdot h_{air}}{\rho_f \cdot h_{jet}}} \quad (3.11)$$

### 3.12 Summary

The main highlights of this chapter are the correct and adequate application of fluid in to the contact region. The main functions of the fluids and the types used in grinding were discussed. The main purpose of the fluid is to aid lubrication, to remove swarf and for bulk cooling. Lubrication reduces frictional forces and subsequently reduces abrasive wear and the generation of thermal heat, leading to improved surface quality and productivity. The life of the grinding wheel is also very important; the porosity of the wheel serves as the transportation of the fluid from entrance zone into the grinding zone. The key point of this chapter is the nozzle jet must flush out chips or transport of the debris away from the abrasive process and the position of nozzle jet to the contact region.

Another issue is the Air barrier effect is a phenomenon where a boundary layer of air develops around a rotating grinding wheel which obstructs the nozzle jet into the contact region. To overcome these problems the main objective of this project is to design high fluid jet, which is needed to penetrate into the air boundary layer. The other key factor is to direct the cutting fluid to the optimal position to accomplish maximum fluid flow penetration into the grinding interface for sufficient cooling.

## **Chapter-4**

# **MQL in Grinding Applications**

## Chapter 4 MQL in Grinding Applications

### 4.1 Introduction

In metal cutting industries, the use of coolants-lubricants plays a significant role in machining process. However, due to environmental and ecological reasons the cutting fluids has become more problematic in terms of generating both high consumption of coolants and discard costs. But the use of cutting fluids generally causes economy of tools and it becomes easier to keep high precision tolerances and to maintain workpiece surface properties without damages. A special attention and stricter laws is taken under the pressure of environmental organizations for industrial waste and pollution aiming to protect the environment. Driven by these laws research centres, universities as well as industries have been led to research alternative production process to reduce or even avoid the production of environmentally aggressive remains. Some of these alternatives are dry machining and machining with minimum quantity lubrication (MQL) method. The efficient use of coolant can be an effective cost saving tool as well as being environmentally responsible (Silva et al, 2005).

The term ‘MQL’ Minimum Quantity Lubrication refers to the use of a precision dispenser to supply in a small amount of fluid to the cutting interface in the form of spray. MQL has been widely used in industrial manufacturing area and studied in many machining processes such as drilling, milling and sawing. However, MQL in grinding is still a relatively new research area, and only a few researchers have studied on grinding with MQL. With a proper selection of the MQL system, nozzle device to cover the wheel width, fluid type, nozzle position and cutting parameters, it is possible to obtain MQL machining performances similar to flood lubrication, in terms of lubricity, tool life, and high surface finish. This MQL application in grinding process can drastically reduces large amounts of flood in machining industries.



## 4.2 Background to MQL

Minimum quantity lubrication ‘MQL’ is also known as ‘Dry Lubrication’ process which, uses a minute amount of fluid mixed with compressed air and delivered in the form of pressurised mist into the cutting interface. Typically, MQL uses within the range of 10-500 ml/hour which, is about three to four orders of magnitude lower than the amount of commonly used in a flood cooling condition. The air pressure supplied to an MQL system has a range of 0.5 to 10 Bars. The air and oil supplied to the grinding zone provides lubrication, thus reduces high frictional heat between the wheel and workpiece. The evaporation of lubricant consumes heat energy and also contributes to cool the workpiece. In machining process used cutting fluids are not safe for the environment as they contain some amount of processed fine metal particles (swarfs) and facilitate the growth of bacteria, also contain additives that are dangerous when they contact with water (Brinksmeier, 1999; Silva et al, 2005).

By considering the above issues, the minimum quantity lubrication and dry lubrication methods are best alternatives, which provide a large reduction in cutting fluids used in grinding applications. The works of some the research in MQL process is given below.

Boubekri, (2012) reviewed the MQL technique for various operations for environmentally friendly and discussed about health concern and issues. To optimize the MQL nozzle Peter, (2008); Theobald, (1980) investigated mist distribution, measurement and size of droplets after spraying from the MQL nozzle on polished silicon wafer with the help of confocal laser scanning microscopy and image processing techniques. Emami *et al*, (2013) demonstrated a theoretical and experimental investigation on the spray atomization and delivery parameters in grinding of  $AL_2O_3$  engineering ceramics. Also he studied liquid droplet size, liquid droplet velocity, nozzle angle, nozzle distance, liquid flowrate and gas flowrate. The results confirmed that optimal spray delivery can reduce the grinding forces and surface roughness.

Rabiei *et al*, (2014) studied the effect of mechanical properties of steels, especially



hardness and flow properties on performance of MQL technique. Two soft and ductile steels (CK45 and S305) and two hard and brittle steels (HSS and 100Cr6) have been used. Three coolant lubricant environments including dry, conventional and MQL fluid technique have been investigated. The main results obtained are MQL technique not only reduce amount of metal cutting fluids but also reduces friction coefficient than conventional fluid. It is mainly due to efficient penetration of oil mist into contact zone. Efficient penetration of lubricant made durable tribo-film with lower shearing strength that leads to better cutting conditions. MQL technique in comparison to fluid cooling can considerably reduce tangential grinding forces, which leads to lower the power.

Yumusak, (2012) worked on the development of an efficient and reliable rocket nozzles design tool and methods depending on the accuracy of the fluid flow models used. To solve the problem of large amount of coolant disposal and to develop a novel method of lubrication of the grinding process Babic *et al*, (2005) used an air jet injection system to create a mist of air and water as a coolant fluid, thus removing ecological hazards. The work of Tawakoli, (2010) examined the effects of MQL parameters by conducting experiments under different MQL conditions in order to determine the process performance in terms of surface roughness, grinding forces, nozzle position and distance from the wheel to the workpiece. Barczak *et al*, (2010) determined the process performance and effectiveness of the MQL method on fine cut plane surface grinding. His work also presents a comparative study of three cooling methods with conventional flood delivery, dry grinding and grinding MQL.

The principle behind the generation of oil mist is well known from engineering principles utilizing the venture effect via supply of high air pressure to create an oil mist that will stick to the targeted area. To compare MQL with dry machining, flood coolant or air cooling, it is necessary to study a number of factors including cutting force on the tool, tool wear, temperature and surface finish. Based on field case studies using end milling, kuroda, (2013) was able to compared cutting forces between the MQL and flood coolant processes.

According to Najiha (2012) work, lubrication and cooling is provided to improve the final quality of the work piece, his study analyses the behaviour of a recently proposed optimization method, which consists of adding water with minimum quantity lubricant (MQL). Rafael, (2013) conducted three different proportions tested in this study with 1/1, 1/3 and 1/5 parts of oil per parts of water and the following outputs variables were evaluated that is surface roughness, roundness errors, grinding power and diametrical wheel wear.

Alves, (2011) worked on analysis and influence of minimum quantity lubrication (MQL) to optimize using different cutting fluid volumes and flow rates on the surface quality and integrity of hardened steel work pieces. The optimized method applies the cutting fluid directly on the cutting area, at high outlet speeds. This optimization generates less fluid jet dispersion in the cutting zone and increases the lubricating and cooling capacity of the fluids, easing the removal of chips.

Tasdelen, (2008) compared dry cutting in terms of tool-chip contact and chip morphology and examined them with scanning electron microscopy (SEM), the MQL and compressed air lowers the contact length compared to dry cutting at short and longer engage times. Gviniashvili, (2003) used wheel, jet velocity and power required for fluid acceleration to determine a suitable fluid value of nozzle outlet to achieve a required fluid film thickness in the grinding zone.

Itoigwa *et al*, (2005) investigated the effects and mechanisms in MQL, and MQL with water in detail by using intermittent turning process of aluminium silicon alloy to elucidate boundary film behaviour on the rake face. In order to obtain good results two types of lubricants considered such as synthetic ester and chilling effect to sustain strength of the boundary film. MQL with rapeseed oil has only small lubricating effect and in light loaded machining conditions and boundary film developed with rapeseed oil is not too strong. MQL with only synthetic ester without water showed lubrication effect but too damage and material pick-up onto the tool surface cannot be suppressed. MQL with water droplets gave good lubrication performance using synthetic ester.



Rahim et al, (2015) attempted to show experimental results of using MQL based synthetic ester as the cutting fluid. Synthetic ester showed more efficient for the machining process as it reduced cutting temperature, cutting force, tool-chip contact length and chip thickness.

Kamata and Obikawa (2007) investigated high speed turning of Inconel-718, with three different types of coated carbide tools using MQL technique and made some comparisons with dry, wet and MQL techniques with respect to tool life and surface finish. The surface finish and tool life attained using MQL was found to be better performance than that in the wet and the dry machining for different coated cutting tools.

The goal is to create a bridge between the specialist area of absolute minimal fluid application and the common industrial approach of ‘more is better’. This should allow some of the benefits of MQL to be applied in more generalized manner. In order to achieve this kind of advance technique the entire grinding process needs to be considered. The research work of Kedare, (2014) was performed the end milling under MQL condition (900 ml/hour) and compared with conventional flooded lubrication (2 lit/min). The comparative effectiveness investigated in terms of surface finish was found to be improved by 27%. The findings of his study showed a drastic reduction of lubricant, reducing the cutting temperature and improved cooling effect, so MQL is considered to be an environmentally compatible lubrication technique. Hadad, (2012) investigated the temperature and energy partition in grinding using MQL technique with  $Al_2O_3$  and CBN wheels by using a thermocouple during grinding in dry, MQL. Dhar *et al*, (2007) investigated turning of AISI 1040 steel and found that the use of MQL reduced the friction at tool-chip interface and deterioration of effective rake angle by BUE formation and wear at the cutting edge. They also recorded reduced auxiliary flank wear as compared to dry turning.

Park *et al*, (2010); Peter, (2008) stated that better understanding in the application of MQL or near dry machining (NDM) is needed for its effective use in practical industrial

applications. In his experiment the combination of confocal laser scanning microscopy (CLSM) and image processing techniques including wavelet transform were used to characterize the droplet sizes and the droplet distribution after MQL oil sprayed onto a polished silicon wafer. Analysis on measuring the volume of each droplet and droplet estimation equation was introduced for extremely small droplets which is difficult to measure. The droplet distribution, which associated with the wetting area by lubricant to cover workpiece area and tool surface for better performance, also can affect the cutting performance.

### 4.3 Cost Benefits of ‘MQL’ Application

Minimum quantity lubrication (MQL) is a modern technique introduced in machining process to reduce the use of coolants in metal cutting process to obtain safe benefits. Metal working fluids cost ranges from average 7-17% of the total machining cost, while the tool cost ranges from 2% to 4%. Therefore, using MQL technique provides a remarkable reduction in the quantity of lubrication and machining costs.

However, due to economic and ecological aspects, some strong efforts are being made to minimize or eliminate the use of these metal cutting fluids in manufacturing fields. In UK (1999) a 10% of total sales of oil in only one year is nearly about (1,000,000 tonnes) was attributed to metal working fluids. The purchase, management and disposal of metal working fluids contribute approximately 15% of overall manufacturing costs. A reduction of 5% in coolants would bring nearly 7000 tonnes per one year, which would have a significant environmental impact (Mortimer, 2005).

The Fig.4.1 illustrates the production and overall cost of the automobile production in German manufacturers; the cost of process fluids is close to 1/5<sup>th</sup> of the 17% of camshaft production and it is close to same cost in UK.

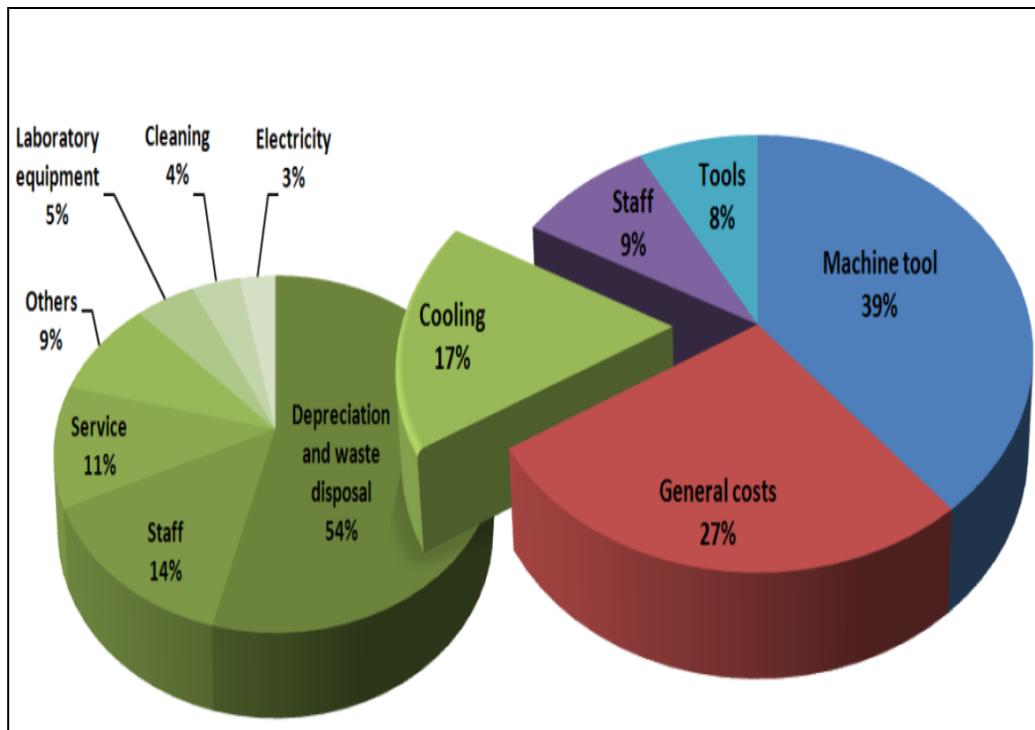


**Figure 4.1: Example of Fluid Costs in Manufacturing**

(Adapted from Brinksmeier, 1999)

By considering this, novel innovations and development activities are focussed only on cost improvement and tools not for minimising the coolants usage (Brinksmeier *et al*, 1999; Brinksmeier *et al*, 1997).

To analyse the cost benefits of MQL, Kuroda, (2013) studied different categories of costs associated with the running of conventional machine tool employing flood coolant in production environment. Further investigation by kuroda reveals that the cost implications of coolant in overall product costs associated with machining operations that indicates an average of 16% product cost from machining operations could be attributed to coolant systems and cutting tools may contribute 4%. It can be concluded that any improvement in consumption costs for machining operations, either in power, tooling or maintenance downtime, has an implication for not only revenue costs but also direct product costs.

#### 4.4 Working Principle of MQL System

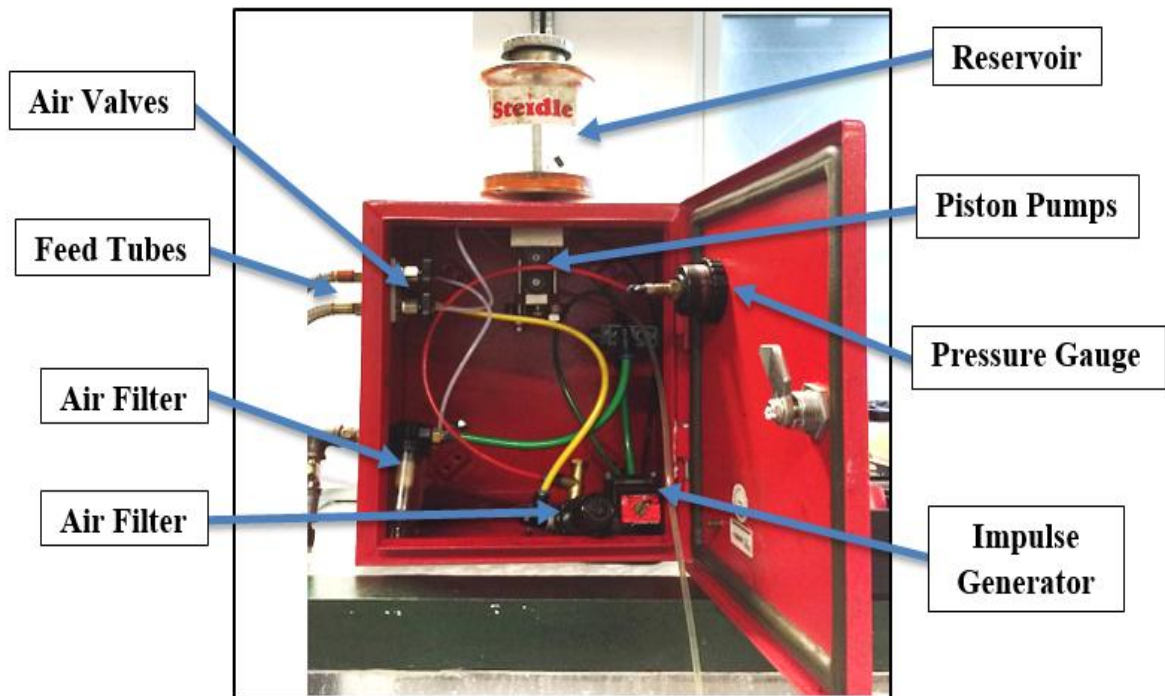


**Figure 4.2: Steidle Lubrimat L-50 MQL System**

Minimum Quantity Lubrication (MQL) is also known as “Micro Lubrication” and near “Dry Lubrication” method requires small amount of fluid which can deliver in form of atomized compressed air flow to the cutting interface. The MQL system used for this study was fabricated by a German company ‘Steidle Lubrimat L50’ lubricating systems for machining illustrated in above Fig.4.2. This model was suited for the test requirement and the purpose of this research work. The working principle of minimum quantity lubrication is combination of two inputs i.e. air and oil.

An impulse generator is used to fine-metered the amount of fluid carried at a given time. The impulse generator operates in the frequency range of 0.1 to 4 Hz. A relatively large reservoir provides sufficient oil pushes into the internal feed tubes with the help of fine-tune pneumatically operated piston pumps and a separately supplied adjustable compressed air flow (Pressure range of 0-10 Bars) splits the media at the nozzle tip

dispense in the form of finely atomized spray to the cutting interface. The reservoir provides continuous working of the system for up to 8 hours, when one nozzle is used and it is easily upgradable with a larger reservoir. The air pressure supplied to the MQL system which consist of a pressure regulator and air filter. The quantities of the air and oil are very small typically ranges from 50-150 ml/hour (0.83 -2.5 ml/min) compared to wet grinding the fluid quantities are typically 4000-26000 ml/min. The application of MQL is efficient in some forms of machining these include drilling, milling and turning and also sufficiently flexible in grinding as well.

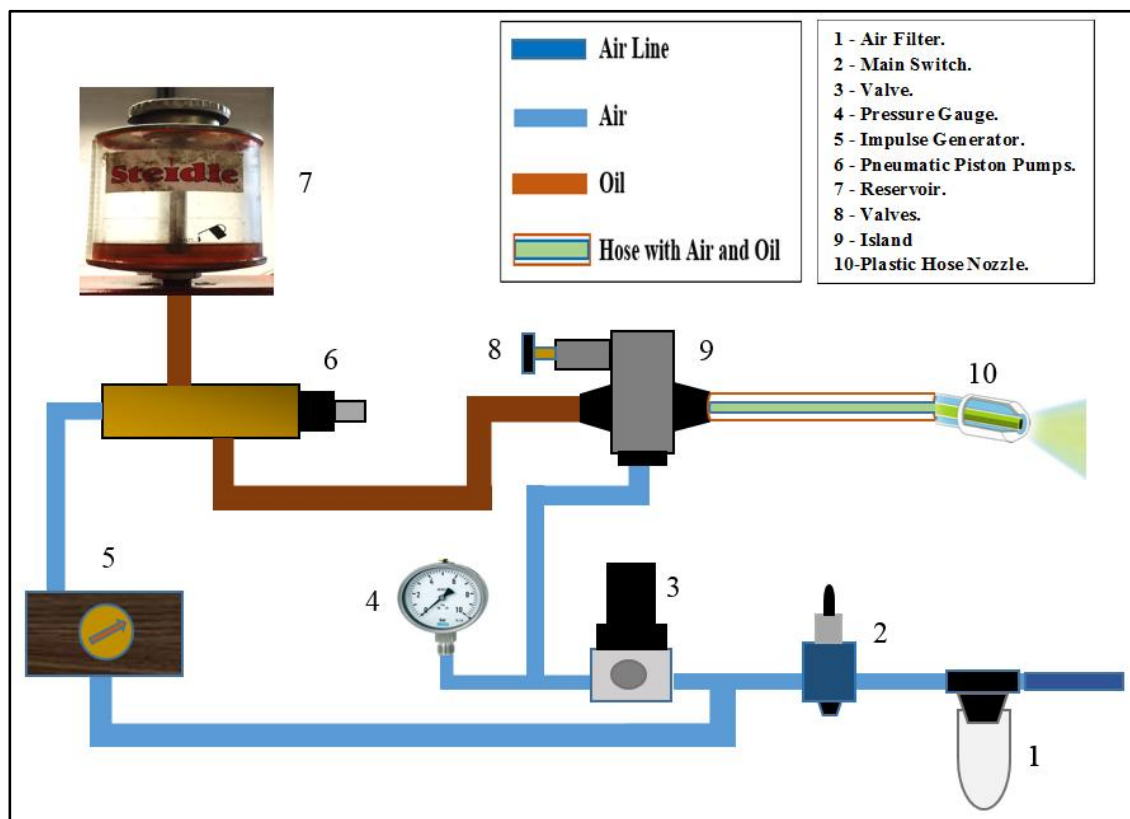


**Figure 4.3: Principle of Operation of Lubrimat L-50 MQL System**

The above Fig.4.3 illustrates a typical (Steidle-Lubrimat L-50 model) MQL system flow pattern configuration. Firstly, the air is supplied to the air filter indicated by '1'; it filters any remaining water droplets and contamination carried within the air line. The main switch '2', cuts off the air access to pneumatic piston pump '6' and impulse generator

'5'. If the switch is in 'ON' position, the air flows in two branches one is to island and the other one is to impulse generator. The first branch supplies air to the island '9'. The pressure from this branch is adjusted with pressure valve '3'. Readings of air pressure can be made using an analogue pressure gauge (pressure gauge from 0-10 bar range) '4' fixed on the door of the MQL housing. The island is equipped with two valves '8' that can be changed manually the pressure of the nozzle.

The other branch of air is supplied to the impulse generator, that may generate an air delay from 0.25 s to 10.00 s. the air coming from the impulse generator goes to the pump and allows it to pump oil from reservoir '7'. The oil gets in to the piston pump by gravitation, and where it pushes the exact amount of oil is delivered to infeed tubes. The pump has a special feature that allows changing of the piston initial position (precise metered adjustment), and thus the volume of oil pumped. When the oil enters into the piston pump (pneumatically operated) where it pushes exact amount of oil that transported into internal feed-tubes (concentric pipes) and the supplied air splits the media at the tip of the nozzle '10', which delivers in the form of atomized air spray.

#### **4.5 Classification of MQL system**

The application of Minimum quantity lubrication (MQL) depends on the type of process work and operation. Due to this, the minimum quantity lubrication is classified into three types of mixing methods (1) Mixing inside the nozzle (Internal) and (2) Mixing outside the nozzle (External) and the third one is lubrication through spraying system (based on excessive pressure system). But the commonly used methods are internal and external. These systems are based upon the principle of total loss lubrication with dry chips and dry workpiece (Brinksmeier, 1999). Some MQL systems have a special mixing chamber prior delivery to the nozzle. Other systems do not have mixing chamber but air and oil are mixed in the nozzle. The latter systems seem to be more simply in use. During the mixing process the oil is pulverised by the pressurised air, thus the mixture is in a form of micro droplets of oil suspended in the transporting flow of air.



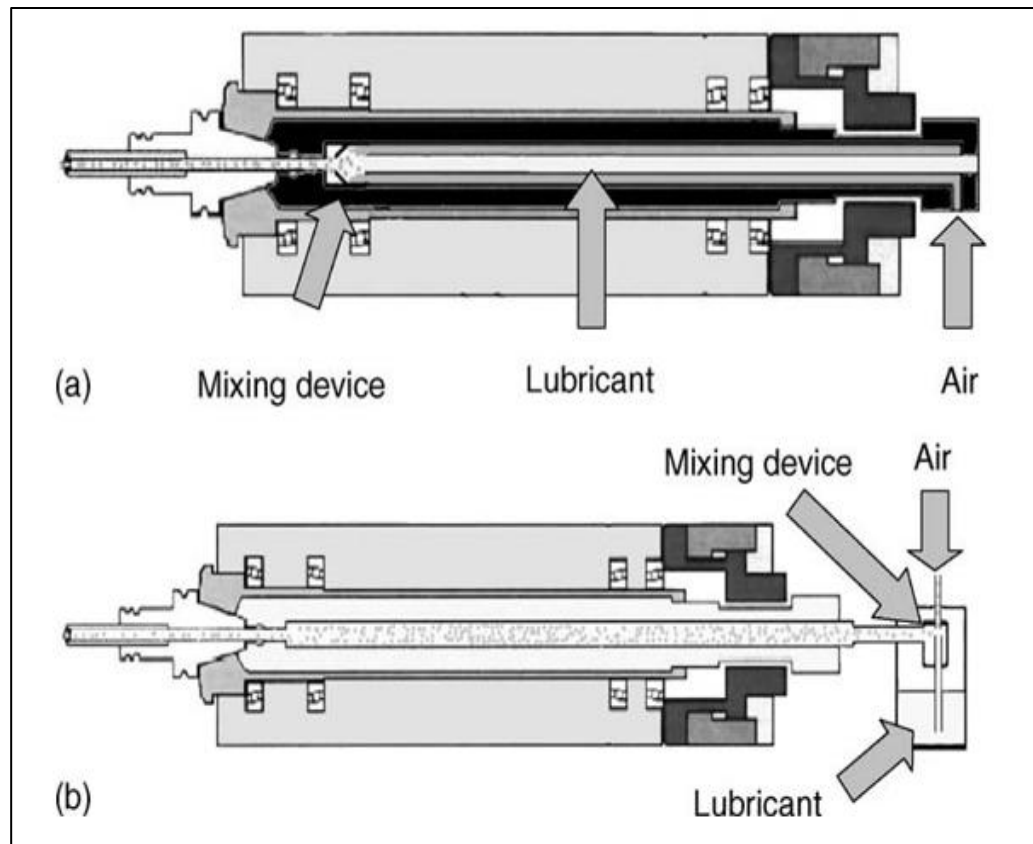


**Figure 4.4: MQL Systems, (a) Internal (b) External Mixing**

(Attanasio et al, 2005)

#### 4.5.1 Internal method

Using the mixing inside the nozzle equipment, pressurized air and lubricant are mixed into the nozzle by a mixing device, as depicted in above Fig.4.4 (a). Several advantages derive applying this method includes mist and dangerous vapours are reduced and the mixture setting is very easy to control.

#### 4.5.2 External method

In the external method the air and oil mixture is obtained in a mixing device positioned in a specific tank as illustrated in above Fig.4.4 (b). Also, in this case lubrication between workpiece and tools can be achieved (Attanasio et al, 2005).

### 4.5.3 Types of MQL Nozzles

In MQL applications there is a wide variety of nozzles exist, but the most commonly used nozzles are (a) Single or Double concentric nozzles (b) Click-fit nozzles and (c) Gas-liquid nozzles.

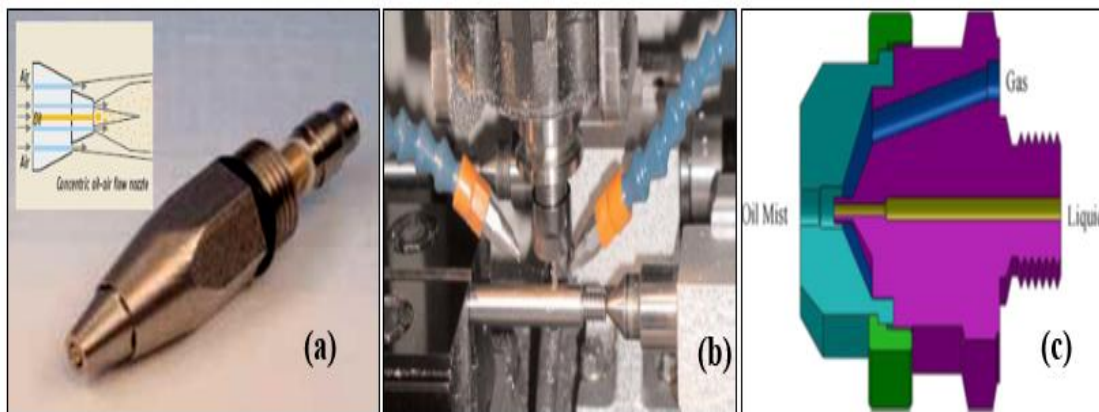


**Figure 4.5: Types of MQL Nozzles**

(SKF Vogel MQL Systems; Emami *et al*, (2013))

The above Fig.4.5 (a) depicts double concentric nozzle where oil feed tube is in centre and its surrounding dual concentric allows to cover by air supply is in inset figure. In this, nozzle oil and air is mixed outside the tip that is external mixing. The Fig.4.5 (b) is commonly used click-fit nozzles and this is more flexible and compactable in MQL applications. The disadvantage of these nozzles is will cover only small area not suitable for grinding application. Fig.4.5 (c) is a high jet spot nozzle; this nozzle can also be used as gas-liquid mixture instead of using air as secondary flow. The gas-liquid/oil is mixed inside the nozzles near liquid tip.

#### *Special purpose MQL Nozzle*

The functions and supply methods of the cooling liquid into the grinding contact zone was emerged in many ways and in this a new system for centrifugal supply of oil mist was described and the experimental investigations conducted into the internal cylindrical grinding process which influence the life of the wheel, machined surface

roughness, grinding power and temperature in the machining zone were analysed. The aim of the experiment was to determine the influence of the application of the centrifugal system of oil mist provision into the machining zone with air pressure of 8.0 bars and flow rate of 80 ml/h and oil used as neat mineral oil VG-48. In comparison with flood cooling this novel system has doubled the wheel lifespan, wheel wear and enabling the slightly reduced grinding power and machined surface. This novel coolant supply system method caused an increase in the workpiece temperature, compared to the flood cooling. The minimum quantity lubrication (MQL) which has become increasingly popular, it allows for a considerable reduction in expenditure while maintaining high efficiency of the lubricating function compared to the flood cooling (Nadolny, 2014).

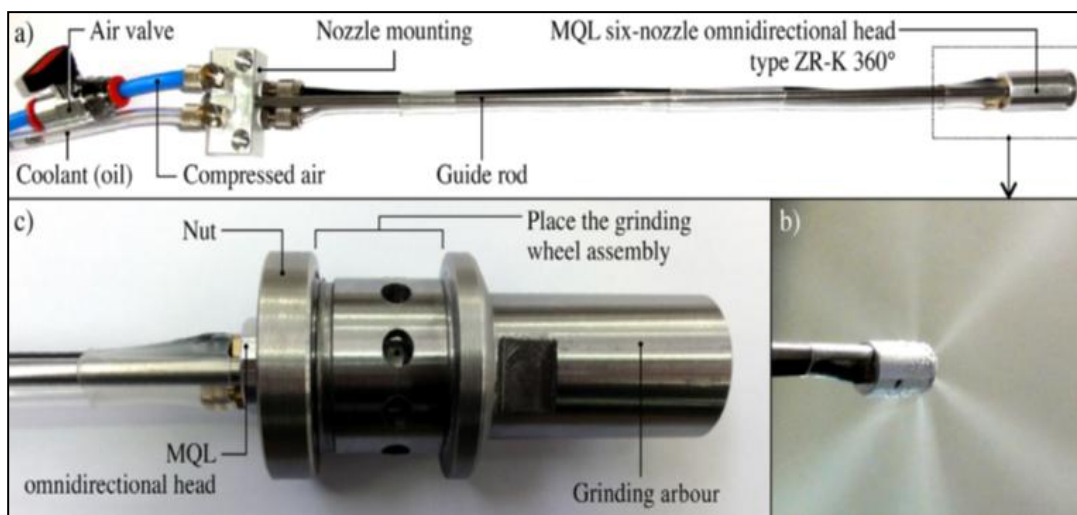


**Figure 4.6: System of centrifugal oil mist supply into a small-sized grinding wheel**

(a) Components of standard MQL set equipped with unidirectional head type ZR-K 360°; (b) way of oil mist supply using six-nozzle head; (c) view of MQL head placed inside the grinding arbor (Nadolny, 2014).

The provision of the oil mist in a centrifugal manner, from the inside of a harbour into the grinding wheel using six-nozzle unidirectional head ZR-K 360° was modified to allow and move along with the feed motion of the wheel.

#### 4.6 Lubricants Used in MQL

The fluids used in MQL process exists various types of oils, commonly used lubricants are vegetable oils, rapeseed oil, petroleum-based oils. In the conventional grinding fluids used to reduce and dissipate heat from the contact zone and transports chips away from the wheel, where MQL lubricants are unable to flush out the chips as they are capable only for reducing heat by reducing friction (Weinert *et al*, 2004). Lubrication is ineffective unless lubricant actually enters in to the grinding contact zone. Even if minute quantities of fluid entering in to the contact zone can be beneficial to process efficiency). This has led to a trend towards MQL systems designed to reduce environmental hazards and disposal costs Barczak *et al*, (2010). For some metals like aluminium and copper they required special forms of oil due to the de-oxidation process and stains can be formed on the surface. Vegetable based oils have a better characteristic and synthetic esters provide wide range of biodegradable depending on their molecular structure of acids and alcohols. Poly esters may probably have suitable viscosities for MQL machining; several poly esters have been examined as lubricants. Based on the test reports poly esters were found to be superior to vegetable oils. In terms of secondary characteristics, biodegradable poly esters were identified as the preferred lubricant for MQL machining (Klock *et al*, 2000; Weinert *et al*, 2004).

Vegetable oils are viable alternative to petroleum-based metalworking cutting fluids. The important factors for selecting the vegetable oils as a feasible choice are:

- Molecules, being long, heavy and dipolar in nature create a dense homogeneous and strong lubricating film that gives the vegetable oil a greater capacity to absorb pressure.
- Lubricating film layer provided by vegetable oils, being intrinsically strong and lubricious, improves workpiece quality and overall process productivity reducing friction and heat generation.
- Higher boiling point and greater molecular weight of vegetable oil result in considerably less loss from vaporization and misting.

- Vegetable oils are non-toxic to the environment and biologically inert and do not produce significant organic disease and toxic effect (Khan, 2009).

Usage of vegetable oils tends to contract metallic surface of the workpiece, due to their polarity in nature the molecules align themselves thus gives superior cooling and better lubricity characteristics. For other metal machining purposes, some oils are specially suggested for these machining processes. However, there is a lack of information and knowledge regarding the specification of oils used in MQL applications. This process needs further research, and that properly chosen MQL oils may reduce environmental and health hazards and either improve or worsen machining conditions.

#### **4.7 Benefits of MQL in Grinding**

In general, the conventional fluid usage is 1-L/min of the fluid per 1 mm of wheel width. In contrast, MQL fluid consumption is typically 30-100 ml/hour, thus it is an environmentally friendly cooling method, no need for waste disposal.

- Biodegradable fluids can be used, no pollutants small.
- No unwanted thermal shock for work piece and tool.
- Safe for the operator and the machine.
- Good anticorrosion and Less Energy Consumption.
- Direct use, no need for the preparation of the coolant.
- No expensive coolant supply systems and their maintenance.
- The power consumed is very less compared to the other operations.
- Less storage place, Costs are limited, cleaner work place and no hazardous to machine environment.

#### **4.8 Lubrication Mechanism in Grinding Process**

MQL is flexible in any type of application by setting up the parameters in right way. In the case of grinding process MQL oil droplets coat the wheel surface and the grits with a thin film of oil, which is transported into the cutting or contact zone. Therefore, an intermediate layer of thin film lubricant is form between the rubbing surfaces, which reduces friction, and subsequently the cutting forces. Due to its thinness the oil coat has

low shear strength between the grains wear flat and the workpiece and this eliminates the formation of strong adhesion.

Obikawa, (2006) Concluded that transportation mechanism of the cutting fluid into cutting interface between flanks wear land and machined surface plays important role and reduces tool wears. His investigation on High-speed grooving of carbon steel was carried out under MQL, dry and wet conditions to investigate the performance of MQL using P35-coated tool.

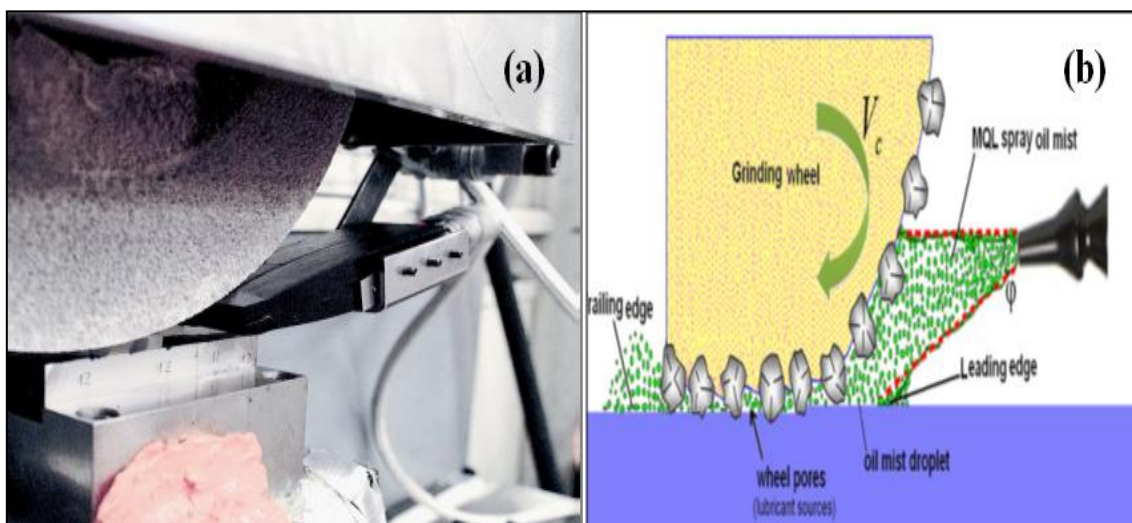


**Figure 4.7: (a) MQL System Setup (b) Lubrication Mechanism in MQL**

(Barczak *et al*, 2010) (Tawakoli, 2010)

MQL reduced both corner and flank wear more efficiently than solution type cutting fluid also reduced with increasing of air pressure drastically, oil supplied at constant of 7 ml/h. The Fig.4.7 (a) depicts an MQL system setup for grinding and (b) sketch of the lubrication mechanism in MQL, where the droplets travel together with the grits and fill the enclosed volume formed between the grits, the bond and the workpiece surface.

The elimination of strong adhesion of grits and workpiece is almost impossible in water-based coolant due to temperatures exceeding boiling point to water. In general, if the lubricant is unable to access the interface between the grain and the workpiece

surface, it is then necessary to limit the region of adhesion to reduce the friction forces exhibited at grain-workpiece boundary.

The pores on the wheel surface entrain and pump the oil mist through the grinding contact and improve further the lubrication effect. Tawakoli, (2010) stated that wheel pores act as pocket source of lubricant; therefore, oil mist requires time to penetrate these lubricant sources. The penetration time of the oil droplets into the lubricant source must be less than the travel time of the lubricant source through the contact zone. The Fig.4.7a illustrates the position of MQL nozzle close to the cutting interface tends to reduce the reversed air flow and improves better lubricity.

Attanasio *et al*, (2005) conducted an experiment based on MQL and tool life test on turning normalized 100 Cr6 steel using commercial triple coated carbide tips. The aim of his research is to determine if ‘MQL’ furnishes some advantages, in terms of tool wear reduction, in comparison with dry cutting. To obtain complete analysis of the influence of lubrication in Turning, the tool flank wear was studied under MQL and dry cutting and SEM analysis of tools was also performed, to understand the mechanism influencing the tool wear when MQL is applied. The cutting parameters includes cutting velocity, cutting feed, cutting depth, cutting length and lubrication type were taken into account and using two different cutting lengths 50 mm instead of 200 mm to evaluate the effect of MQL efficiency, and his experimental results confirmed that in turning with MQL technique could furnish advantages in terms of tool life when properly applied. (Attanasio *et al*, 2005). Klocke, (2000) considered that MQL is a flexible system for grinding and machining applications

## **4.9 Application of ‘MQL’ in Various Processes**

### **4.9.1 MQL in Milling**

In milling, general problems will occur when the work material was adhering to the cutting edges and surface roughness on the slot in up cut milling to reduce tool life. By considering the geometrical design of the cutter the increase in the number of teeth from



will result in long life too. For a good milling process, the chip size must be large which shows the maximum number of teeth (Inasaki, 2011). Lutao, (2012) conducted an experiment with different modes of MQL technique for optimal conditions in end milling of a forged steel (50 CrMnMo) with nozzle position in relation to feed direction and nozzle elevation angle.

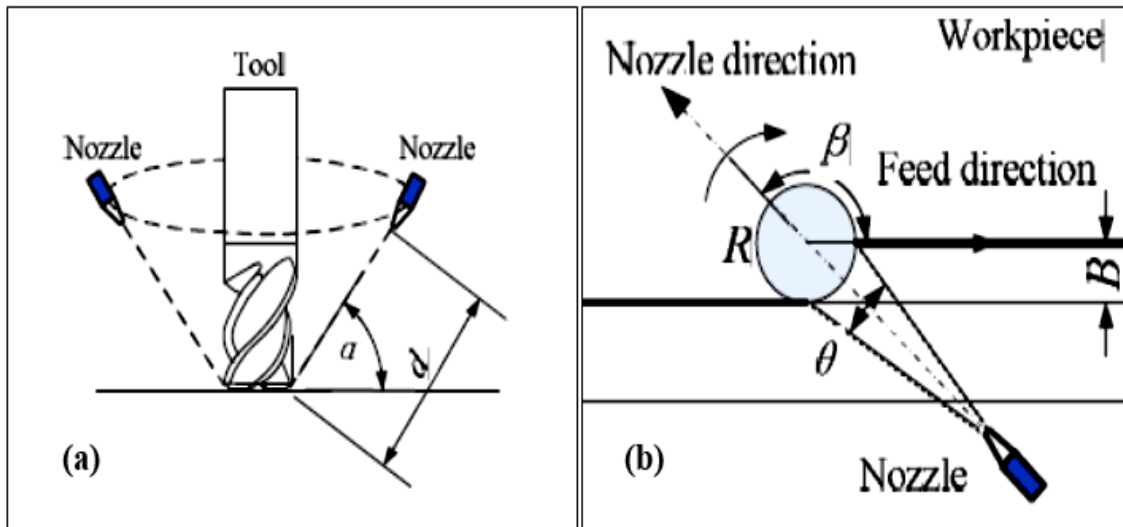


**Figure 4.8: (a) Schematic View of Nozzle Position  
(b) Nozzle position along Feed Direction for Cutting Test**

(Lutao, 2012)

The investigation results showed that the MQL technique lowers the tool wear and surface roughness values compared that of conventional flood and dry cutting conditions.

$\alpha$  = Elevation angle of nozzle

$\beta$  = Nozzle direction in relation to feed direction

$\theta$  = Spray cone angle of the nozzle

$R$  = Radius of cutting tool

$B$  = Width of cut

$d$  = Distance from the nozzle tip to the cutting zone.

The relative nozzle feed angle  $120^\circ$ , the elevation angle  $60^\circ$ , and distance from nozzle tip to cutting zone at 20 mm provides the prolonged tool life and reduced surface roughness values. Increase of oil flowrate from 43.8 ml/hour to 58.4 ml/hour leads to reduce flank wear. Higher flowrate and air pressure enables improvement in tool life and surface finish. The fact is due to the oil mists can penetrate in the inner zones of the tool edges in a very efficient way.

#### 4.9.2 MQL in Drilling

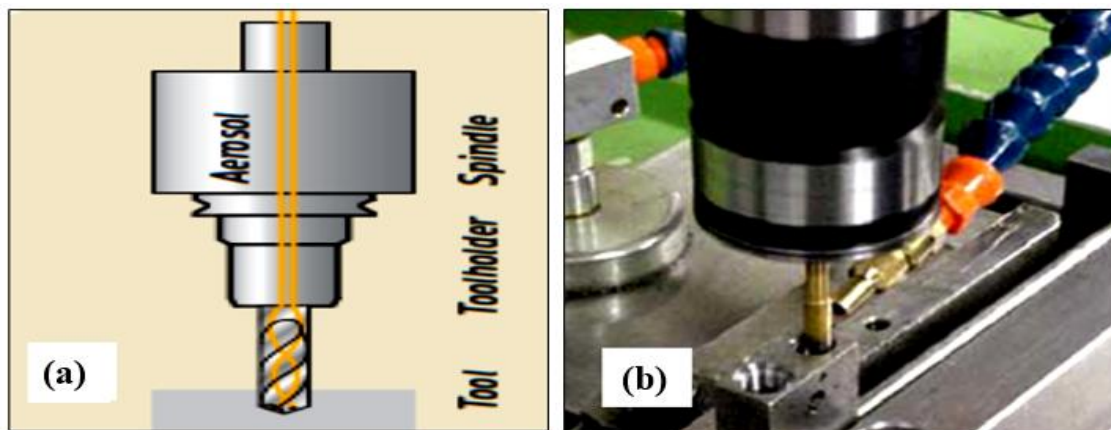


**Figure 4.9: (a) Internal; (b) External MQL in Drilling**

(SKF Vogel MQL Systems)

The MQL in drilling may be used two types of methods (a) Internal and (b) External methods presented in Fig 4.9, the difference is the air and oil mixture is transported internally to the cutting zone and the same mixture is delivered externally.

The internal delivery method is mostly considered as efficient in MQL applications dry machining including some modifications like sharp and stable cutting edges for small cutting forces which is an advanced design of cooling channels to allow a secure minimum quantity lubrication aerosol, need wide chip openings which makes sure that the chips should be removed properly, and obtain a smooth surface to reduce friction and wear of the surface.

Meena, (2011) conducted an experimental investigation on the role of MQL drilling on cutting forces, tool wear and surface roughness of newly produced ADI (Austempered Ductile Iron) at industrial speed-fed combinations by TiAlN-coated tungsten carbide tool. MQL drilling performance compared with dry and conventional drilling process under the same conditions results obtained significant reduction in tool wear, cutting forces and MQL drilling, mainly through reduction in the cutting zone temperature. Surface roughness and tool life was better than that of dry drilling and comparable to flooded drilling up to 40-holes drilled. Tool life in dry drilling of ADI is 80-holes while in MQL drilling are 110-holes using TiAlN-coated tungsten carbide tool. Le Coz *et al*, (2012) proposed a new temperature measurement technique for rotating cutting tools for aeronautic industry. Firstly, to optimise the cutting conditions during drilling of Ti6Al4V titanium alloy with MQL. Second one to test thermal behaviour of three different coated tools during dry milling of an aeronautic aluminium alloy.

#### **4.9.3 MQL in Turning**

Hadad and Sadeghi, (2013) found that the among of all three types of turning wet, dry and MQL of AISI 4140 alloy steel, MQL produced the best surface quality for the entire range of depth of cut. They also noticed that the minimum cutting force was required to perform turning operation with the MQL as compared to dry and wet turning for the entire depth of cut values. Gaitonade, (2008) aimed to determine the optimum amount of MQL and the most appropriate cutting speed and feed rate during turning of brass using K10 carbide tool. The optimization results obtained using Taguchi technique indicated that MQL of 200 ml/hour, cutting speed of 200 m/min and feed rate of 0.05 mm/rev is essential for minimization of surface roughness and specific cutting force under different conditions of MQL. Khan, (2009) used vegetable oil-based cutting fluid in MQL on turning performance of low alloy steel AISI 9310, also compared with dry and wet machining in terms of chip-tool interface temperature, chip formation mode, tool wear and surface roughness his results showed substantial reduction in tool-wear and enhanced tool life and surface finish.



The work of Rakurthy, (2013) machining experiments were carried out to understand the effects of targeted cooling for annealed AISI 1045 steel-CVD multicoated tool combination resulting in the following findings. The application of fluids upon the rake face produced lower temperatures along the cutting edge as well as lower residual stresses on the machined surface. Higher the amount of fluid applied lower the residual stresses.

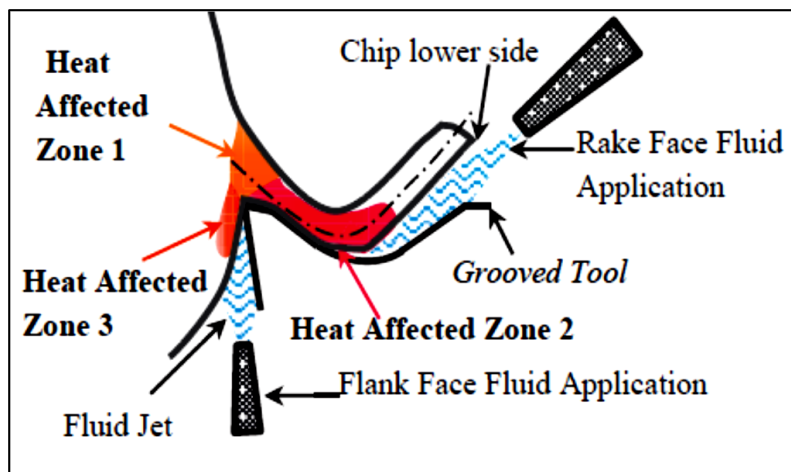


**Figure 4.10: Schematic Representation of targeted MQF application in machining**  
(Rakurthy, 2013)

The attempt is to quench the temperatures at ‘just machined subsurface’ resulted in a higher magnitude of compressive residual stresses. Targeting MQF effectively in a portioned and independent manner on the rake and flank faces improves the subsurface integrity. Thus a higher quantity fluid application on the rake face can be eliminated which can enhance sustainable manufacturing.

#### 4.10 Comparison of MQL with Conventional Coolant Systems

Comparison of MQL with either dry machining, flood coolant or air cooling it is necessary to study a number of factors including cutting force on the tool, tool wear, temperature and surface finish. Based on field case studies using end milling, Kuroda were able to compare cutting forces between the MQL and flood coolant processes.

MQL samples at varying ml/hr. delivery rates consistently reduced cutting force on the tool compared to dry machining with air-cooling only. At higher rates of 16 ml/hr. MQL was able to match the cutting force measure of flood coolant systems which was operating a much higher consumption rate of 258 ml/hr (Kuroda, 2013).

While cutting forces was comparable with flood coolant and temperature was considered within acceptable limits and stable with the MQL process, tool wears is also an important factor in the cost analysis and process stability. After 12 m of machining, flute edge quality was analysed and showed comparable and low wear conditions same as flood coolant.

Surface finish was the final element studied by Kuroda, (2013) and this, too, can be influenced by a verity of factors such as the tool itself, material, feed rates, etc. the MQL could achieve a better surface finish for turning of special materials such as titanium. A 60 mm blank was machined to three separate diameters employing flood coolant compare to three separate MQL mist pressures. The sterling results indicated that the surface finish measured in (Ra) was actually lower than the performance achieved by flood coolant (Kuroda, 2013).

#### **4.11 Utilization of MQL with Water in CBN Grinding**

When MQL with or without water is used a wheel loading grout is formed by the mixture of oil and chips, being responsible for scratching the work piece and worsening both surface roughness and roundness precision with the increase of water less grout is formed and better results can be obtained. It was observed that increasing water parts in traditional MQL improved surface roughness among all the proportion tested, 1:5 parts of oil/parts of water provided the best results, reaching values close to even lower than 0.75 mm/min feed rate conventional cooling-lubrication, with high amount of water in its composition. The traditional MQL produced worst results, a grout was formed by the mixture of machined chips and oil, and even high-velocity compressed air jets were not able to remove it properly from the cutting zone.



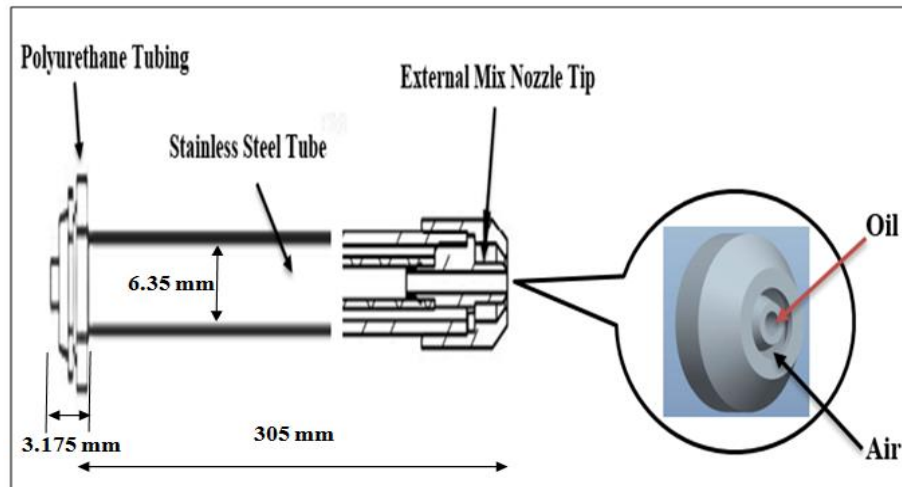
Researchers improved the traditional MQL with adding water to it, water has a higher cooling capacity than oil (two times the specific heat of pure oil), but its lubricating capacity is much lower therefore, this method presents higher cooling capacity than traditional MQL, due to adding water. The resultant water droplets sprayed are covered by a thin layer of oil which may evaporate on the work piece surface, thus promoting cooling MQL with addition of water is efficient than traditional MQL due to the improvements observed in both finishing quality and lowers tool wear. When using MQL with water, for higher additions of water about 1:5 parts of oil/parts of water showed better results (Rafael, 2013).

The MQL and compressed air lower the total natural contact length due to the cooling effect of air that results in chip up curling that decreases the contact length. For compressed air and MQL is the same for long engagement times. The oil droplets decrease the friction at sliding region, which is observed as thinner clad material at sliding region for MQL. At the very short engagement times the decrease of friction in the sliding region starts to affect the whole contact length lubrication effect overcomes the cooling effect. The amount of oil influences the contact length at very short engagements times and the chips for dry cutting are wider have side curl due to speed difference at outer and inner diameter of the work piece. A change from dry to MQL can result in benefits due to shorter contact length but a change from emulsion to MQL should be evaluated in terms of many other parameters such as tool life, surface finish, forces, etc. (Tasdelen, 2007)

#### **4.12 Investigation of Flow Behaviour in MQL for Modification of Nozzle Design**

The minimum quantity lubrication (MQL) is a sustainable manufacturing technique, which has the potential of replaced the conventional flooded lubrication methods and the dry machining. The work of Najiha, (2012) investigated the flow behaviour of lubricant and air mixture in a certain pressure at a tip of a nozzle specially designs for MQL to help design modification for future work on MQL.

The nozzle used is stainless steel of 6.35 mm diameter and 305 mm long while the polyurethane tube is 3.175 mm illustrated in below Fig.4.11 (a). Computational Fluid Dynamics and ANSYS-Fluent solver used for transient, pressure-based, three-dimensional analysis is performed with viscous, realizable model.



(a) MQL Concentric Tube Exit

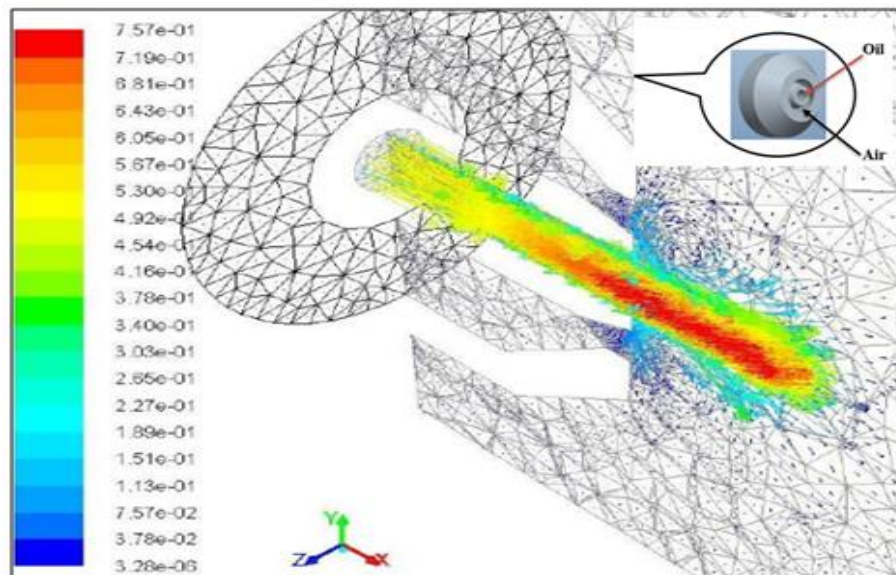


Figure 4.11: (b) Velocity Vector and Vol. Fraction Contour of Air-Fluid Mixture

(Najiha, 2012)

Mixture of compressed air and lubricant are modelled as multiphase volume of fluid, viscous, standard k- $\epsilon$  model. This model is most suitable model for fully turbulent flow. The lubricant volume flow is approximately 0.08 ml/cycle of the pump pushed through a capillary tube coaxial within another tube through which the pressurised air carries the mixture is sprayed in the form of mist to the friction zones to the desired location (Najiha, 2012).

The above figure Fig.4.11 (b) shows the sectional view of MQL nozzle and velocity vectors, contours of volume factors for the lubricant without any compressed air supply. It can be seen that the maximum velocity of the lubricant is 0.757 m/s, which is very small for carrying the lubricant to the cutting zone. Oil drops just after exiting the nozzle tip in the form of droplets; hence the compressed air is used as spraying medium. The position of the lubricant drops from the nozzle tip is plotted against the volume fraction. It can be observed that the lubricant covers only a small distance of 1.5 mm from the tip of the nozzle. The small distance between the nozzle tip and the tool-work piece interface results in an interaction with chips.

Therefore in order to make an aerosol spray, which carries the lubricant to the tool-work-piece interface, compressed air is supplied to the nozzle. The compressed air flow lubricants drop at the external of the nozzle and then velocity vector creates eddies when compressed air exists in the nozzle. The lubricant is dispersed with the compressed air become the mist after a certain distance, the lubricant is completely mixed with the air to form the spray; therefore, one phase air exists only. This shows the average velocity of air-lubricant mixture is 600 m/s, which is large enough for carrying the lubricant to the cutting zone. Oil drops mixed with the compressed air forming an aerosol spray. Path lines for the flow of lubricant drops is clearly show that the lubricant drops travel to some distance before mist is formed. When air is supplied to the nozzle, the distance travelled by the lubricant is increased to 5-6 mm approximately after which the lubricant fraction in aerosol becomes negligible. This distance is important with respect to the effective dispersion of the spray. The rise in volume fraction at 12.5 mm

is mainly due to some eddies formed in simulation, resulting in oil volume fraction increasing at that location. This is not a point of concern as the nozzle distance in machining setup is not more than 5-6 mm. Thus, this phenomenon is not commencing any problem (Najiha, 2012).

The work of Najiha, has shown the fluid flow behaviour of oil and air mixture in a certain pressure at a tip of a nozzle specially designs for MQL to help design modification for future work on MQL. The delivery of proper mist sprays which influences the grinding process and large reduction in usage of coolants. The objectives and main task of this project are to develop high jet velocity nozzle with less lubricant to penetrate into the cutting zone.

#### **4.13 Summary**

A broad review of MQL system delivery and working process was discussed and presented in detail. The main key points of this chapter are the MQL background, economics, together with potential savings were discussed. The cost benefits associated with the machining and usage of coolants. One of the main advantages of using MQL method is the drastic reduction in the consumption of the bulk coolants in metal cutting industry. The use of coolants-lubricants plays a significant role in machining process, economy of tools and it becomes easier to keep high precision tolerances and to maintain workpiece surface properties without damages. MQL is flexible in using drilling and milling but spot nozzles are not fit for the purpose as the wheel width is wider to cover sufficient lubricant in grinding. Taking into consideration the project main aim and task is to develop dual flow nozzle, air & oil as lubricant to dispense very minute amount of fluid in grinding application. Another main issue is the environmental and ecological reasons, the cutting fluid has become more problematic in terms of generating both high consumption of coolants and discard costs. Special attention and stricter laws is taken under the pressure of environmental organizations for industrial waste and pollution aiming to protect the environment. MQL method is efficient in using less coolant application which reduces these ecological problems.



## **Chapter-5**

### **Nozzle Initial Simulation Using CFD**

## Chapter-5 Nozzle Initial Simulation Using CFD

This section presents 3D solid modelling and simulations for the design and development of the nozzle model using ‘SolidWorks’ software. The initial work used ‘COSMOS Flowworks’ CFD simulation; this inbuilt CFD Flowworks allows studying original designs directly in ‘Solidworks’ without any design modifications for a computational fluid dynamics application. By iterating between Solidworks and the CFD package radically new generation of parametric multi-purpose nozzle system, which incorporate a dual flow coupled to deliver a low volume at required pressure for both MQL and conventional grinding fluid application was developed. This was achieved through a detailed systematic optimization process at the design stage using CFD simulation.

### 5.1 Flow Straightener Designs

In the fluid flow, the conditioners or flow straighteners are often used to achieve the desired performance. A flow conditioner tends to increase the laminar properties of the fluid flow by removing turbulence and recirculation elements inside the pipe or nozzle. Flow Straighteners are grouped into three general classes based on their ability to correct the mean velocity profile, turbulence structure and bulk swirl.

The first class of straightener is designed primarily to counteract swirl by splitting up the flow into a number of parallel conduits. Fig.5.1 (a) shows a Mitsubishi flow straightener, which consists of a concentric circular pattern of holes through a disk. This type of straightener does not attempt to produce a uniform velocity profile immediately downstream of the flow. The second class of straightener is designed to generate an axisymmetric velocity profile distribution by subjecting the flow to a single or series of perforated grids illustrated in Fig. 5.1 (b) (Baines-Jones, 2007).



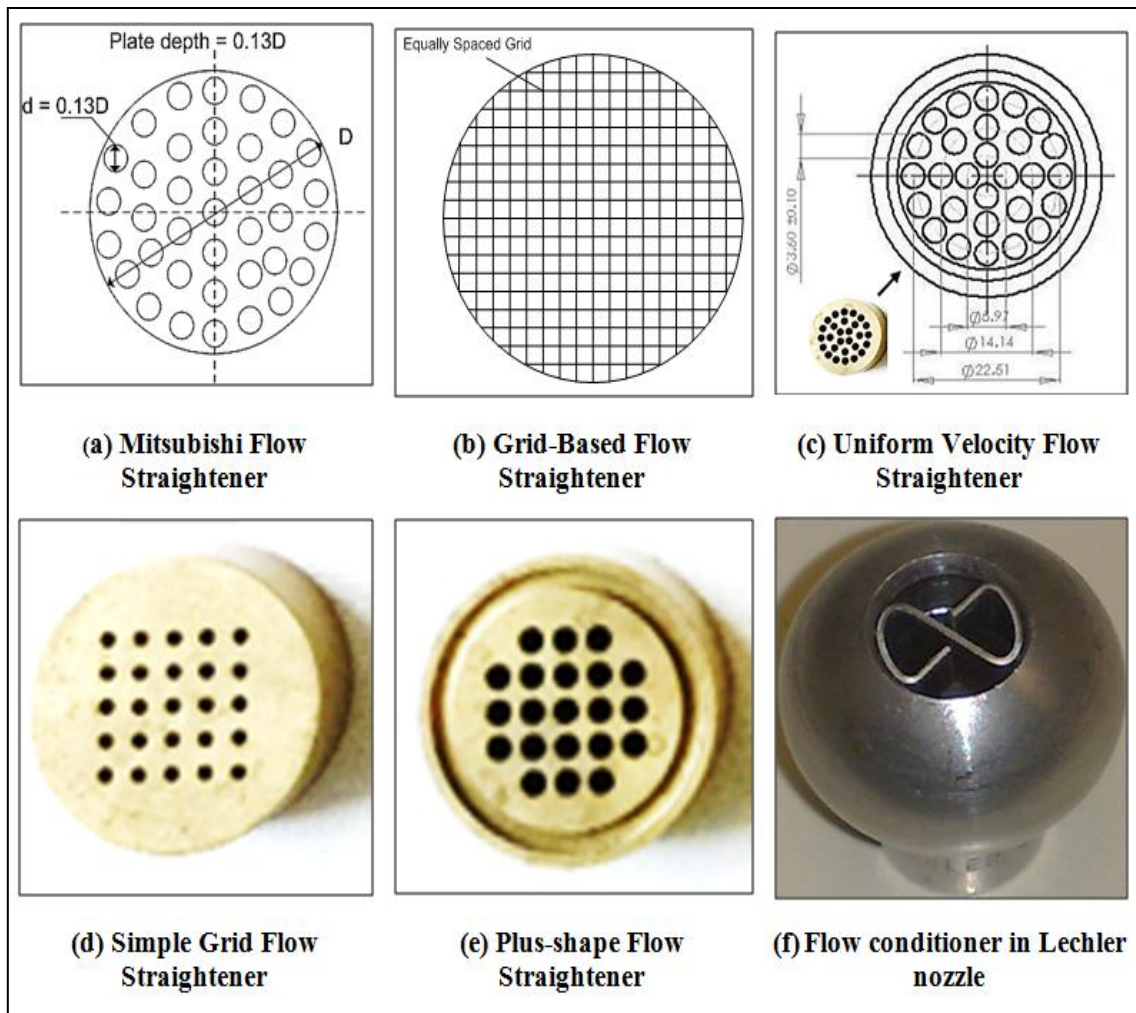


**Figure 5.1: Various Types of Flow Straighteners (AMTReL)**

This straightener has little effect on reducing the swirling effect. Fig. 5.1 (c) depicts the third class of flow straightener is designed to generate a fully developed velocity profile. Fig. 5.1 (d) shows a simple grid flow straightener leading to a turbulence inside the nozzle cavity and is not much fit for the purpose. And in Fig. 5.1 (e) is a cross-shaped flow straighteners which has little effect on reducing the recirculation and swirling effect. Fig. 5.1 (f) depicts an “8” shaped flow straightener (Lechler Nozzle) set in the flow used to increase the pressure in Lechler articulated nozzle. These flow straighteners have some problems in the real applications, and this is shown in Fig. 5.2.

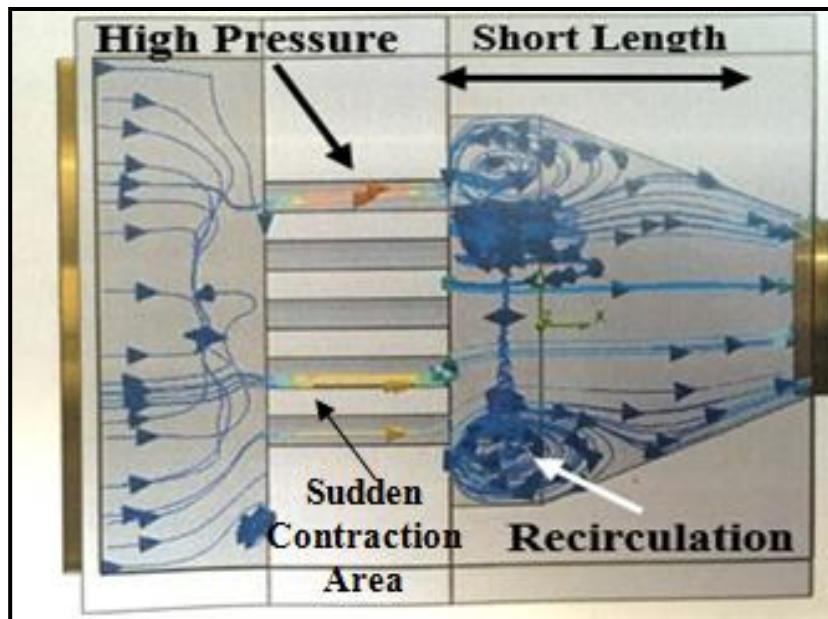


**Figure 5.2: Simple Grid-Flow Straightener in a Taper Nozzle**

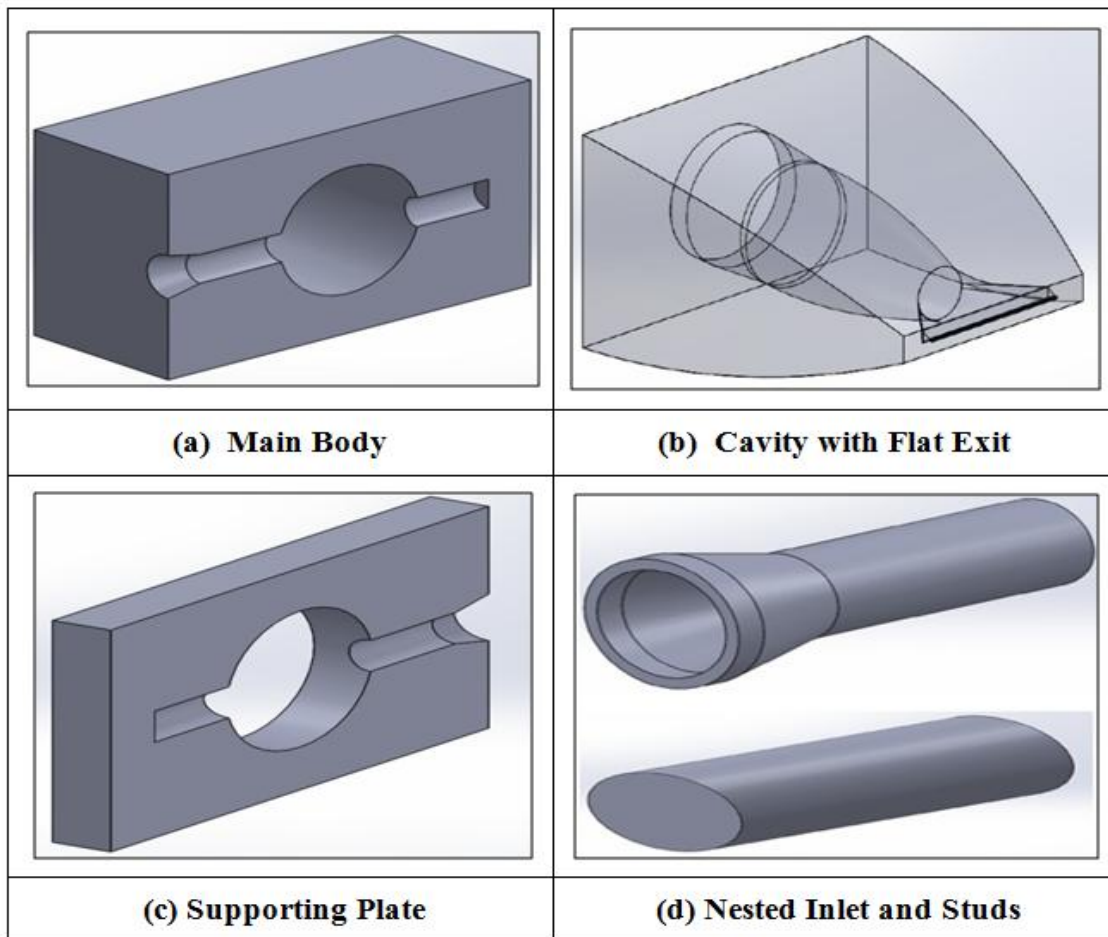
Here it is observed that the performance of taper nozzle with this flow straightener creates a turbulence and stagnation zones after immediate exit of the straightener. In general, a flow straightener does not induce any effect with short length and sudden contraction profile in nozzle cavity.

However, above mentioned problems in the interaction and performance of the fluid flow straighteners in the nozzles needed further investigation to fully understand and optimise the performance of the nozzle being developed. This basic understanding helped to design and implement a universal dual flow nozzle for conventional fluid and MQL application. Therefore in this work a novel concept of developing flow conditioner and its performance is modified and scaled, and extended to the outcome of the final design.

## 5.2 Geometry of the Models

All the geometry of the CAD models were designed in SolidWorks software at the initial stage and then used to run the CFD simulation. In this section each individual component, structure and function is discussed in detail.

### 5.2.1 Primary Nozzle Design (Main Nozzle)



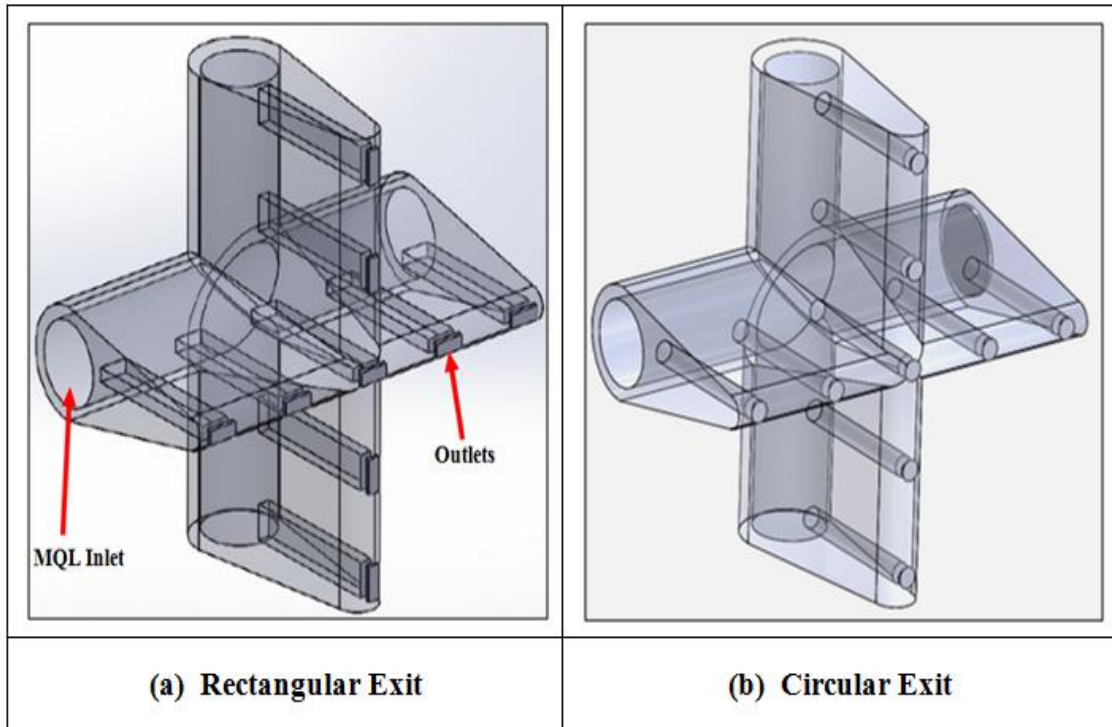
**Figure 5.3: Nozzle Components**

Fig 5.3 illustrates the nozzle model contains six components arranged in a systematic way to deliver dual flow system for grinding application. The nozzle is divided into two flows, namely primary flow (Main Nozzle) and secondary flow (Nested Nozzle). Primary flow is a plane nozzle, with only the main body.

### 5.2.2 Secondary Nozzle Design (Nested Nozzle)

Hydrofoils are used as flow conditioner device if one refers to the flow condition in Lechler Nozzle. Here a cross-shape hydrofoil sits in the centre of main nozzle cavity. The hydrofoil shape helps in increasing pressure of the coolant in the main nozzle and

straightening the fluid flow up to the exit. Both aeroplane wing aerofoil and hydrofoil have a characteristic shape of a rounded leading edge followed by a sharp trailing edge.



**Figure 5.4: Hydrofoil (Flow Conditioner)**

Two hydrofoil models have been designed in this work with two different exit slots. One has rectangular exit slots Fig 5.4 (a) and other one has a circular exit slots Fig 5.4 (b). The internal flow cavity structures of both models are shown in Fig. 5.4. The two models were investigated to test their effect and influence in the nozzle cavity. The simulation results and performance of both models rectangular and circular orifices are discussed in below Fig 5.5.

### 5.3 Fluid Flow in the Nested Nozzle

To identify the best performing nested nozzle outlet profile, a comparative study was made by analysing the fluid pressure distribution or the fluid velocity distribution within the part.

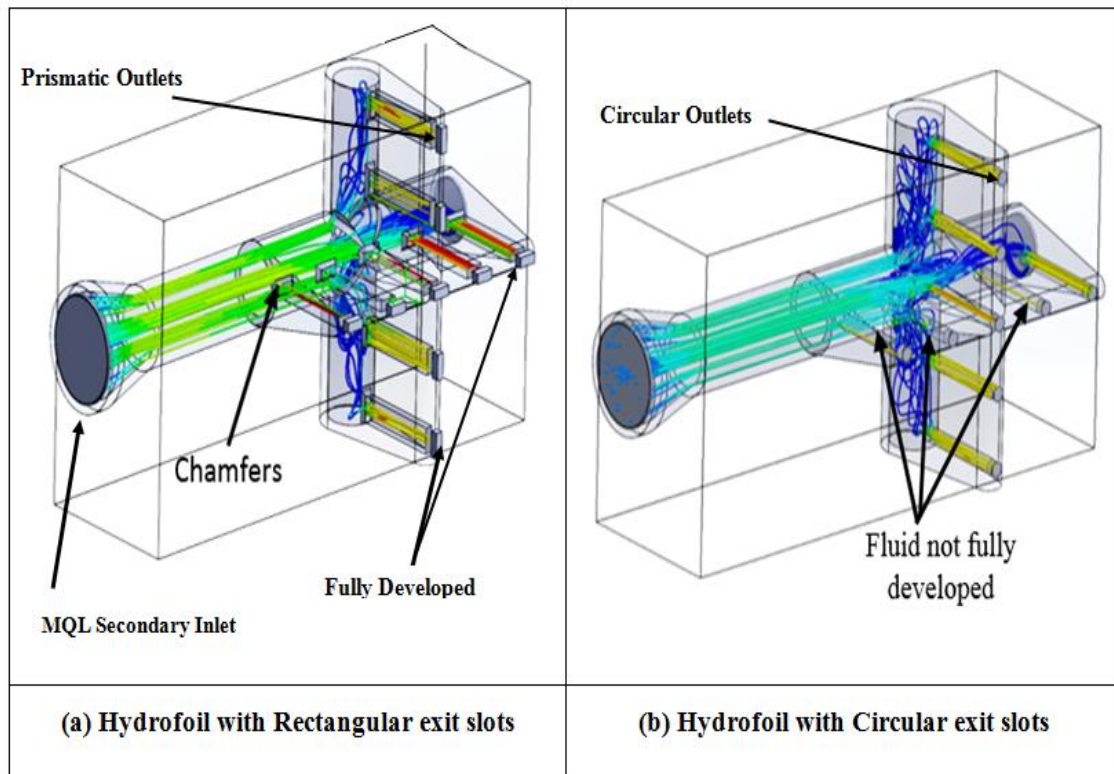


**Figure 5.5: Flow profile in nested nozzle with rectangular and circular exit**

The above Fig.5.5 illustrates, the secondary nested nozzle designed in a form of hydrofoil which serves as a flow conditioner. The exit of the secondary nozzle can be reconfigured in various shapes. Comparing prismatic and circular exist profiles with it was observed that prismatic openings performed better in terms of flow pattern in the secondary nested nozzle this is illustrated in Fig 5.5 (a). It is observed that circular exits do not provide the same jet velocity as the prismatic exits Fig 5.5 (b). In some cases the fluid did not flow through some of the circular exits. Therefore preference was given to prismatic exit though their manufacture is not easy. Thus the study is focused on the analysis of the fluid pressure and velocity distribution with the variation of inlet flow. With the rectangular outlet, the fluid distribution is more even in each outlet compared with the circle outlet. According to the Bernoulli's principle,

$$H = P + \frac{v^2}{\rho} \quad (5.1)$$

The Bernoulli's effect is the lowering of fluid in the cavity regions where the flow velocity is increased. where,  $H$  = height (mm),  $P$  is the pressure (Pa),  $V$  is the velocity (m/sec) and  $\rho$  is the fluid density ( $\text{kg}/\text{m}^3$ ). Therefore any increase in the fluid speed is proportional to the increase in dynamic pressure and kinetic energy.

To improve the prismatic exits, fillets were added to avoid sharp corners, recirculation zones and stagnations. It is observed that higher velocity occurred in the direction of the supply pipe. The vertical wings of the cross hydrofoil did not get enough flow as expected. In addition large stagnation was observed at the end of the supply pipe. This early finding gave an indication how to improve the design to achieve desired results. It is now planned to concentrate the exit hole around the cross but leave the body of the secondary nozzle to act as flow conditioner.

#### **5.4 Initial investigation into Minimum Quantity Lubrication (MQL) Nozzle**

In general commercial MQL systems are equipped with standard spot nozzles which are typical not adequately configured for MQL application to grinding process. Fig.5.6 (a) shows a model of new design, which incorporates 2-cores of spot spray encapsulated in a nozzle cavity that covers the desired wheel width.

In the case using 2-core infeed tubes, the oil and air mixture creates turbulence, and the exit fluid velocity is developed only half way of the nozzle exit as shown in below Fig 5.6 (a). This is due to short nozzle cavity length. Figure 5.6 (b) depicts, the air and oil exit tip of internal feed tubes. The MQL system pushes exact amount of oil to the internal feed tube where a separately supplied air splits the media in the form of atomised spray.

Using the below model and fitting the nozzle internal cavity with three cores (3-internal feed tubes); a more efficient nozzle was created. This new model covers the wheel width of 40 mm and allows effectively coating the wheel surface with needed amount of lubricant. However, the amount of oil supplied to the three cores seems to be increased and fully develops the fluid mixture up to the exit.

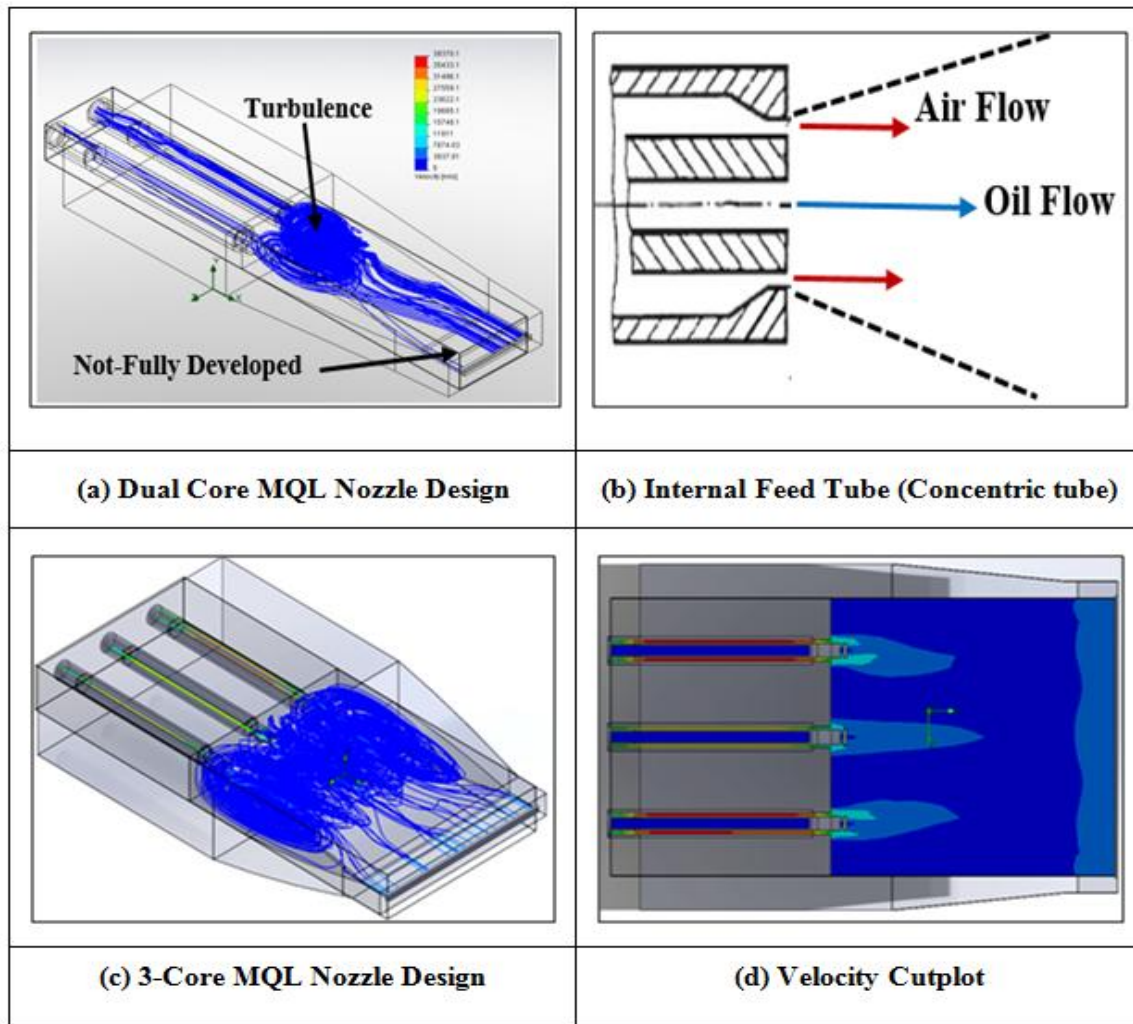


**Figure 5.6: MQL Flow in Nozzle with 3-Core Inlets**

Fig.5.6 (c) shows an initial flow profile in the MQL nozzle, where the recirculation is observed. This secures a good mixture of oil and air. However the velocity distribution in Figure.5.6 (d) suggests that the nozzle cavity is not adequate and need some modification to achieve a better performance. The shape of core exits needs a convergent profile, to optimise the turbulence, and the nozzle cavity needs shortening and re-profiling to follow the shape of the flow. However, referring to the novel modular and adaptable nozzle design presented in below (Section 5.10), it is possible to use the nested nozzle to supply oil and air effectively and having an MQL nozzle by altering the supply holes of the secondary nozzle.

### 5.5 Nested Nozzle Design (Flow Conditioners)

In this work an attempt is made to develop nested nozzles. Here the relationship between the flows and the pressures in the main and nested nozzles will be investigated in order to optimize the design. The purpose of this is to reduce the amount of coolant used with reference to traditional flood cooling.

A research has been made on several existing models on internal fluid flow behaviour. The pressure cone is the main component in this nozzle design as it works to increase the pressure inside the main nozzle chamber, on the one hand. This allows increasing exit velocity. On the other hand, the external profile of the pressure cone/nested nozzle acts as a hydrofoil for flow condition. Several design optimisations and modifications has been undertaken in order to select the best performing profile.

The concept of pressure cone or nested nozzle is designed based on "Bernoulli's principle" that any fluid flowing from large cross section to the smaller cross section tends to increase in the fluid velocity occurs simultaneously with decrease in pressure or a decrease in fluid potential energy. The principle is applied and developed and introduced a hydrofoil shape nested nozzle illustrated in Fig.5.7 (1). The hydrofoil consists of an inlet and outlets and the outer body is in aerofoil shape with trailing edges this shape helps to act as flow conditioner inside the main nozzle cavity. In this two hydrofoil models one is with rectangular outlets and other circular outlets has been designed and simulated. The rectangular outlet showed better performance then circular one. Based on this hydrofoil another model has been designed, tapered pressure cone illustrated in Fig.5.7 (2) this model has five openings, four around its cone and one on its centre. When the fluid flows through the cone the flow splits into five openings but due to large openings of the pressure cone area the flow could not able to create pressurising action inside the nozzle cavity. By modifying this tapered cone into conical shape Fig.5.7 (3) the fluid trajectories shown a smooth flow over the cone with no stagnations or recirculation is observed inside the nozzle cavity which is depicted in Fig 5.18. This conical shape cone when performed with hydrofoil, a large turbulence is

forming between cone and hydrofoils (see Fig.5.19). Considering this conical shape profile as a base design, a new curved shape with through hole is designed which is depicted in Fig 5.7 (4). This model has smooth curved shape that fluid flow sticks to its surface creating a laminar flow. Due to its through hole at its centre the fluid flow speed is dropping (see Fig.5.23). This cone is further modified into a solid egg shape cone illustrated in Fig.5.7 (5). This cone design is performed well compared to all other previous designs; as a result the fluid speed is gradually increasing up to the main nozzle exit. Taking this model into consideration an internal flow system is also designed shown in Fig.5.7 (6). This internal flow system is applied for two models one is tapered cone and egg shape cone. The working principle of this final design consists of an internal flow system with inlet and outlets, when the tapered cone is placed inside the nozzle, it blocks the main nozzle internal cavity and it creates pressurizing action and increases fluid speed inside the nozzle cavity but this model has turbulence and recirculation zones (see Fig 5.25). After reviewing some working models related to flow over cylinder and oval shapes (see Fig.5. (8) and (9)). This gave a new idea for development of egg/elliptical shape nested nozzle. This model is designed to perform "Coanda Effect" which the fluid sticks on its surface and tends to flow in laminar form; the internal structure of this cone is illustrated in Fig 5.10. This egg-shape cone performs in 3-stages one is its body acts as flow conditioner, second is its internal flow system which accelerates the fluid additionally in the main nozzle cavity and third is its body which creates pressurizing action in the nozzle chamber (see Fig 5.34).

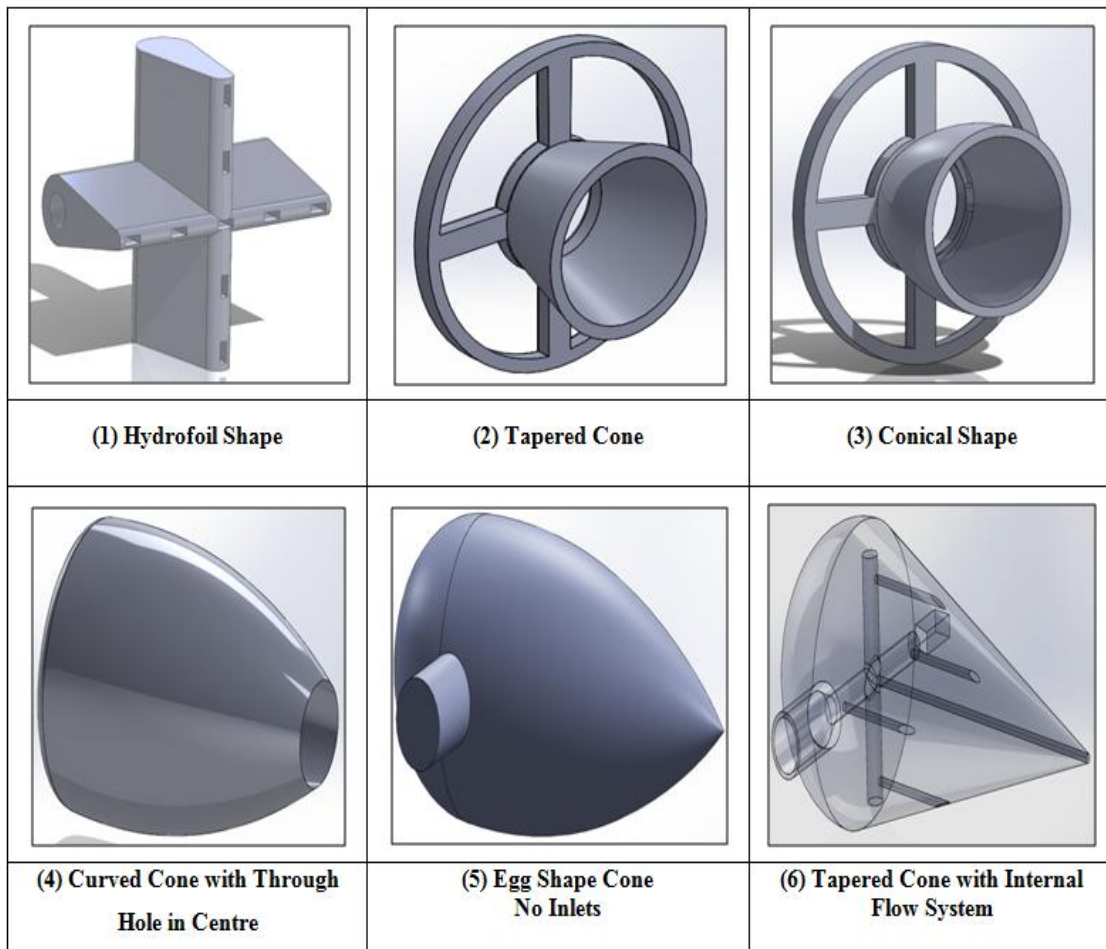


**Figure 5.7: Transformation of Pressure Cone Design**

It is essential to avoid areas of recirculation and stagnation; however recirculation has an apparent benefit in MQL application as it allows for a good mixture of air with oil before exit. An attempt has been made in using inverse pressure to induce ‘Coanda effect’ in order to increase pressure in the main nozzle cavity.

### 5.6 Diffuser as Pressure Cone

The notion of pressure cone is introduced in this study and Fig.5.8 depicts the results of an initial investigation into the action of a pressure cone in a flow within a diffuser. Introducing the diffuser, that is a device use to keep or increase aflow velocity when, the frlow moves from a narrow duct into a sudden expanded duct. It is seen that the

pressure increases in the diffuser. Here the angle of the cone plays an important role, however it does lead to some stagnation in the inner surface of the cone.

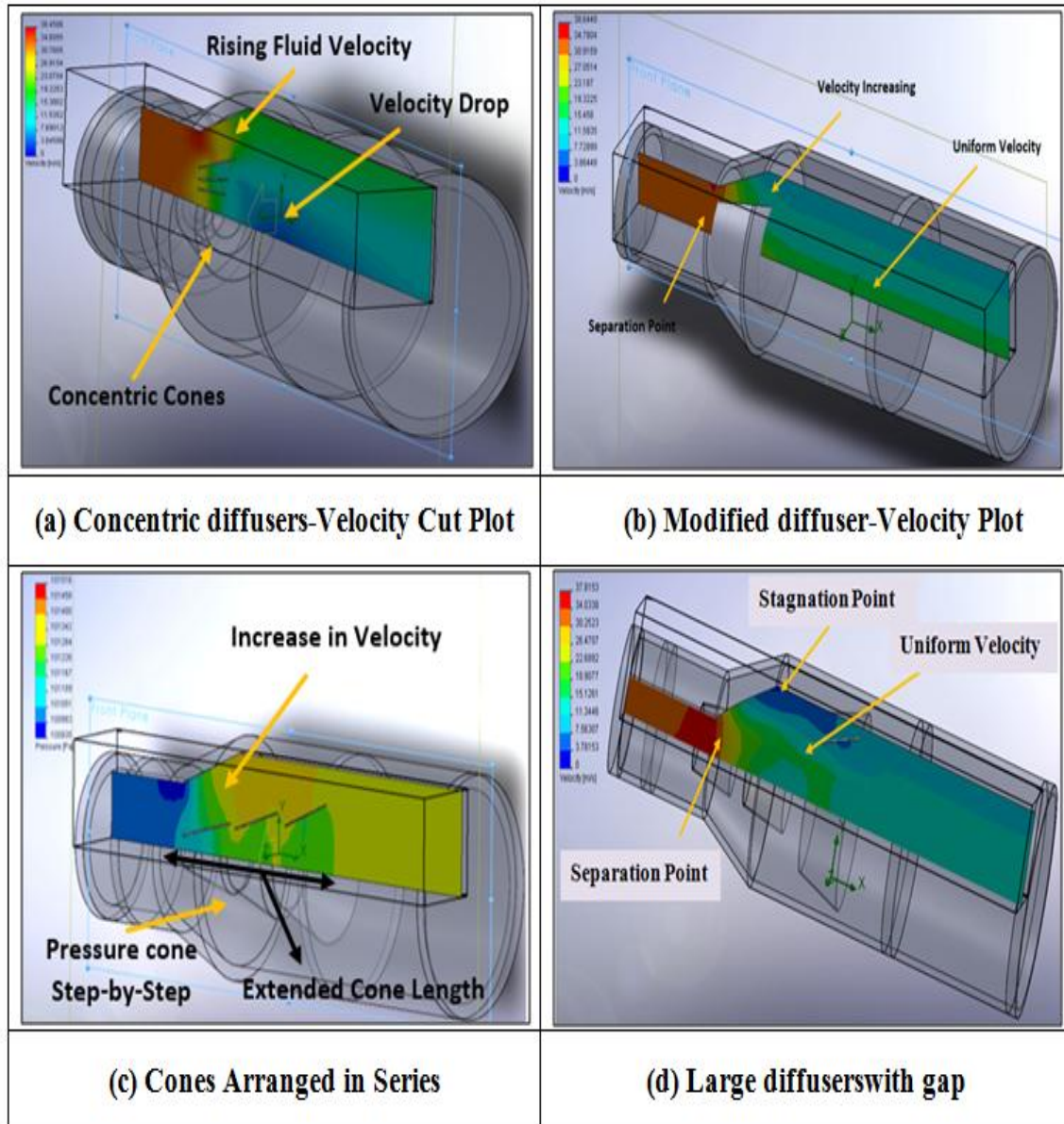


**Figure 5.8: Effect of pressure cones in a diffuser, pressure profile.**

In this investigation three types of cone positions has been studied. Fig.5.8 (a) illustrates that the three cones are arranged concentrically one in another. The simulation results of this model reveals that the fluid velocity is increasing between the top of the cone and

the main nozzle wall. This uniform velocity is continued up to the exit only at the top internal surface.

A low velocity is observed in the middle of the cone this lead to further modifications of the model by moving cone further in adequate positions and diffuser angles see Fig.5.8 (b). It is is observed that in the middle of the diffuser compared to the previous model as shown in Fig.5.8 (b). In the third model 5.8 (c) the diffusers are arranged in a series but stagaerred one from another. This model achieved some good results with referrence to the plot of the regions where the velocity is gradually increasing under the cones with no recirculations or stagnations. This is due to the effect of diffuser extended length.

In the final model the cones are placed making gap of 10 mm in between them as illustrated in Fig.5.8 (d). In this model large cones with gap and due to the gaps in between the cones, turbulence and stagnation points are observed near the fluid saperation point and diverged area. This is because when the fluid strikes the diffusers from the inlet here, the large diffusers are not making enough pressure inside them which leads to velocity drop near the cone area. The effect of diffusers in this model performed poorly because the body of the diffusers staggered at distance acted as obstacles in the flow, thus induced recirculation. Out of all models the results of diffusers arranged in series has performed well. The results obtained here led to the idea of reverting the diffuser into a cone. This idea is implemented and investigated in the next section.

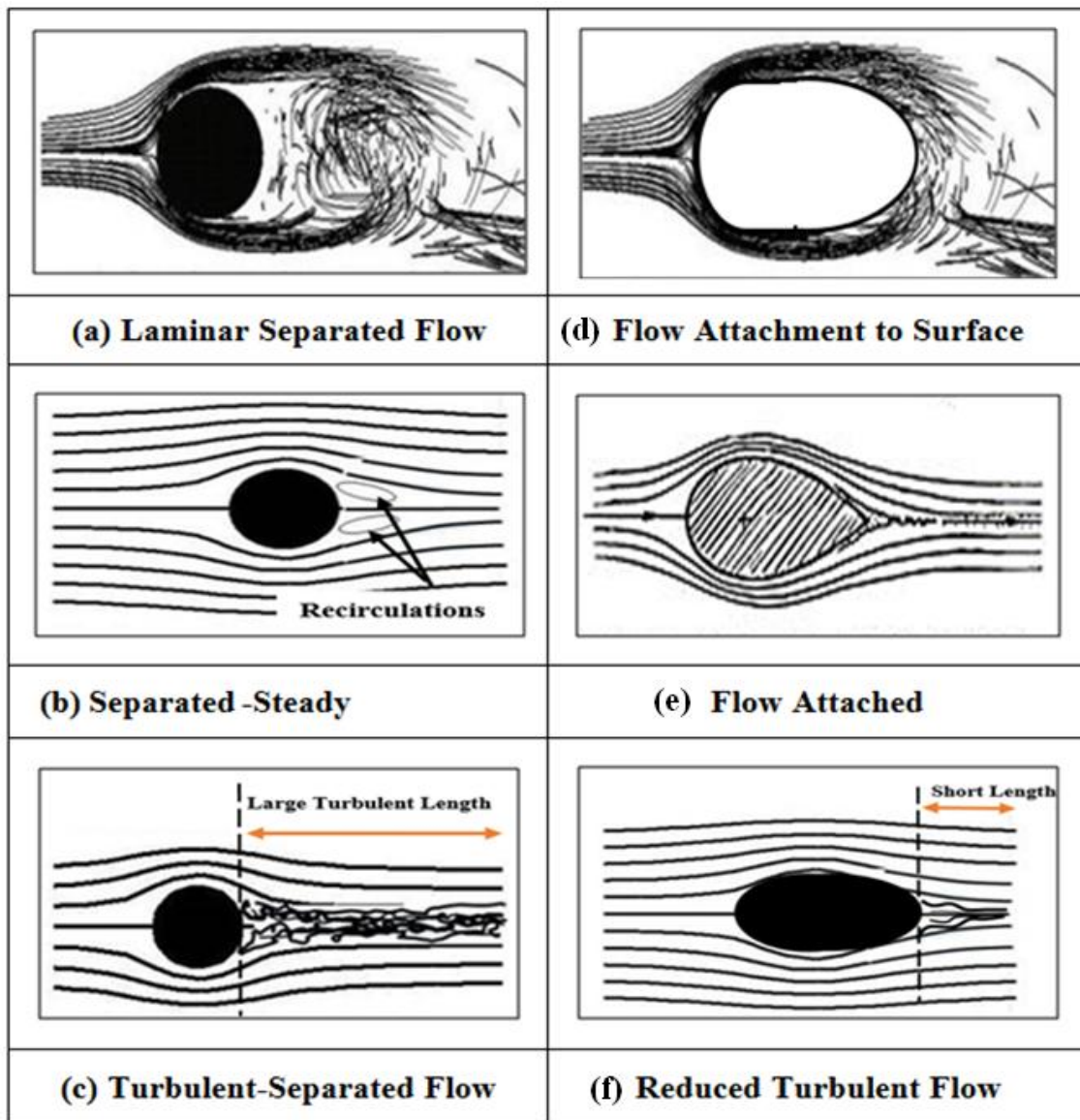


**Figure 5.9: Flows over Cylindrical Vs Elliptical/ Egg Shape Cone**

(Adapted from NASA.gov.com)

The recirculation and turbulence caused by the staggered duffusers, also entailed the study of the effects of shapes on the flow patterns. Fig.5.9 illustrates the fluid flow behaviour over cylindrical shape surfaces verses various types of external profiles. The obstacles in the flow here are of different shapes including elliptical and egg-shape, which will be considered in developing new pressure cones.

### 5.7 Design of Pressure Cone as a Nested Nozzle

Referring to Fig.5.9, the egg shape cone provides flow without turbulence or large eddy vortices. Therefore this shape was selected for further investigation to develop the nested nozzle. This nested nozzle is designed in such a way to increase the pressure inside the main nozzle chamber with a small gap between the internal wall of the nozzle and external surface of the cone. The nested nozzle (pressure cone) has five inlet holes aligned four in vertical plane and four in horizontal plane with fifth hole in the centre. Each hole has 1.5 mm diameter. It is possible to use a tapered angle so that the liquid inside the duct pressurised further in order to accelerate the low velocity fluid around the nested nozzle.

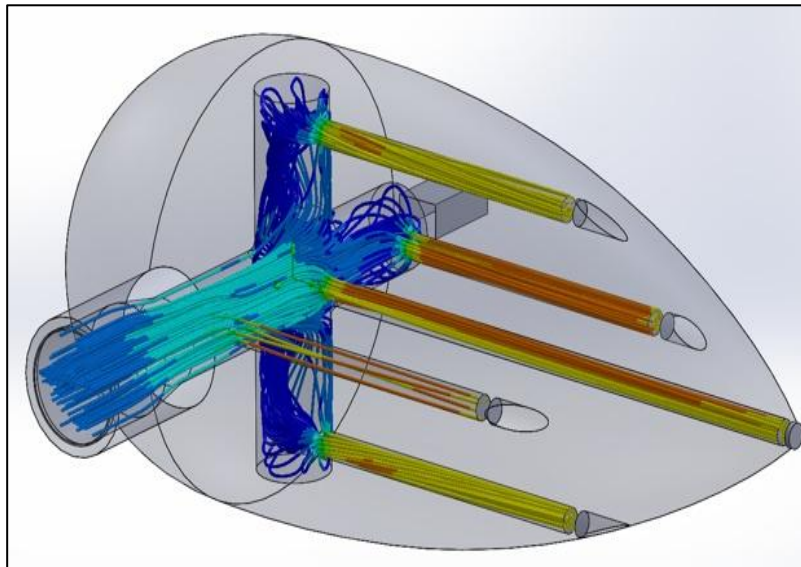


**Figure 5.10: Egg-Shape Pressure Cone Velocity Streamlines**

Another purpose of this pressure cone is to act as a flow conditioner and the shape is designed in the form of elliptical profile (egg-shaped) to stick the flow on the surface of the cone by means of “Coanda effect” without any recirculation zones. The shape of the cone of the secondary nested nozzle can be reconfigured in various shapes such as conical shape, concentric oval shape. The conical shape pressure cone is not suitable for this purpose due to eddy and recirculation zones that were identified see Fig.5.25 and

Fig.5.26. This gave an indication as to how to improve the cone and nozzle design to optimise the flow and the overall nozzle efficiency.

Egg-shape pressure cone achieved better results compared to all other cone designs this is due to the shape which uses the advent

age of “coanda” effect. The inlet pipes and the five holes are placed in cross shape and create high pressure inside the nozzle cavity which tends to high velocity.

The study was focused on the analysis of the fluid pressure distribution and the fluid velocity distribution with the variation of inlet flow. With the pressure cone, the fluid distribution was more even in each outlet compared with the conical outlet.

### 5.8 Nozzle Cavity Design

Using the knowledge acquired through the literature review a concept of new Nozzle design was developed. This concept was studied using 3D solid modelling, CFD flow

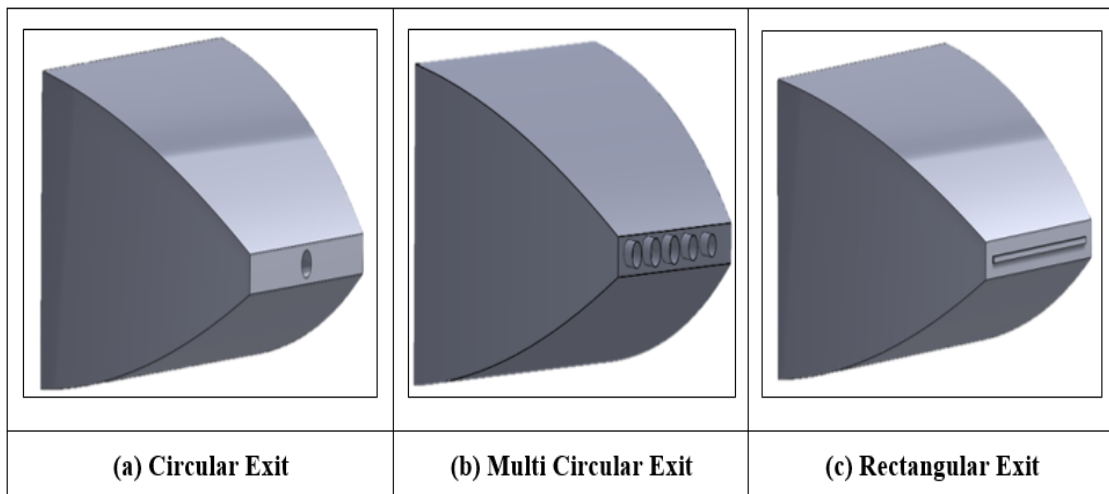


**Figure 5.11: Nozzle exit configurations**

simulation with design and simulation iterations before actual implementation. In the modelling process, three different nozzle exits were investigated, namely, (a) single orifice, (b) multiple orifices and (c) rectangular slot exit as illustrated in Fig.5.11. The nozzle cavity is a modified Rouse-nozzle to accommodate a nested secondary nozzle acting as a flow conditioner. Therefore the nozzle chamber was extended and

converged into aforementioned nozzle exits. Single circular exit was for study purpose as it may suitable for narrow wheel, therefore a row of cone shape exits was studied.

## **5.9 Basic Studies of Internal Fluid Flows**

This section presents the internal nozzle cavity problems, simulations and performance of some existing coolant nozzle designs. The discussion on 2-Dimensional and 3-Dimensional cross-sectional CAD models used in experimentation and theoretical work by (Gviniashvili, 2003) is given.

### **5.9.1 Problems with Existing Nozzles**

In Fig 5.12, illustrates some of the existing models all these models a reverse flow is observed in the nozzle cavity due to sudden expansion and contraction of the nozzle chamber. However the simulation provided an insight to the nature of flow in the nozzle and at the exit orifice. This gives an idea of fluid behaviour inside the nozzles, which is not covered previously. The nozzle with rectangular long exit slot outlet proposed by Gviniashvili (2003) focused on these types of nozzles experimentally and theoretically related to energy loss using conservation of energy equations. But his results do not give suggestion to the user how to improve the nozzle design to reduce areas of stagnations.

## 5.9.2 Effect of Internal Cavity Profiles

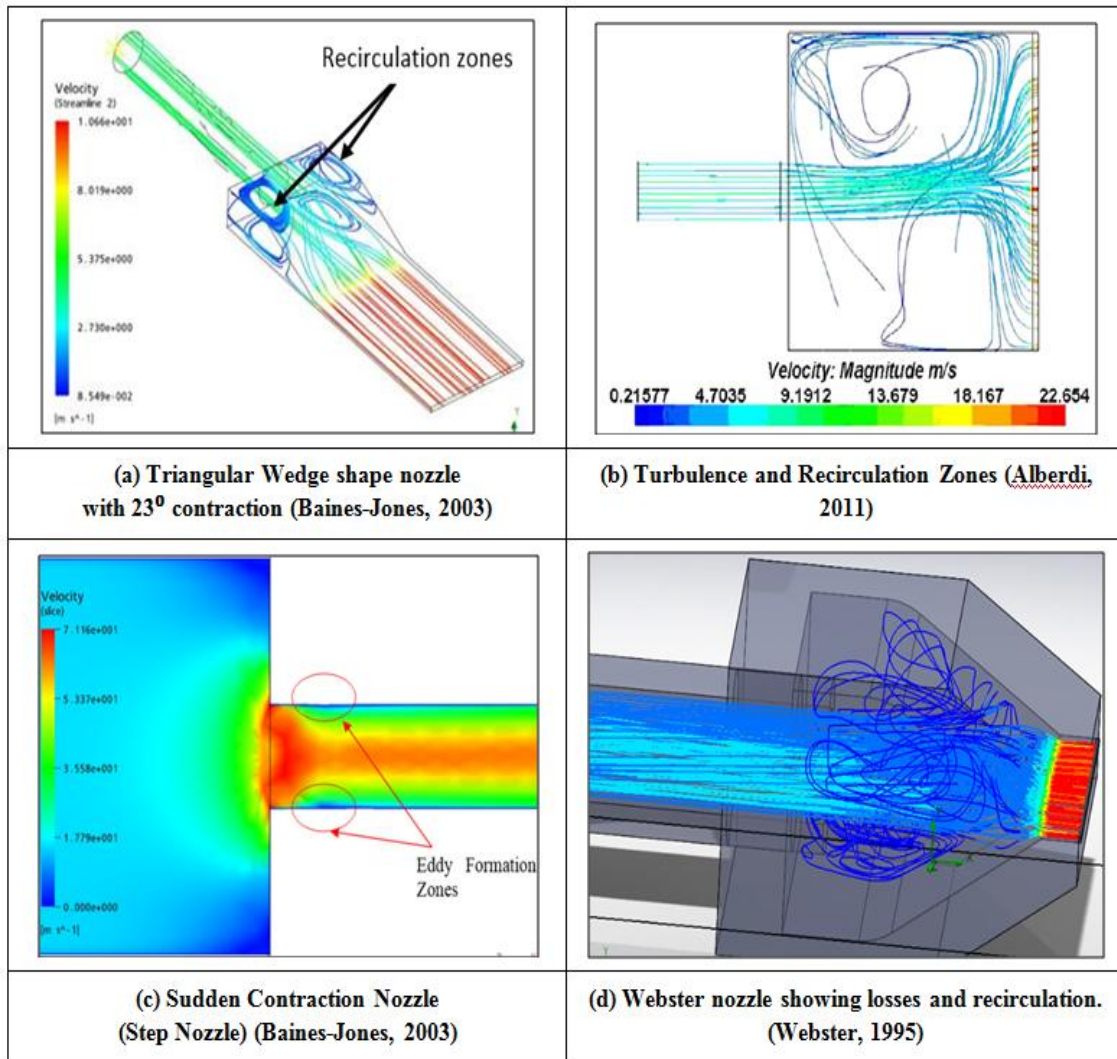


**Figure 5.12: Turbulence, Recirculation and Stagnations in Nozzle Cavity**

The results of nozzle with long slot in Fig.5.12 (a), shows that the flow trajectories of the fluid exhibits relatively high reverse flow and stagnation points is occurred in the large nozzle cavity and also large turbulent flow. When, the fluid exits from the large cavity of flow into the narrower cavity, the velocity of the fluid increases significantly because of the smaller cross-section. However, before uniform velocity is reached at some distance within the narrow cavity there is a flow region of varying velocity at the interface of the two varying volumes.

This is mainly caused by changes in internal geometry of the large chamber; also the velocity profile of the nozzle exit shows regions of varying velocities. Lower velocity is observed at the outer edges of the exit flow and high velocity is observed at the centre of the outlet this is due to interior wall friction of the nozzle.

Alberdi, (2011) studied two approaches aiming to the optimisation of fluid application in grinding Fig.5.12 (b). The influence of nozzle design on the development of velocity and pressure fields was studied using CFD simulation. Subsequently, he attempted to correlate the effect of nozzle geometry on grinding process conditions.

Baines-Jones, (2003) Jyotirishwar, and Sourav (2015) studied the flow characteristics of a cutting fluid flowing through a sudden contraction nozzle Fig.5.13 (c). The main aim of his work is to study laminar fluid flow characteristic flowing through a sudden contraction nozzle for different Reynolds number ranging from 100 to 500 for a fixed aspect ratio 0.28.

The Webster nozzle has become more popular in recent years; however, in this nozzle the generation of stagnation and recirculation zones lead to energy losses that reduce the fluid performance. At the exit of the nozzle velocity variations has been observed with the non-uniform flow towards the grinding wheel and inner pressure maps showed that pressure tend to concentrate at the centre of the exit of the nozzle, with significant losses at its edges.

The famous Webster nozzle does not always perform as it is claimed. This is because these nozzles are designed based on empirical estimations of what flow is needed. Fig 5.12 (d) illustrates the internal flow behaviour of the Webster nozzle, and it shows key problem of losses due to recirculation. Therefore, this nozzle is not optimised, though it has an acceptable performance in some cases. This basic analysis gives an attention to improve the nozzle design where the area of recirculation zones and stagnations is observed in this stage of nozzle design.

### 5.9.3. Good Performance of Modified Nozzle Designs

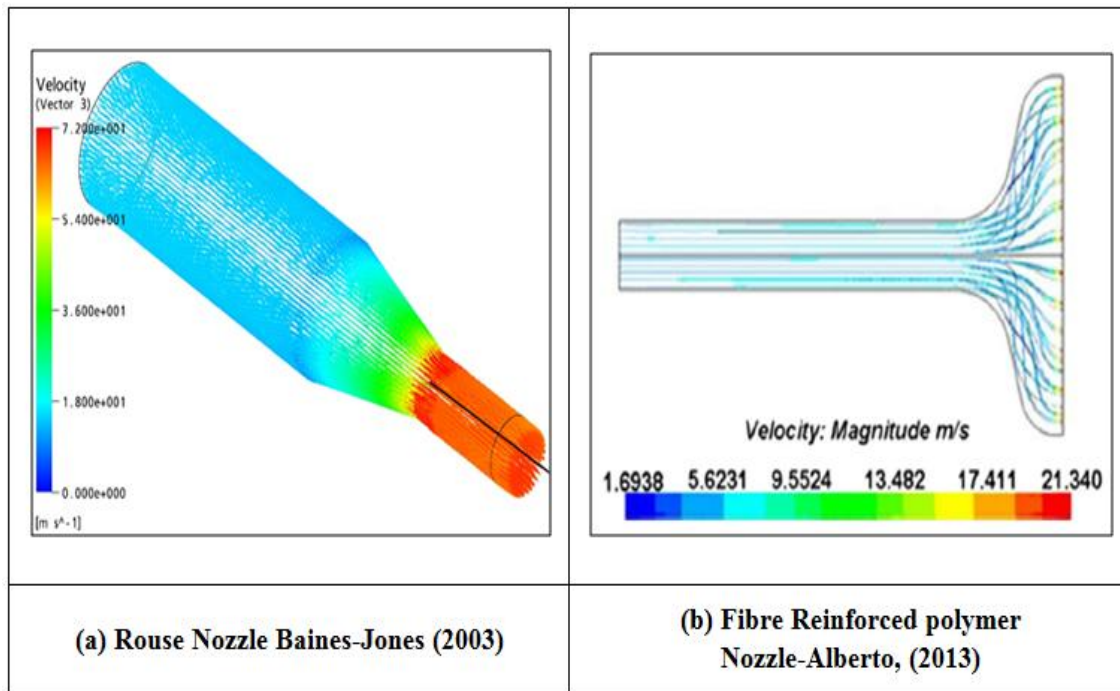


**Figure 5.13: Improved and Modified Nozzle Designs**

Fig.5.13 (a) depicts the Rouse-shape sloped nozzle showing that the fluid exhibits no reverse flow in the area of contraction from the supply pipe to the converging section even with a large turbulent flow. The fluid exits the converging section and flows to the narrower chamber where the velocity of the fluid increases significantly because smaller cross-section. However, before uniform velocity is reached at some distance within the narrow chamber there is a flow region of varying velocity at the interface of the two varying volumes. This is due to change in section and appearance of vena contracta. This agrees with the work proposed by McCarthy and Molloy (1973), later investigated by Cui (1995).

Fig.5.13 (b) Alberto, (2013) studied two approaches aiming to the optimisation of fluid application in grinding. The influence of nozzle design on the development of velocity and pressure fields was studied using CFD. Subsequently, he attempted to correlate the effect of nozzle geometry on grinding process conditions.

The results showed that using the newly developed composite nozzle a 30% of reduction in coolant was achieved and approximately 60-80% pump pressure and power reduction was also achieved compared to commercially available nozzles. In addition, to this some improvements in wheel life and also in surface finish were achieved.

### 5.10 Preliminary Simulation Work

The novelty in this work presented here reflects the need of high performance nozzles. To achieve this, a concept of new novel modular adaptive design with nested flow nozzles (Secondary Nozzles) was designed to implement a new concept of ‘*Dual and Triple Flow*’ delivery was developed. This concept was studied using 3D solid modelling, CFD flow simulation with design and simulation iterations before actual implementation. In optimisation process the nozzle internal cavity and nested nozzle model were modified in a series of steps from initial design stage to final design stage. Here the ‘*Nested Nozzle*’ acts as a flow conditioner allows to straightening the fluid flow in the nozzle cavity. A flow conditioner is a device that used to straighten and align the fluid flow within a duct for better flow efficiency. Flow straighteners are widely used in pump and pipeline systems to produce a consistent, swirl-free and distortion-free highly repeatable velocity flow profile. In this work various types of nested nozzles (Flow Conditioners) designs has been tested in simulation.

Another aspect of the novelty is the ‘*MQL flow*’ delivery, which intends to reduce further the quantity of fluid used.

The combining of these two new approaches to nozzle design; a new optimized universal, multipurpose and multi-phase flow nozzle was derived. It is anticipated that the outcomes of this research work will bring the following benefits:

- New generation of modular multi-phase flow nested nozzles
- New design of universal nozzle for MQL and conventional fluid application in grinding



- Drastic reduction of amount of coolant as per MQL
- Considerable reduction of fluid requirement in flood cooling
- Low pressure requirement in conventional coolant application
- Improved and high performance nozzles for conventional and MQL application in manufacturing.

In this preliminary simulation work various types of secondary/nested nozzles (flow Conditioner) and internal cavities were designed and simulated to develop multi-purpose nozzle system to deliver a low volume at required flow pressure for both MQL and conventional fluid application to the grinding contact zone.

### 5.10.1 Initial Nozzle Simulation

All the initial nozzle designs and simulations were performed in SolidWorks software. The flow simulation embedded within Solidworks is called 'COSMOSFloWorks'; this package allows the user to simulate range of physical process using a model designed directly in SolidWorks.

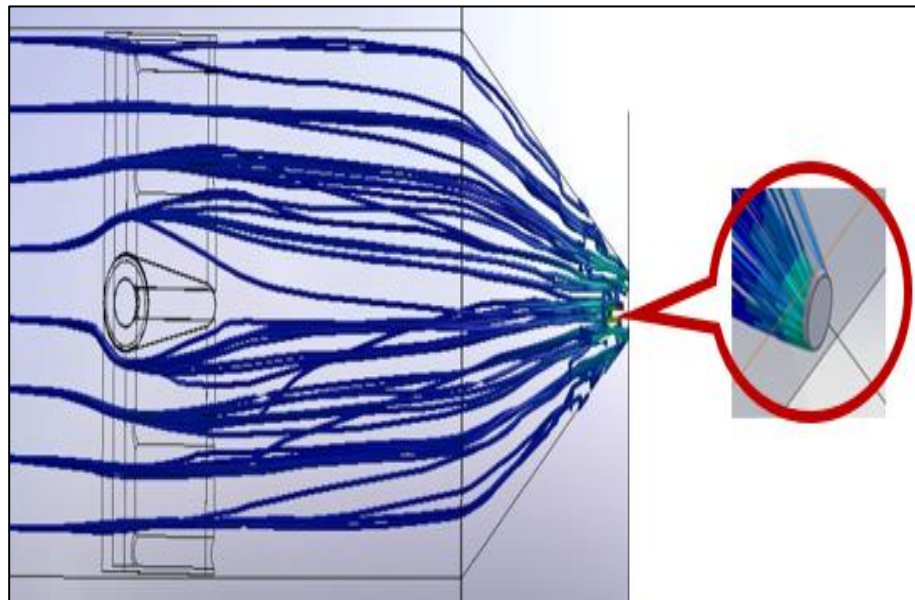


**Figure 5.14: Nozzle with Hydrofoil Circular Exit**

(Previous nozzle with slight turbulence near Hydrofoil and opening)

In this study, two types of media i.e. air and water was used for internal flow analysis. This allowed selecting an optimal design by comparing the performance of internal flows in the main nozzle and the interaction of the flow with the nested nozzle.

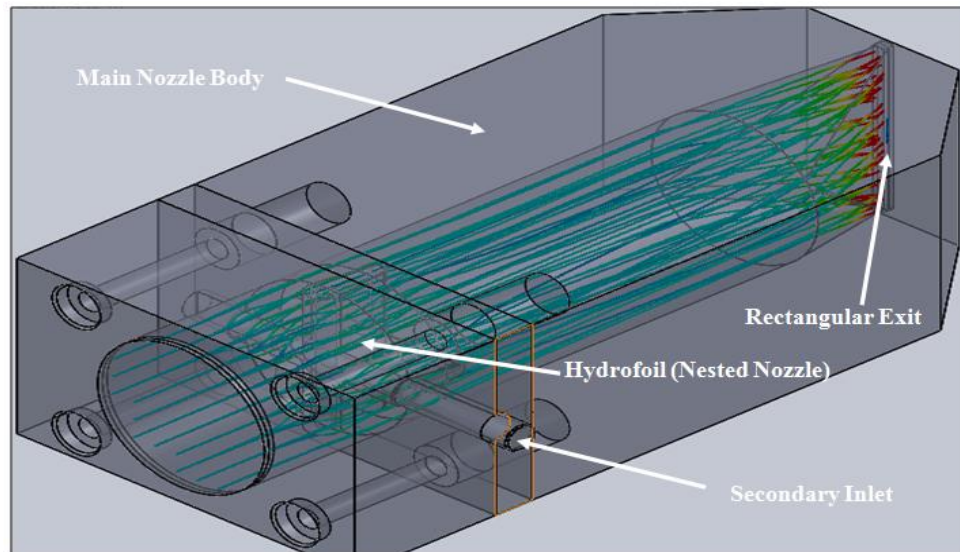


**Figure 5.15: Nozzle with Hydrofoil Rectangular Exit**

(Initial design of a nested nozzle showing its flow profile with no recirculation)

The simulation was performed with taper nozzle end with circular exit, and rectangular exit slot, both of this nozzle system consists of a main body, nozzle cavity and a hydrofoil (nested nozzle) with different exit slots is illustrated in above Fig.5.15. The fluid flow profile of the main nozzle had neither recirculation nor turbulence. It is also seen that the conditioner placed in the flow served its purpose by straightening the fluid and allowing the flow to develop fully up to the exit. However, no peak velocity is observed in this in circular exit model shown in Fig 5.14. This is because the large volume inside of the nozzle has not developed enough pressure up to the exit. Fig.5.15 this is a modified nozzle extended nozzle cavity length; in this, the fluid flow profile of the main nozzle cavity has neither recirculation nor turbulence. It is also seen that the conditioner placed in the flow served its purpose by straightening the fluid and allowing the flow to develop fully up to the exit.

1.	Inlet Flowrate	20 L/min = 0.34 kg/sec
2.	Secondary Inlet flowrate	No Fluid Inside
3.	Nozzle exit Opening Dimensions	25 mm x 40 mm x 1 mm
4.	Fluid Type	Water
5.	Outlet Pressure	Static Pressure

**Table 5.1: Nozzle Input Parameters**

The above two nozzle model simulations gave better idea and insight of the fluid flow behaviour and nested nozzle performance. Based on this nested nozzle concept some of the other various types of flow conditioners were studied to achieve an optimised multipurpose nozzle design.

### 5.10.2 Model of the Nozzle with Hydrofoil (Nested Nozzle)

In this section an attempt is made to improve the nested nozzles. Here the relationship between the flows and the pressures in the main and nested nozzles is investigated in order to optimize the design.

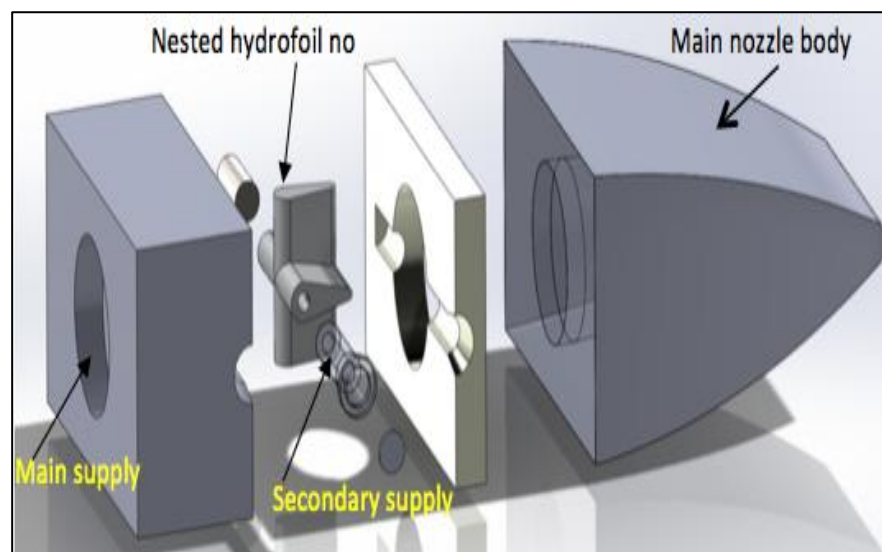


**Figure 5.16: Internal View of Nozzle Components**

The purpose of this is to reduce the amount of coolant used with reference to traditional flood cooling. Fig.5.16 shows, the exploded view of structural composition of a nested nozzle system which consists of six components: the main supply block, the nested nozzle and its elements and the main nozzle body. To positively exploit the side effects of the nested nozzle, it is designed in a form of hydrofoil, thus its body acts as flow conditioner for the main stream.

### 5.10.3 Fluid Flow in Main Nozzle No-Nested

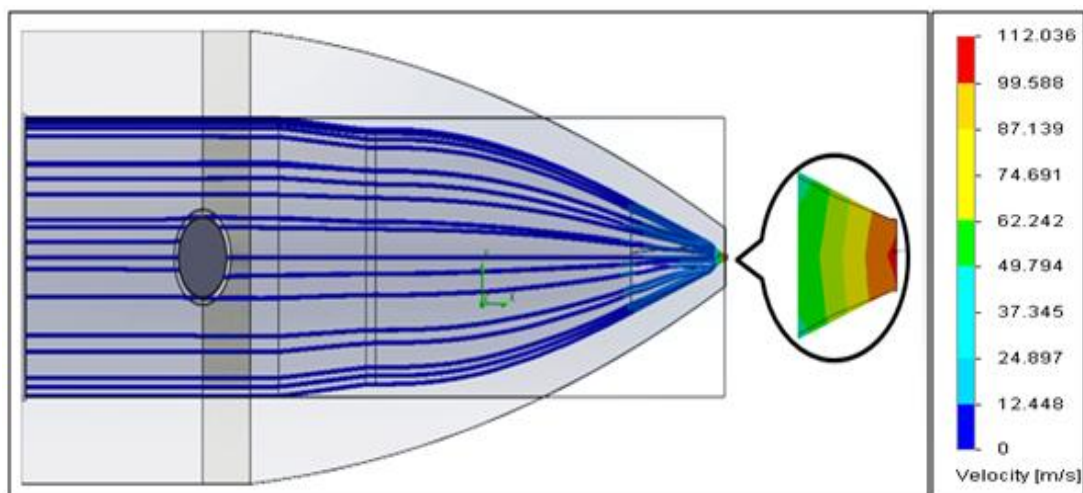


**Figure 5.17: Plain Nozzle Flow Streamlines (Flow Trajectories)**

No.	Input Parameters	Values
1.	Inlet Flowrate	50 L/min = 0.85 kg/sec
2.	Secondary Inlet flowrate	No Hydrofoil
3.	Nozzle exit Opening Dimensions	10 mm x 0.5 mm x 40 mm (Rectangular Slot)
4.	Nozzle Inlet Diameter	35 mm
5.	Fluid Type	Water
6.	Outlet Pressure	Static Pressure

**Table 5.2: Nozzle Input Parameters**

The flow in the main nozzle was studied with and without the nested nozzle and the pressure cone. Fig 5.17 shows the flow profile in the empty main nozzle with no nested and hydrofoil with a rectangular exit slot. A fully developed flow stream is observed with the exit jet reaching 112 m/s. This nozzle produced a clean laminar flow with no turbulence and nor recirculation. The shape of the exit has a smooth transition to the converging main nozzle and does not generate cross flow and turbulence. Therefore, this nozzle cavity is seen as good enough to serve its purpose and will be modified only to help improve the effect of pressure cone.

#### 5.10.4 Nozzle with Pressure Cone (No-Hydrofoil)

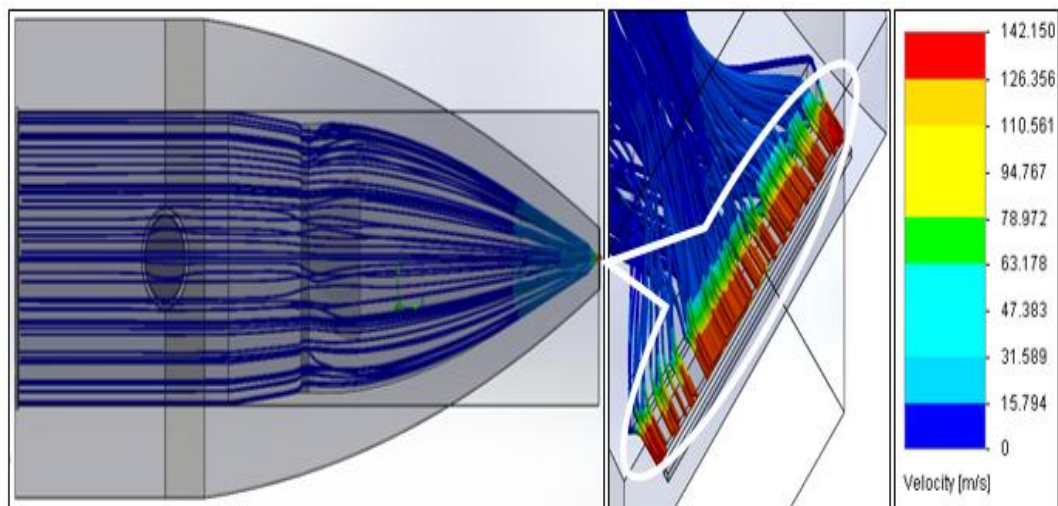


**Figure 5.18: Flow Trajectories of Nozzle with Cone**

Fig.5.18 is the performance of main nozzle after introducing the pressure. It is seen that the pressure cone does not disturb the flow and turbulence is not generated. However, this simple device increased the exit jet velocity from 112 m/s up to 142 m/s with the same flow rate. This increase is explained by the effect of the size ratio of the main cavity and the cone.

If it is achieved an increase of over 25% in jet velocity by introducing a pressure cone, this means that with a proper design one could effectively reduce the flow rate, proportionally keeping the high target jet velocity.

### 5.10.5 Nozzle Simulation with Hydrofoil (No-Cone)

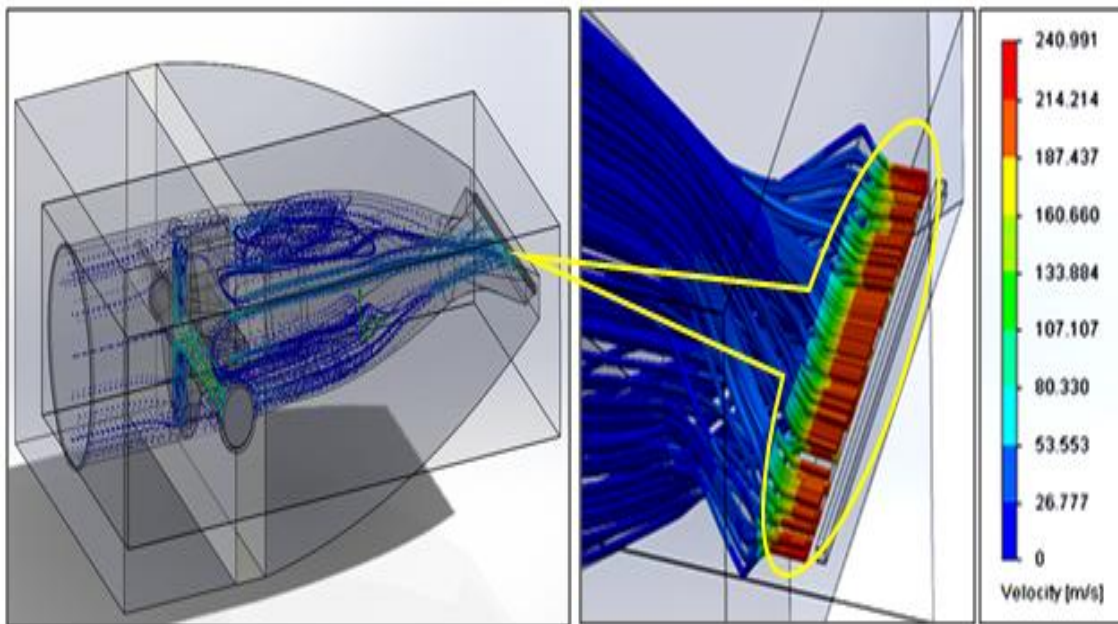


**Figure 5.19: Velocity Streamline of Nozzle with Hydrofoil**

Fig.5.19 shows the flow trend in the main nozzle when the nested nozzle is supplied with a secondary flow. It is seen that at the immediate exit of the nested nozzle, the two flows mix up causing recirculation before exiting the main nozzle at a velocity exceed 200 m/s. The recirculation is generated by the 9 prismatic jets of the nested nozzle because these jets flow at high velocities (119 m/s) and meet with low speed main stream ( $< 26$  m/s). The high speed jets are decelerated while trying to speed up the main flow. This causes the flow from the nested nozzle to back off forming a whirlpool.

Though the jet velocity reached 240 m/s at the nozzle exit due added flow, it is observed that the location of the secondary nozzle did not provide the expected effect. The recirculation, however gives room for further exploitation in the development of a modular multipurpose nozzle, where the whirlpool could be used to achieve a homogenous mixture of air and oil in MQL application. Therefore this initial model leads to two applications namely conventional and MQL lubrication.

### 5.10.6 Nozzle Simulation with Pressure Cone and Nested Nozzle

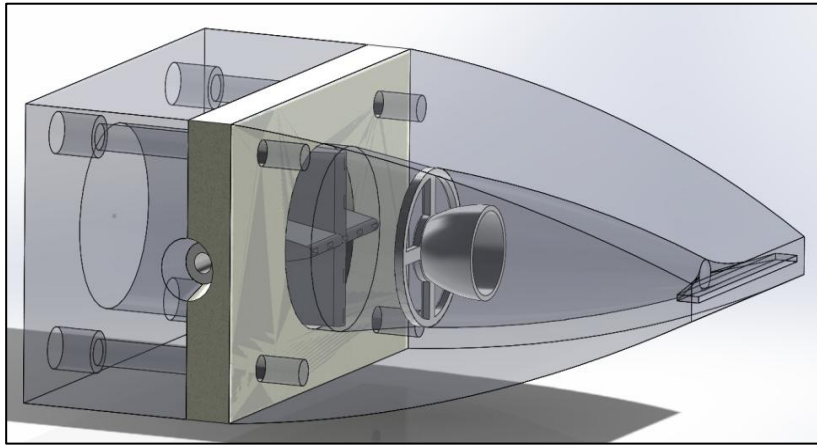


**Figure 5.20: Assembly Model**

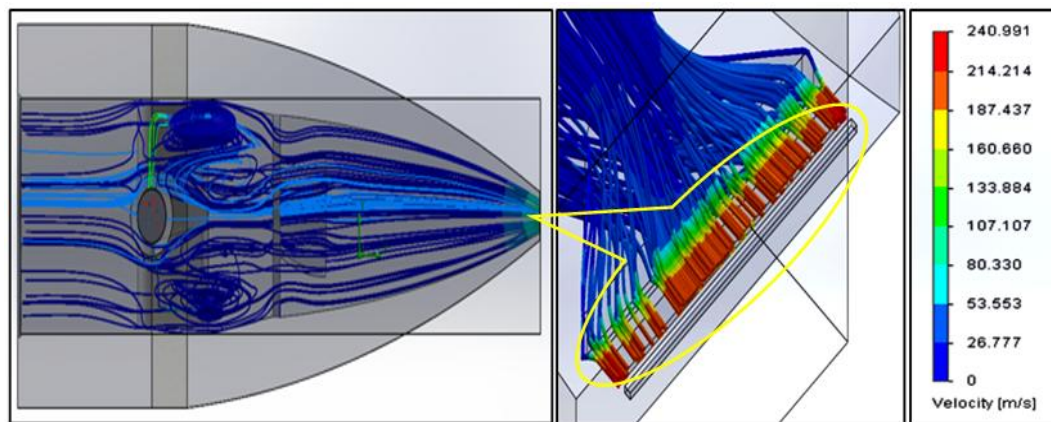


**Figure 5.21: Dual flow system with hydrofoil and Pressure Cone**

Fig 5.20 depicts the assembly model and Fig 5.21 presents the behaviour of the flow in the system with all its components in place and with the fluid being supplied to both main and nested nozzles. The velocity profile shows that in dual flow, the introduction of the pressure cone does not bring a net gain. This may be due to the increased internal pressure in the main nozzle cavity caused by the secondary flow, which dwarfs the effect of the pressure cone. This result points to the need of improvement and optimisation of the design. Two design iterations were undertaken and the comparative results are given in the table below, where a clear improvement of the system is observed.

No.	Components	Flow rate	Basic design	Improved design
1.	Main Nozzle Only	50 l/min	109.116 m/sec	112.036 m/sec
2.	Nozzle with Pressure cone	50 l/min	138.013 m/sec	142.150 m/sec
3.	Nozzle with Hydrofoil	50 l/min	238.190 m/sec	240.970 m/sec
4.	Full model simulation	50 l/min	231.897 m/sec	240.991 m/sec

**Table 5.3: Comparative Results with Water**

As in other case the nozzle with hydrofoil with rectangular exit slots, a laminar flow is observed in the nozzle cavity up to the exit. The model is designed in such a way to create a high pressure in the nozzle chamber to secure high exit velocity. However, in the configuration for the air as fluid in MQL turbulence and recirculation is desired to provide a good mixture of air with oil droplets before exiting the nozzle. This is observed in this nozzle with some increased velocity. Modifying the nozzle exit and extending the length of the cavity showed better performance.

#### 5.10.8 Nozzle Simulation for MQL

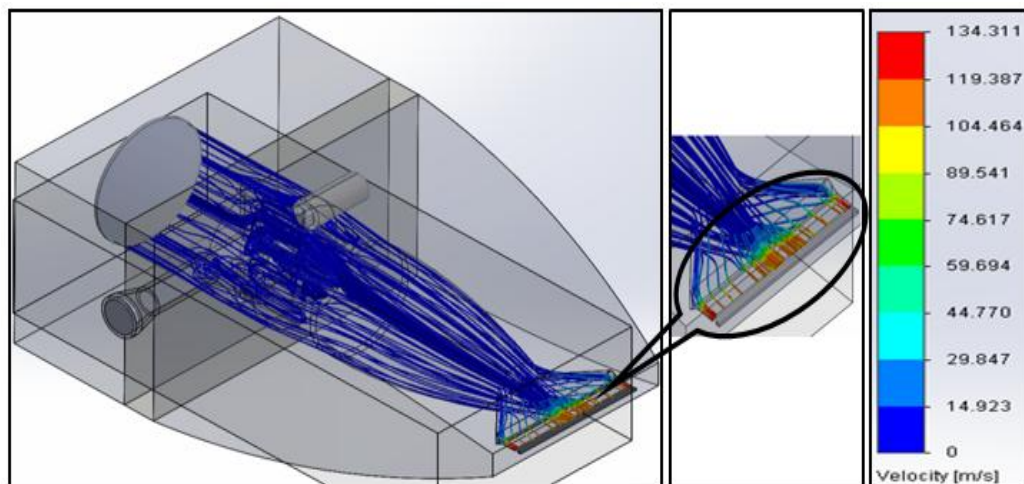


**Figure 5.22: Flow Profile with Air as Fluid for MQL**

Fig.5.22 shows the results of the simulation with air as fluid. Here, the flow of the oil is neglected as it supplied in minute quantity of droplets. The fully developed flow of air exits the nozzle at a velocity exceeding 120 m/sec. The recirculation help to mix the oil with the air thoroughly before the mixture exits the nozzle. This result shows that it is possible to use this new modular nozzle for both flood and MQL applications.

### 5.10.9 Nozzle with Hydrofoil and Curved-Shape cone

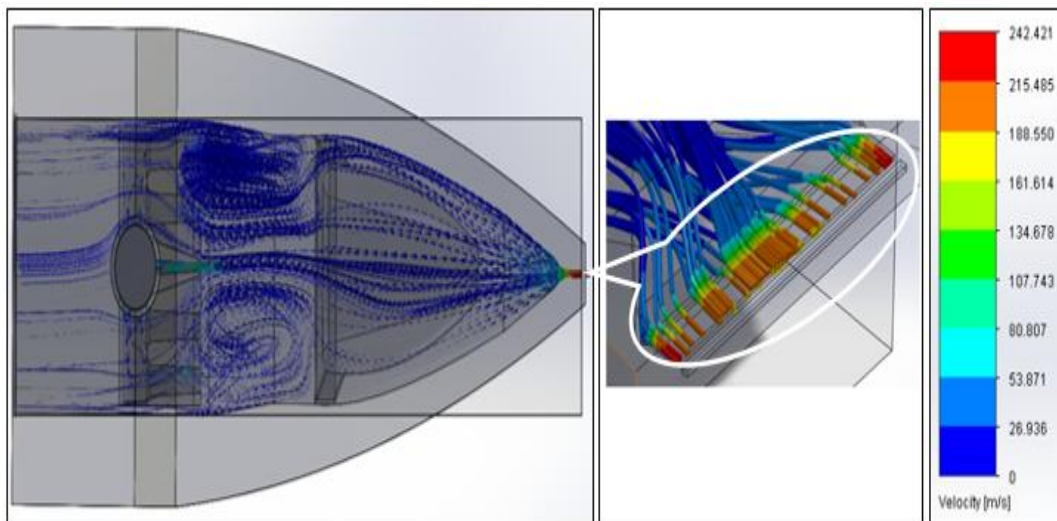


**Figure 5.23: Turbulence near Hydrofoil**

The simulation results of nozzle with hydrofoil and curved shape cone is presented in Fig 5.23. Here, turbulence is occurred in between the hydrofoil and cone. It is observed that normally the hydrofoil creating turbulence after immediate exit of rectangular slots, but in this case the cone has through hole in its centre is creating pressure inside the nozzle cavity but the above the cone it seems that the flow is laminar form. Hence the cone needs some further improvement by removing the hole at its centre to become complete solid block in order to increase the pressure in cavity.

### 5.10.10 Full Design Iterations

It is assumed that to be good design when the volumetric flow rate of the fluid at the inlet is same and the result of maximum fluid velocity at the outlet, it is then considered

as the better design compared with the previous nozzle designs to achieve this research work objective. The results obtained after the modifications in the improved design.

According to the results obtained, the fluid passing through the improved design has the highest velocity at the outlet nozzles compared with the previous design. The fluid in the improved design is accelerated faster, thus the maximum velocity is gained at the outer nozzle. The flow condition is affected by the length of the convergence area; therefore the smaller the divergence area the highest the flow velocity can be obtained. The length with the constant diameter does influence the maximum velocity at the nozzle, but the length of convergence area has a much stronger effect on it. It is shown that the improved design has the higher fluid velocity because velocity increased when outlet cross section gradually decreased according to the equation  $Q = VA$ .

Where;  $Q$  = volumetric flow rate,  $A$  = area and  $V$  = velocity.

However at this early stage of this investigation, the position of the pressure cone relative to the nested nozzle is not well defined yet; thus further simulations are needed in order to optimise the design. This new concept shows a complex structure set to develop a new generation of low volume at increased pressure generated by internal inserts in the main nozzle cavity achieve high exit jet velocity. However at this conception stage, the design for manufacture has not been taken into account, only the flow process is of interest, therefore nozzle dimensions are not finalised.

## 5.11 Types of Internal Nozzle Cavity profiles

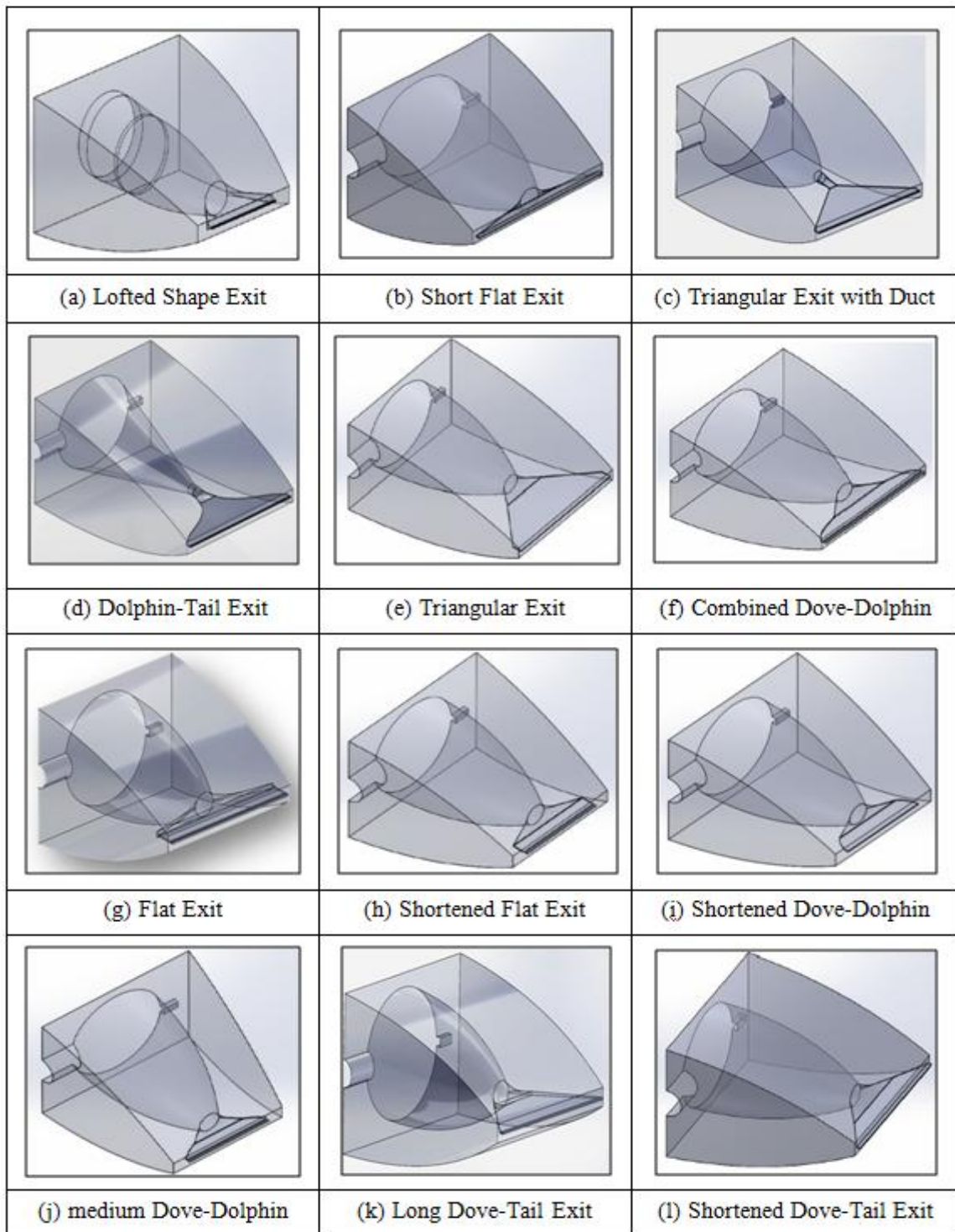


Figure 5.24: Nozzle Exit and Cavity Profiles

The nozzle chamber design-1 Fig.5.24 (a) has a flat exit with 15-mm in length, 0.5-mm Exit opening and 40-mm in exit width. The exit profile is designed like a lofted to allow fluid to develop very smoothly. The opening of nozzle of 0.5 mm will allow the flow to achieve high velocity due to the generated high pressure by the nested nozzle. The exit profile of the nozzle in Fig.5.24 (b), (d) and (e) is designed following the flow profile obtained in the initial CFD simulation. This profile is derived from the velocity cut plots the fluid flow that depict the flow pattern formed in the horizontal plane of the nozzle. The nozzle cavity is also changed into a conical shape and a throat between nozzle cavity and nozzle exit is round. In design (c), nozzle chamber is separated from the exit with an extended circular duct, with the intension to pressurise further the fluid before its diversion in the exit cavity. The nozzle exit opening is 0.3 mm. In the design (k) in Fig.5.24 the exit profile has been modified into long dovetail shape because as flow comes from high volume to a narrow passage where the velocity increases. Consequently, the exit profile is designed in diverged shape in order to cover the entire wheel width. The designs Fig.5.24 (f), (g), (h), (i), (j) are modified followed by trimming the edges to converge its shape to fully develop flow in the exit cavity. Fig.5.24 Design (l) is the converged final actual shortened Dove-tail model. The simulations and optimisation of these nozzle exits showed in appendix-1.

### 5.12 (Set-1) Study of Conical-Shape Nested Nozzle

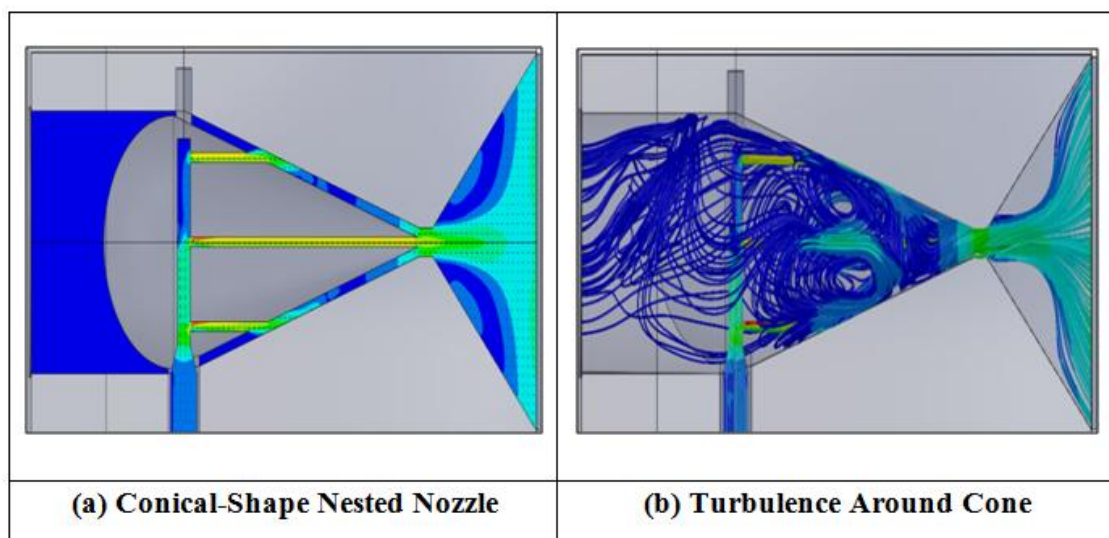
To replicate the fluid application used in some aerospace processes, 120 litre/min was used as baseline. A series of simulation were carried out with different flow rates in the range of 120 litre/min to 60 litre/min with increments of 20 lit/min. for example a 120 lit/min supply is split into 90 lit/min for main inlet flow and 30 lit/min for nested flow rates.

In the attempt to reduce manufacturing time and cost, a simplified form of the pressure cone was considered, i.e. a simple cone with spherical base. The simulations showed a rather interesting behaviour with no direct applications.



**CFD Input Data**

No.	Input Parameters	Values
1.	Main Inlet Flow	30 litres/min
2.	Nested Inlet Flow	70 litres/min
3.	Cone Type	Conical Shape with 5-Outlets
4.	Fluid Type	Water
5.	Phase	Dual
6.	Nozzle Exit Cavity	Triangular Exit
7.	Nozzle Exit Aperture (Opening)	0.3 mm x 40 mm

**Table 5.4: (Set-1) CFD Input Parameters****Figure 5.25: Conical-Shape Nested Nozzle with Triangular Exit**

The nozzle configuration with conical pressure cone and the dovetail exit profile did not perform as expected. The conical shape through with spherical base generated a head resistance causing immediate turbulence when the fluid hits cone, though a coanda effect was expected by attaching the fluid to the cone. The fluid existing from the nested flow created a further recirculation of the fluid, which swirled in the throat. However, in the exit cavity, it is observed that Dolphin-tail shape is formed, in Fig 5.25 (b). It is also

observed that a high-pressure zone is formed in the centre of the exit aperture. This can be explained the fact that the fluid attached itself to the wall of the nozzle exit and this could lead to increased pressure in the middle.

### 5.13 (Set-2) Conical-Shape Nozzle with Dolphin-Tail Exit

#### CFD Input Data

No.	Input Parameters	Values
1.	Main Inlet Flow	30 litres/min
2.	Nested Inlet Flow	70 litres/min
3.	Cone Type	Conical Shape with 5-Outlets
4.	Fluid Type	Water
5.	Phase	Dual
6.	Nozzle Exit Cavity	Dolphin Tail Exit
7.	Nozzle Exit Aperture (Opening)	0.3 mm x 40 mm

**Table 5.5: (Set-2) CFD Input Parameters**

The same CFD input data is applied to this Conical-shape with Dolphin-Tail model

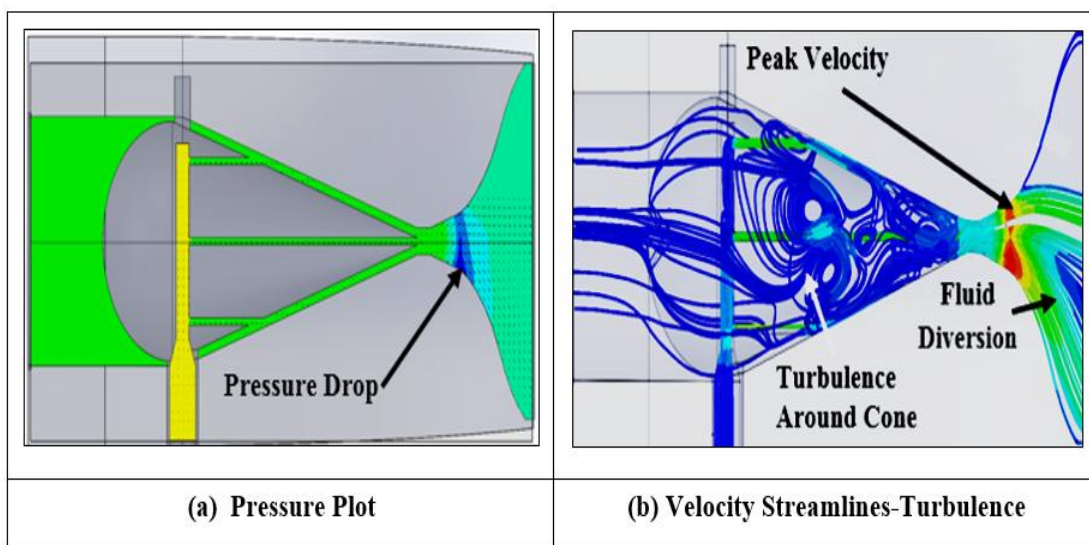


**Figure 5.26: Performance of Dolphin tail Profile with 100 litres/min (30/70 l/min)**

As the flow streamlines indicated the preferable fluid flow pattern in a shape of dolphin tail, thus then nozzle exit cavity was reshaped to match this profile. However, using the same flow parameters as in previous simulation, the results obtained were not conclusive. The pressure profile depicted in Fig 5.26 (a) shows an uneven pressure drop in the nozzle throat. It is thought that the triangular shape of the pressure cone could have led to the way of the fluid flow to one side of the nozzle, which is accentuated by the swirl of the fluid in the throat. This is illustrated in Figure 5.26 (b). The turbulence created by the conical pressure cone can be exploited in MQL application using dovetail exit as this would allow for a better mixing of oil before exiting the nozzle.

#### 5.14 (Set-3) Nozzle with Egg-Shaped Pressure Cone (Nested Nozzle)

In this section the nozzle optimisation process is presented in detail with design set wise from initial stage to final stage. The egg shaped pressure cone is designed in such a way to increase the pressure inside the nozzle chamber with some gap in between the internal cavity wall surface and external surface of the cone. The pressure cone which has five straight fit exit outlet holes designed in a cross-shape and each diameter hole of 1.5 mm. The pressure cone is optimised for internal and external dimensions by simulating only cone to achieve good design and later is simulated the whole component by placing inside the nozzle chamber.

#### CFD Input Data

No.	Input Parameters	Values
1.	Main Inlet Flow	30 litres/min
2.	Nested Inlet Flow	70 litres/min
3.	Cone Type	Egg Shape with 5-Outlets
4.	Fluid Type	Water
5.	Nozzle Exit Cavity	Dove Tail Exit
6.	Nozzle Exit Aperture (Opening)	18 mm x 0.3 mm x 40 mm

**Table 5.6: (Set-3) CFD Input Parameters**



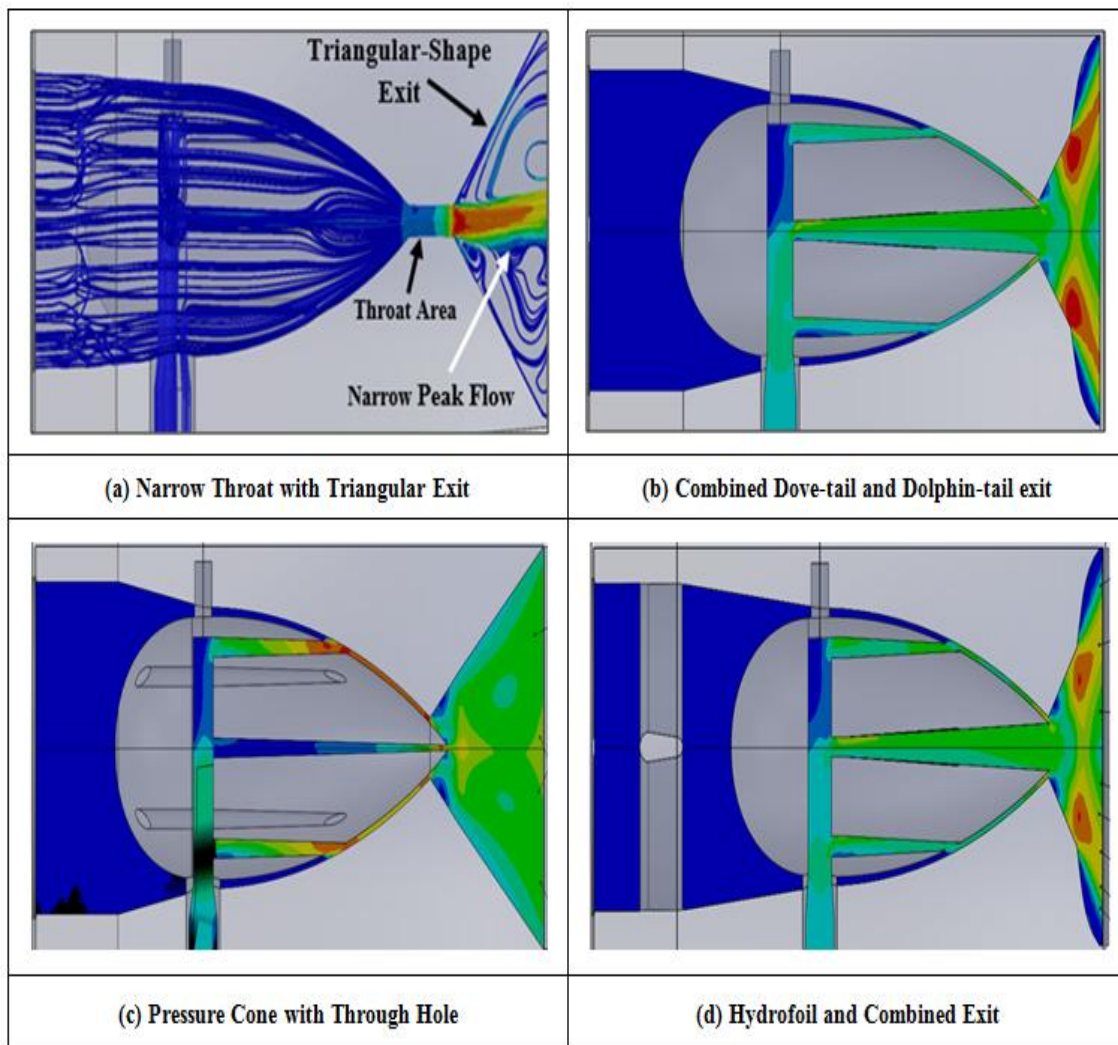


**Figure 5.27: Other Nozzle Exit Profiles**

The profile in Fig 5.27 (a) was developed to overcome the cross firing explain simulation (Set-6). However, the fluid in the exit cavity simply stagnated and only the middle core achieved higher velocity. Therefore the design was also removed from further investigation. The profile in Fig 5.27 (b) and (d) are same except a hydrofoil is added at the rear side of the nozzle; and it shows another version of combined dovetail and Dolphin tail, where high velocities are observed at the edges of the dovetail profile. However, the velocity profile varies along the nozzle width with low velocity in the middle. Consequently, this nozzle was rejected from further studies. Fig 5.27 (c) is

same as dove tail design except the cone is modified with through holes in order to increase the flow rate but the result of this design also same as the design in set-6.

### *Simulation setup*

#### **5.15 (Set-4) Nozzle with Pressure Cone (Dual Flow)-Flat Exit**

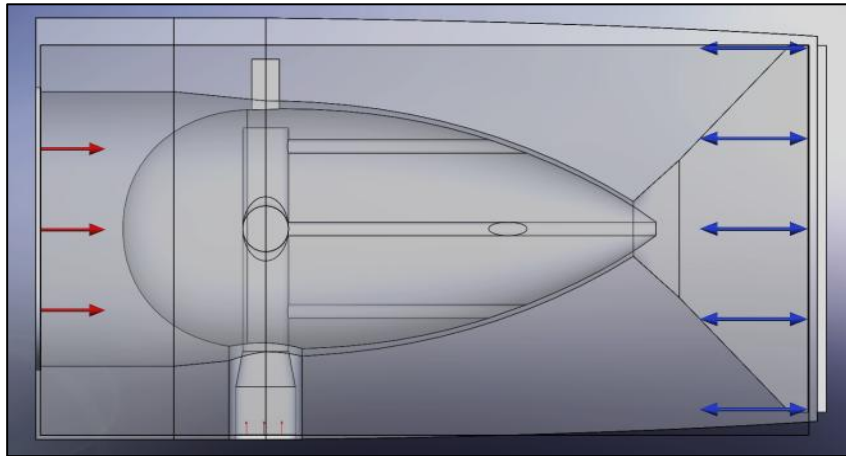


**Figure 5.28: Simulation Setup**

#### **CFD Input Data:**

No.	Input Parameters	Values
1.	Main Inlet Flow	30 litres/min
2.	Nested Inlet Flow	90 litres/min
3.	Cone Type	Egg Shape with 5-Tapered Outlets
4.	Fluid Type	Water
5.	Phase	Dual
6.	Nozzle Exit Cavity	Flat Exit
7.	Nozzle Exit Aperture (Opening)	5 mm x 40 mm x 0.3 mm

**Table 5.7: (Set-4) CFD Input Parameters**

The above Fig 5.28 illustrates the simulation setup with the exit boundary condition set at static pressure.

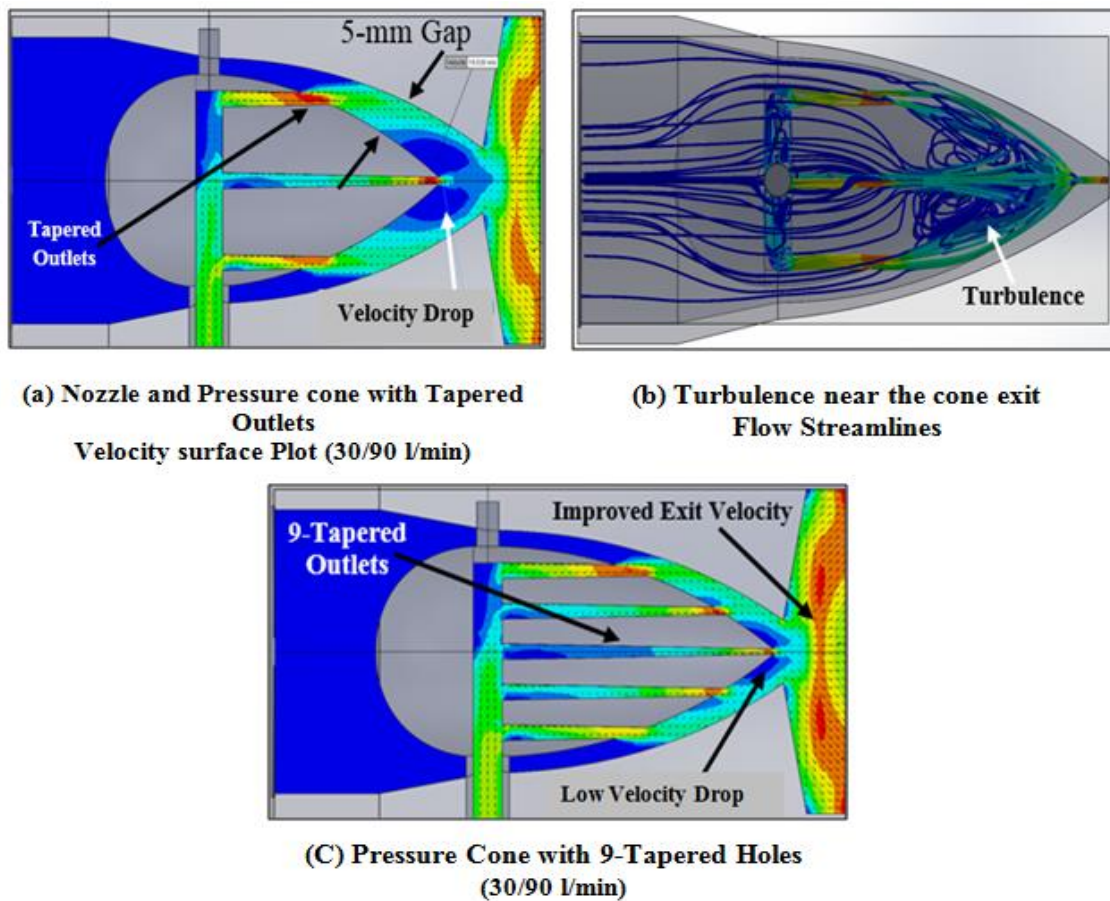


**Figure 5.29: Design-1 (30/90 l/min) with 5-mm gap between cone and main nozzle**

The nozzle has a flat exit with 15-mm in length, 0.5 mm opening and 40-mm in width. The exit profile is designed like a lofted to allow the flow to smoothly develop. The opening of 0.5 mm allows the flow to achieve high velocity due to the generated high pressure by the nested nozzle. The results in the above Fig 5.29 (a) nozzle with flat exit of flow rate (30/90 l/min) with 5-mm gap between cone and main nozzle, shows that the idea of accelerating the low flow using a nested nozzle works in principle. It is observed that the flow is accelerating at the exit of the nested nozzle at about 145 m/s and keeps this velocity until a further acceleration at final exit. In Fig 5.29, it is seen that the existing fluid from the nested nozzle attached itself to the wall of main nozzle cavity and lead to a recirculation volume around the tip of the pressure cone. This is caused by the large gap (5-mm) in between the pressure cone and the internal wall of the main

nozzle. The turbulence and recirculation is a desired effect for MQL application to allow oil droplets to mix very well with air vortexes before exiting. However, for flood coolant application this is resolved by controlling the gap between the two bodies. This offers a controlling tool for adjustment in this universal modular design approach. In Fig 5.29 (c) it is observed that with increase of cone internal outlets from 5 to 9, the flow is accelerating on both exits of the nozzle i.e. nested nozzle exit and main nozzle exit reached at about 155 m/s, compared to the previous model with Fig 5.29 (a) the flow in the main exit is improved and a little bit converged peak velocity also seen in the main exit. Another observation is that a low velocity drop appeared between the cone and main exit.

#### 5.16 (Set-5) Nozzle with 1-mm Gap between Cone and Main Nozzle (Dual Flow)

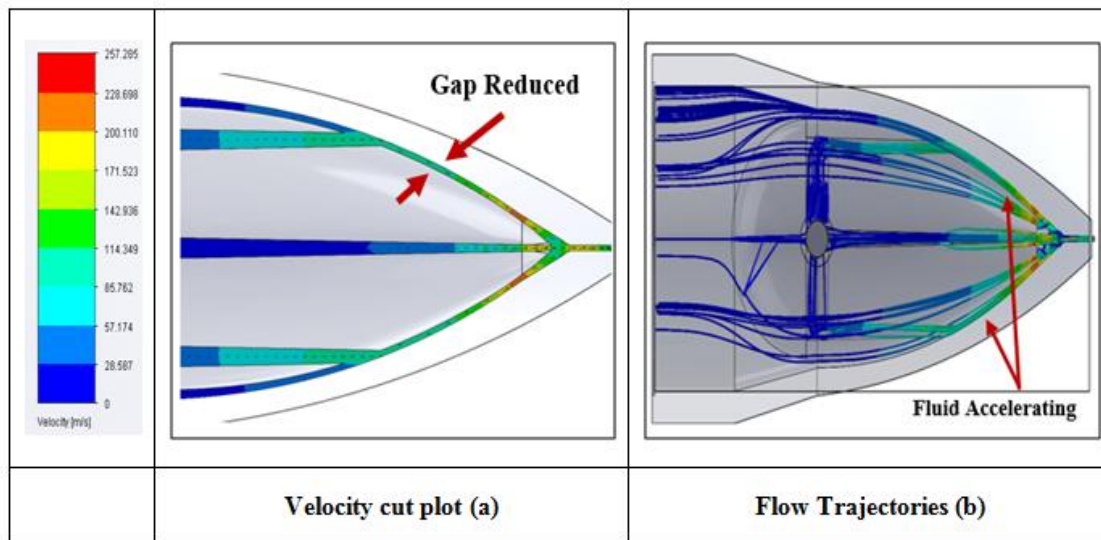


**Figure 5.30: Design-2 (120-l/min) with 1-mm gap between the cone and main nozzle**

The same CFD input data is applied to this nozzle, the recirculation and stagnation zones encountered in design Fig.5.25 (Set-1) are resolved by reducing the gap between the nested nozzle and the main nozzle cavity. Consequently, in Fig 5.30 neither turbulence nor recirculation is observed. It is seen that a gap of 1mm provided the desired performance hence this will be used in further design iterations.

**5.17 (Set-6) Nozzle with Pressure Cone (Dual Flow)-Flat Exit**

**CFD Input Data:**

No.	Input Parameters	Values
1.	Main Inlet Flow	30 litres/min
2.	Nested Inlet Flow	70 litres/min
3.	Cone Type	Egg Shape with 5-Tapered Outlets
4.	Gap between cone and cavity	1-mm
5.	Fluid Type	Water
6.	Phase	Dual
7.	Nozzle Exit Cavity	Flat Exit
8.	Nozzle Exit Aperture (Opening)	5 mm x 40 mm x 0.5 mm

**Table 5.8: (Set-6) CFD Input Parameters**

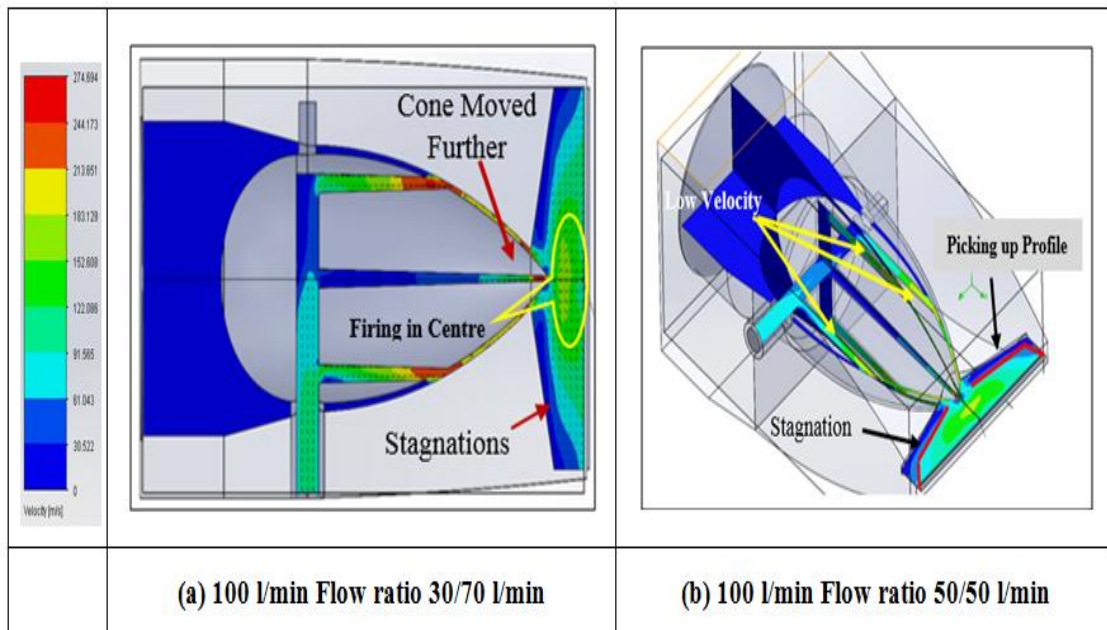


**Figure 5.31: Nozzle with Flat Exit of 1-mm gap between the cone and main nozzle**

In this design the pressure cone is moved further close to the nozzle exit chamber. Here, the focus was translated onto the nozzle exit profile. Fig 5.31 (a) shows how this design distributes the flow evenly to cover the required wheel. This simulation was performed with two different inlet flow i.e. 30 litre/min into main nozzle and 70 litre/min in the nested nozzle, and equal flow in the two inlets 50-50 litres/min where a slight increase in exit jet velocity was observed illustrated in Fig 5.31(b). However, as revealed in CFD simulation, the velocity profile is not even, and it is observed that the exit velocity has increased but regions of stagnations are formed along the walls of the exit cavity. This is due to the fluid attaching itself to the back walls of the exit cavity caused angle at two edges of the exit slot. Using these results, the profile of the exit cavity was modified to fit the profile of flow streamlines that had no stagnation. This leads to the nozzle design in Fig 5.32 (a).

#### **5.18 (Set-7) Nozzle Cone Shortened Flat Exit (Single Flow)**

The nozzles 5.32 (a) to (d) is performed with 1-mm gap, single phase flow (no fluid in nested nozzle) with flow rate of 50 litres/min. In this optimisation, the nozzle exit is modified with various forms of edges illustrated in above Fig 5.32. The formation of this converged nozzle exit is investigated in a series of modifications and simulations performed on each exit design. The exit design of Fig 5.32 (b) is shortened exit profile chosen from Fig 5.31 (b) because in this case the fluid is attached to walls of the internal exit forming stagnations. Therefore by shortening this nozzle exit and picking the exact flow profile a new converged nozzle is derived. Other nozzle exit profiles were explored these are the variation of dovetail and Dolphin tail.

It is also observed that the profile in Fig 5.32 (c) performed very well providing high exit velocity over entire width of the nozzle. It is concluded that by trimming the edges on both sides of the nozzle to remove stagnation areas and shortening the length by a few millimetres could result in uniform jet velocity. Fig 5.32 (e) the same nozzle is studied with dual flow with flow ratio of 30litres/min in main inlet and 50 litres/min in nested inlet flow.



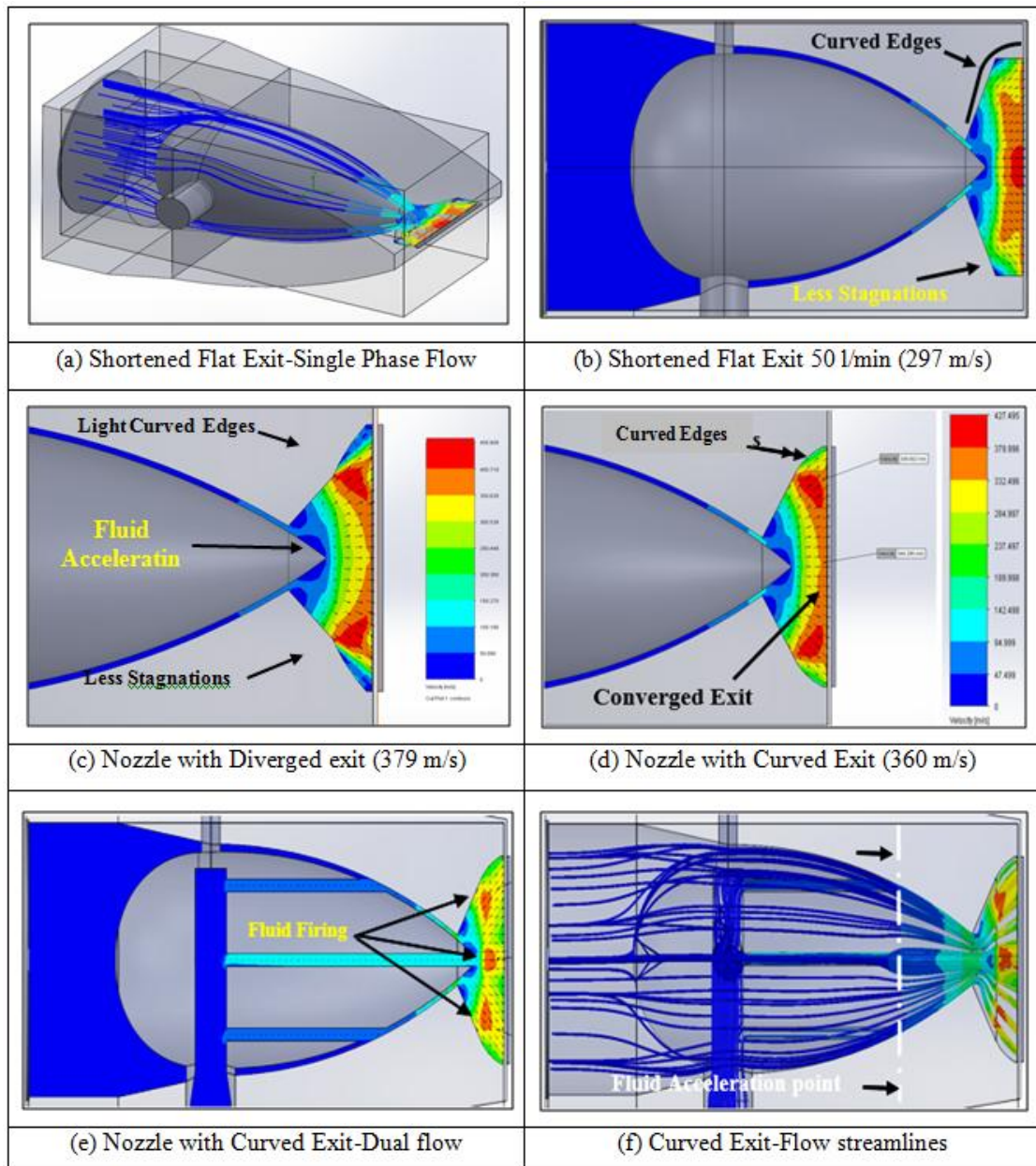


**Figure 5.32: Nozzle with Modified Exit (30/50 litre/min-Single Phase Flow)**

In this case the fluid is firing with peak velocity in the exit this is mainly due to the nested flow effect, in the Fig 5.32 (d) the velocity near the cone exit is dropped; in this case there is no nested flow as in the case of Fig 5.32 (e) a small drop in velocity appeared. It is understood that the fluid in the cone (internal outlets) pumping more velocity after immediate exit of the cone and this fluid after entering the main exit it is

cross-firing. In this simulation it is observed that the fluid acceleration point is starting earlier as shown in Fig 5.32 (f). Still this model needs further modification until its reach the nozzle exit convergence.

**5.19 (Set-8) Nozzle with Cone Dolphin-Tail Exit (Dual Flow)**

**CFD Input Data**

No.	Input Parameters	Values
1.	Main Inlet Flow	30 litres/min
2.	Nested Inlet Flow	70 litres/min
3.	Cone Type	Egg Shape with 5-Tapered Outlets
4.	Gap between cone and cavity	1-mm
5.	Fluid Type	Water
6.	Phase	Dual
7.	Nozzle Exit Cavity	Dolphin Tail Exit
8.	Nozzle Exit Aperture (Opening)	5 mm x 40 mm x 0.5 mm

**Table 5.9: (Set-8) CFD Input Parameters**

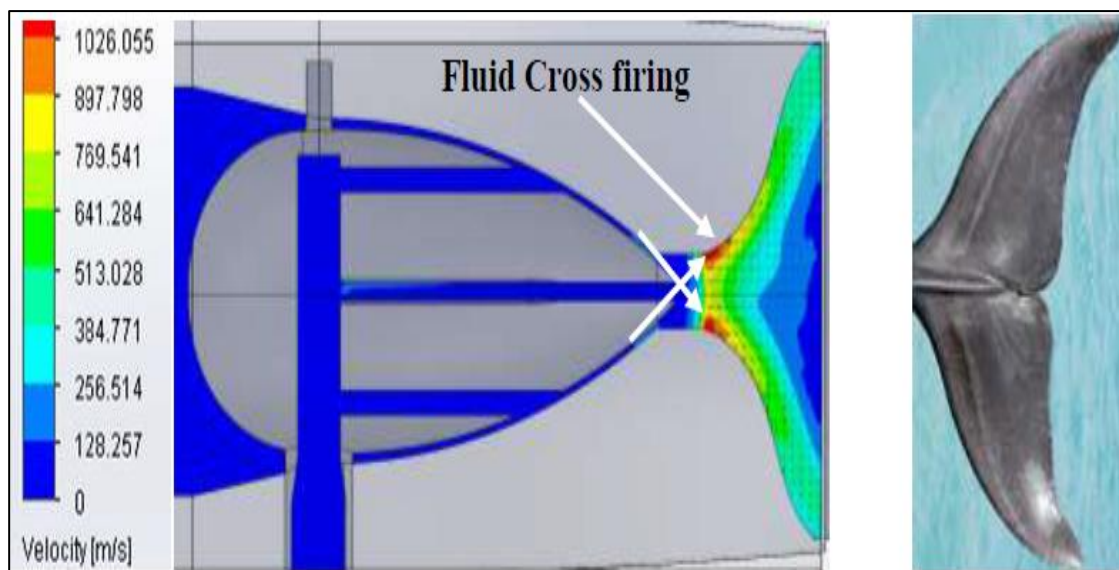


**Figure 5.33: Performance of Dolphin-Tail Exit 100 litres/min (Flow ratio 30/70)**

Following the streamlines in the preliminary simulation, it was observed that in the exit cavity, the previously observed Dolphin-tail profile was formed again (see Fig 5.25 (b)). Thus this profile was investigated and the above Fig 5.33 shows that an area of low velocity is created in the middle of the nozzle, which is similar to the median notch in Dolphin-tail. Extremely high velocities are reached at the wall towards the exit of the throat. These extreme velocities are at the area where the jet lands flowing tangentially to the cone. This higher velocity creates low pressure at the exit of the nozzle and the fluid attaches itself to the walls and low velocity fluid is gathered in the middle of the nozzle. Therefore in order to employ this profile the throat must be shortened to allow a uniform acceleration of the fluid.

### **5.20 (Set-9) Nozzle with Cone Dove-Tail Exit (Dual Flow)**

#### ***Principle of Acceleration Using Dual Flow***

It is observed that in below Fig 5.34 (a) nozzle no-cone the fluid comes at low velocity in the main nozzle up to the throat and fluid velocity increased after immediate exit of the aperture. Fig 5.34 (b) nozzle with cone (no-fluid in nested cone) here, also same cone the fluid comes at low velocity in the main nozzle once the low velocity fluid reaches the nested nozzle, the fluid inside the cavity pressurises tends to increase the exit velocity. Fig 5.34 (c) nozzle with cone (dual phase) in the main nozzle once the low velocity fluid reaches the nested nozzle it acquires additional momentum from the jets of the nested nozzle and an initial acceleration begins. The fluid is then fully accelerated up to the velocity of the fluid from the nested nozzle. The streamlines in Fig 5.34 (c) neither recirculation nor backward flow is showed. However, in Fig 5.34 (b), where the total amount of fluid in supplied to the main nozzle, it is seen that the fluid stays at low velocity and does not accelerates until after the throat. Also low velocity is generated in the middle of the nozzle, and the average velocity at the exit is lower than the velocity in Fig 5.34 (c). Fig 5.34 (b) shows the effect of the insertion of the cone. A net fluid acceleration is observed. Therefore, this result shows the advantage of splitting the fluid in dual flow and the use of nested nozzle with pressure cone.

**CFD Input Data**

No.	Input Parameters	Values
1.	Main Inlet Flow	30 litres/min
2.	Nested Inlet Flow	70 litres/min
3.	Cone Type	Egg Shape with 5-Outlets
4.	Gap between cone and cavity	1-mm
5.	Fluid Type	Water
6.	Nozzle Exit Cavity	Dove Tail Exit
7.	Nozzle Exit Aperture (Opening)	15 mm x 40 mm x 0.3 mm

**Table 5.10: (Set-9) CFD Input Parameters**

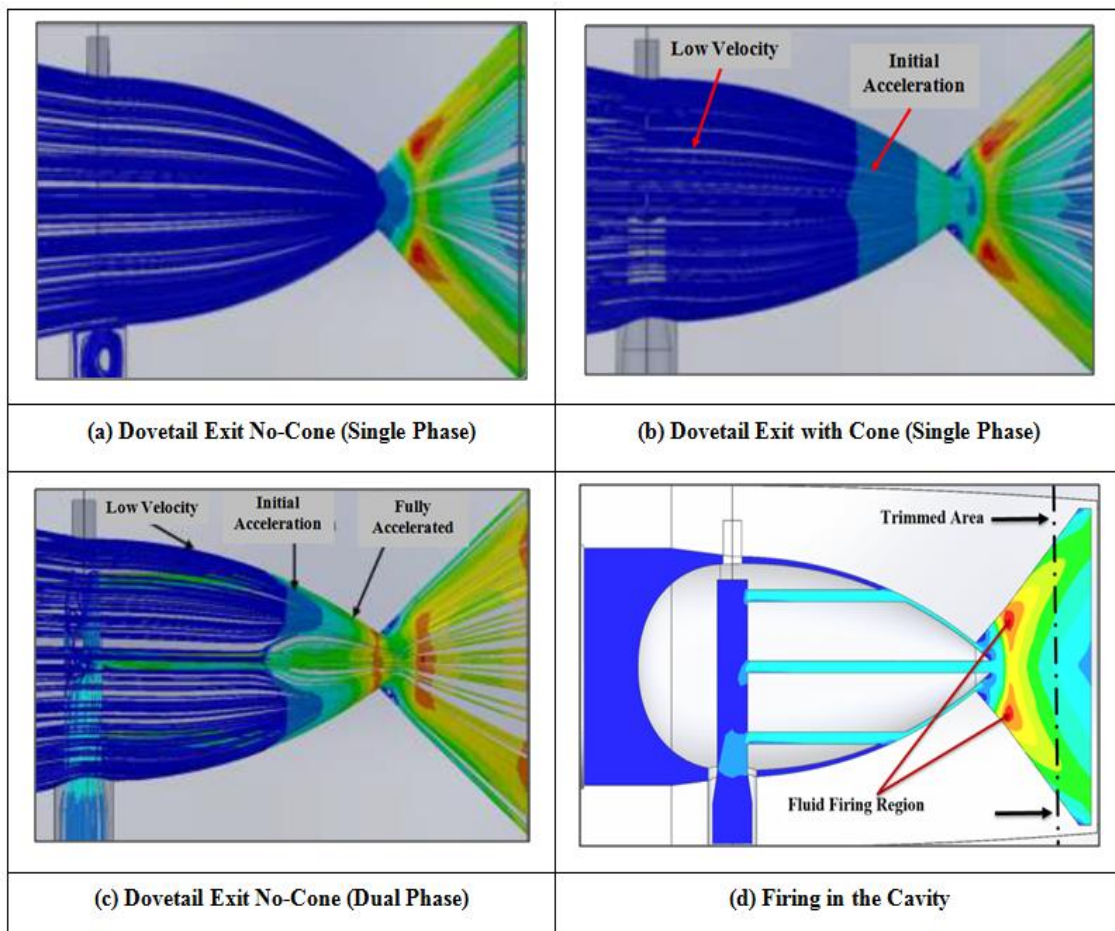


**Figure 5.34: Pressure Developments with cone and without cone**

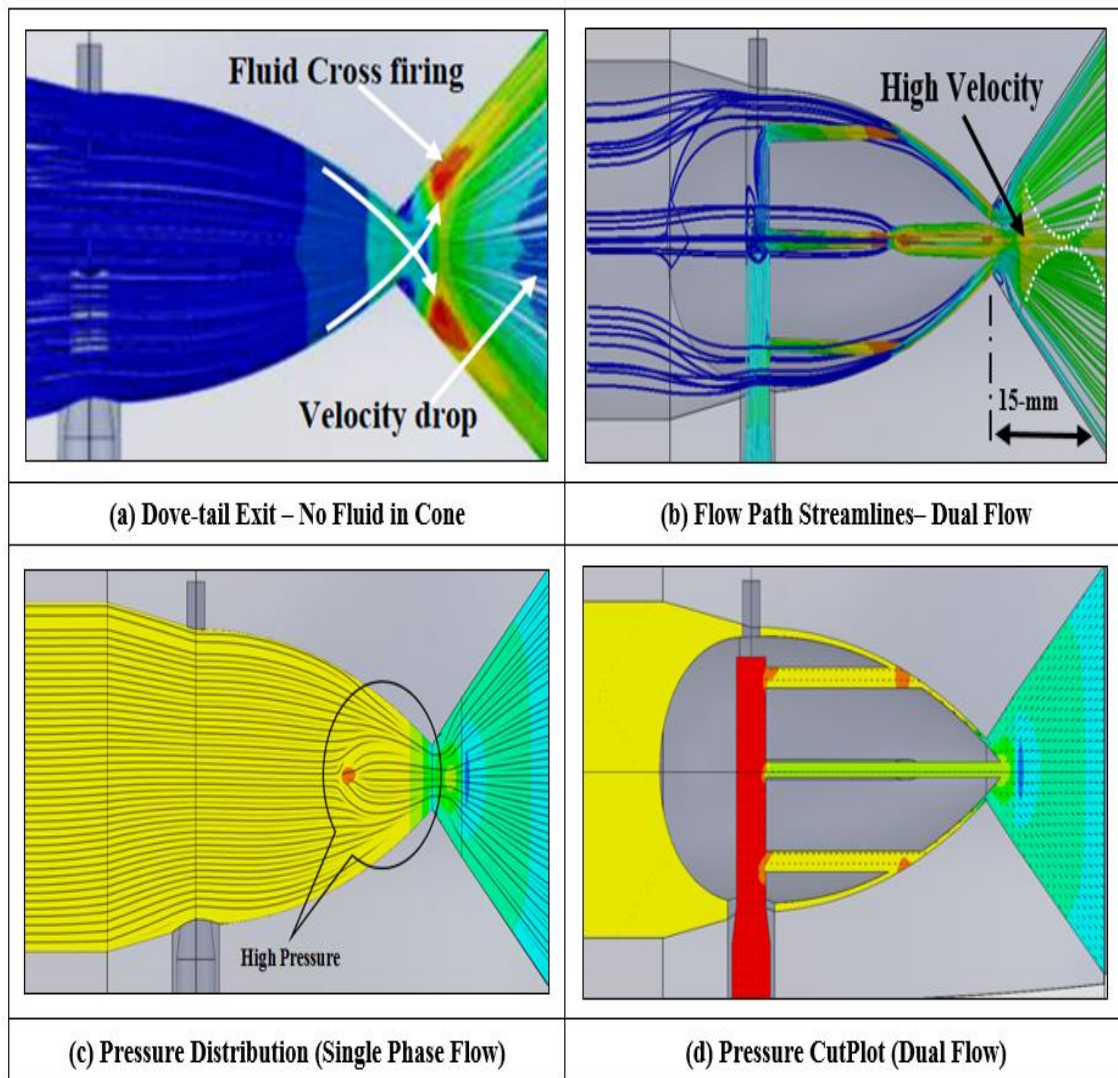


**Figure 5.35: Dove-Tail Nozzles with Cone**

In the attempt to resolve the problem mentioned in ‘Dolphin-tail’ profile, a dovetail shape was investigated. Fig 5.35 (a) shows that the cross-firing of the fluid (see position of arrows) still exist if only the pressure cone is inserted without secondary flow. However, as the secondary fluid is switched on, this problem is resolved as illustrated in Fig 5.35 (b). It is observed that instead of the velocity drop, high velocity appeared in a diamond shape with a repeating pattern, indicated by dotted line in Fig 5.35 (b). Fig 5.35 (c) & (d) shows the pressure distribution in the nozzle where pressures drop is observed in the exit cavity straight ahead of the pressure cone.

### 5.21 (Set-10) A Novel Modular Adaptable Universal Nozzles

This concept will be studied using 3D solid modelling, CFD flow simulation with design and simulation iterations before actual implementation. Here, the nozzle system consists of 6- components that are presented in below.

#### Geometry Model of Nozzle with Egg-Shape Pressure Cone- Dove-Tail Exit

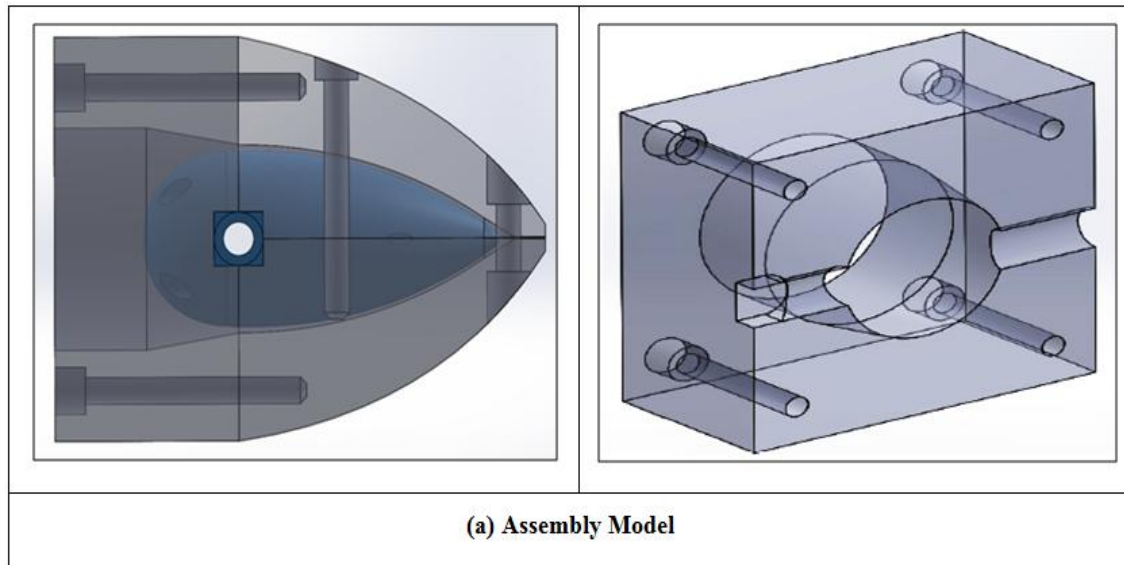


**Figure 5.36: Geometry of Actual Nozzle Model**

#### CFD Input Data

No.	Input Parameters	Values
1.	Main Inlet Flow	30 litres/min
2.	Nested Inlet Flow	50 litres/min
3.	Cone Type	Egg Shape with 5-Outlets
4.	Nozzle Exit Cavity	Dove Tail Exit
5.	Nozzle Exit Aperture (Opening)	10 mm x 40 mm x 0.3 mm
6.	Fluid type	Water

**Table 5.11: (Set-10) CFD Input Parameters**

The Fig 5.36 depicts geometry models of nozzle design, in this part of work, the fluid velocities are explored throughout the profile. This is achieved by sectioning the nozzle using vertical and horizontal planes and recorded the velocities along the nozzle interior cavity. In this investigation reduced flow rate (80 lit/min) is used with a flow ratio of 1/3, meaning that 20 litres in main inlet and 60 litres into nested nozzle inlet. The dovetail profile is employed here with exit dimensions of 10 mm x 40 mm x 0.3 mm.

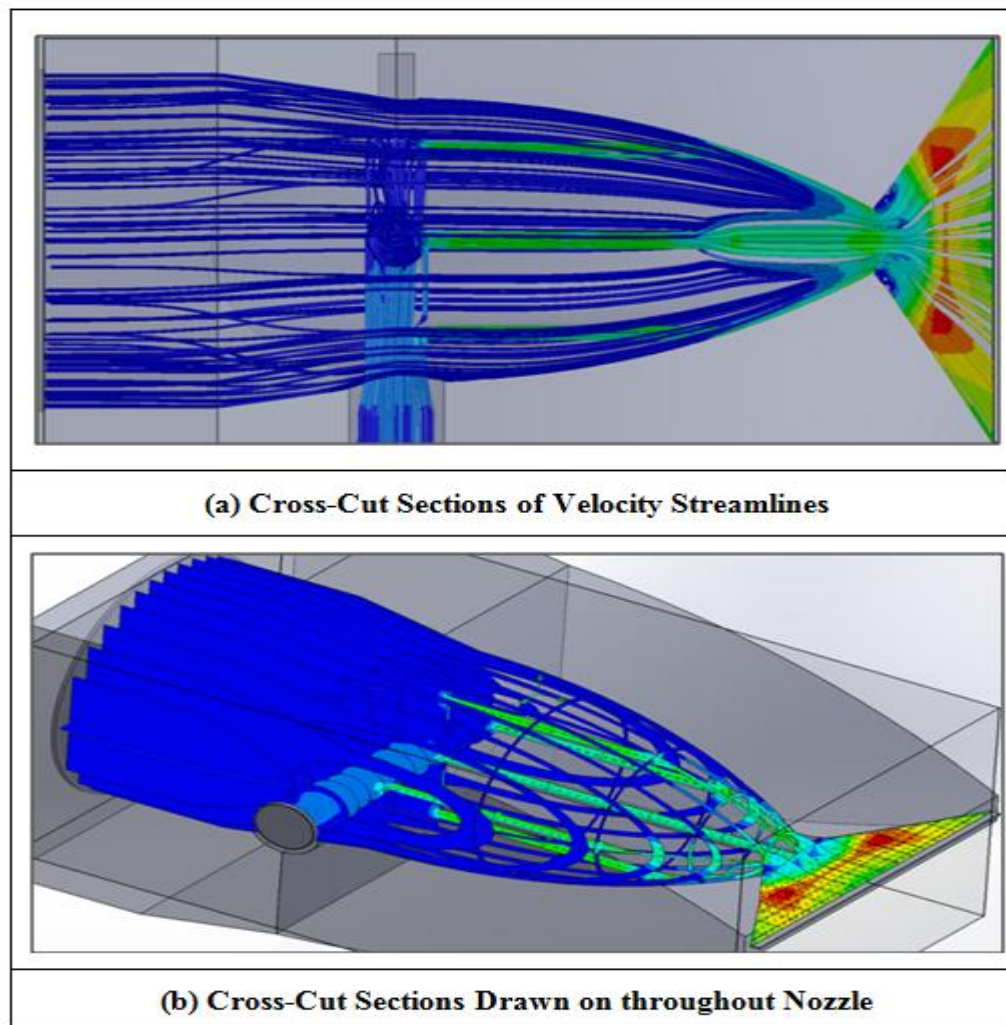


**Figure 5.37: Vertical and horizontal cross cuts**

(a) The flow streamlines and in (b) its corresponding sliced profile using vertical planes along the nozzle. This reveals how the fluid behaves inside the bulk of the fluid.

Figure 5.38 (a) is the front view of the flow profile using cross section planes. However, Figure 5.38 (b) is the combined longitudinal and cross sectional cuts around the throat of the nozzle. Figure 5.38 (c) depicts a 3D velocity profile of the flow in the nozzle throat and the exit cavity where the variation of velocities can be observed. It shows that

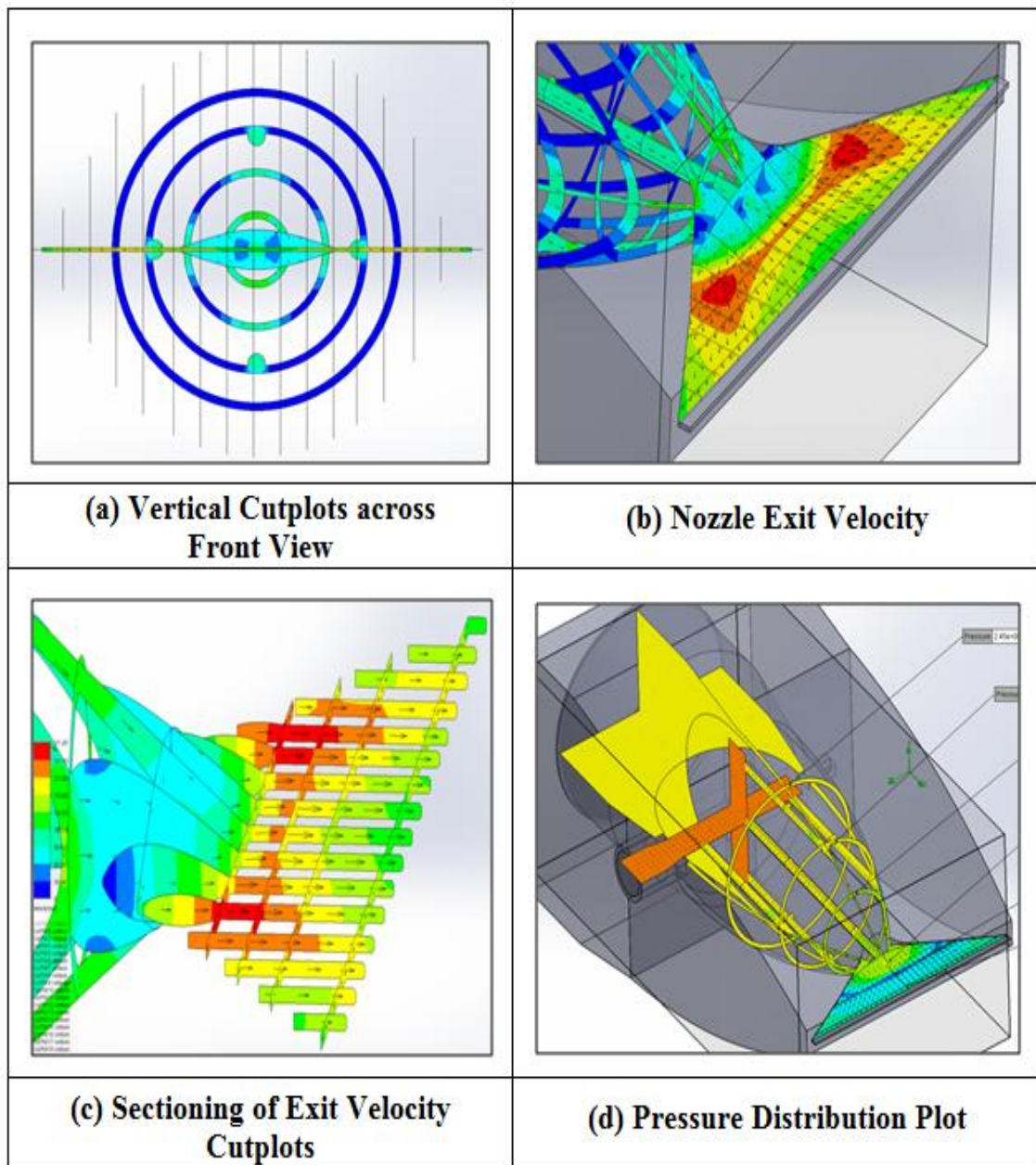


**Figure 5.38: Velocity Field in Cross-section of Dovetail profile**

The velocity vector field forms a wedge with its acute angle located at the bottom area see Fig 5.38 (c). However, due to fluid attachment to nozzle walls, this vector field close to the walls regain the shape of classical velocity profile of a fluid flowing in a duct. The Fig 5.38 (d) depicts the horizontal and vertical pressure distribution plots with measured points around cone surface. The modifications of nozzle exits are presented in a series in appendix A-1.1.

### 5.22 Nozzle with flow rate 80 litres per min (Flow Ratio 2/6 may be use 1/3)

Using cut plane passing through the centre line of the nozzle, a graph of the velocities along the nozzle is obtained as illustrated in Fig 5.39. It shows that a peak velocity of 220 m/s is reached in the area of cross firing. This graph reveals that by optimizing the length of the exit cavity and its shape it is possible to get exit velocity of 180 m/s or higher. The velocity and pressure cross cuts is presented in appendix (A-1.2 to A-1.4).

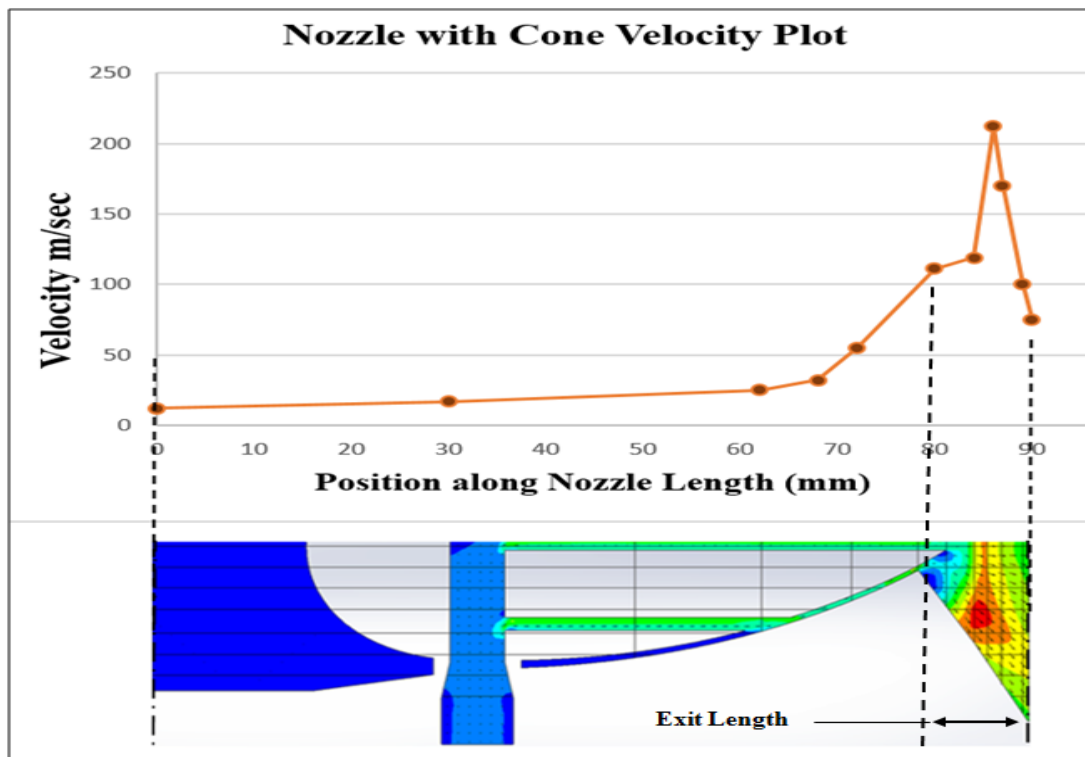
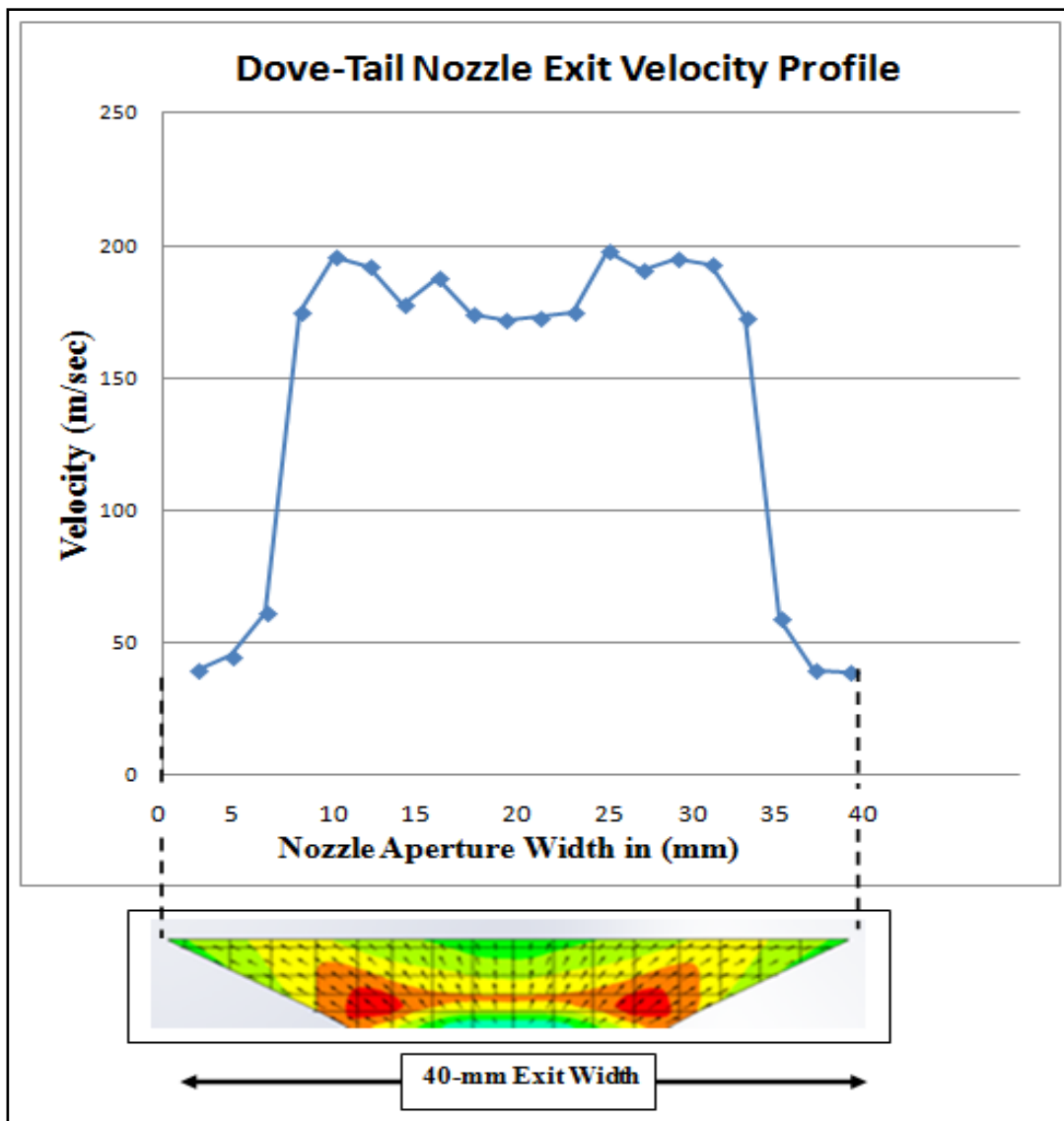


Figure 5.39: Velocity Graph across the Nozzle Length

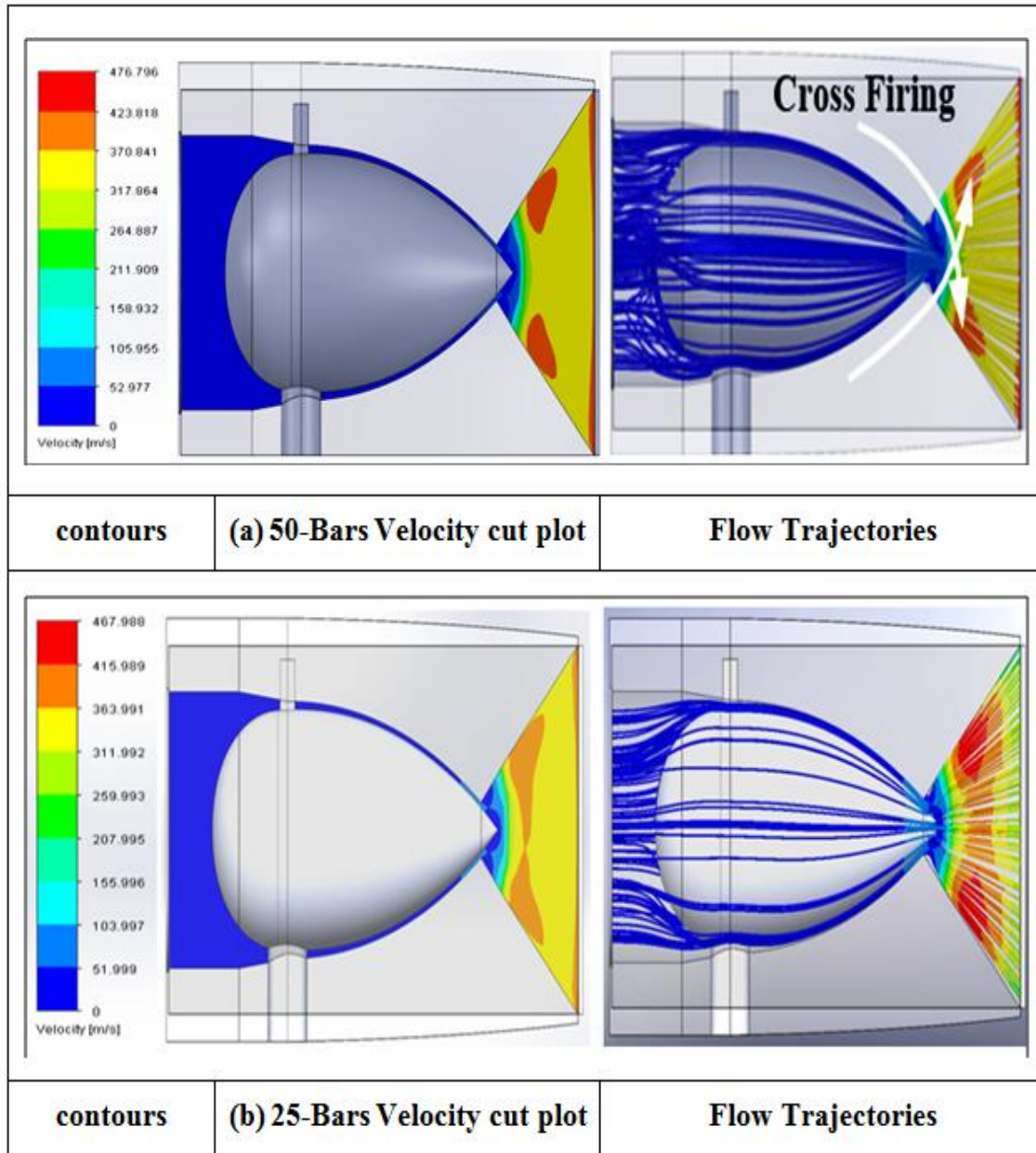


**Figure 5.40: Dove-Tail Nozzle Exit Velocity Profile**

The above Fig.5.40 depicts the velocity profile drawn across the nozzle aperture after immediate exit of the nozzle across the width of 40-mm and picked 20-points on exit face. The graph represents the fluid behaviour inside the exit cavity has the peak velocity is observed firing in the centre opposite to each other. These firing points are clearly shown indicated by the line graph. The fluid inside the cavity is fully developed and converged, and this firing peak jet velocity would match the wheel width for adequate lubrication near the grinding contact zone.

### 5.23 Nozzle Simulation with Air Flow for MQL (Single Phase)

The nozzle being designed is intended to be a universal with multiple applications. In this section of the work, the performance of the nozzle is investigated for MQL application. In MQL the supply of oil is ultimately small at no pressure, therefore, it was assumed that the oil is supplied to the nested; this means that there is no flow.



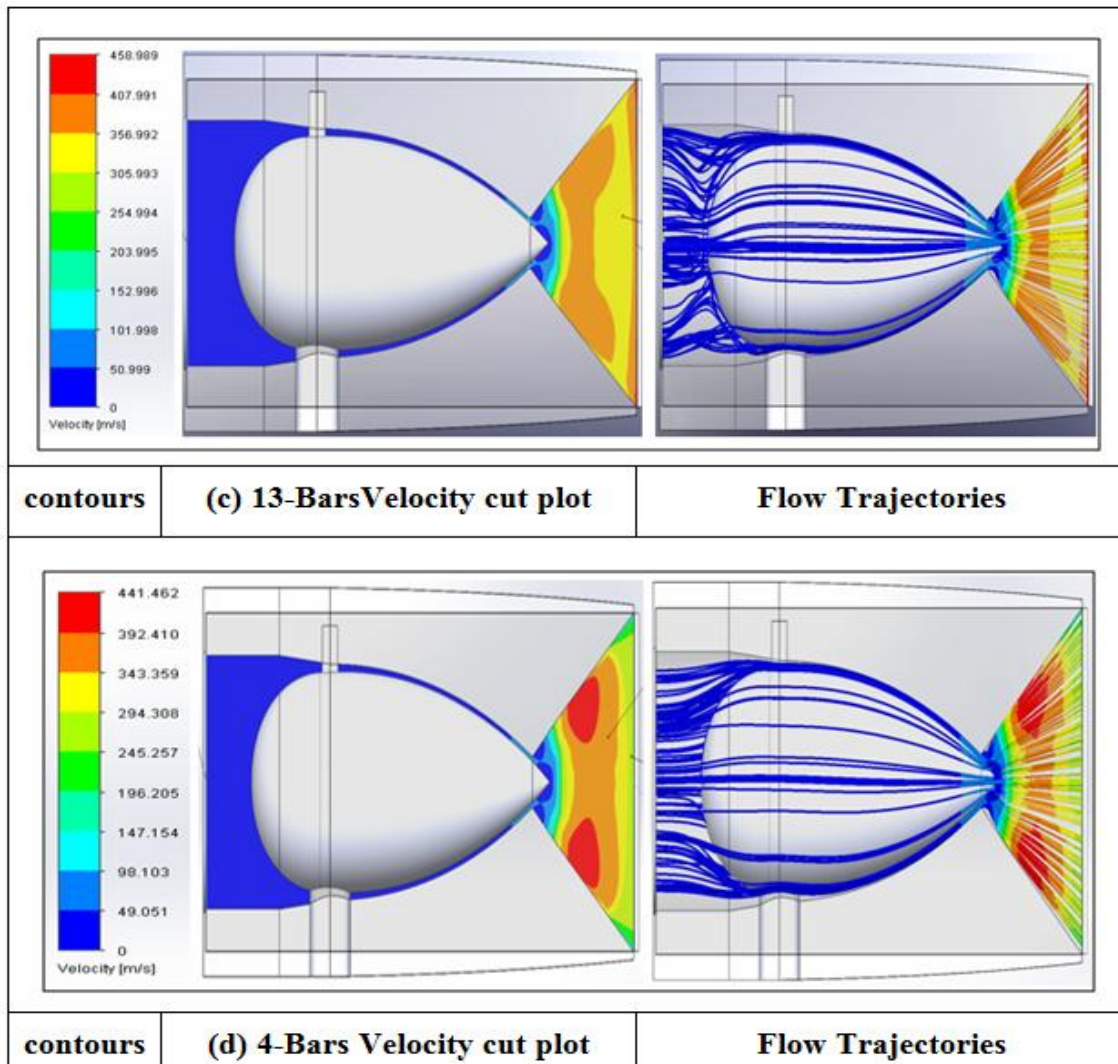


**Figure 5.41: Simulation with Air at 50, 25, 13 and 4 bars**

The transport fluid (air) is supplied to the main nozzle at various pressures, i.e. 50, 25, 13 and 4 bars. The nozzle exit is flat with 15mm length, width is 40 mm, exit aperture is 0.3 mm, and 1mm gap was set between the pressure cone and nozzle body.

The results of the simulation presented in Fig 5.41 shows similar flow behaviour as with water. Higher jet velocities are observed in cross-firing zones. However, here at low supply pressure e.g. 4 bar (see Fig 5.41 (d)), the cross firing creates an interconnected volume of fluid with high homogeneous velocities across the nozzle width. This offers a room for optimising the length of the nozzle exit cavity to secure that the exit velocity is

same along the exit profile. The given configuration of the nozzle with 4 bars provides a blade of air at a uniform sonic speed at the exit. By varying the aperture of the exit and the length of the exit cavity, it is possible to define the desirable exit velocity.

Using this principle, Fig 5.41 shows the results of the simulation with air as fluid. Here, the flow of the oil is neglected as it supplied in minute quantity in form of drops. The fully developed flow of air exits the nozzle at a velocity exceeding 129 m/sec. This result shows that it is possible to use this new modular nozzle for both flood and MQL applications.

#### 5.24 Nozzle with Air Simulation - Velocity Vs Pressure

The graph below Fig.5.42 illustrates the nozzle input pressure verses exit velocity. Here, the graph presented the nozzle with various flow rates of only air as taken fluid input flow. Increasing the air input flow rate the exit velocity gradually increasing, this confirms that pressure cone creating high pressure internally with given input flow rate.

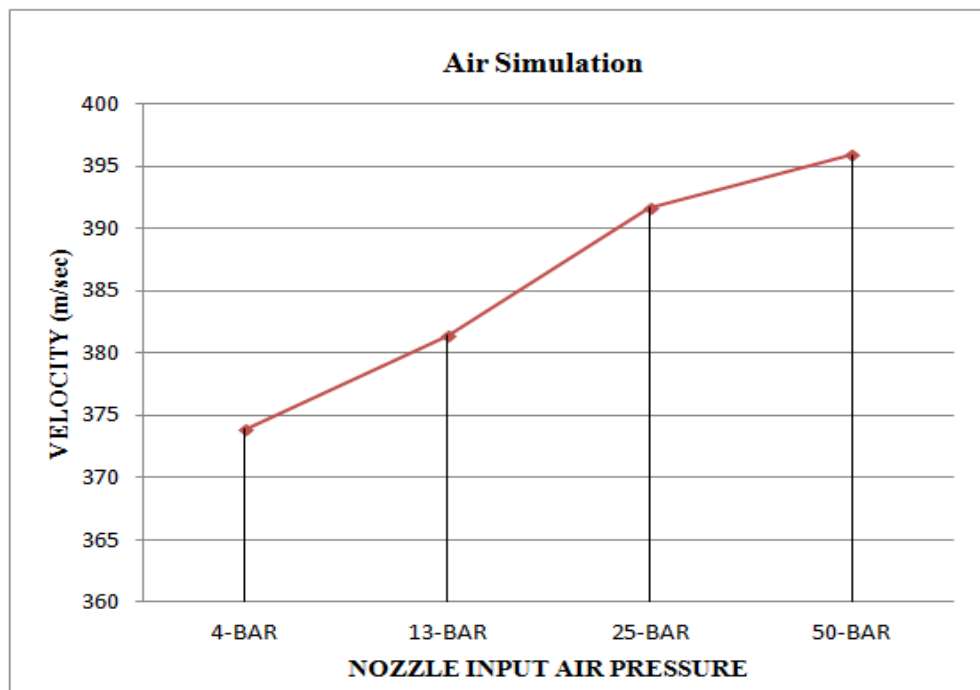


**Figure 5.42: Nozzle Air Pressure Vs Velocity**

This stage of the project focused on the development of a multipurpose nozzle that could be used for both flood and MQL cooling methods. A range of volumetric flow rates was investigated including MQL. The performance of the nozzle was characterised in terms of internal flow patterns and exit velocities. The velocity profile across the nozzle was investigated and suitable nozzle exit profile was identified for flood and MQL application.

For the internal flow simulation the COSMOS FloWorks CFD package is used at this early stage. However, for the final actual model, the refinement and studies of internal and external flow simulations were performed with more advanced ANSYS CFX.

In this simulation air and water are used as main fluids to study the behaviour of the flow in the nozzle cavity and use the flow pattern to improve and optimise the design. The following parameters were used for this initial study. The inlet flow rate was set at 120 l/min to replicate industrial application. Having identified the key parameters for the nozzle design, the project now enters the manufacturing and testing stage.

### **5.25 Summary**

The overview of set of CAD models, Initial nozzle simulation work along with nozzle design techniques is identified. Various exit profiles and nozzle cavities were designed for the improvement of nozzle efficiency. The development of nested nozzles and concept of pressure cones were introduced and after several modifications, the dove-tail exit profile was achieved with satisfactory results. A range of nozzles with air as fluid media simulations were performed for MQL applications in grinding. Now, the optimised nozzle model is performed with fundamental studies concerned with contained fluid flows. A proposed ANSYS CFX solution is developed in the next chapter where this area of work also contains detailed analysis of simulations of internal and external fluid flow behaviour.

### Key Findings

1. The introduction of pressure cone (nested nozzle) which acts as a flow conditioner straightens the flow into laminar showed better performance.
2. The output jet velocity is depending on gap between the cone surface and nozzle internal cavity surface, the minimum gap was set to 1-mm, increasing the gap reduces the velocity and reducing the gap increasing velocity.
3. The internal fluid behaviour pattern showed wedge shape acute angle formation.
4. With the help of vertical and horizontal cross cuts within the nozzle body and exit cavity showed velocity variations.
5. The internal rouse shape profile and pressure cone showed laminar flow.
6. The nested cone with internal inlets tends to increase additional acceleration on primary flow.
7. Hydrofoil and taper nested nozzles showed more turbulence compared to egg shape pressure cone.

## **Chapter-6**

### **Investigation into the Performance of Final Nozzle**

## **Chapter-6 Investigation into the Performance of Final Nozzle**

### **6.1 Introduction**

Computational Fluid dynamics (CFD) allows simulating the behaviour of fluid flows and other physical processes, which includes heat transfer, environment and other related processes. This new flow works technology is emerging into a highly powerful tool for analysis of fluid flow problems in all kinds of industries and areas. CFD is used to visualize the actual fluid flow behaviour at the initial stage or to analyse existing complex components to improve the design modifications.

### **6.2 Background of ‘CFD’**

The motion of fluids is governed by Bernoulli’s and Euler equations, which describe the conservation of momentum and mass of fluids (Euler, 1955). From the mid-1970s, complex mathematics required to generalize the algorithms began to be understood, and general-purpose CFD solvers were developed and large amounts of time was required to set up simulations. Consequently, CFD was used almost exclusively in research. Recent advances developments in computing, graphics and interactive 3D manipulation of models, have made the process of creating a perfect CFD model.

CFD tool helps engineers in understanding the problem in robust models appropriately and offers practical ideas to solve and for the best decision making about the most flawless and product designing.

As a result, computational fluid dynamics (CFD) is now an established industrial design tool, helping to reduce design time scales and improve processes throughout the engineering world and analysing results much less labour intensive, reducing time and hence cost.



### 6.3 Overview of ANSYS CFX

ANSYS CFX is a general-purpose computational fluid dynamics (CFD) software suite that combines an advanced solver with powerful pre & post processing capabilities.

It contains broad physical modelling capabilities needed to model flow, turbulence, heat transfer, and reactions over objects. It uses the finite-volume method to solve the governing Navier-Stokes equations for fluid, which are derived from the conservation of mass equation (6.1), the conservation of momentum (6.2) and the conservation of energy (6.3) equations.

$$1) \frac{\partial \rho}{\partial t} + \nabla \cdot (\rho \vec{V}) = 0 \quad (6.1)$$

$$2) \rho \frac{\partial \vec{V}}{\partial t} + \rho (\vec{V} \cdot \nabla) \vec{V} = -\nabla \rho \vec{g} + \nabla \cdot \tau_{ij} \quad (6.2)$$

$$3) \frac{\partial}{\partial t} \int e * \rho dV + \int (\check{u} + \frac{p}{\rho} + \frac{V^2}{2} + gz) \rho V \cdot \check{n} dA = \dot{Q}_{net in} + \dot{W}_{net in} \quad (6.3)$$

The difficulty arises from the fact that the conservation of mass, momentum and energy are coupled and non-linear set of differential equations making them practically impossible to solve analytically for practical engineering problems. Hence CFX software is utilized to provide reasonable approximation upon solving the specified governing equations (CFD Training manual, 2013).

Generally the way in which computers deal with continuous flows is to discretise domain of interest into small sub-domains using technique called Finite Volume Method (FVM) where the equations can be solved for each volume individually (ANSYS CFX Introduction, 2013).

It includes

- An advanced coupled solver that is both reliable and robust,
- Full integration of problem definition, analysis and results presentation,
- And an intuitive and interactive setup process, using menus and advanced graphics.

### 6.3.1 Turbulence Models

ANSYS offers a number of advanced turbulence models in the form of algebraic, one equation, two equation and Reynolds stress models. The most widely used turbulence models are Reynolds-Averaged-Navier-Stokes (RANS) models that are based on time-averaged of the equations. The standard k- $\epsilon$  model is used in the prediction of most turbulent flow calculations because of its robustness, economy, and reasonable accuracy for a wide range of flows. However, the model performs poorly when faced non-equilibrium boundary layers. It tends to predict the onset of separation too late as well as to under-predict the amount of separation (Introduction to CFX, 2009).

### 6.3.2 Shear Stress Transport Model (SST)

The shear stress model is a combination of the k- $\epsilon$  in the free stream and the k- $\omega$  models near the walls. One of the most effective is the shear stress transport model (SST). This model is based on (k- $\omega$ ) model and has the same automatic wall treatment. For flow separation, the shear-stress transport (SST) model has become accepted as the two-equation model industry standard. The SST model unifies the advantages of the most widely employed two-equation (k- $\omega$  and k- $\epsilon$ ) models and is the most reliable model for fluids with flow separation. The model works by solving a turbulence/frequency-based model (k-  $\omega$ ) at the wall and k-  $\epsilon$  in the bulk flow. A blending function ensures a smooth transition between the two models. The shear tress model performance has been studied in large number of cases. This model is contained in ANSYS CFX with robust near wall predictions for turbulent flows.

Separation influences the overall performance of many devices, such as diffusers, turbine blades and aerodynamic bodies. Separation also has a strong influence on wall heat transfer and multi-phase phenomena. Generally separation occurs when the boundary layer flows far enough against an adverse pressure gradient that the velocity of the boundary layer relative to the body totally drops to zero. The fluid detached from

the surface of the body, and instead forms recirculation, eddies and vortices (Introduction to CFX, 2009).

### **6.3.3 ANSYS CFX Turbulence Near-Wall Treatment**

The ANSYS CFX introduced a formulation for wall function-based models, so called scalable wall functions. This is the only available formulation allows users to apply arbitrarily fine grids without violating the underlying logarithms profile assumptions. For shear stress model, the new boundary treatment exploits the simple and robust near wall formulation of the  $k-\omega$  model and switches automatically from a low-Reynolds number formulation to a wall-function treatment based on grid density. The user can then make optimal use of the advanced performance of the turbulence model for any given grid.

The  $(k-\epsilon)$  model fails to predict or capture the physics of this separation flow entirely, where the shear stress transport model (SST) is based on  $(k-\omega)$  model has the same automatic wall treatment. It accounts for the transport of the turbulent shear stress and gives accurate predictions on the onset and the amount of flow separation zone in close agreement with data.

In some situations, such as boundary layer separation, wall functions do not correctly predict the boundary layer profile. In these cases wall functions should not be used instead, directly resolving the boundary layer can provide accurate results. Not all turbulence models allow wall functions to be turned off (Introduction to CFX, 2009).

## **6.4 Multiphase Fluid Flow Models**

A multiphase flow is a flow with simulations of different phases, where phase refers to solid, liquid or vapour state of matter. A phase is an identifiable class of material that has a particular inertial response to and interaction with the flow and potential field in which it is immersed (Stefan, 2011). There are four main categories of multiphase flows are; gas-liquid, gas-solid, liquid-solid and three-phase flows. A flow pattern describes



the geometrical distribution of the phases and the flow pattern greatly affects the phase distribution, velocity distribution for certain flow situations. For some simple shapes, for example horizontal and vertical pipes, the flow patterns that occur for different phase velocities have been summarised in a so-called flow map. In the Figure 6.1 visualises the flow configuration for some possible flow regimes.

Dispersed flow is a flow where one phase is widely distributed as solid particles or bubbles in another continuous phase depicted in Fig 6.1 (a). The two extremes in a flow map is dispersed flow and separated flow.

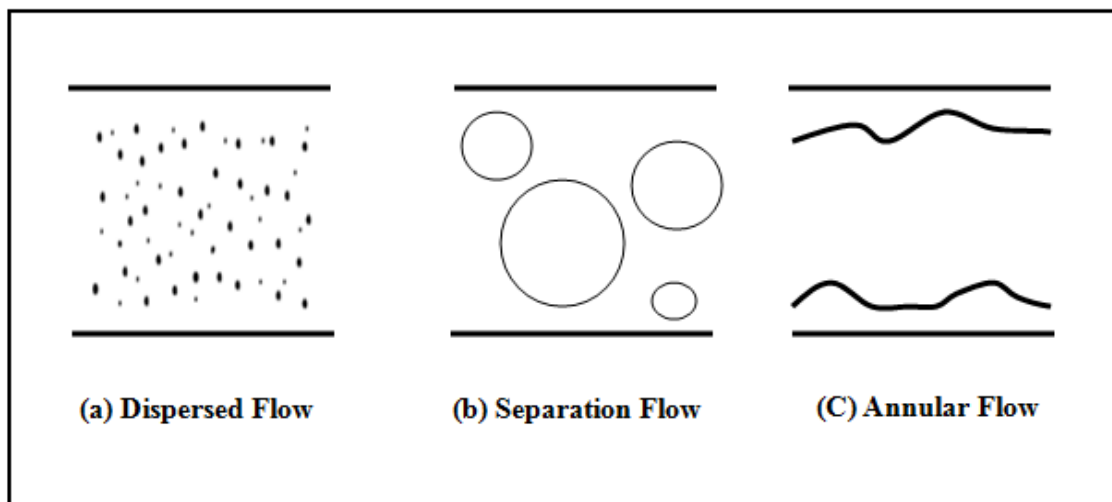


**Figure 6.1: Example of typical Flow Patterns for Flow in Horizontal Pipes**

(Adopted from Elin, 2013)

In separated flow illustrated in Fig 6.1 (b) there is a distinct boundary between the phases. Examples of separated flow is stratified flow where one phase is flowing on top of another or annular flow in a pipe with a liquid film along the pipe and a gas core in the middle see Fig 6.1 (c). Several intermediate regimes also exist, which contain both separated and dispersed phases such as for example annular bubbly flow. Due to growing instabilities in one regime, transition to another regime can occur. This phenomenon complicates the modelling of multiphase flow even further as the

transition is unpredictable and the different flow regimes are to some extent governed by different physics (Elin, 2013).

#### 6.4.1 Multiphase Flow Regimes

These can be divided into three types: Gas-Solid flows, Liquid-Solid flows: Gas-Liquid or Liquid –Liquid.

*Multiphase flow regimes are:*

- Droplet flow includes absorbers, atomizers, combustors, cryogenic pumping, dryers, evaporation, gas cooling and scrubbers.
- Bubbly flow examples include absorbers, aeration, airlift pumps, cavitation, evaporators, floatation and scrubbers.
- Slug flow examples include large bubble motion in pipes or tanks.
- Stratified/free-surface flow examples include sloshing in offshore separator devices and boiling and condensation in nuclear reactors.
- Fluidized bed examples include bed reactors and circulating fluidized beds.
- Slurry flow examples are slurry transport and mineral processing (Stefan, 2011).

#### 6.4.2 Method of Choosing Appropriate Multiphase Model

Initial step in solving a multiphase fluid flow problem is to find out which of the flow regimes provides adequate guidelines to determine appropriate models for each flow regime, and how to resolve the degree of inter-phase coupling for multiphase flows involving bubbles, droplets, or particles, and the adequate model for different amounts of coupling (Stefan, 2011).

- At present, there are two different approaches for the numerical calculation of multiphase fluid flows: Euler-Lagrange and Euler-Euler approach.

In the Euler-Lagrange approach, particles are tracked on the level of a single particle where particle refers to either a solid particle or a gas/fluid bubble/droplet. Conservation

equations are solved for the continuous phase and the particle phase is tracked by solving the equations of motion for each particle, see equations 6.4, 6.5 and 6.6.

$$\frac{\partial \alpha_f \rho_f}{\partial t} + \nabla \cdot (\alpha_f \rho_f \mathbf{u}_f) = S_{mass} \quad (6.4)$$

$$\frac{\partial \alpha_f \rho_f}{\partial t} + \nabla \cdot (\alpha_f \rho_f \mathbf{u}_f \mathbf{u}_f) = \alpha_f \nabla p - \alpha_f \nabla \cdot \boldsymbol{\tau}_f - S_p + \alpha_f \rho_f \mathbf{g} = 0 \quad (6.5)$$

$$\frac{\partial \mathbf{u}_p}{\partial t} = \sum F \quad (6.6)$$

Here " $\alpha$ " is volume fraction, " $S_{mass}$ " is a mass source term existing in the case of exchange of momentum between the phases and "F" is force. Subscript "f" and "p" refers to the fluid and particle phases, respectively.

The forces acting on particles vary depending on the flow situation. The drag force is generally included and other forces that can be of importance are of example lift force, virtual mass force. When performing modelling the modeller has to judge which forces that are of importance to include on the right hand side of equation (6.6). Adding more forces to model increases accuracy but also increases complexity.

As this modelling approach resolves information on the level of a single particle it is quite computationally expensive. To reduce the computational cost one can choose to track clusters of particles instead. However, this approach is still computationally expensive and therefore Euler-Lagrange modelling is suitable for dilute dispersed flow, meaning flows with a low volume fraction of the dispersed phase (Elin, 2013).

In addition to the regular transport equations, a transport equation for the volume fraction is also solved for each phase. The sum of the volume fractions should be equal to one. The governing equations for a two-fluid model with two continuous phases are shown below.

$$\frac{\partial \alpha_k \rho_k}{\partial t} + \nabla \cdot (\alpha_k \rho_k \mathbf{U}_k) = 0 \quad (6.7)$$

$$\frac{\partial \alpha_k \rho_k U_k}{\partial t} + \nabla \cdot (\alpha_k \rho_k U_k U_k) = -\alpha_k \nabla P + \alpha_k \nabla \cdot \tau_k + \alpha_k \rho_k g_k + S_k = 0 \quad (6.8)$$

$$\frac{\partial \alpha_k}{\partial t} + \nabla \cdot (\alpha_k U_k) = 0 \quad (6.9)$$

Here “ $U$ ” is the mean velocity field and “ $P$ ” is the mean pressure shared by the phases. The subscript “ $k$ ” refers to the “ $k^{th}$ ” continuous phase.

To track the different phases, a transport equation for the volume fraction is also solved. The phases are allowed to move with different velocities by using the concept of slip velocity, which in turn includes further modelling (Elin, 2013).

The volume of a single phase cannot be occupied by any other phase; the concept of “phasic” volume fraction is used. Therefore, it is assumed that volume fractions are continuous functions of both space and time and the total sum is equal to one.

In common uses there are three different Euler-Euler multiphase models are: The volume of fluid (VOF), mixture model and Eulerian model.

### 6.4.3 Volume of Fluid (VOF) Model

The volume of fluid VOF model is a type of a surface-tracking technique, which belongs to the Euler-Euler framework where all phases are treated as continuous, but in contrary to previous presented models the VOF model does not allow the phases to be interpenetrating.

The VOF method uses a phase indicator function, sometimes also called a colour function, to track the interface between two or more phases. The indicator function has value one or zero when a control volume is entirely filled with one of the phases and a value between one and zero if an interface is present in the control volume. Hence, the phase indicator function has the properties of volume fraction. The transport equations are solved for mixture properties without slip velocity, which means that all field

variables are assumed to be shared in between the phases. The equations for the VOF method are as follows:

$$\frac{\partial \rho_m}{\partial t} + \nabla \cdot (\rho_m \mathbf{u}) = 0 \quad (6.10)$$

$$\frac{\partial \rho_m \mathbf{u}}{\partial t} + \nabla \cdot (\rho_m \mathbf{u} \mathbf{u}) = -\nabla P + \nabla \tau + \rho_m \mathbf{g} + S = 0 \quad (6.11)$$

$$\frac{\partial \alpha}{\partial t} + \nabla \cdot (\alpha \mathbf{u}) = 0 \quad (6.12)$$

Here  $\rho_m = \sum \alpha_k \rho_k$ . The subscript “*m*” refers to mixture properties. In this model, there is a single set of momentum equations, which is shared by all fluids. The volume fraction of every fluid in each computational cell is tracked all over the domain (Elin, 2013).

**The Mixture Model** was made for flows of two or more fluid or particulate phases. This model shares a characteristic with the Eulerian-model the phases are treated as interpenetrating continua. The mixture model solves the mixture momentum equation and specifies relative velocities in order to describe the dispersed phases. It can be used without relative velocities approach for the dispersed phases in order to model homogeneous multiphase flow (Stefan, 2011).

**The Eulerian model** is the most complex of the Euler-Euler models. This model solves a set of momentum and continuity equations for each phase. Coupling is achieved by use of the pressure and inter-phase exchange coefficients. Exchange of momentum between different phases depends on the type of mixture being modelled.

### 6.5 Performance & Characterization of Final Nozzle

This section presents the refinement of the actual nozzle (Final Optimised Nozzle) by investigating the model in detail. This refinement includes the internal and external flow studies and meshes optimisation in order to improve the efficiency and accuracy of the nozzle model.



### 6.5.1 Geometry Creation of the Model

Here ANSYS was used and its workbench design modeller software provides a single geometry source for a complete range of engineering simulation tools. The development of 3-D model of the nozzle is set as a modular sub-assembly of three key components namely, the main body, nozzle chamber and an egg shaped pressure cone as shown in Fig.6.2 (a). This new concept aims at developing a new generation of nozzles with advanced performance that secures low volume of fluid at low pressure. The engineered nozzle profile is optimised to increase the pressure internally in the nozzle chamber. This is achieved using a principle of ‘Nested Nozzle’, where a small nozzle is inserted in the main nozzle. Here the nested nozzle plays a triple role: (a) its body acts as a flow conditioner for the main flow; (b) its body is designed to perform pressuring action on the main low volume low pressure flow, (c) its jet is used to accelerate the low flow stream to high speed at the main exit. In the previous chapter, the modelling process, various types of nozzle chambers with different exit profiles have been designed and simulated to check the performance of the nozzle. This allowed optimising the profile as shown in figures below and each model is discussed in detail.

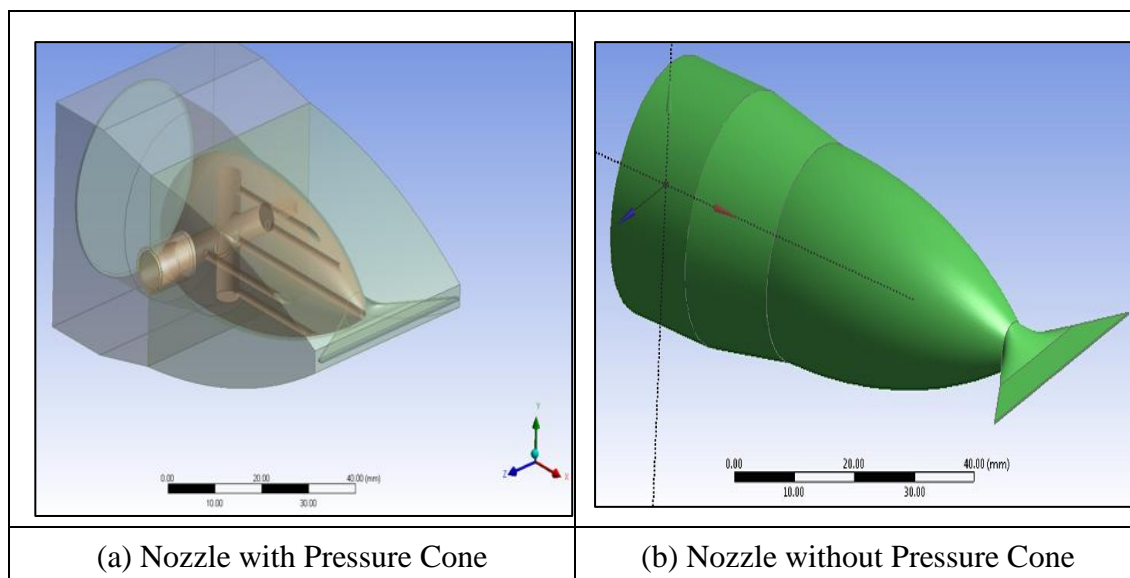


**Figure 6.2: Final Nozzle Model Design**

This model was developed by number of modifications and optimisation methods using ‘Solidworks’ and CFD simulations. Here, this model the flow behaviour and nozzle performance efficiency is investigated using ANSYS CFX.

The above Fig.6.2 (a) is an assembly model, in order to perform simulation ignoring external body of the nozzle and choosing only internal flow profile, which becomes actual 3-D solid model of the fluid flow region Fig 6.2 (b).

### 6.5.2 Meshing

Mesh Quality indicates the accuracy of results, hence better the mesh quality, and better the simulation results. In general, tetrahedral mesh, hexahedral mesh will always give more accurate results because the mesh elements are always aligned to the flow direction, but it is not possible to mesh entire geometry using hexahedral mesh. Hence, it is used only at regions of key interest. ANSYS CFX provides two types of meshing ANSYS CFX Mesh and ICEM CFD Mesh products.

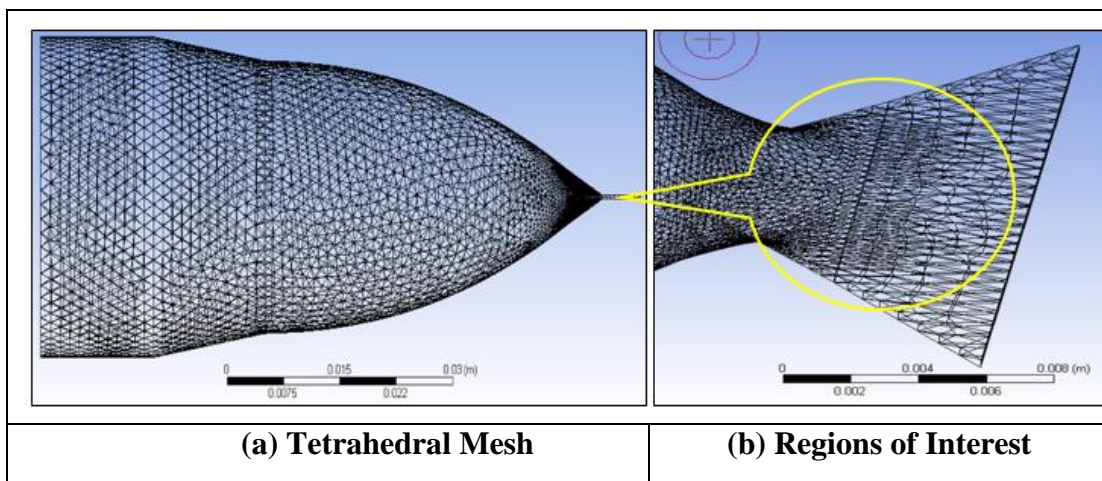


**Figure 6.3: Mesh formation and Regions of interest**

For this research work ANSYS CFX TETRA is used to provide high quality mesh for accurate results. To achieve the convergence, minimum three convergence runs are required for accurate results otherwise it is needed to further refine the mesh for full convergence.

Fig.6.3 shows convergence study used in this example with velocity at the outlet selected as the location. After four refinements, it is clear that no further refinement is necessary for the preliminary studies. As illustrated in Fig.6.3 (a) used tetrahedral mesh, one of the key concepts of mesh is mesh convergence; that is performed on model by refining the mesh in specific regions of interest depicts in Fig.6.3 (b).

1. **Mesh Skewness:** It is a quantitative or quantitative parameter that decides whether mesh is having a large amount of skewness or it is an ideal or a square.
2. **Mesh Smoothness:** It describes as to how smooth the mesh is, how its transition whether it is an abrupt or in a smooth manner.
3. **Mesh Aspect Ratio:** It is the ratio of the largest dimensional length of an element to the smallest length.
4. **Mesh Density:** It means how closely or coarsely mesh elements are placed. Resizing the mesh size in different regions of CFD space, where then flow is very close to wall, to define mesh so that the triangular and quadrilateral and other shapes are packed together closely in order to capture the boundary layer, but away from the walls/surfaces elements that are larger or coarsely spaced

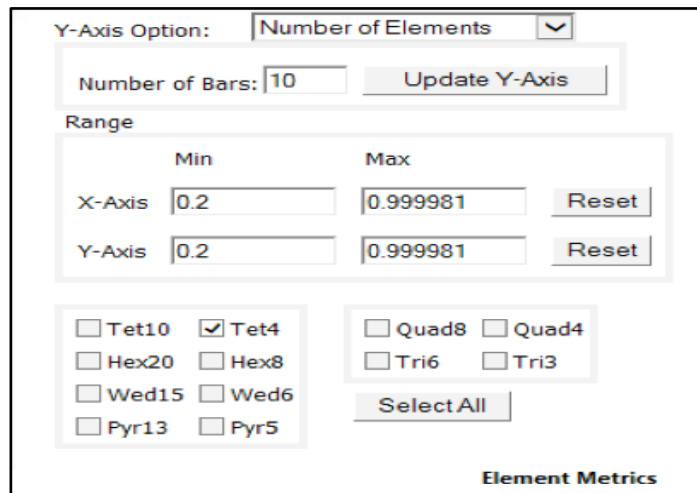


**Figure 6.4: Mesh Statistics**

$$\text{Mesh Quality} = \frac{R_{\text{inside}}/R_{\text{outside}}}{(R_{\text{inside}}/R_{\text{outside}})_{\text{Ideal}}}$$

Fig. 6.4 shows the statistics of the meshing setting used and the mesh quality is defined as: An aspect ratio of one indicates perfectly regular volume and an aspect ratio of zero indicates that the element has zero volume.

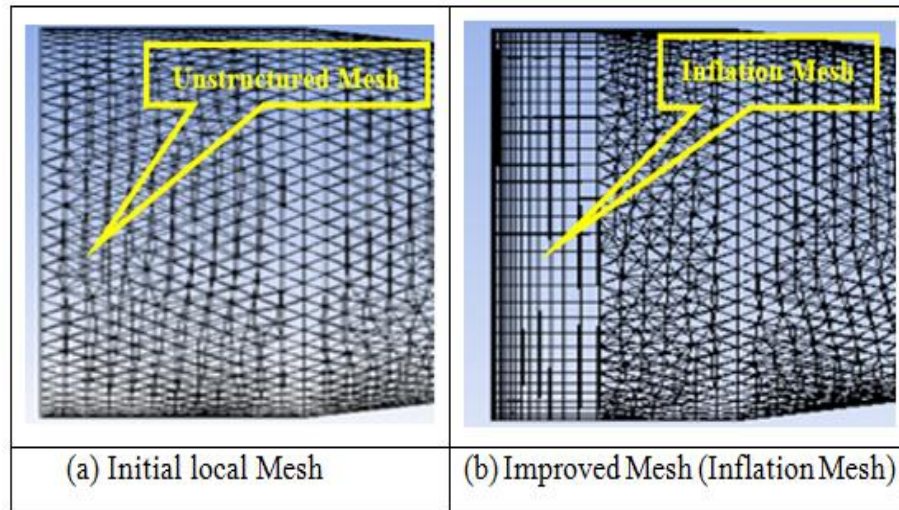


**Figure 6.5: Mesh Improvement using layers of Inflation mesh**

The above Fig.6.5 (a) depicts the initial mesh and Fig.6.5 (b) inflation mesh layers near critical areas. The use of inflation layers allows closing focus on expected recirculation zones near walls. Table-6.1. shows the quality of mesh criteria after both tetrahedral and prismatic meshing using ICEM and five smoothing operations.

<b>Tetrahedral Meshing</b>				
Global Element Scale	Global Element seed size	Triangular Tolerance	Smoothing Iterations	Minimum Quality
0.2 mm	5	0.001mm	5	0.4 mm
<b>Prismatic Meshing (Inflation Meshing)</b>				
Height Ratio	Number of layers	Vol. Smoothing	1 <sup>st</sup> Layer Smooth	Surface Smooth
1.3	5	1	2	0

**Table 6.1: Mesh Criteria for Nozzle**

Fig 6.6, shows the first step of internal flow analysis defining whether the simulation is steady or transient. Most of the work in this thesis is concerned with steady state problems as transient problems increase the inaccuracy and complexity of the results.

Pre-Processing			
Fluid Type	Water	Inlet Speed	
Simulation type	Steady State	Outlet Pressure	Rel: 0 Pa
Reference Pressure	1 atm	Wall Criteria	No-Slip
Heat Transfer	None	Advection Scheme	Upwind
Turbulence	SST	Convergence	Auto Time Scale
Solver	CFX 11.0	Time Scale	Conservative

**Table 6.2: Pre-Processing Physics Definition**

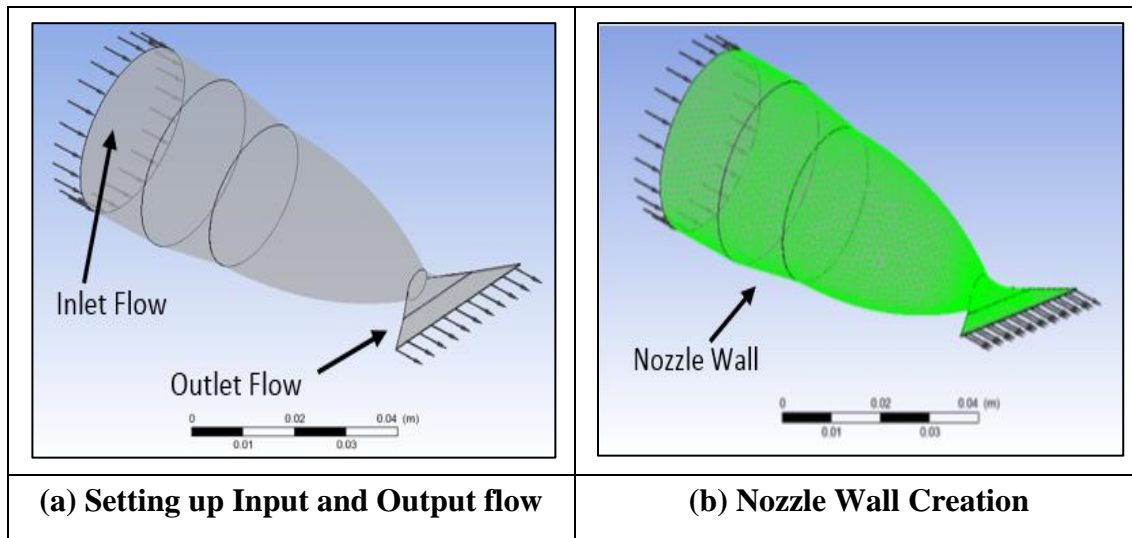


**Figure 6.6: Example of Nozzle Domain Setup**

In this simulation water is used as a fluid is close enough to emulsions used in machining. The reference pressure is set to atmospheric, so all other pressures are in reference to this. No heat transfer analysis is set as this is of no interest in this work for analysing internal flows of a single fluid at ambient temperature.

## 6.6 Nozzle Simulation Results

This section presents the results of the simulation of the nozzle without the inner cone.

### 6.6.1 Nozzle No-Cone (Flow Rate 10-Litre/min-Single Phase Flow)

The below Fig.6.7 represents the results of nozzle without the cone at flow rate 10 litre/min. it shows the velocity profile in the nozzle cavity with the velocity vector for the total velocity (fluid speed in x, y, z combined).

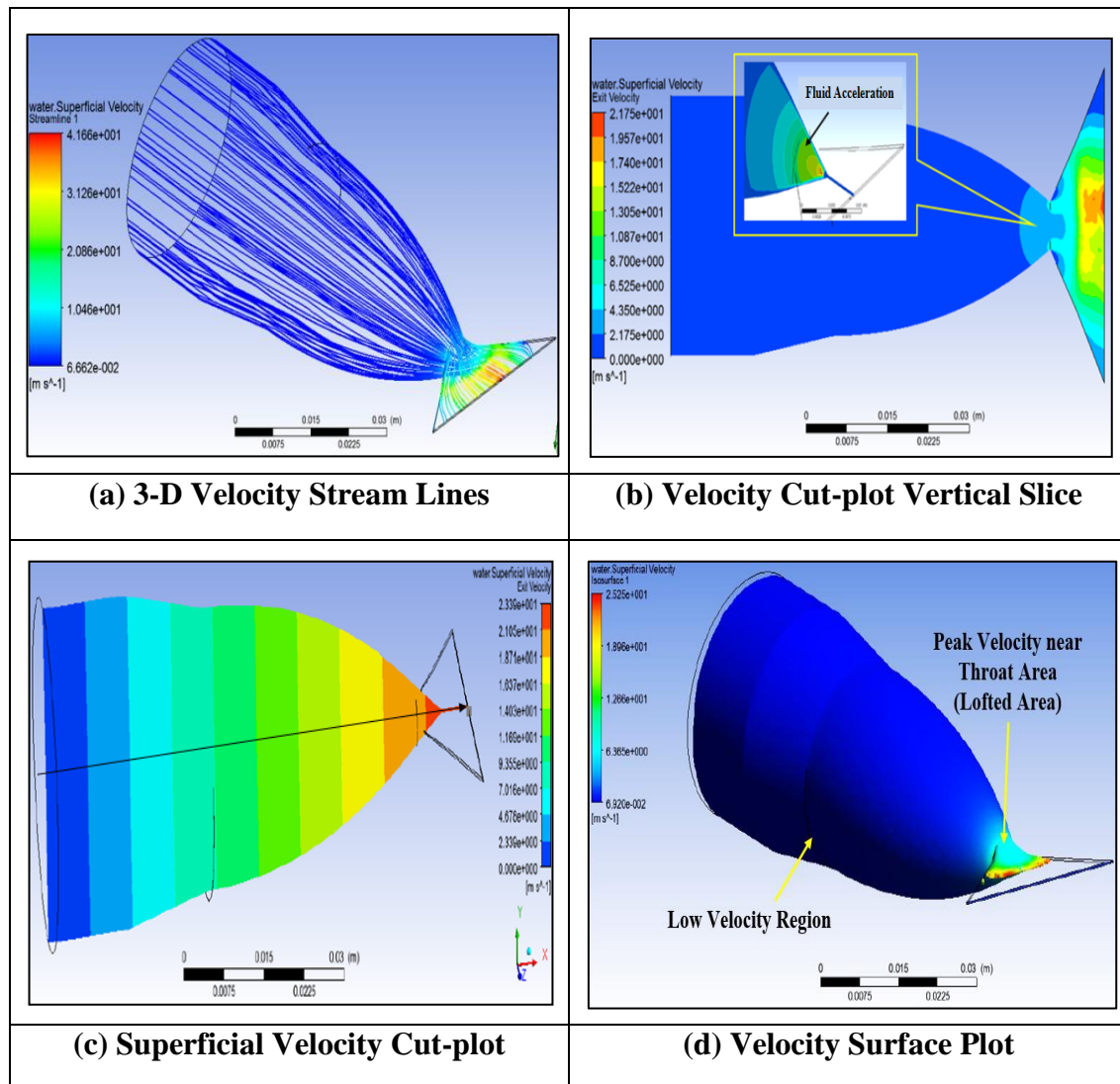
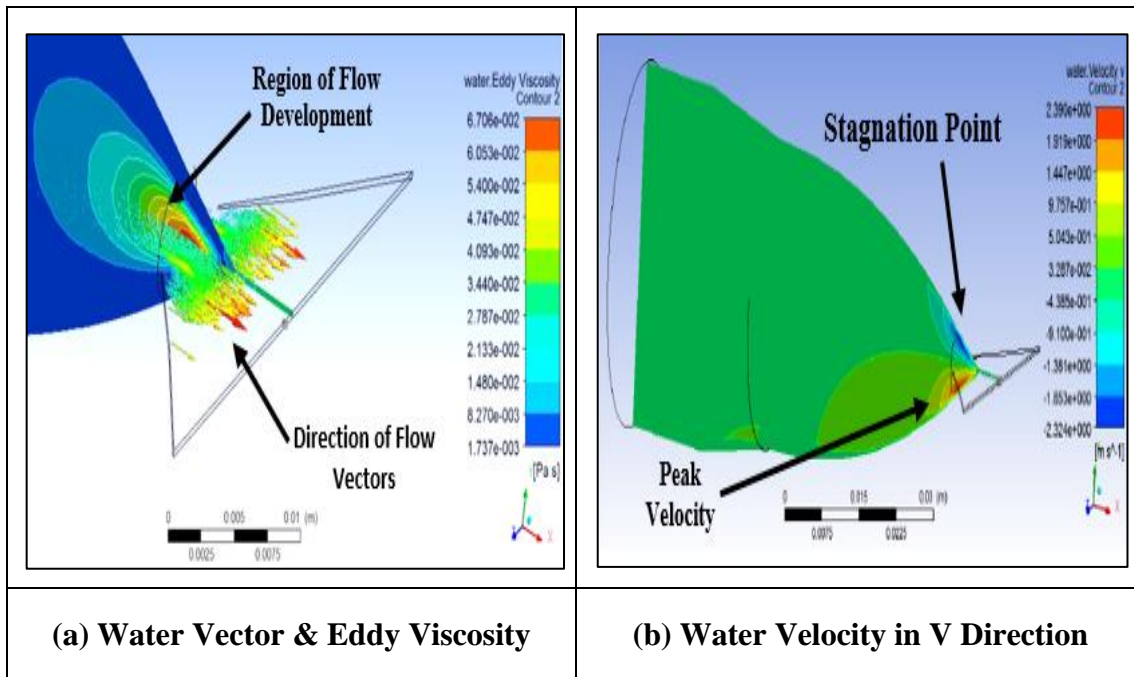


Figure 6.7: Nozzle with Dove-Tail Exit No-Cone (Flowrate 10 L/min)

In Fig.6.7 (a) exhibits no reverse flow near the throat area from the supply line to the narrow convergent region. With the help of velocity cut-plot which is drawn vertically and horizontally, it is observed that with low flowrate the fluid is gradually rising near the lofted throat area illustrated in Fig.6.7 (b). A high velocity region is observed in centre of the exit cavity with a fully developed flow fluid. This is because the internal profile of the nozzle is designed in a Rouse-shape, which accelerates the fluid without recirculation.

With help of velocity cut-plot drawn vertically and horizontally it is observed that with low flowrate the fluid is gradually rising near the lofted throat area illustrated in Fig.6.7 (b). A high velocity region is observed in centre of the exit cavity with a fully developed flow fluid. This is because the internal profile of the nozzle is designed in a Rouse-shape, which accelerates the fluid without recirculation.

However, before uniform velocity is reached at some distance within the narrow chamber there is a flow region of varying velocity at the interface of the two cavities. This is mainly due to the change in the section inlet area to outlet region. The cut-plot slice drawn in middle of the nozzle vertically indicates the water superficial velocity is developing in a systematic manner from inlet up to the exit as illustrated in Fig.6.7 (c). The velocity near the surface of the walls is presented in Fig.6.7 (d) and a varying velocity of the fluid is observed near the throat area only after crossing the lofted region, then the fluid is uniform up to the exit.



**Figure 6.8: Turbulence and Eddy Cut-plots**

Investigating the flow behaviour near the converging section (lofted area) a velocity plane is drawn near the throat area for a detailed study. The Fig.6.8 (a) is a water vector and eddy viscosity plot drawn vertically and horizontally indicating that no eddies or turbulence is formed near the throat area and the velocity vectors shows that the flow in nozzle cavity is uniformly accelerating. A small area of stagnation point and large area of high velocity region is observed near top and bottom portion of the lofted boss region illustrated in Fig.6.8 (b). Also the fluid flow is splitting near the lofted area this is mainly due to shape of the loft.

## 6.6.2 Nozzle Velocity Plot No-Cone at 10-Litre/min-Single Phase Flow

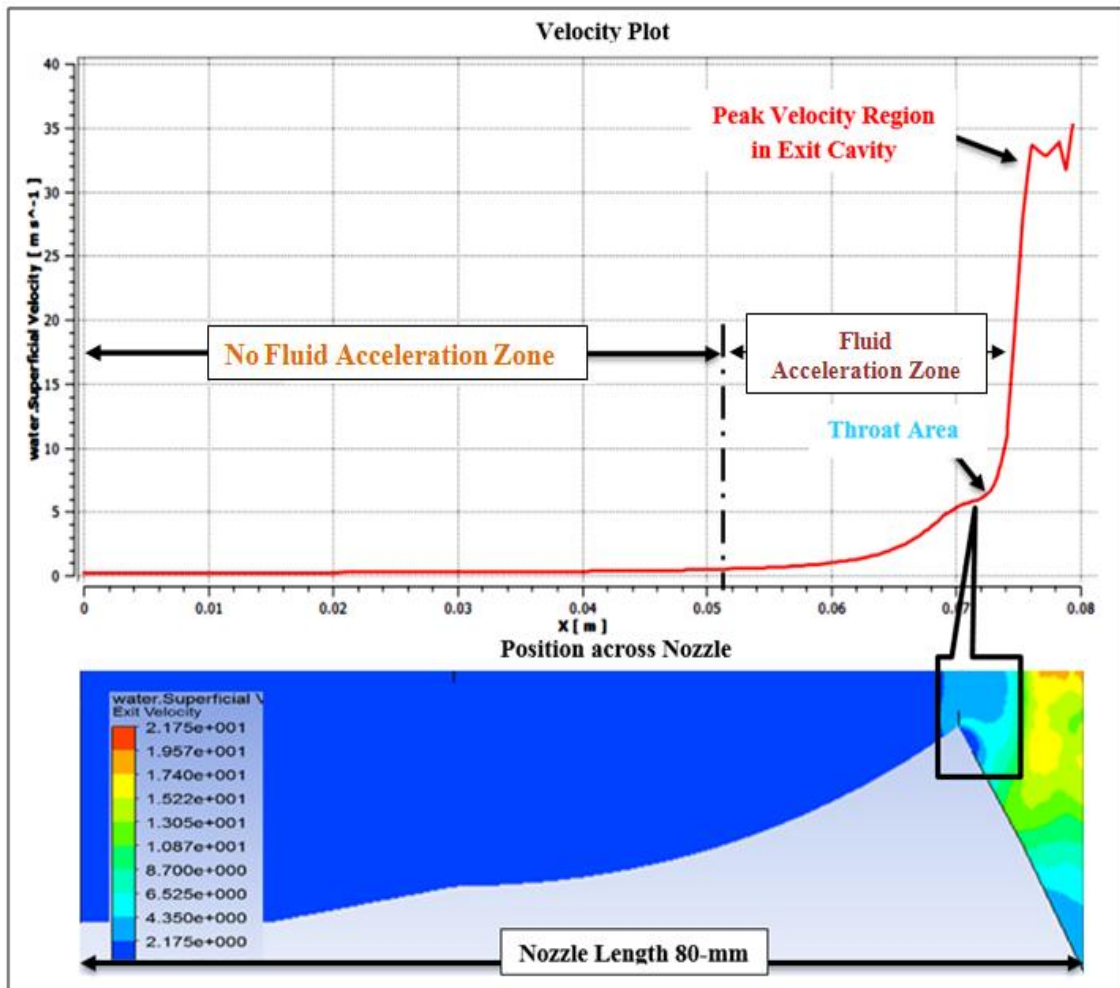


**Figure 6.9: Water Superficial Velocity across Length of Nozzle (mm)**

Fig.6.9 depicts the velocity in a plane (velocity Line) passing through the centre line of the nozzle along the nozzle length. This plot reveals that a low uniform flow followed up to the distance of 0.05 m and after crossing this region the fluid start accelerating up to the throat; here the fluid acceleration is further increased due to the structure of throat and exit cavity of the nozzle reached with a peak velocity of 21.7 m/sec. Also a line graph is drawn on nozzle exit face shows a velocity profile illustrated in Fig. 6.10. This two line graphs indicates the actual fluid flow behaviour inside the entire nozzle cavity with respect to the supplied inlet flowrate and outcome of the exit velocity.

### 6.6.3 Nozzle Exit Velocity Profile

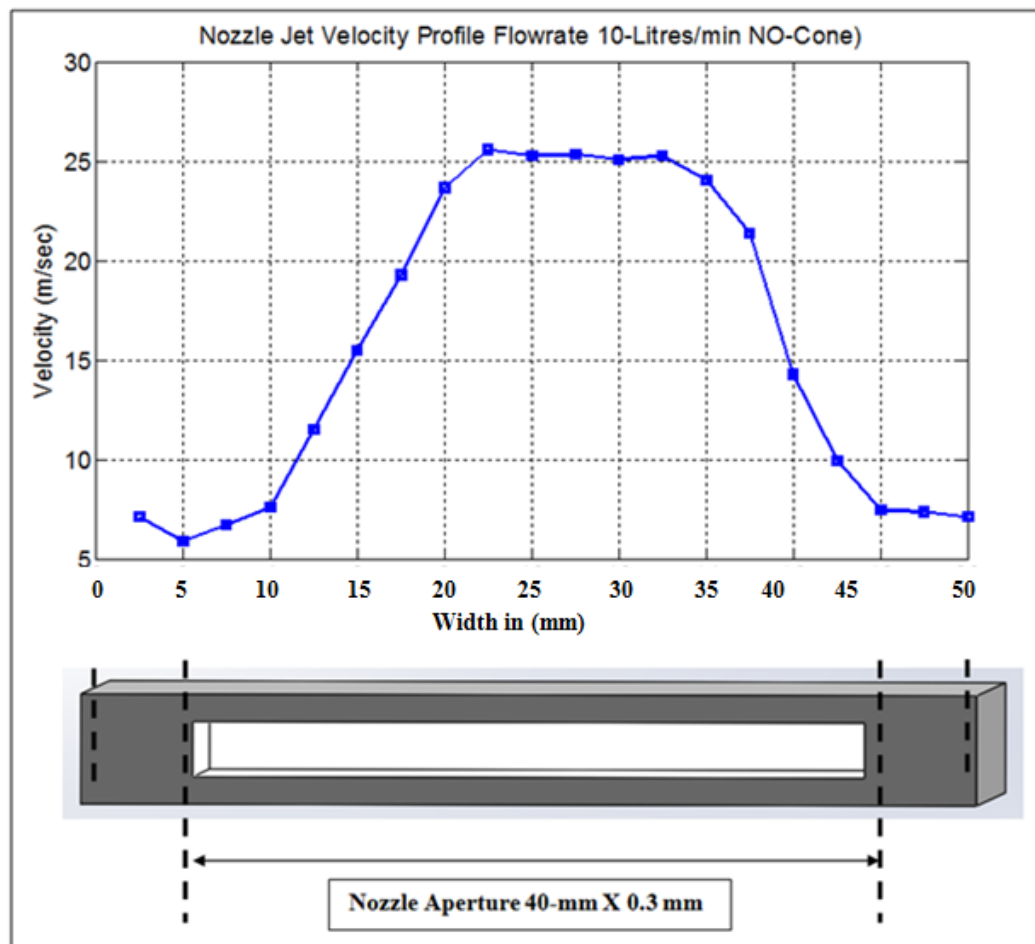


**Figure 6.10: Nozzle Exit Velocity Profile (Flow Rate 10 l/min No-Cone)**

Fig.6.10 shows the jet velocity profile at the immediate exit of the nozzle. The total width of the nozzle is 60-mm and nozzle aperture is 40-mm x 0.3-mm. On the middle layer 20-points picked with an interval of 3-mm distance is equally selected on nozzle exit face to draw a velocity profile. Here it is observed that the jet velocity is in parabolic shape this means high velocity is reached in centre of the exit and low velocity at the corners of the exit. This profile confirms that the nozzle exit width covers the wheel width with high velocity. With the supplied flow rate the nozzle exit is achieved of velocity 25 m/sec.

## 6.6.4 Pressure Plot (10-Litre/min-Single Phase Flow)

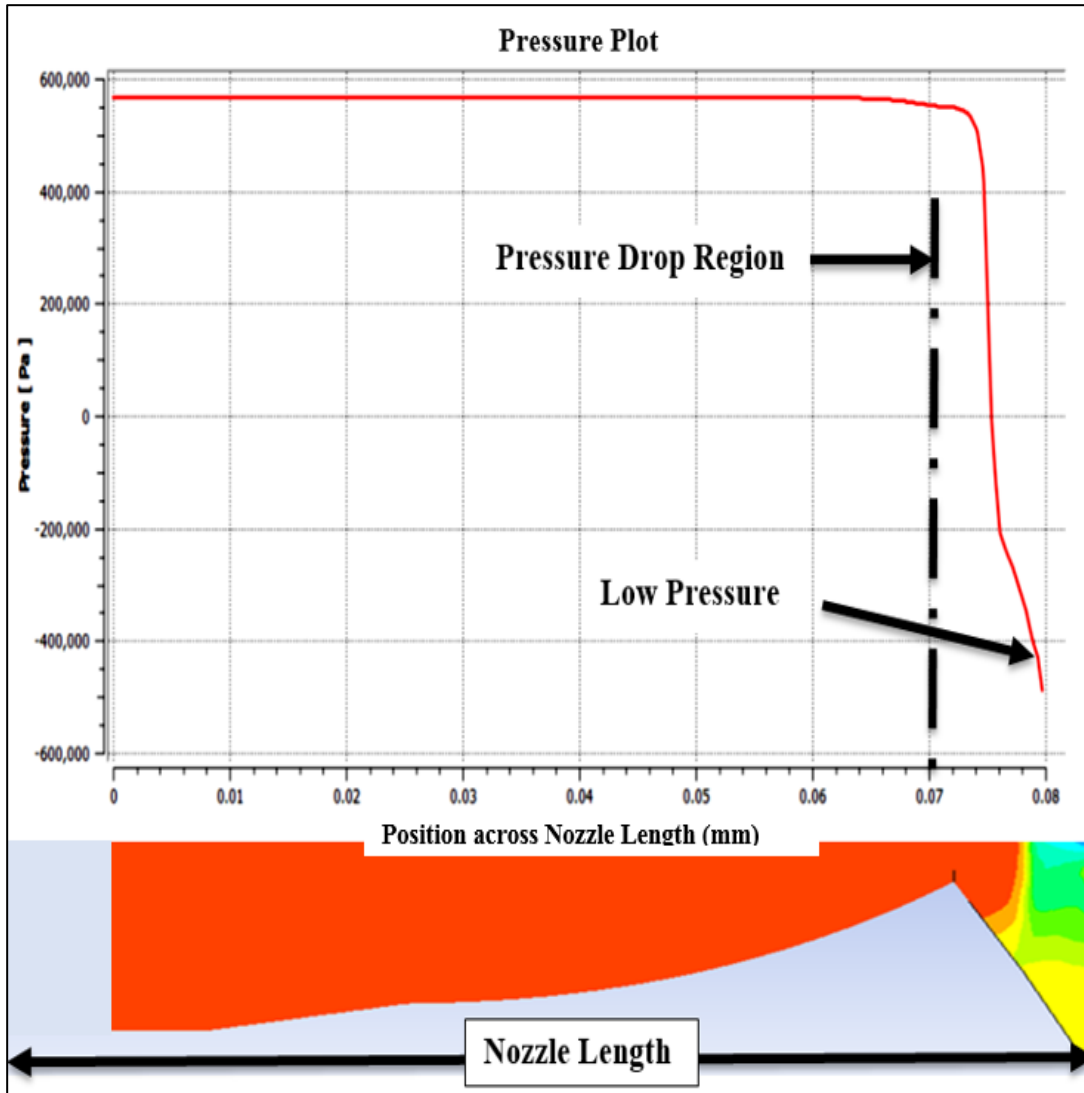


**Figure 6.11: Pressure Plot across Length of Nozzle (mm)**

Fig.6.11 shows a pressure contour drawn an axis line passing through in middle of the nozzle, here high pressure is formed only in large section of the nozzle and when it reached the narrow section the pressure gradually dropped due to the expanding cross section of the exit cavity. The Convergence of the process was reached after 100 iterations with an upwind and  $1e^{-06}$  target. Here, the residuals appear smooth and this gives a confidence in the results.

### 6.6.5 Plain Nozzle without Cone at 5-Litre/min-Single phase Flow)

The below Fig.6.12 (a) shows the results of simulation with a reduction of flow rate and four changes are found. One, the flow in the exit cavity is not fully developed and a sudden drop near the throat compared to the previous simulation Fig.6.12 (a) also a stagnation zones appeared at the exit corners. The supply of low flow rate 5-litre/min no-cone gave an average jet velocity of 16 m/sec. The supplied flow rate is not enough to develop fully in the exit cavity.

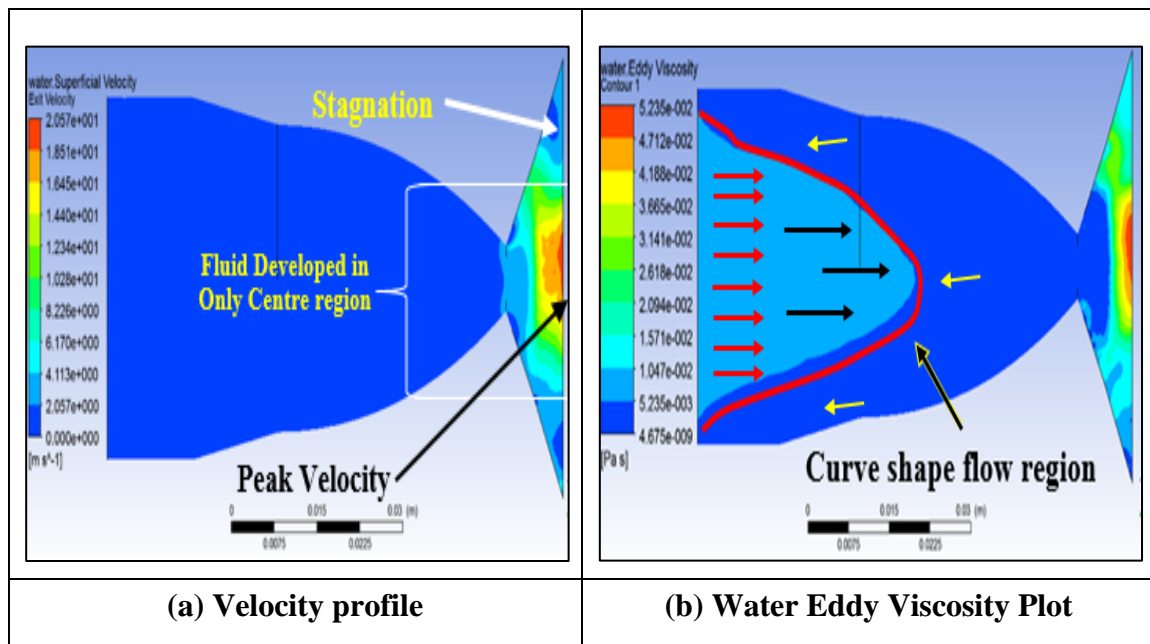


**Figure 6.12: Velocity Profiles of Nozzle Exit**

Investigating the water eddy viscosity plot a curved shape formation is appeared at rear side of the main nozzle inlet area with rising fluid shown in Fig.6.12 (b). This is the main cause of when the inlet flow enters into the main cavity the flow velocity stands up to certain distance and with opposing force that pushes back to the inlet flow, and in this process the fluid formed with curved shape. This flow pattern of this example is showed in the external flow jet velocity coherence length in chapter-8. In order to overcome this problem flow conditioner is inserted into the main cavity in the attempt to straighten the fluid into laminar form up to the exit. The performance of nozzle with

cone is presented in below section in comparison of both models 10 & 5 l/min with cone.

### 6.6.6 Nozzle Velocity Plot across length (5 Litre/min Single Phase Flow)

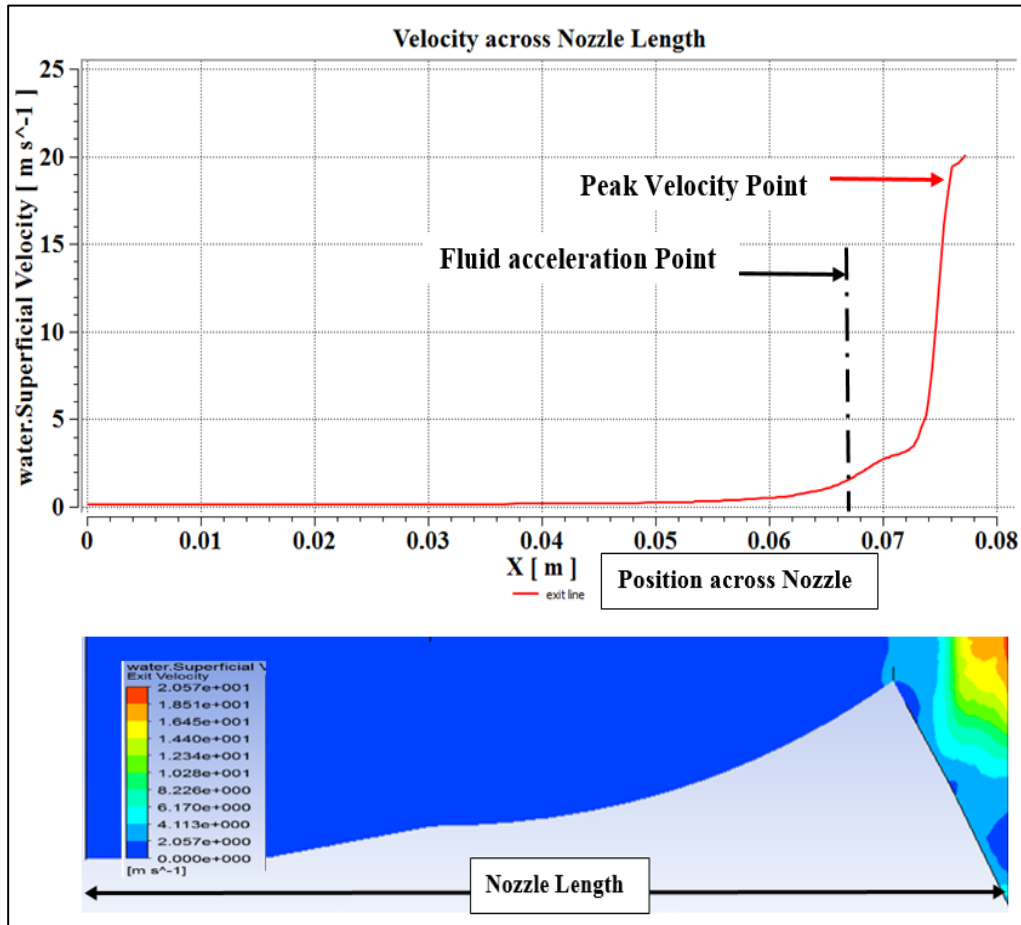


**Figure 6.13: Nozzle without Cone (Flow rate 5 Litre/min Single Phase Flow)**

Fig.6.13 depicts the velocity plot across the nozzle length and in this case the fluid velocity start accelerated at a point of 0.07 m and followed up to the exit. Comparing the previous simulation of 10 lit/min the fluid acceleration started at 0.05 m which is developed early. It means that the difference between the two flow rates is showing accelerating point difference of 20-mm distance with reduction of 5-lit/min flow rate. The average exit jet velocity reached with 10-l/m is 18 m/sec and 5-l/m is 12 m/sec.

### 6.6.7 Nozzle Exit Velocity Profile Plot (5 Litre/min Single Phase Flow)

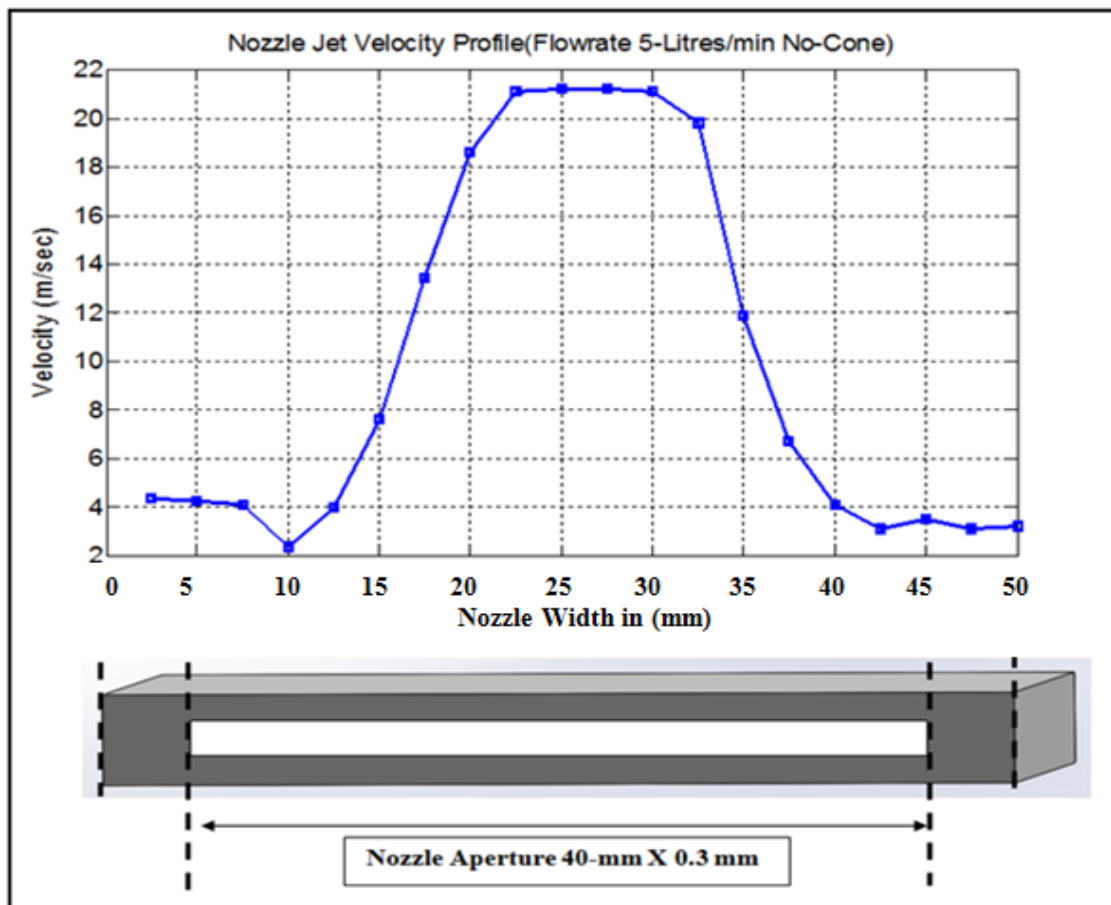


**Figure 6.14: Nozzle Exit Velocity Profile No-Cone**

Fig.6.14 illustrates the nozzle jet velocity profile and it reveals, that the actual fluid jet profile has an inverted “U” shape but by capturing the velocity points within the jet fluid showed in a parabolic shape. It is understood by this graph that the ends of the exit profile has low velocity and the jet is projecting high velocity in centre of the flow.

### 6.7 Nozzle with Cone at Flow Rate (10-Litre/min-Single Phase Flow)

Fig.6.15 (a) illustrates the nozzle with cone, which shows the effect and performance of cone in the main nozzle. the velocity cut plot it reveals that the fluid comes at lower velocity in the main flow once this low velocity fluid strikes the cone and enters into the narrow region of 1-mm gap, there it acquires additional momentum due to very narrow

gap thus develops pressure around the cone and the fluid is then fully accelerated up to the exit. It is also observed that the flow enters into the nested inlets fills and sticks in it, and this flow does not affect the internal flow of the nozzle. The effect of pressure cone in the main nozzle creating high pressure up to the nozzle throat illustrated in above Fig.6.15 (b).

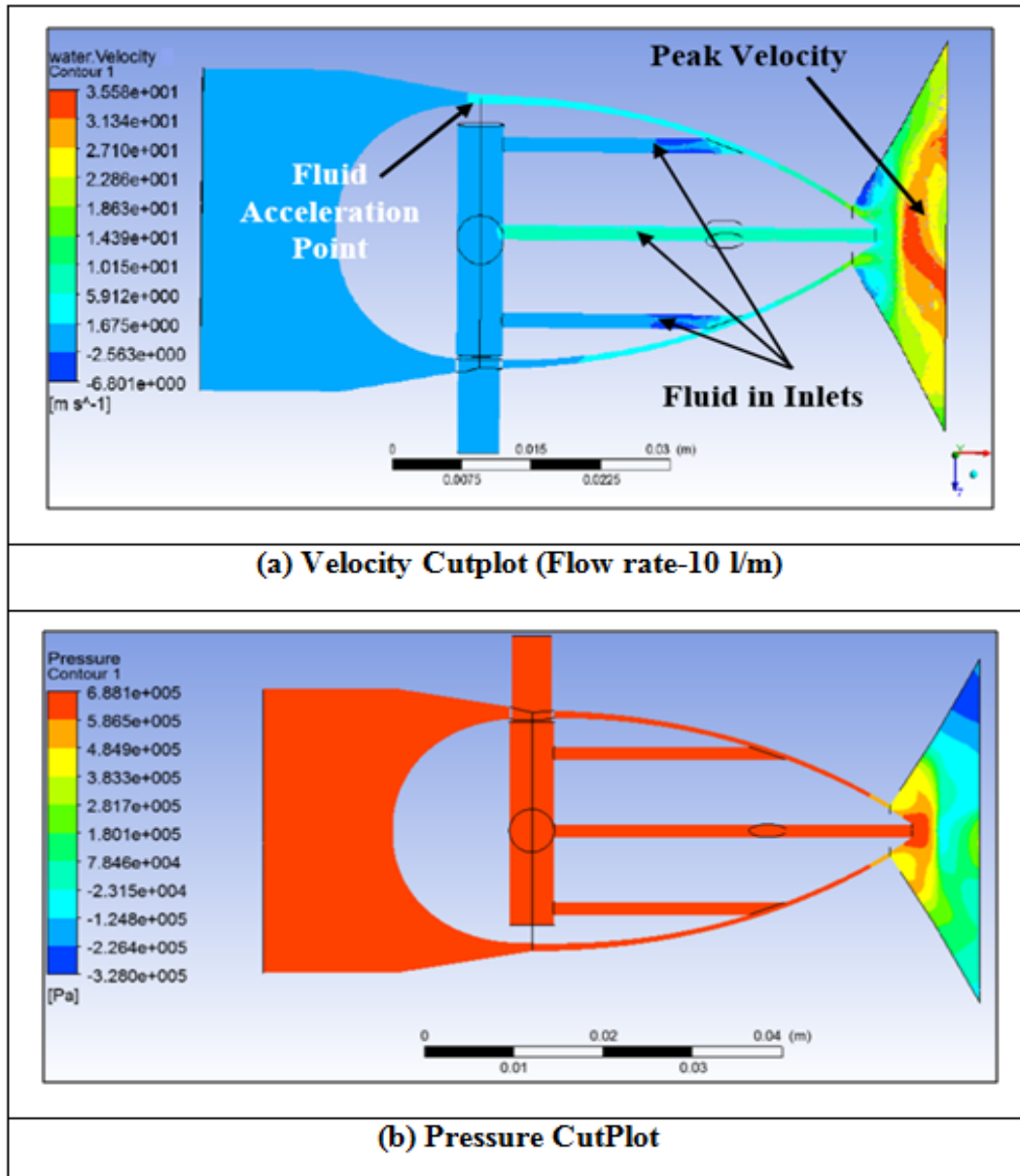
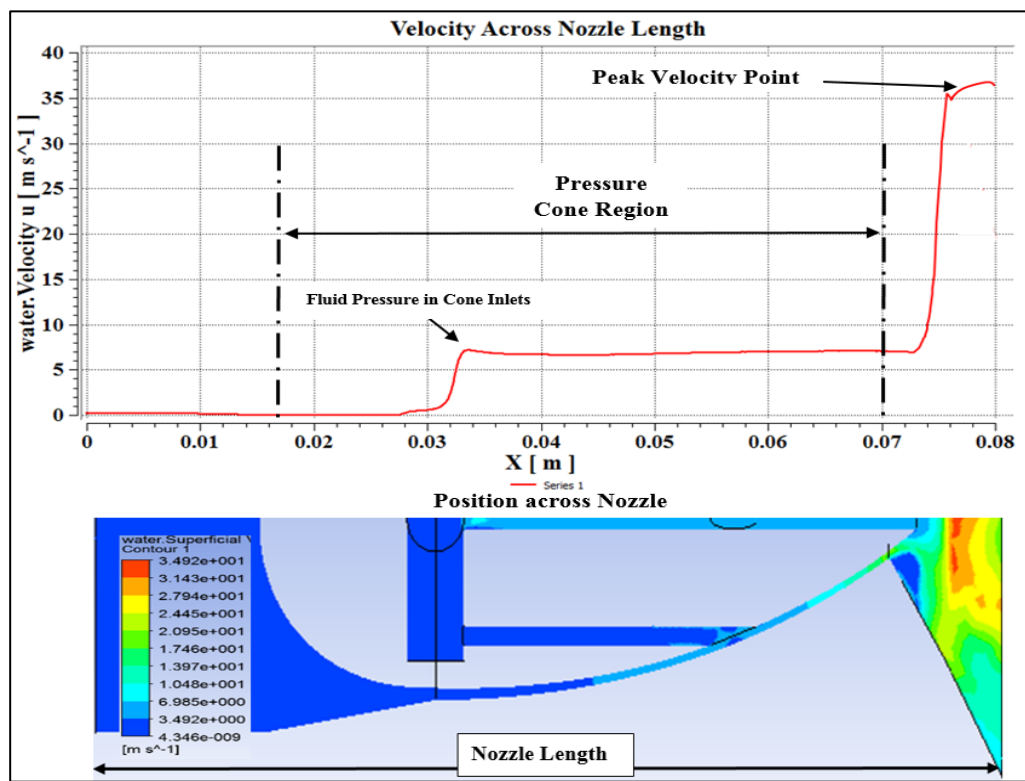


Figure 6.15: Nozzle Velocity Exit Profiles

The regions of low and high pressure across the nozzle length are explained in detailed in below Fig.6.16. The introduction of the cone showed a better performance, comparing both results of the nozzle with/without cone at 10-l/min. Since the outlet velocity and flow around the cone is being examined, it was observed that better result is obtained with increase in jet velocity. Fluid acceleration in the main nozzle increased earlier and the fluid is fully developed in the exit cavity.

### 6.7.1 Nozzle Velocity Plot with Cone (10-Litre/min-Single Phase Flow)



**Figure 6.16: Velocity across Nozzle length**

Fig.6.16 illustrates the velocity plot across nozzle length and gives a good insight of influence of the cone effect. The inlet fluid flow reached uniformly at a distance of 0.03 m where, the velocity increased due to the nested cone and flow uniformly up to the outlet tip of the nested cone is indicated by arrow. After the immediate exit of the nozzle throat, the fluid velocity increased in exit cavity with jet velocity of 35 m/sec.

## 6.7.2 Nozzle Pressure Plot with Cone (10-Litre/min-Single Phase Flow)

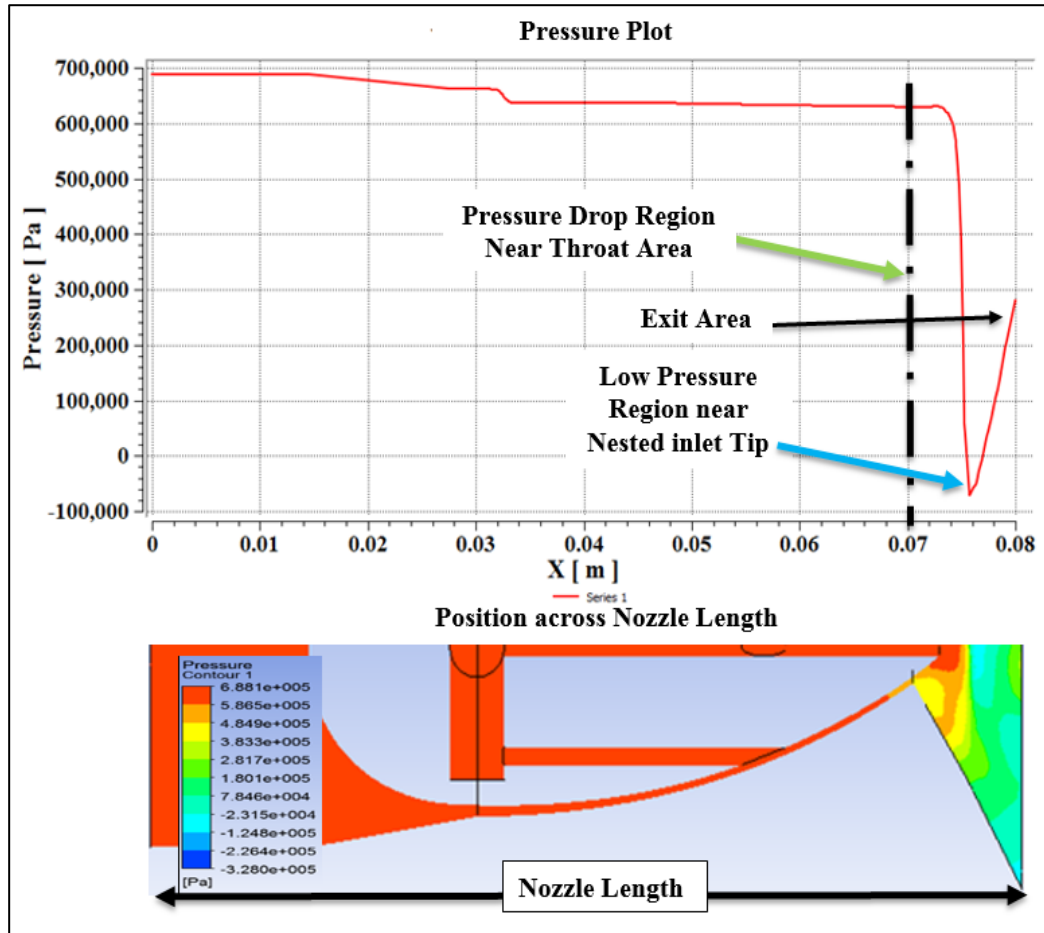


**Figure 6.17: Pressure Plot across Nozzle length**

The above Fig.6.17 illustrates a pressure plot of nozzle with cone 10-l/min single phase flow only coolant. From the plot it is clearly revealed that the high pressure is followed from the main inlet up to the cone area narrow passage and then the fluid pressure is gradually decreasing middle of the cone up to the lofted exit cavity due to the cone effect. This region has a very narrow passage way (1-mm) in the cavity and creates high pressure inside the nozzle cavity. After crossing the point at 0.07 meters, the pressure starts falling in the lofted throat area and again arises a bit due to varying the cross sections of the nozzle large volume to low volume. This pressure variation tends to raises the velocity in the exit cavity, as the pressure decreases velocity increases.

## 6.7.3 Exit Velocity Plot (10-Litre/min-Single Phase Flow)

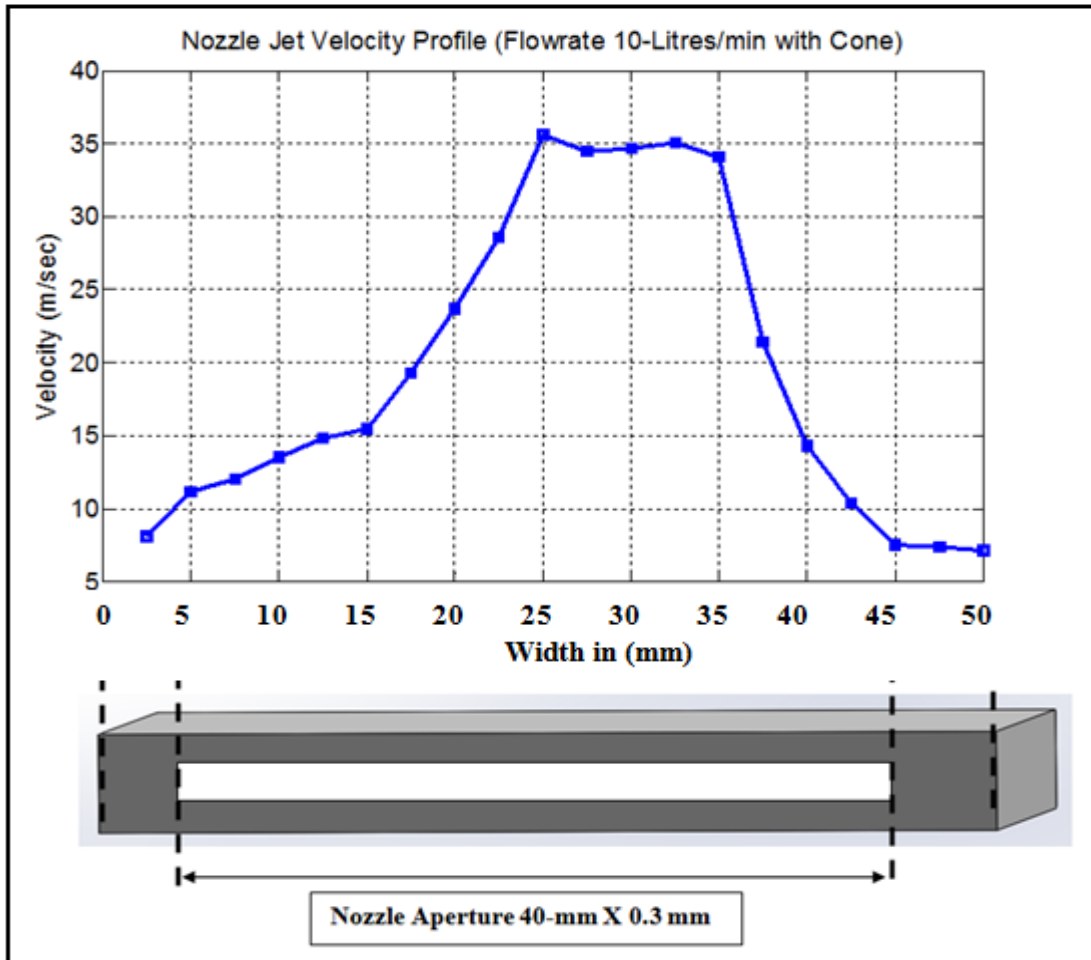


**Figure 6.18: Jet velocity Profile across Nozzle Width (With-Cone)**

The above Fig.6.18 depicts, the velocity profile plot drawn after immediate exit of the nozzle of 40-mm x 0.3-mm width. In this plot the peak velocity is achieved at the centre of the exit with a velocity of 35 m/sec. The shape of the flow formed like a conical profile with fully developed flow in the nozzle exit cavity. The peak velocity formed in the centre is caused by the insertion of the cone. Based on the Rouse-shape internal cavity profile and the elliptical shape cone with sharp tip at its end, allows the fluid sticks on its surface of the cone and tends to flow in the same shape which results high speed in the centre of the exit.

## 6.8 Nozzle with Cone at Flow Rate 5-Litre/min-Single Phase Flow)

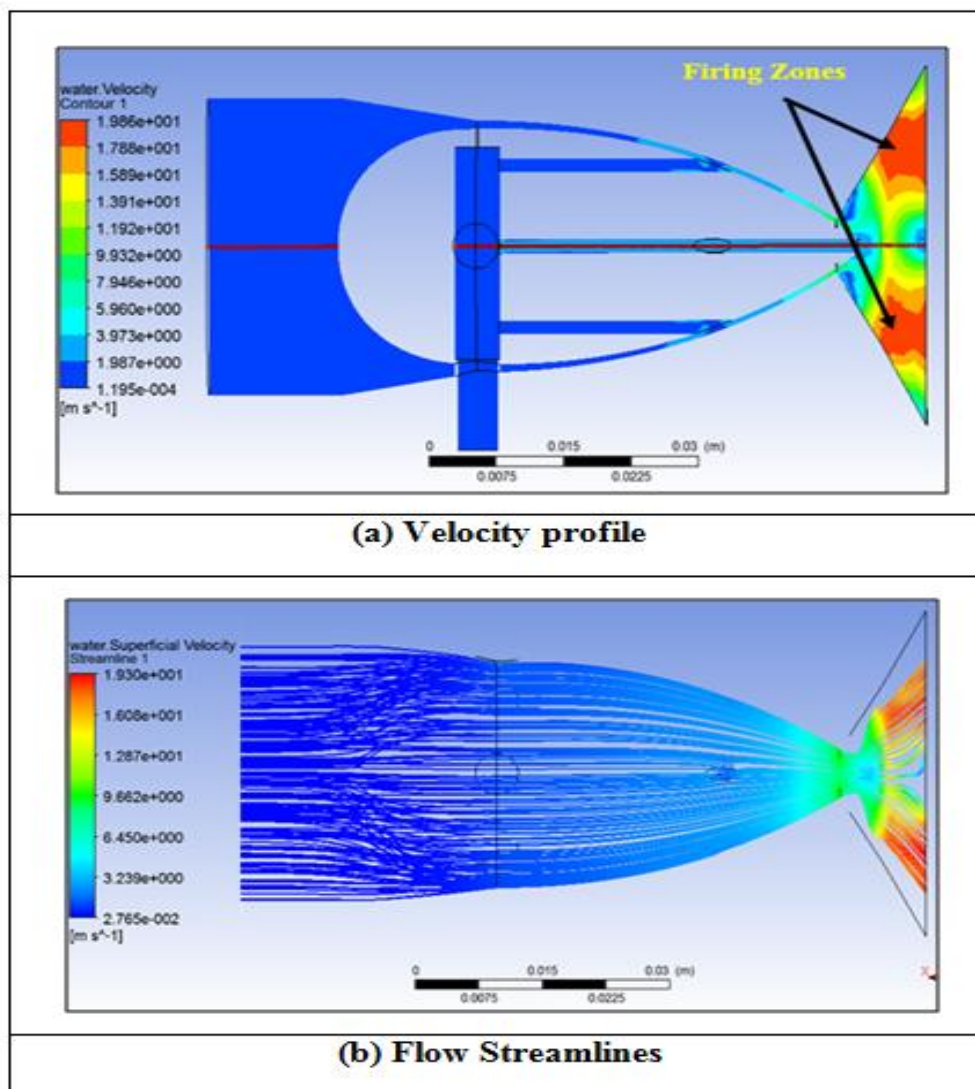


**Figure 6.19: Velocity Profiles of Nozzle Exit**

The simulation of nozzle with nested cone with flow rate of 5-l/min single phase flow is depicted in above Fig.6.19 (a). Here, in the exit cavity it is observed that high velocity appeared at both ends of the exit cavity this is due to the effect of cone cross firing from the narrow gap. The low flow rate easily entering into the narrow gap is accelerated more at the outlet tip of the nested cone and fluid start firing on both ends. But the entire length of the exit showed increased average velocity of 20 m/sec.

## 6.8.1 Nozzle Velocity Plot with Cone (5-Litre/min-Single Phase Flow)

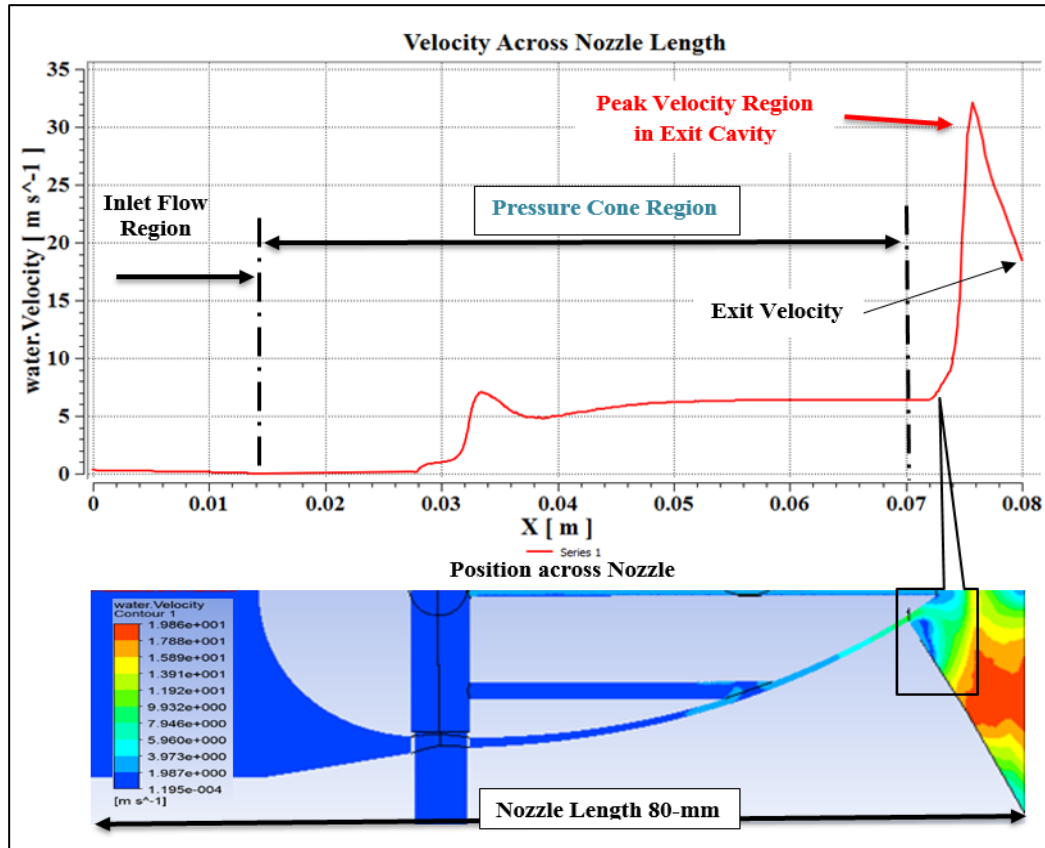


**Figure 6.20: Velocity plot across Nozzle length**

Fig.6.20 illustrates, the velocity plot drawn across the nozzle length horizontally to visualize the actual fluid flow region around the main inlet, cone and exit cavity width. The above simulation is performed with a supply flow rate of 5-litres/min with cone. From the simulation results it is observed that near the throat area the fluid velocity is increased up to 35 m/sec and drop and falls with a registered velocity of 20 m/sec after immediate exit of the nozzle. As in this case, the cone effect has shown improved exit velocity of same flow rate compared to the nozzle with no-cone. Also, it was observed that the fluid in the exit cavity forming cross firing on both ends of the exit. Whereas, comparing to the nozzle with supply flow rate of 10-l/min the exit cavity is fully developed. This was mainly caused by the supply flow rate; the low flow rate could not able to create the required pressure and fluid speed in the cavity.

## 6.8.2 Nozzle Exit Velocity Profile with Cone (5-Litre/min-Single Phase Flow)

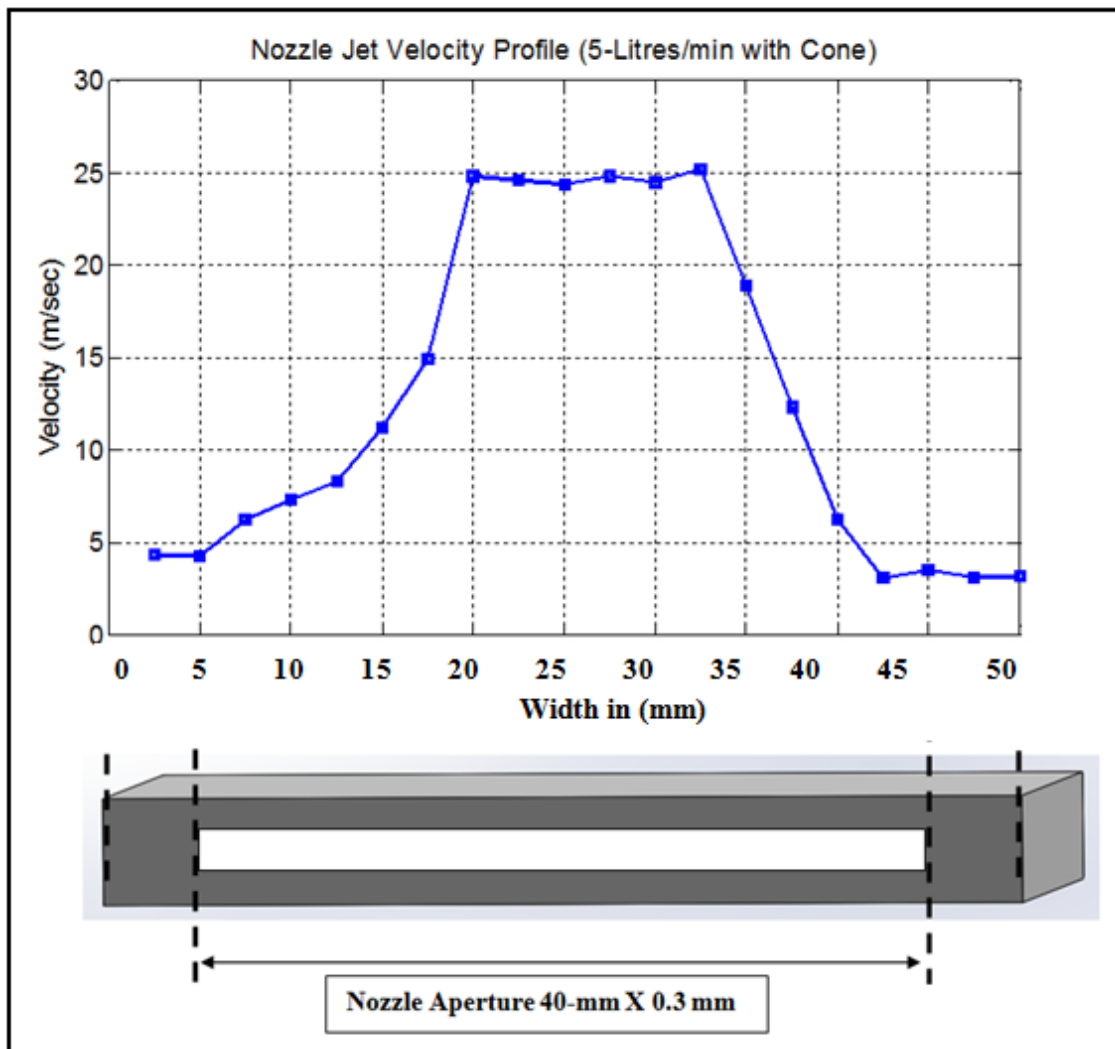


**Figure 6.21: Nozzle Jet Velocity Profile (With-Cone)**

A velocity profile is also drawn after immediate exit of the nozzle to visualize the fluid flow behaviour is depicted in the above Fig.6.21. The nozzle with cone at supply flow rate of 5-lit/min has registered with a peak velocity of 25 m/sec. As in this case also the profile is in conical shape. In the exit it was observed that the profile maintaining same jet speed with straight line in the centre, two peak velocity regions in the middle of the flow this is the effect of cross firing of the nozzle exit this region would matches the enough velocity with respect to the wheel speed.

**6.9 Nozzle with No-Cone (Single Phase) with Various Flow Rates**

In this refined simulation where the performance of the main nozzle is studied, the pressure cone is removed. Water was used as main fluid at the following flow rates: 40, 50, 60, 80, 100 and 120 Litres/min.

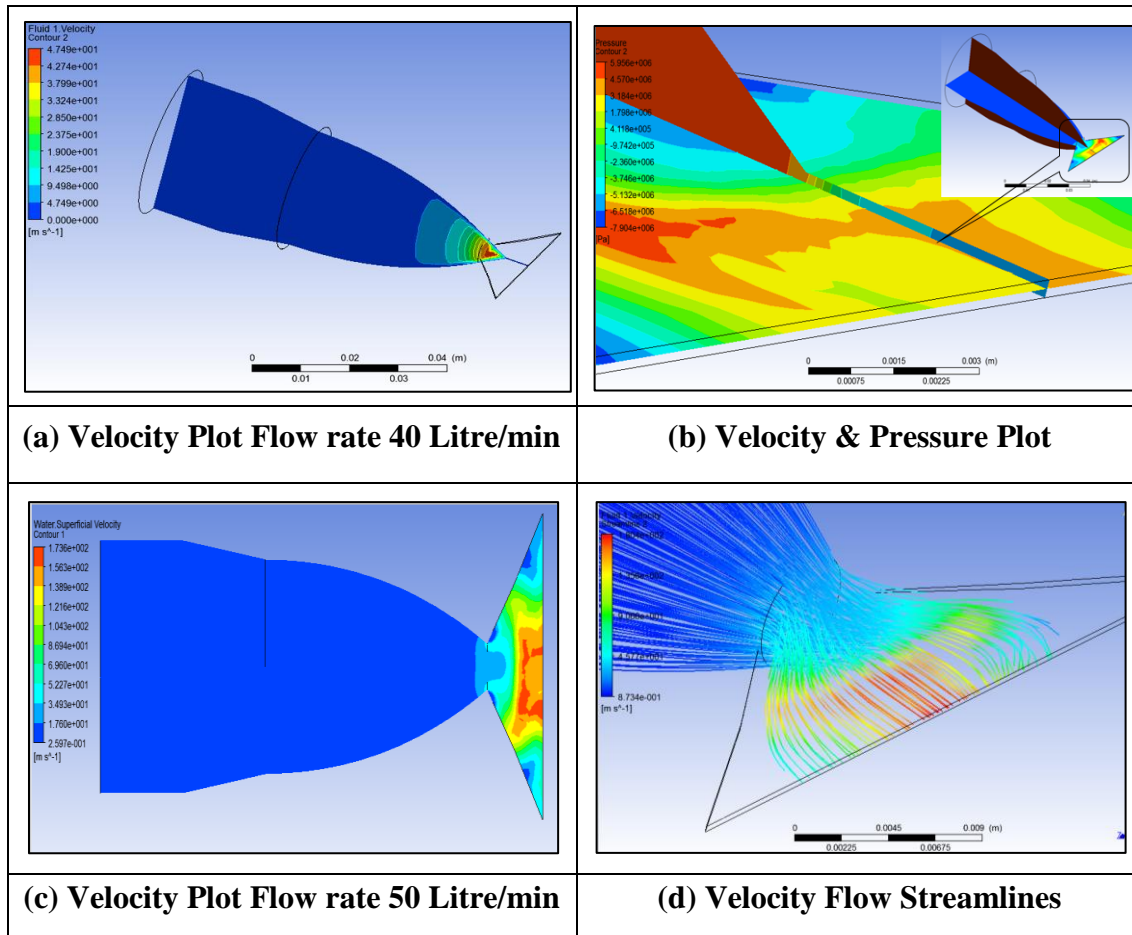


**Figure 6.22: Velocity Profile for Nozzle with No-Cone Flow rate 40 & 50 litre/min**

Three types of simulations were undertaken i.e. water only, water and air and then air and oil. Fig.6.22 (a) illustrates the performance of the main nozzle cavity without the pressure cone for a flow rate of 40-l/min of water. It is observed that the fluid has low velocity at the two tips of the exit cavity. However, high velocity flow was formed in the middle of the exit. This is because the main mass of the fluid is concentrated in the immediate middle of the nozzle exit, whilst only limited fluid reached the extreme tips

of the exit cavity. Fig.6.22 (b) is 2-plane plot of pressure and velocity profiles, where pressures are depicted in the vertical plane. As the exit cavity is only 0.3 mm a close up view is given where the horizontal plane with velocity profile is seen crossing the vertical plane with pressure profile. In Fig 6.22, for 40 & 50 l/min, the velocity of the fluid at the extreme tips of the exit cavity has increase but yet not to the desired state.

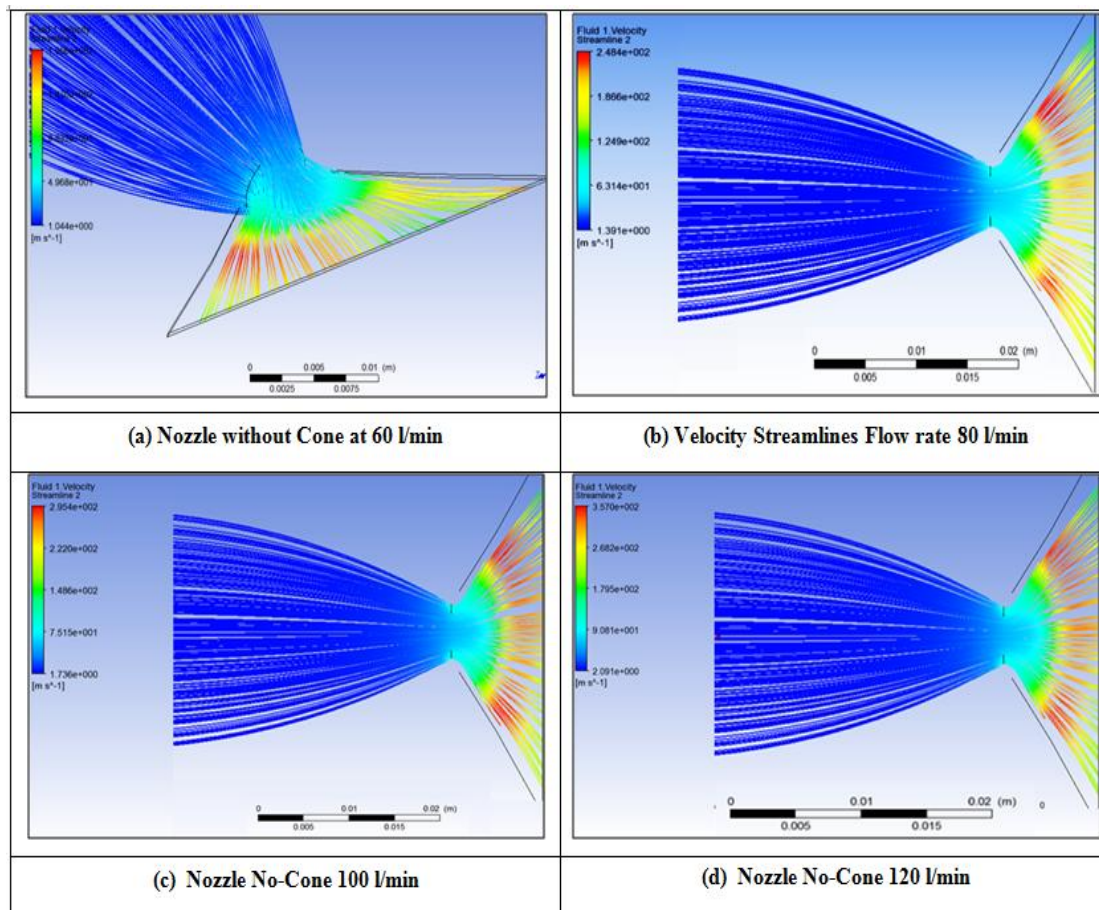


**Figure 6.23: Velocity Profile for Nozzle with No-Cone Flow rate 60 to 120 litre/min**

Fig.6.23 puts side by side the performance of four flow rates (60, 80, 100 and 120 l/min). Here it is seen that in all cases the fluid accelerates uniformly and reaches a peak velocity towards the second half of the exit cavity. This suggests that the exit cavity needs shortening to harvest the highest velocity as in this study the exit length is 10 mm. It is expected that by shortening the exit by 2-3 mm one could deliver peak velocities.

## 6.9.1 Nozzle Exit Velocity Profile Plot with various Flow Rates (No-Cone)

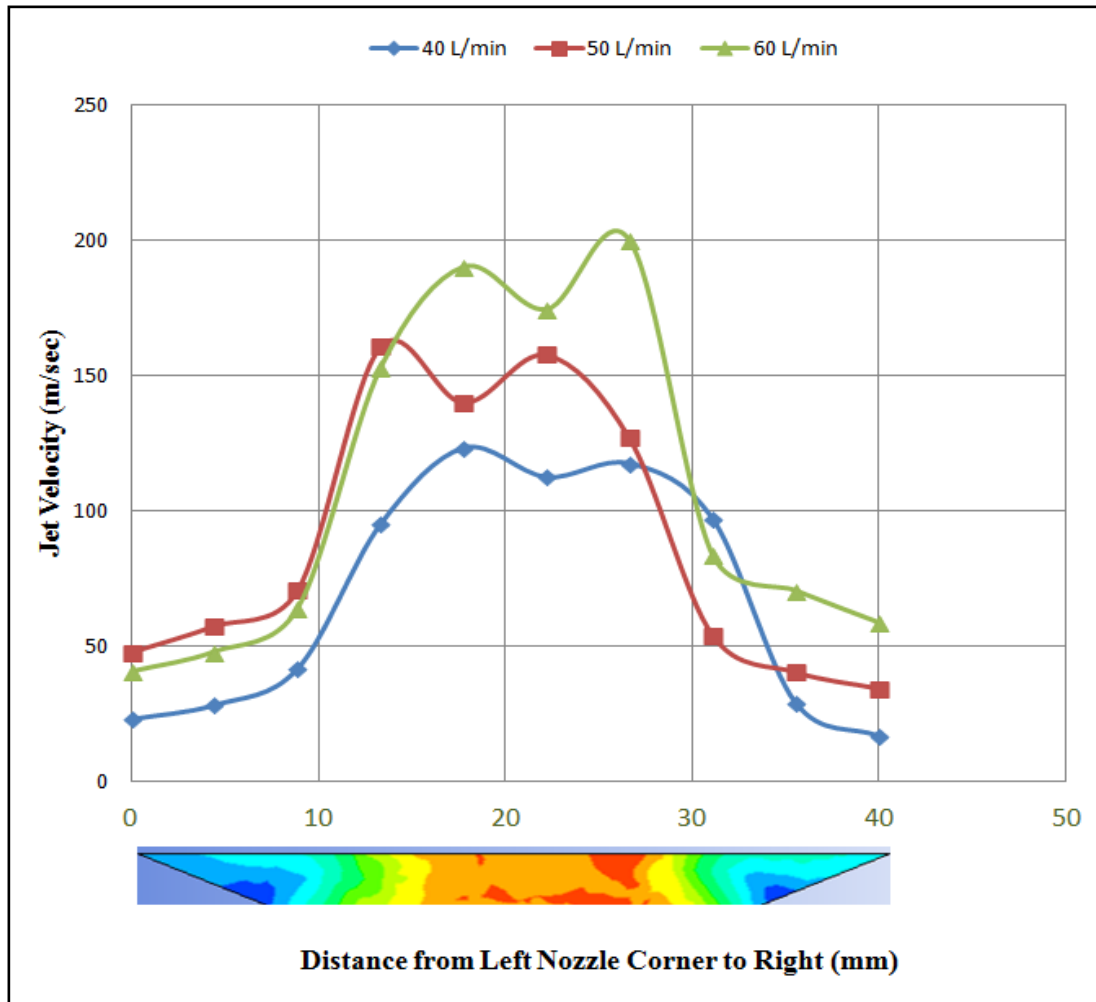


**Figure 6.24: Velocity profile in the centre line across the nozzle exit**

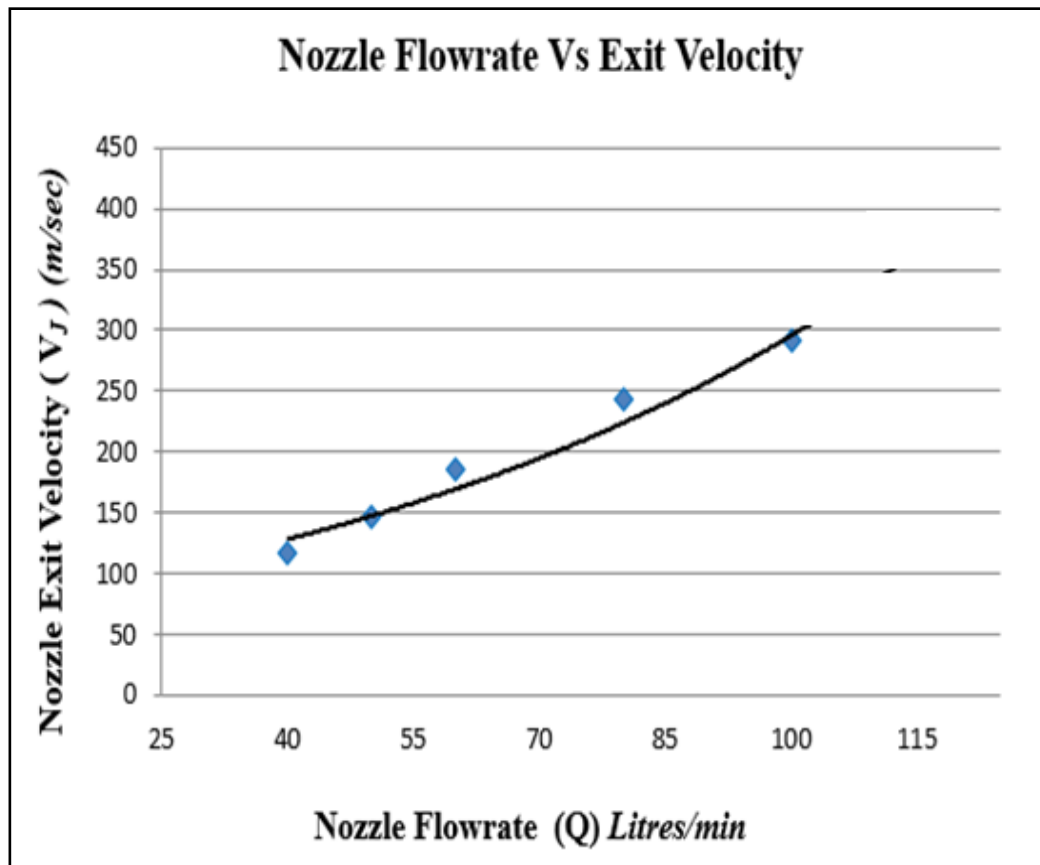
Fig.6.24 shows the jet velocity at the immediate exit of the nozzle for a range of flow rates. Here, it is observed that for 40-60 l/min the jet profile is uniform and symmetrical across the nozzle. However, for 80-120 l/min the peak velocity is skewed from the middle of the nozzle exit towards the right. The reason is unclear and need further study. However, this graph shows that flow rates up to 60 l/min are good enough to generate stable velocities up to 120 m/s which are adequate for grinding application. Therefore, above 60 l/min the skewed profile of 80-120 l/min is not an issue for direct application rather a scientific understanding.

### 6.9.2 Comparison of Nozzle Simulation Results

Flowrate L/min	Nozzle No-Cone Exit Velocity (m/sec)	Nozzle with Cone Exit Velocity (m/sec)	Percentage Increase (%)
5-L/min	16	19.5	21.8%
10-L/min	21.7	35.5	63.6 %

**Table 6.3: Comparative Results of Various Flowrates and Nozzle Exit velocities**

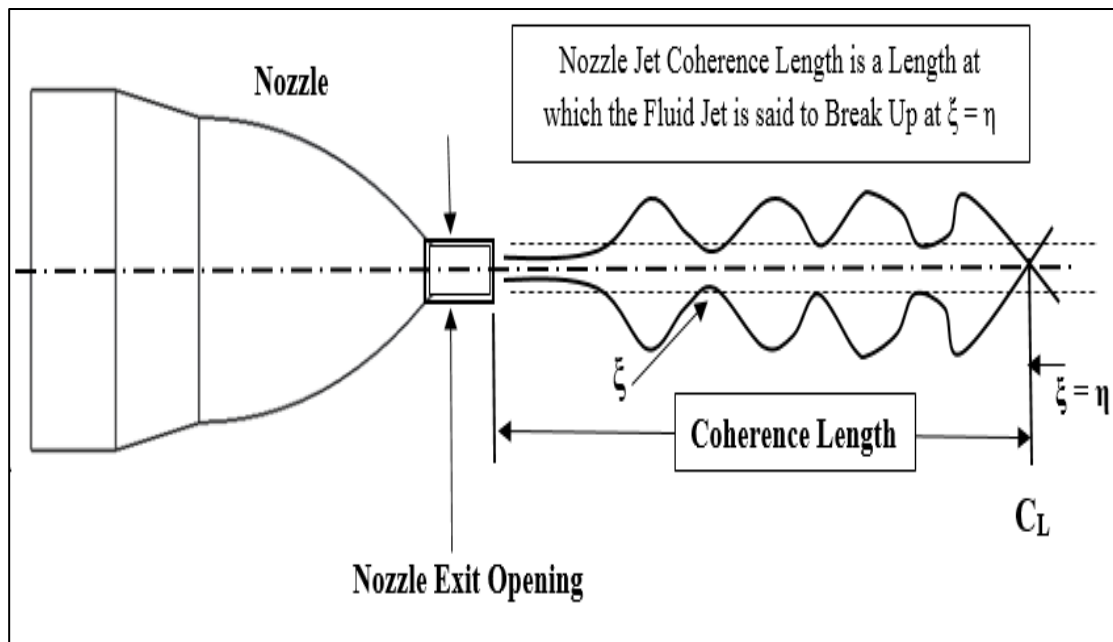
The above table-6.3 presents the simulations values of nozzle jet velocities with a range of flow rates and nozzle conditions. Using the jet velocities of nozzle with cone and without cone gives comparative results and also an insight into the effect and influence of this new novel adaptive nozzle model. The first simulation is performed nozzle without cone with flow rate at 10 l/min showed 21.7 m/sec and the same flow rate with cone is 35.5 m/sec which is an increase of 13.8 m/sec. The percentage increase in velocity by introducing this cone is achieved 38.8 % in the case of 10 lit/min. whereas the flow rate with 5-litres/min is 17.9 % increase in velocity. Fig. 6.25 illustrates the output jet velocity as a function of input flow rate. It is seen due to inadequate design of nozzle, industrial applications use up to 120 l/min, with associated high cost of pumping and fluid maintenance. Whereas in this optimised design a cut down of 50% i.e. 60 l/min of flowrate secures the need of 120 m/s jet velocity.



**Figure 6.25: Nozzle Exit Velocity Vs Various Flow rate**

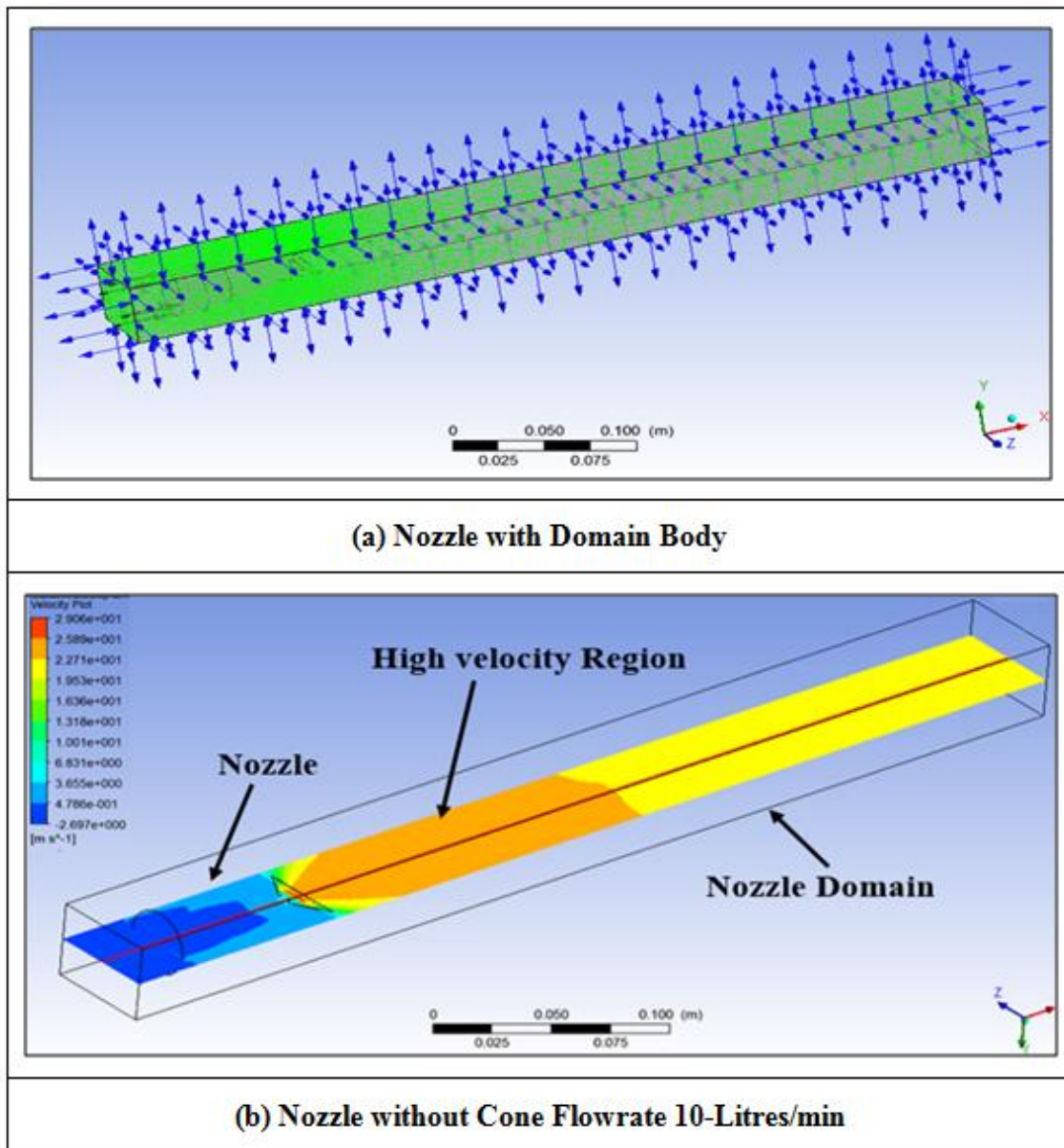
### 6.10 Nozzle Jet Coherence Length Determination from Fluid Jet Break Up

The delivery of adequate supply of coolant to the grinding cutting interface is achieved through nozzle orifice. The geometry and internal profile of the nozzle influences the fluid velocity and flow pattern on exit from the nozzle orifice. The performance and efficiency of the grinding process requires that the fluid is delivered in a systematic manner to ensure that desired fluid jet velocity has adequate coverage of the cutting interface. The sufficient coverage of fluid is based on visual inspections of the jet coherence length. In this section the work provides a new insight into an analytical model to predict the nozzle jet coherence length of a novel modular adaptive nozzle design is presented. Many researchers worked and investigated on the flow of jet issuing from differing nozzles in differing industrial applications.



**Figure 6.26: Schematic for the definition of Nozzle Jet Coherence Length**

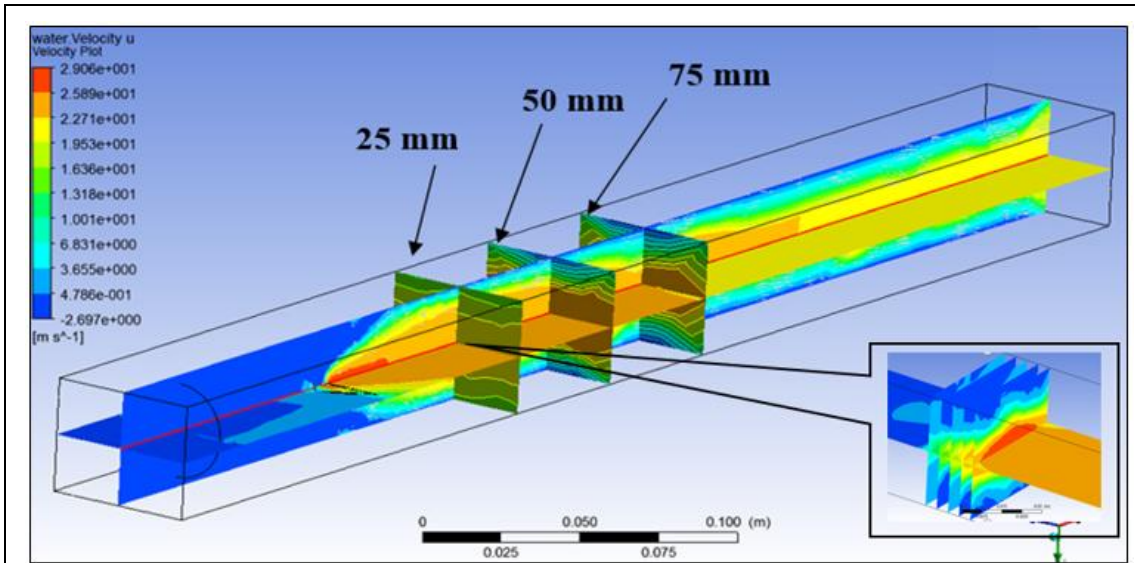
This is a theoretical basis of jet break up, but many relations come from confirmation experiments. McCarthy and Molloy (1974) undertook an experiment evaluation of the break up length. Their relationships form in the ways shown in Fig.6.26 giving relationships between the jet break up length  $L$  (coherence Length  $C_L$  in this work) and jet velocity  $V_J$ .



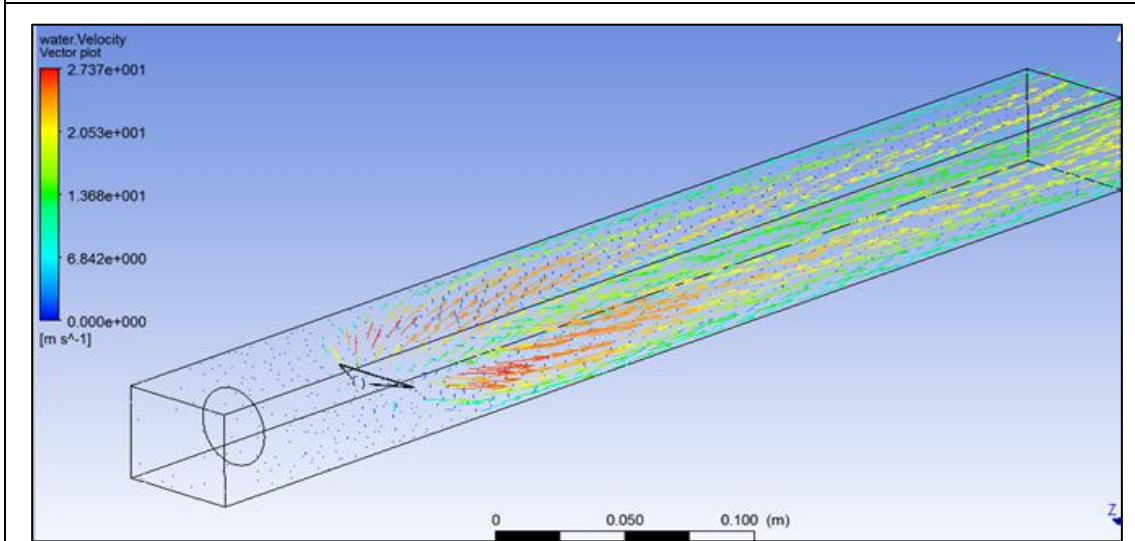
**Figure 6.27: Velocity Contour Plots Drawn on Horizontal and Vertical Planes**

Fig.6.27 (a) illustrates the meshing of the area on interest, whereas Fig.6.27 (b) shows the jet fluid emerging from the nozzle and flowing into the computational domain chamber containing air. The free surface model employed allows the water to interact with air at the boundary between two. The velocity exhibits the expected behaviour in that jet becomes thicker due to overall spreading of the fluid however, the peak velocity

decreases. The fluid simulation using SST model for turbulence and multiphase physics to study the speed conservation length shows that the jet hold its speed over approximately 90 mm with exit of peak velocity of 30 m/sec. The arrangement of slices is presented in appendix (A-2.4 to 2.6).



(a) Planes drawn On Horizontal velocity Cutplot (Inset Plane Slices)



(b) Velocity Vector Plot

Figure 6.28: Cut planes where jet velocities were recorded

Fig.6.28 (a) shows the fluid jet out of the nozzle with vertical and horizontal slices drawn to convey the fluid flow behaviour. The simulation is performed to determine the nozzle coherence length in order to position the nozzle relative to the cutting interface. This process is performed in a systematic manner by placing a set of velocity cut plot slices positioned at various distances from nozzle orifice up to fluid jet Fig.6.28 (a) and the inset figure shows slice planes at regular intervals up to the 50-mm distance. The velocity points are captured on every slices middle layer with a series of 20-points horizontally. Fig.6.28 (b) illustrates a total velocity vector plot of a jet flow direction in a domain. A series of velocity profiles are plotted as shown in Fig.6.29.

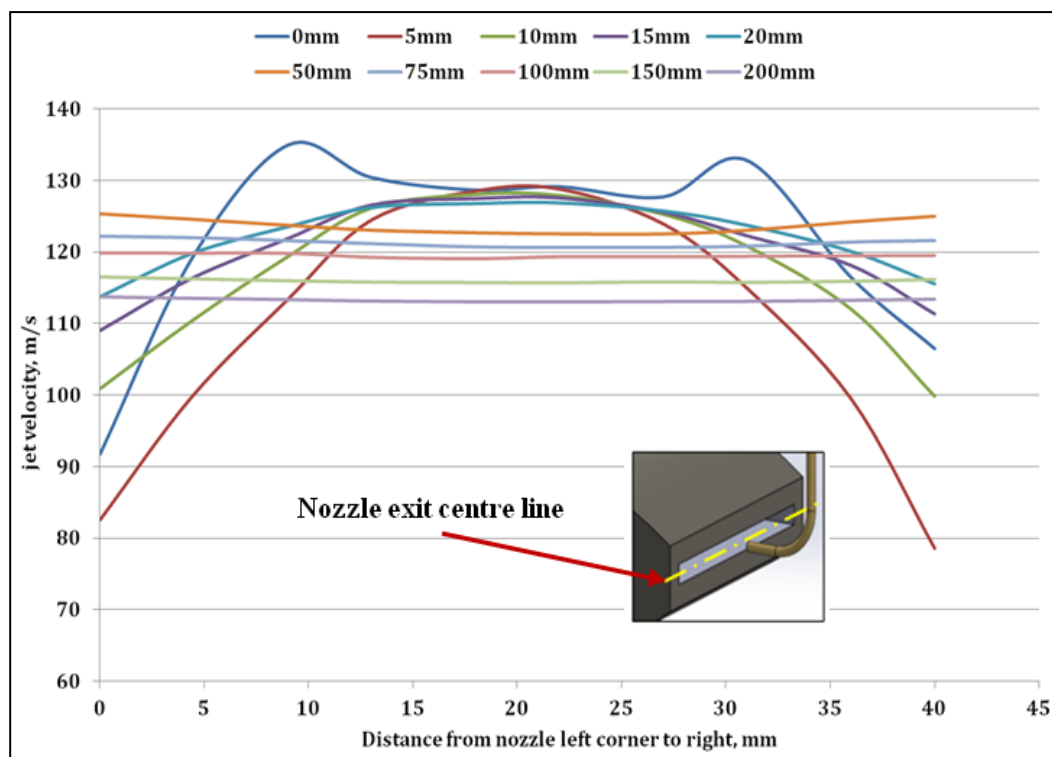


**Figure 6.29: Velocity profile in the centre line across the nozzle exit up to 200 mm**

Fig.6.29 displays the jet velocity profile across nozzle width and away from the exit at distance 5-200 mm for a flow rate of 50 l/min. It shows that the jet keeps a stable average velocity of around 120 m/s across the nozzle. Here the line denoted by “0 mm” is the velocity at the immediate nozzle exit in the centre line, where higher jet velocities

present a turbulent profile due to the effect of exit edge shape and burst into atmospheric pressure. However, at 5 mm away from the exit the jet displays a profile similar to laminar flow. Therefore, it is preferred to position the nozzle a bit back about 50 mm for improved performance or very close to the wheel for cleaning purpose. Fig 6.28 (a) shows the planes (velocity Slices) kept where the velocities were captured to illustrate the jet profile.

### 6.11 MQL Nozzle Simulation with Cone (Air & Oil Multi-Phase Flow)

The dual (multiphase) flow model is made of two inlets: the main inlet which is air inlet at 4-bar and the secondary flow of low volume oil (MQL). The MQL flow is supplied through the pressure cone at a flow rate of 100 ml/hour. The most time consuming is the meshing, refining and adaptation, especially for the zone of tiny features such as the five oil ducts. Fig.6.30 (b) shows a typical meshing configuration used in this study. The following parameters were used for this refined simulation.

#### ***Input Data***

Fluid type: Oil & Air

Main inlet flow: Air at 4 Bar

MQL inlet flow: Oil at 100 ml/hr

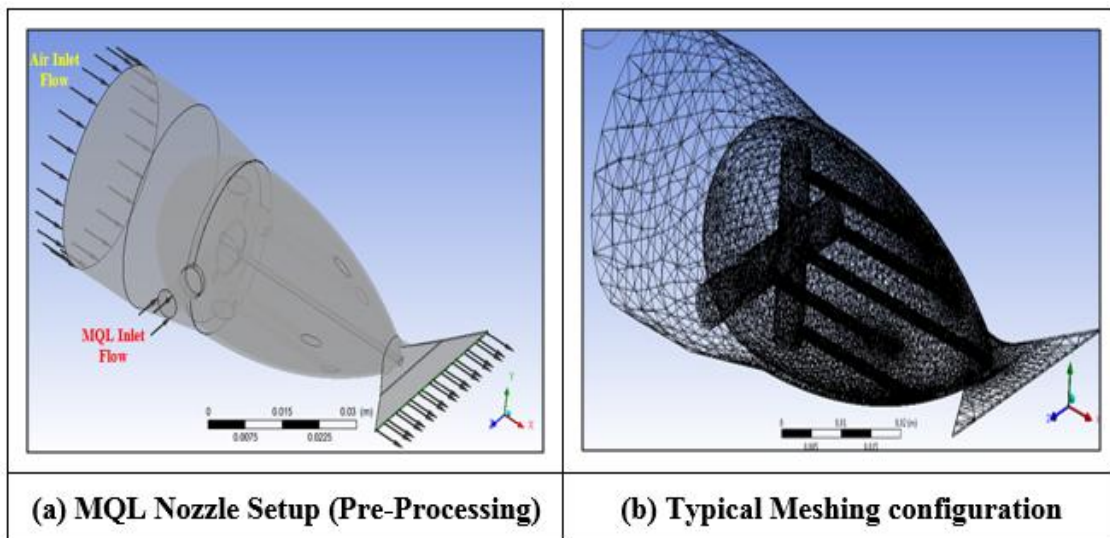


**Figure 6.30: MQL Nozzle Configuration**

The Fig.6.30 (a) shows the pre-processing setting of the MQL nozzle. The main inlet flow is supplied with air with 4-bar and a 100 ml/hr flow rate is supplied into the nested inlet flow. The simulation results of this MQL nozzle showed good performance, in Fig.6.31 (a) with the help of surface plot it is understood that the acceleration of air and oil appeared to be a multi-layer formation which is gradually increasing and passing through the throat up to the nozzle exit. It is also observed that the air and fluid acceleration point formed early with multiple layers and a fully developed with high jet velocity of 25 m/sec, which is indicated by arrows.

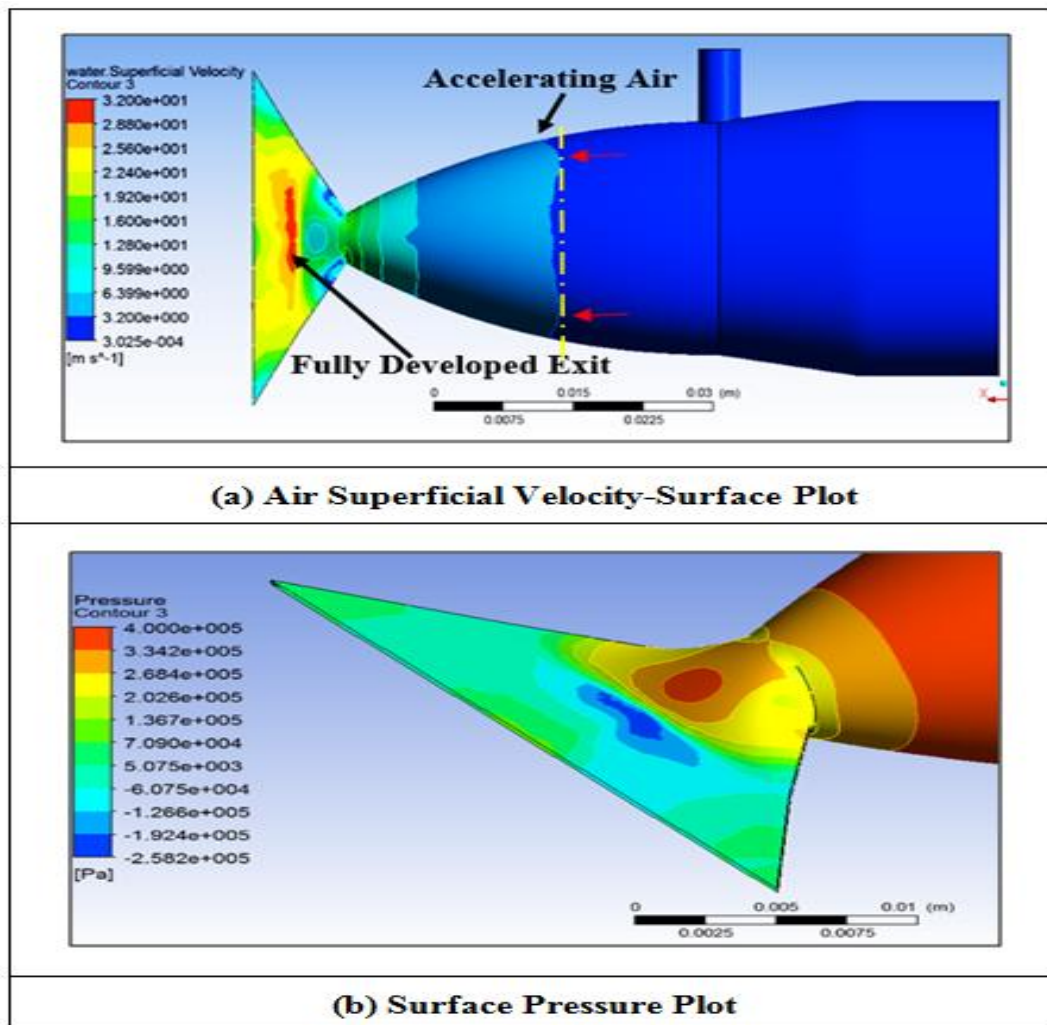


Figure 6.31: MQL Nozzle Simulation for Air & Oil Multi-Phase Flow

The velocity streamlines of this MQL nozzle showed fully laminar flow from inlet to the exit. The flow behaviour of air pressure inside the nozzle is firing only in centre of the exit cavity this is due to 'Coanda Effect', where the cone shape drags the air to low pressure area (negative pressure) which resulted in middle area. The surface pressure plot of this nozzle depicted in above Fig.6.31 (b), has a layers of air pressure contours formed near the throat area that shows the acceleration of the air passing from high pressure region main nozzle to the low pressure exit cavity region. The MQL simulations showed in appendix (A-2.1 to 2.3).

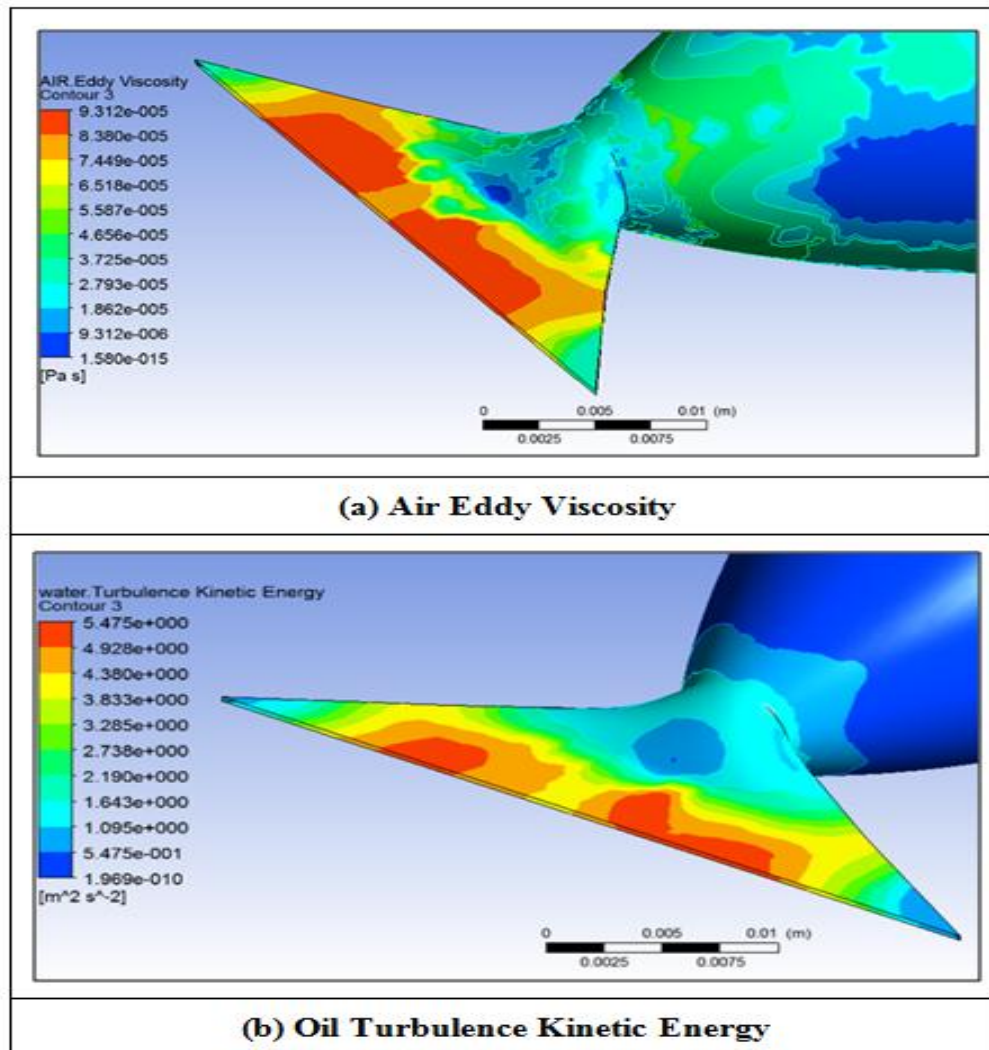
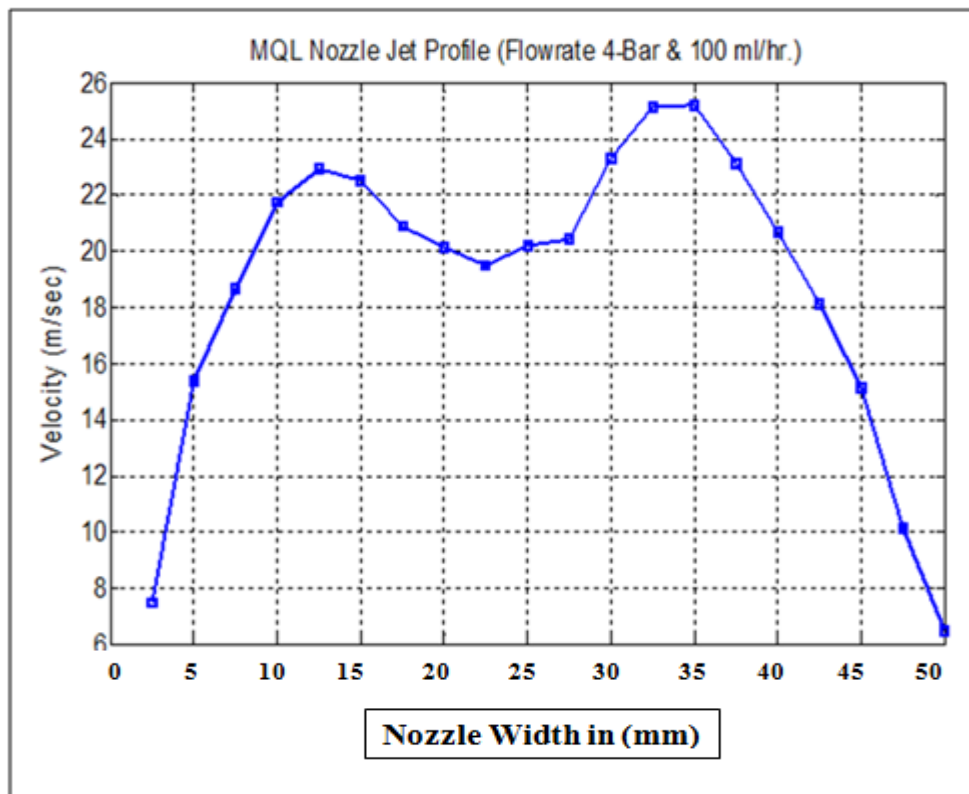


Figure 6.32: Multiphase Nozzle Simulation

The above Fig.6.32 (a) illustrates the air eddy viscosity plot, to study the strength or resistance of the fluid creating any frictional forces near the walls. These opposing forces or wall surface roughness tends to increase the temperature of the fluid within the nozzle. The viscosity is a measure of fluid thickness or resistance to gradual deformation by shear stress or tensile stress. For liquids, normally viscosity is a property arises from collisions between neighbouring particles in a fluid that are moving at different velocities. In this simulation air and water is used as a fluids, from the main inlet air is forced through a narrow passage. Thus fluid particles generally move faster near the axis of the inlets or and more slowly near its walls due to wall roughness. Therefore, to overcome this problem some stress is needed to increase the pressure difference between the two ends of the nozzle and friction between particles layers to keep the fluid moving. The plot shows that air distribution on cone surface has a medium viscosity and some areas showing lower viscosity. For a given velocity pattern, the stress required is proportional to the fluids viscosity.

Fig.6.32 (b) depicts the oil turbulence kinetic energy, and is characterised by measured root-mean-square (RMS) Velocity fluctuations. Normally turbulence is a type of fluid or gas flow that undergoes irregular fluctuations, swirls, mixing, or in contrast to laminar flow, in which the fluid moves in smooth paths or multi-layers. In turbulent flow the speed of the fluid at a point is continuously changing in both magnitude and direction. Turbulence can be visualized by irregular swirls of motions called eddies. In this simulation the turbulence kinetic energy plot no recirculation or eddies is seen on surface of the cone and nozzle area. The fluid is accelerating near the throat due to varying section and high velocity reached in exit cavity. The cone almost induces laminar flow near the walls whereas in some critical areas (near cone outlets tip area) and at exit cavity the flow seems to be fully developed without any eddy formations.

## 6.11.1 MQL Nozzle Velocity Plot (Main Inlet 4-Bar, Nested Flow 100 ml/hr)



**Figure 6.33: MQL Air Exit Jet Velocity**

The above Fig.6.33 depicts, the MQL nozzle simulation with air & oil used as fluids. The main inlet flow was set to 4-bar air pressure and 100 ml/hr. was set into nested nozzle. Here, also same the nozzle exit width is divided into 20-points with distance of 3-mm is drawn exactly after immediate flow exit of the nozzle orifice which is in middle layer. Here, the jet profile formed like a spline shape. The drop in velocity in the middle is caused by the pressure difference between the tip of the cone and the firing points (see Fig.6.31 b) that create a negative gradient that holds back the acceleration of the fluid in the middle of the nozzle. As the speed of the MQL oil supply is in droplets with low pressure and high air supply around the cone surface this resulted in spline shape formation. This can be eliminated with an increase in the supply of air pressure shown in Fig 6.35.

6.11.2 MQL Nozzle Velocity Plot (Main Inlet 6-Bar, Nested Flow 100 ml/hr.)

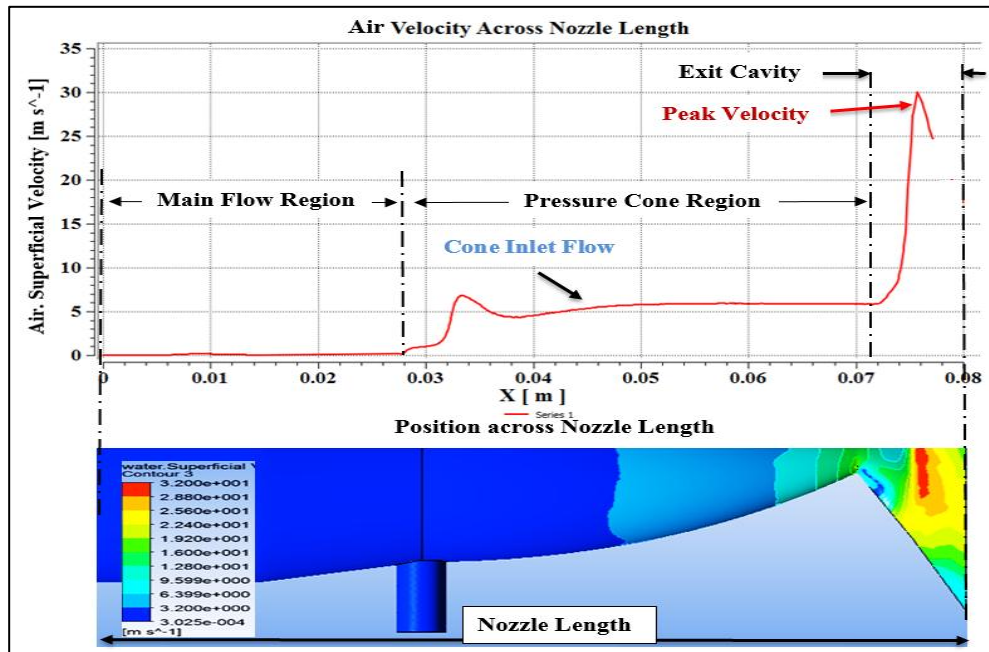


Figure 6.34: MQL Air Exit Jet Velocity across Nozzle Length (6-bar)

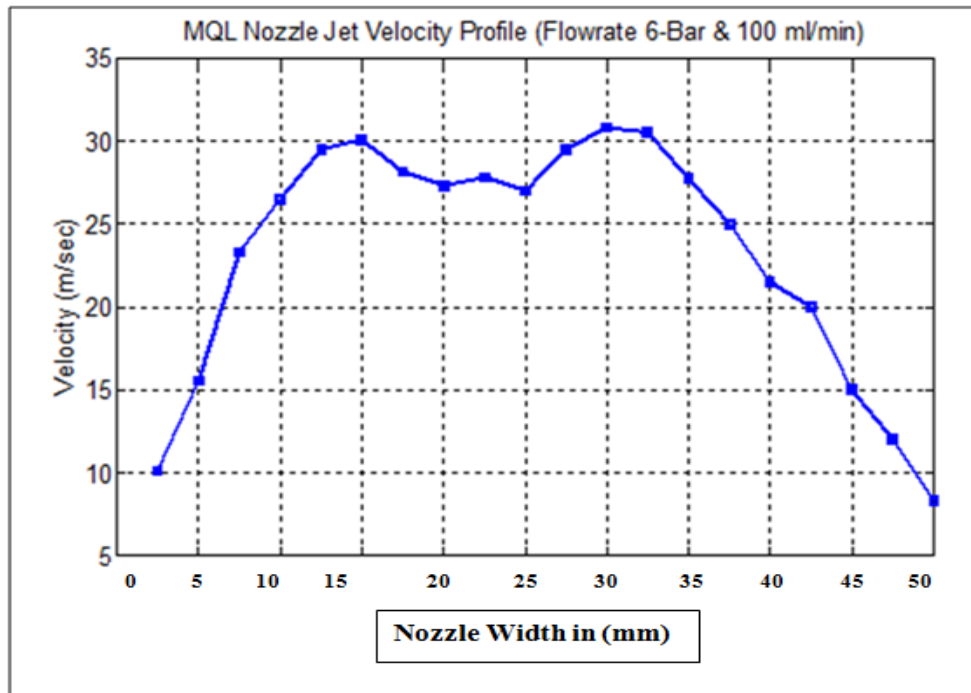
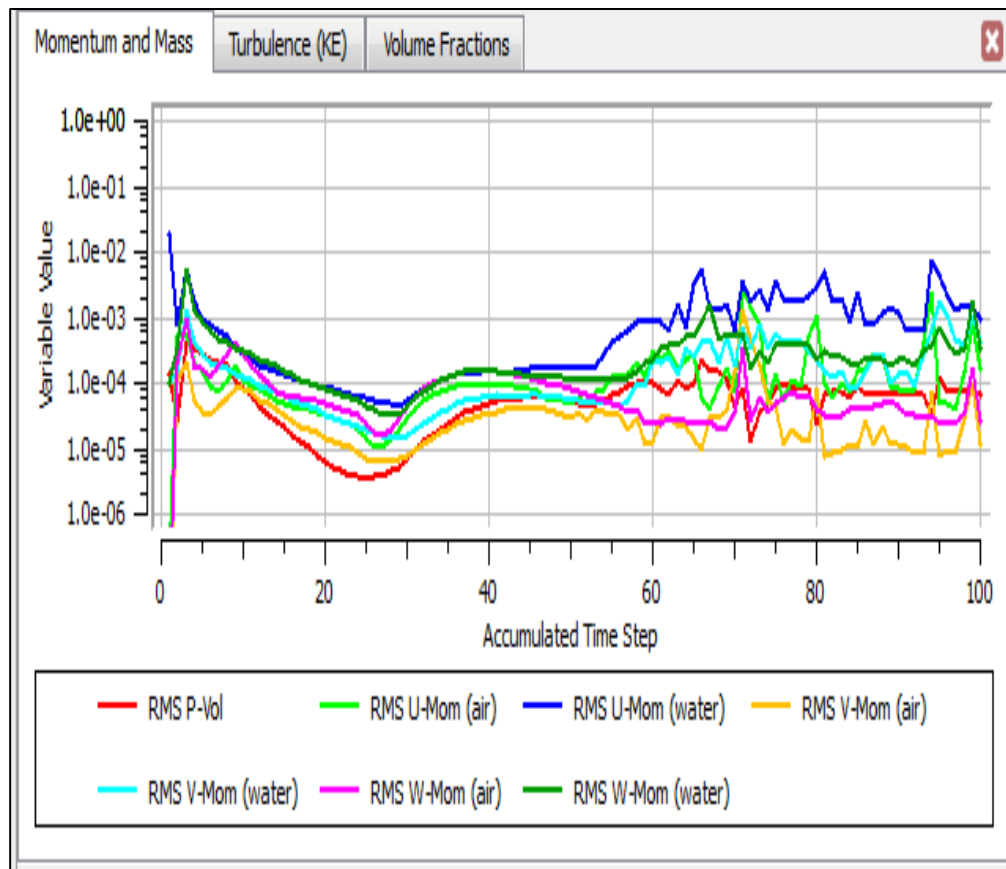


Figure 6.35: MQL Air Exit Jet Velocity



**Figure 6.36: MQL Nozzle Convergence Plot**  
**(Flow rate Main flow 6-Bar, Nested Flow 100ml/hr)**

The above Fig 6.34 depicts, the MQL nozzle simulation with air & oil used as fluids. The main inlet flow was set to 6-bar air pressure and 100 ml/hr was set into nested nozzle. The MQL air and fluid jet velocity points picked exactly after immediate flow exit of the nozzle orifice which is in middle layer of the exit. Here, it is observed that the drop in velocity in the middle of the jet profile formed like a spline shape caused less as compared to 4-bars (see Fig 6.33). In these both simulations showed that increasing air input pressure influences the nozzle exit profiles as illustrated in above Figures 6.33 and 6.35. The convergence of the MQL simulations presented in Fig 6.36 that the internal fluid flow smoothly converged up to the cone. The percentage increase in MQL simulation of both 4-bar & 6-bar is 20.9 % in MQL.

## 6.12 Summary

This area of work contains detailed analysis of simulations of internal and external fluid flow behaviour using ANSYS CFX tool and the nozzle optimisation techniques. The final nozzle model was refined with mesh convergence by concentrating in critical areas. Now this CFX advanced tool was used for the wall treatment and external fluid jet behaviour measuring of jet coherency was determined. After several modifications the dove-tail exit profile was achieved with satisfactory results. A range of nozzles with air & oil as fluid media, simulations were performed for MQL applications. Now in the next chapter-7 & 8 the nozzle model is performed with an experimental work, concerned with contained fluid flows with proper testing arrangement.

## Key Findings

1. A fluid firing is observed in the nozzle exit cavity this is due to fluid acceleration in the narrow gap between the cone and internal cavity surface.
2. The peak velocity profiles were recorded up to 150 mm length of jet stream.
3. The fluid acceleration was observed, that fluid passing after the half of the cone length and an additional momentum was seen near the cone inlets.
4. Using ANSYS CFX tool, the meshing near the areas of interest shown actual fluid flow behaviour which helps in mesh modification.
5. The velocity profile after immediate exit of the nozzle was observed that peak velocity is achieved at the exit centre followed up to the length of 80 mm this can matches exactly the wheel width (contact zone).
6. The introduction of pressure cone performance shown increase in jet velocity.
7. In MQL flow, multiphase simulation using velocity, surface and fluid superficial plots was given good insight at the fluid acceleration and drop off regions.
8. In the determination of coherence length, the air in the computational domain showed some effect on jet stream.
9. Supply of large input flowrates (above 60 lit/min) showed high cross firing in the exit cavity.

## **Chapter-7**

# **Experimental Methods and Techniques**

## **Chapter-7 Experimental Methods and Techniques**

### **7.1 Introduction**

This chapter discuss the experimental procedure and equipments used for nozzle characterisation. The data collection was recorded using LabVIEW tool to characterise the nozzle performance and to present the nozzle jet velocity profiles. The collected data is then transferred to build a 3-dimentional surface plot of nozzle jet velocity profiles using MATLAB. In this work, to measure the pressure within this exit flow, a differential type pressure transducer was used. The nozzle validation tests and experimental program of work is discussed and completed in this chapter. The experimental method consists of the following procedures:

- Experimental techniques and methods used in this work.
- The design setup of the test rig and Inspection Chamber.
- The procedure for each test of the nozzle.
- Results and discussion of each flow test.

### **7.2 Experimental Methods and Apparatus**

All the nozzle experimental tests were conducted in the advanced manufacturing technology research laboratory (AMTReL) at Liverpool John Moores University. The main body of the initial nozzle testing utilised the “Jakobson Surface-Grinding Machine” for basic understanding of grinding fluid flow supply and measurement system. Additionally the test rigs were manufactured for inclusion on the grinding machine to transform this into the nozzle measurement centre and inspection chamber. A Pitot tube measurement system is fixed on machine head allows moving in up and down position. The coolant delivery system is also installed to supply the flow to the

nozzle arrangement. In this the novel modular adaptable nozzle has been presented and tested during the experimental work for this thesis is given below.

1. Nozzle without Pressure Cone
2. Nozzle with Pressure Cone
3. Nozzle with pressure Cone Multiphase (MQL)
4. Nozzle with Pressure Cone exit Opening with 0.4 mm
5. Nozzle with Pressure Cone Exit Opening with 0.5 mm

The main body of the experimental work focussed on the MQL nozzle & nozzle with pressure cone (secondary Nozzle) which results in large reduction of lubrication in grinding applications. This experimental procedure of nozzle calibration tests is performed in a detailed, systematic list of the experiments that were conducted to analyse the objectives to set out within this research work. The nozzle within each set of tests, only some of the variables was changed to allow for comparison between nozzle and the system constants. The nozzle experimental setup and jet coherency length tests with discussions are presented in this chapter.

The experiment of these nozzle types i.e., nozzle with cone, without cone and MQL nozzles conducted with different flowrates. The nozzle exit coherency length tests were performed and nozzle position setup is done by using inspection test rig with movable clamp and rotary adjustment. The importance of jet lies in the overall trends of coherence length to a variety of fluid flow patterns, nozzle exit jet velocity and tests parameters.

### **7.3 Fluid Pressure Measurement**

The main objective of the pressure measurement in this work was to investigate the fluid behaviour of the jet after the immediate exit of the nozzle. Measuring the pressure then converting to velocity, allowed for velocity measurement of the entire jet. It is important to keep the system as steady as possible to collect or record the data of flow test readings taken are all within a less percentage error of each other. In the below

Fig.7.1 depicts a dynamic supply system with air flowing through a Pitot tube supply pipe.

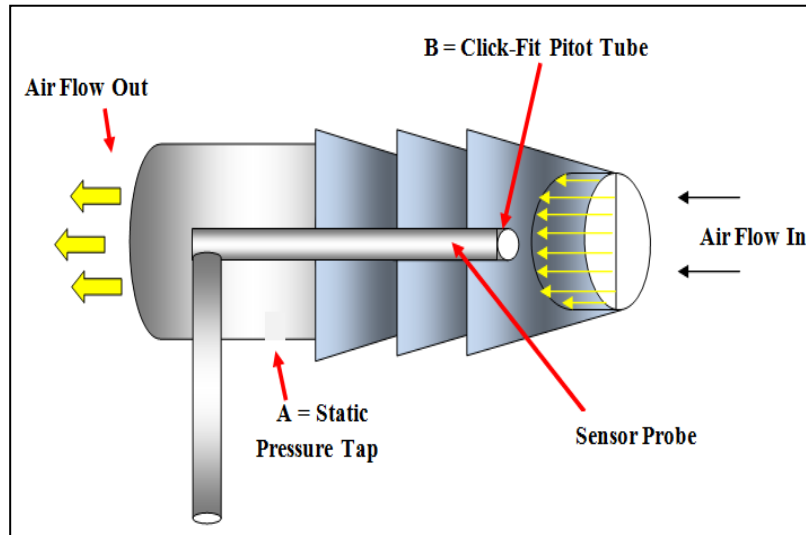


**Figure 7.1: Pitot tube Pressure Measurement in Dynamic Fluid System**

A static pressure tap is located in the pipe wall at point A. The Pitot tube inserted into the flow, measures the total pressure at point B in the system. The total air pressure measured at this point is the stagnation pressure where the value obtained when fluid flow is decelerated or reduced to zero velocity in an isentropic process. This process converts all of the energy from the flowing air into a pressure that can be measured. The stagnation or total pressure is the static pressure plus the dynamic pressure. Measurement of the dynamic pressures allows determination of the velocities and flow system.

The use of a Pitot tube pressure measurement system allowed for the measurement of pressure losses within the pre-nozzle delivery arrangement. This is an important factor when considering overall system design for the coolant supply into the grinding zone. Research into losses in pre-nozzle delivery arrangements was undertaken within the laboratory. The important concept grasped from this study was the reduction in the pre-nozzle delivery systems measured with a pitot tubing system.

## 7.4 Pressure Transducer

The pressure is measured in a variety of ways using transducers, sensors, piezo-resistive, piezo electric and simple gauges. The pressure transducers convert the mechanical pressure to an electrical signal and these are slightly more complex. Simple pressure gauges use simple mechanical method to measure the pressure.

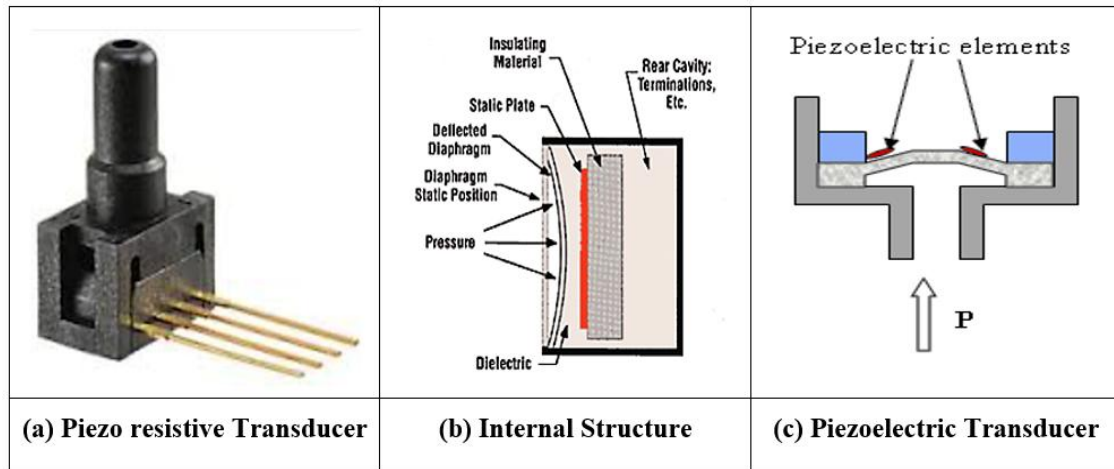


**Figure 7.2: Working Principle of Pressure Transducers (NI National Instruments)**

The piezo resistive effect, involves pressure or stress changes in resistance across the piezo material are the product, not a charge or voltage or it is a phenomenon the insulated material is deformed due to an applied load or stress, an electric potential is generated. This electric field is directly proportional to the material deformation, and therefore applied load or pressure. It is change in electrical resistance of a semiconductor material stress shown in above Fig.7.2 (a). The internal structure illustrated in above Fig.7.2 (b) it consist of a diaphragm, insulating material and a static plate when the force exerts the diaphragm bends and send signals to the system. Piezoelectric transducer or sensor is a device that uses electric voltage effect to measure changes in shape piezoelectric elements, which depicts in above Fig.7.2 (c). These sensors are used in various processes such as pressure, acceleration, strain and force by converting in to electric charge.

Piezoelectric transducers are relatively inexpensive, easy to fix, and these transducers used for quality assurance and process control and often used in industrial and laboratory units. In order to obtain accurate data with these transducers some of the steps required prior to collecting data. The pressure device used in this experiment is a differential type pressure transducer with a range of 0-100 PSI and a full-scale output of 0-225 mV. This gave a sensitivity of 2.25 milli Volts/Psi at a recommended excitation voltage of 10V shown above Fig.7.2 (a). This type of pressure transducer has a small inlet hole in which the pitot tube is inserted, making it suitable for the exit –flow velocity measurement. It also has its own static pressure tap to give total pressure measurements. Probe specifications presented in appendix A-3.1.

### **7.5 Measurement Technique**

The measurement system of nozzle jet velocity profiles to build a 3-D surface plot is considerably crucial part. For this experiment choosing the right transducer which can led to obtain accurate results, the use of several more expensive sensors for measurement of pressure by others researchers within the laboratory proved some inaccurate and trouble for the exit flow problem. The target is to create the sensor probe that could be positioned at a set distance from the nozzle exit and readings taken of the pressure allowing for calculation of the nozzle jet velocity at a range of points, and building a 3-D surface plot image of the jet profile at that point. Using of expensive transducers, the cost of instrumentation to record this data would be considerably larger. The other disadvantage would be in the use of more than one sensor, increase the cost of the overall measurement system as well as incurring errors between each sensor unless significant time was spent calibrating each sensor independently and keeping a record of each data point separately for final processing. Hence, only one pressure sensor was used for this experiment. The air pressure was recorded continuously with slow motion at each interval of the traverse of the Pitot tube across the fluid jet stream. This measurement was repeated by three times at each step to allow for the capture of the mean pressure using averaging.

## 7.6 Nozzle Inspection Test Rig

The nozzle inspection chamber and test rig was built around the Jakobson surface-grinding machine which consists of inbuilt lateral traverse mechanism in the X and Y planes for nozzle position adjustment. The surface grinder was also adapted nozzle positioning system, and the traverse Pitot tube measurement system was fixed.

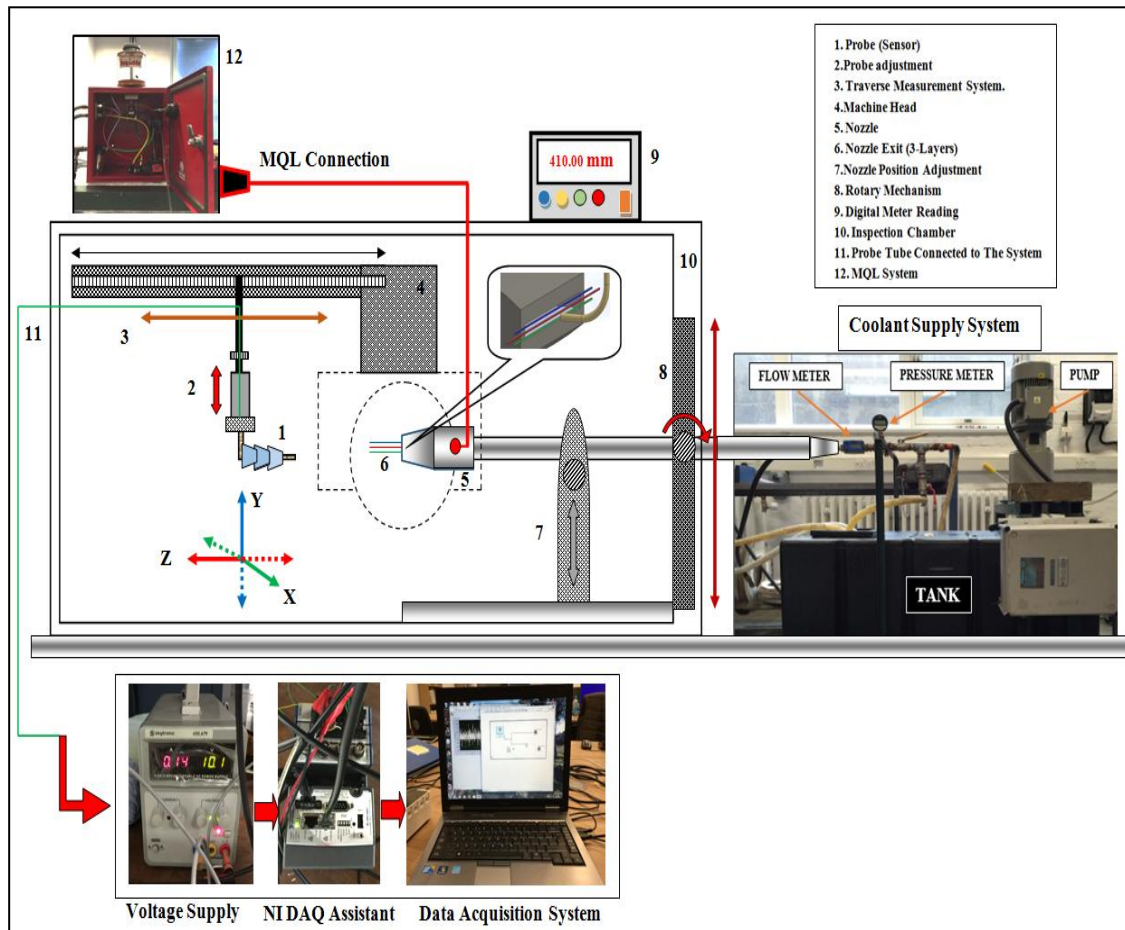


**Figure 7.3: Nozzle Inspection Test Rig**

The inspection chamber consists of a up and down movable system to measure the (+y to -y direction) to act as an observation medium which allow access for nozzle and machine tool adjustment and a detachable back panel allowing the machine spindle and wheel to be moved in both X and Y directions for part setting. The above Fig.7.3

illustrates the whole setup for nozzle testing includes inspection chamber, traverse pitot tube measurement system, MQL system, Coolant delivery tank and air supply line, NI DAQ Data Acquisition system, Voltage generator and System monitor.

### **7.7 Nozzle Positioning System**

Nozzle position is one of the main aspects in grinding process for proper or adequate cooling of the workpiece to protect from high thermal effects. In industries most of the grinding operations are performed on CNC controlled machines which is automatically position the wheel or tool with respect to the workpiece. In cylindrical grinding machine parts are automatically loaded into the machine centres in place then the spindle is activated and the wheel is positioned to contact the workpiece (in relation to the axis on machine tool) in order to form the workpiece into a desired shape with high quality. The wheel-workpiece contact zone is then supplied with a coolant from nozzle or multiple-nozzles to reduce the high heat temperature created by friction generated between the wheel and the plastic deformation of the workpiece. The coolant nozzle must be adjusted with respect to a particular wheel-workpiece combination, to provide the coolant in a proper position.

Typically, coolant is provided to the grinding contact through a nozzle connected to a flexible hose. The nozzle and hose are manually positioned each time however, can be dangerous and difficult for operator to accurately position with respect to grinding contact during in motion. It would therefore be desirable to provide a coolant nozzle position system and method that aids positioning of the nozzle with respect to grinding contact zone. The system maintains its setup position during the entire grinding process (Ebbrell, 2003).

For repeatable measurements and accurate nozzle positioning, a system feeding back from a linear scale and rotary actuator into display was created is shown in below Fig7.4. This system allowed for accurate positioning of then nozzle in the Y and Z-axis as well as then nozzle angle with reference to an angle of zero representing tangential fluid supply.

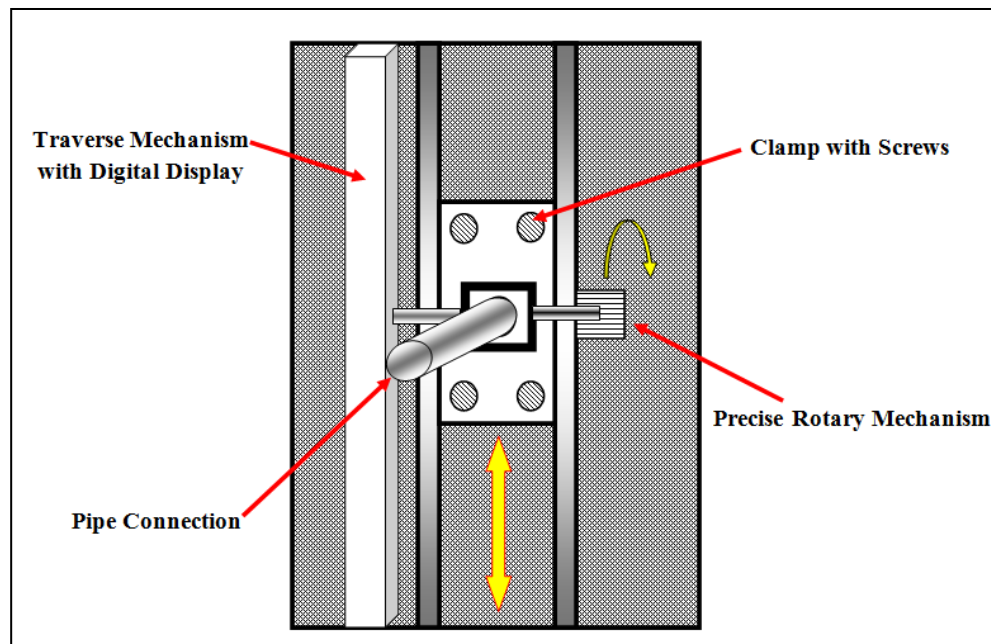


**Figure 7.4: Nozzle Positioning System with Rotary Mechanism**

It is suggested that nozzle has a significant effect on the useful flowrate supplied to the grinding contact. The importance of nozzle position and shape are demonstrated by (Webster, 1995). The delivery of fluid approximately tangential to the grinding wheel is a common approach. The delivery of fluid via a tangential jet led to increased side leakage, raising the nozzle slightly reduced side leakage to a negligible quantity.

### 7.8 Fluid Delivery System for Nozzle

In this nozzle validation test the fluid delivery system was built separately to supply the flow to the inspection chamber on a movable platform with flow measurement equipment shown below Fig 7.5. A rotameter type of flowmeter was fixed in between the pump and the nozzle system. The flowmeter was factory calibrated before being supplied to the laboratory. A simple calibration test is performed with water and then air separately with flow rate of 10 l/m. the flow meter used was an OMEGA FTB792-L turbine flow meter. This was supplied with an analogue output to trace the changes in flowrate due to fluctuations from the pump. Just before the flowmeter. The pressure

gauge of (OMEGA DPG1000B-500G 0-500PSI) was fixed. An analogue output was fed into the data acquisition system to eliminate (through adjustments from the input signal) any errors due to fluctuations in the supply flow. The equipments used in experiment are showed in appendix A-3.2.

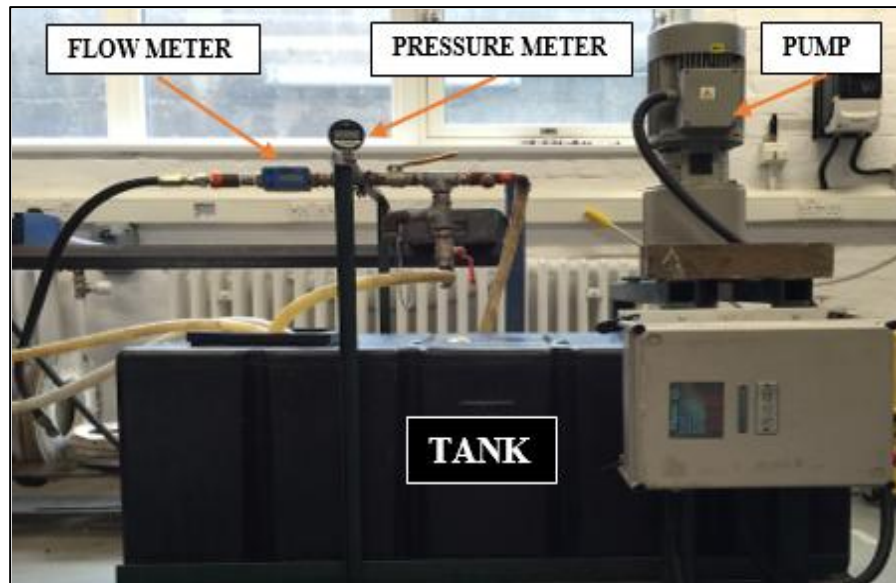


**Figure 7.5: Coolant Supply System**

The pipe system used for the coherency testing comprised of three main sections. The first section, connecting the pump to a filter, the pressure gauge, the control valves and the flow-meter, consisted of 0.5 inch BSP connectors for each device, connected to a straight shaft pipe with an internal diameter of 19 mm. The second section connecting the fluid delivery system to the nozzle system which is made from a 19 mm diameter hydraulic braided pipe. The last section is a straight aluminium pipe of same 19mm diameter that connects the hydraulic pipe to the nozzle. Although losses occurs in each section, these were kept to a minimum by avoiding as many elbows bends and restrictions as possible before the straight supply area. These losses could not be neglected if they were varying however, so to keep a constant experimental method, the position of the delivery system was kept fixed in a constant configuration for all the nozzle calibration tests.

The coolant supply used in the experimentation was delivered directly from a pump salvaged from the existing suprema coolant delivery system within the laboratory. The maximum delivery pressure with the 19-mm open pipe was measured and found to be 4.5 bars to control the supplied pressure and flow-rate of the fluid, two control valves were installed. The first fluid to pass into the nozzle and the second controls flow return to the coolant tank.

### 7.9 Pitot Tube Measurement System to Determine Jet Coherency

A pitot tube system device was designed and implanted to investigate the jet coherency for flows exiting a range of nozzles illustrated in Fig.7.6 (a). In addition, the system was allowed for measurement of the flow after it passed through a range of flow conditions. A transverse measurement system, previously for traversing the grinding wheel on the machine tool feeds into a linear scale mounted on top of the inspection chamber.

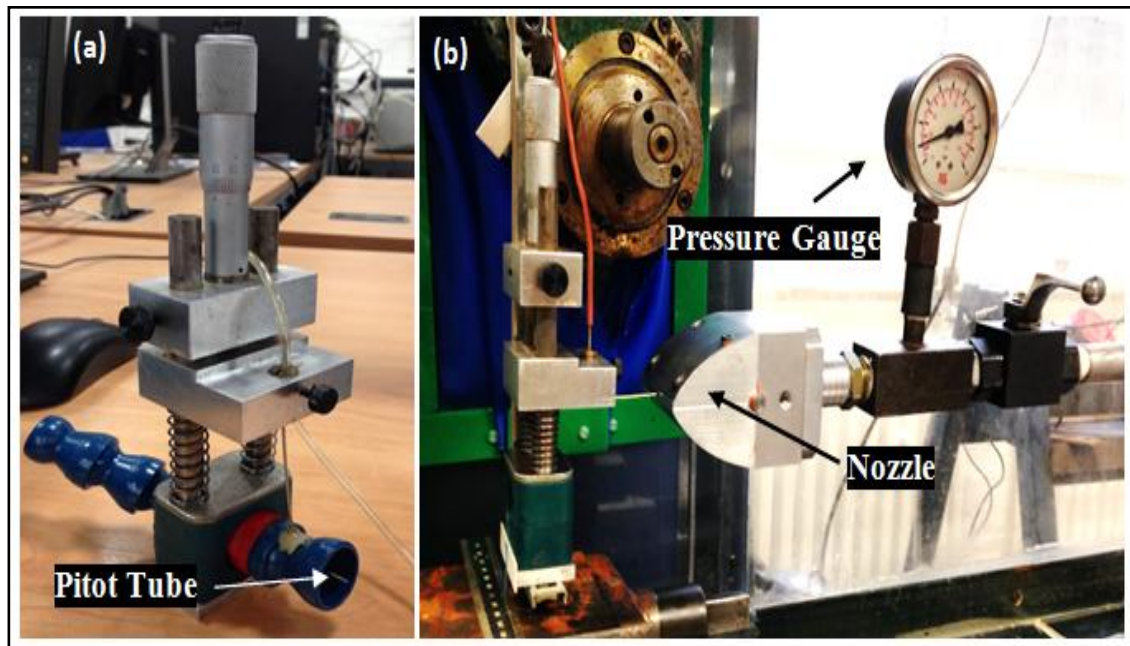


**Figure 7.6: (a) Pitot tube System (b) Sensor probe directed to nozzle exit**

The scale measures the pitot tubes movement in both X and Y directions and has a resolution of 0.1 mm. The pitot tube was fixed to the traverse measurement device with

the use of two rigid bars with adjustable locking connections for accurate and repeatable positioning. For repeatability of the position, each set of results was calculated three times and then averaged. The coherence length of the jet was measured by traversing the tube across the fluid stream area with overlap on either side. The below Fig.7.7 illustrates the basic understanding of the nozzle exit jet measurement system with 3-layers.

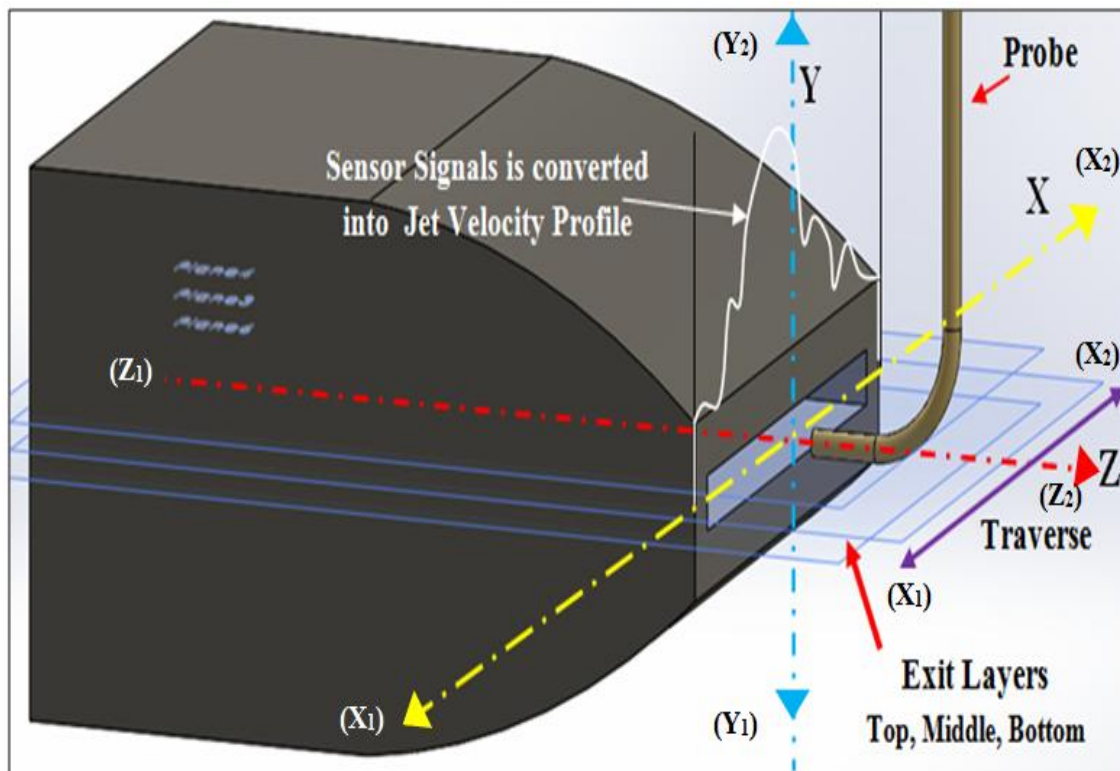


**Figure 7.7: Nozzle Jet Measurement System**

The probe motion starts from the nozzle width left to right across the fluid stream to capture the data same as in Fig 7.6 (b). This figure also shows the clear understanding of probe traverse motion from ( $X_1$  to  $X_2$ ) horizontal direction also in the same way from ( $Y_1$  to  $Y_2$ ) vertical direction, ( $Z_1$  to  $Z_2$ ) away from the nozzle until fluid jet breaks up (0-100). A sample formation of the jet velocity profile is drawn after immediate exit of the nozzle middle layer indicated by white line curve.

### 7.10 Nozzle Test with Coolant

The nozzle test is performed with coolant with two different flowrates of 5 liters/min and 10 liters/min respectively. The coolant supply to nozzle system is connected from the coolant tank through the flow meter and pressure meter and a valve to the nozzle shown in below Fig.7.8. The flowmeter allows controlling the fluid flow and a valve is to turn off after an interval of the jet stream measurement. The Pitot tube is positioned accurately in line to the nozzle exit as shown in Fig.7.8 (a). The traverse motion of the probe allows capturing the jet stream flow from 0 to 100 mm or up to its coherence length depicts in Fig.7.8 (b).

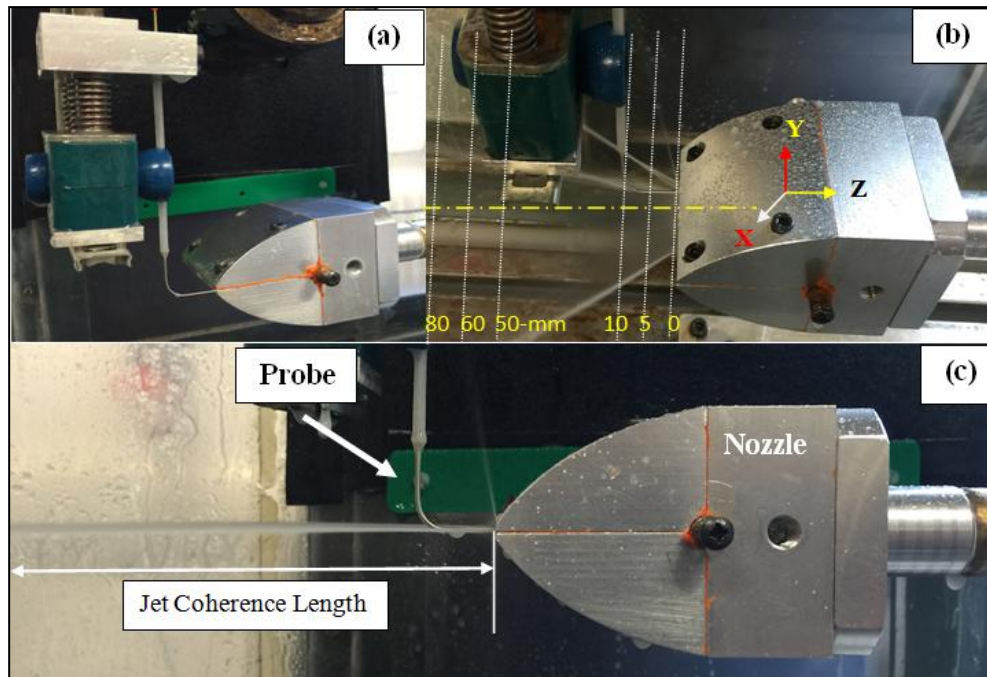


**Figure 7.8: Pitot tube Motion through the Nozzle Exit Fluid Stream**

This method is considered as an effective and economical means of measuring jet velocity and coherence length of the jet stream. This assumption is a good method comes from the fact that the rigid bar should not interfere with the flow upstream. Using the Pitot tube measurement system, the jet velocity profiles and coherence length was

determined from actual pressure readings. The coherence length is vital importance to position the nozzle before grinding process Fig 7.8 (c). It is accepted that the fluid jet should cover the entire grinding contact. Any misdirected of the nozzle position and distance coverage during grinding will not be cooled effectively. The true effectiveness of jet is performed only when it is close to contact zone. This confirms that the total thickness and width of the jet should cover the workpiece area and contact zone.

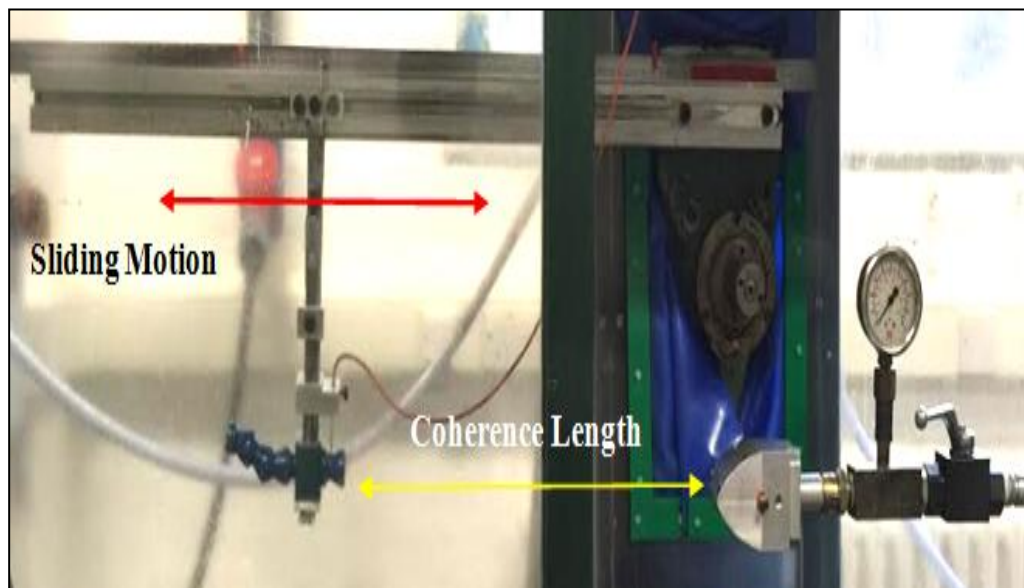


**Figure 7.9: Sliding System Fixed on Machine Head**

The traverse system can move in the both X & Y directions, the only other Z-axis movement was achieved by varying the distance of the pitot tube from the nozzle outlet using a sliding system which is measured mechanically as shown in below Fig.7.9. This mean the effective jet velocity and coherence length could be measured at any distance from the nozzle exit  $Z=0$  to a physically allowed maximum distance of  $Z=200$  mm. It is accepted that the nozzle closer to the grinding contact zone, the better the fluid delivery leads to the better cooling effect. Most attention was focussed on the close range spectrum at values for Z-axis approaching to zero. To build a complete 3-D surface plot of the jet, the measurements of Z-axis is ranged from 0 mm up to 100 mm from the nozzle orifice as shown in the above Fig.7.8 (a) & (b).

### 7.11 Nozzle Test with Air for ‘MQL’

The experimental work of MQL nozzle was designed to test the effect of flow pattern on nozzle exit flows. Here, in this experiment two types of tests are conducted, firstly the nozzle is performed only with air as fluid media for investigating the coherence length of MQL effect. The below Fig.7.10 depicts basic connections of MQL supply system. The design and testing of several air inlet flows allowed for investigation of their influence. Air pressure was set to 4 and 6-bars using a pressure gauge which is fixed before entering the nozzle. A traverse Pitot tube system was used to measure and collect data of air jet flow across nozzle exit with several intervals as shown in the Fig.7.6 (b).

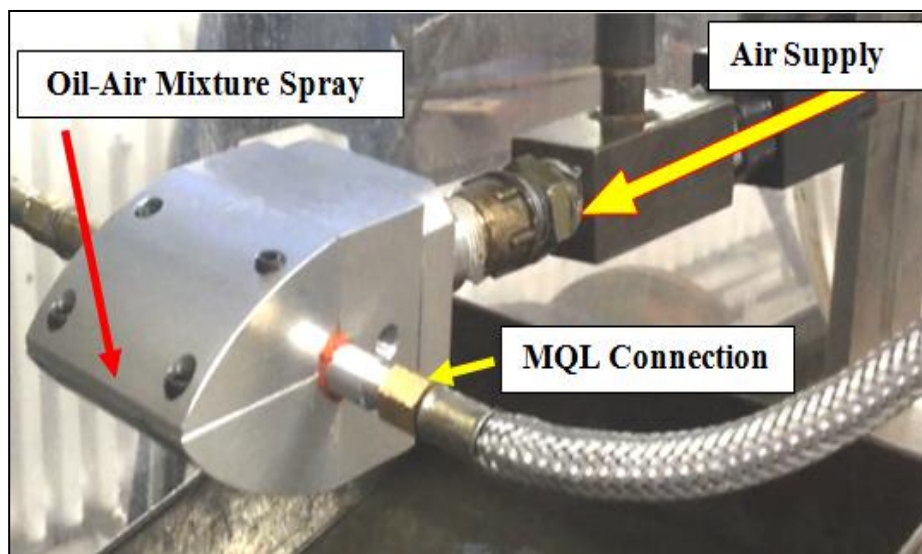


**Figure 7.10: MQL Nozzle Experimental Setup for Testing**

The MQL droplet formation is depends on proper supply of air and quantity of fluid, which covers the length between nozzle exit and the grinding contact zone. To implement this, the coherence length is required to position the wheel-workpiece-nozzle system for MQL application. Once the data is collected throughout the nozzle jet stream, the data is then transferred to the MATLAB to build jet velocity profiles and 3D surface plots to visualize the actual fluid jet behaviour.

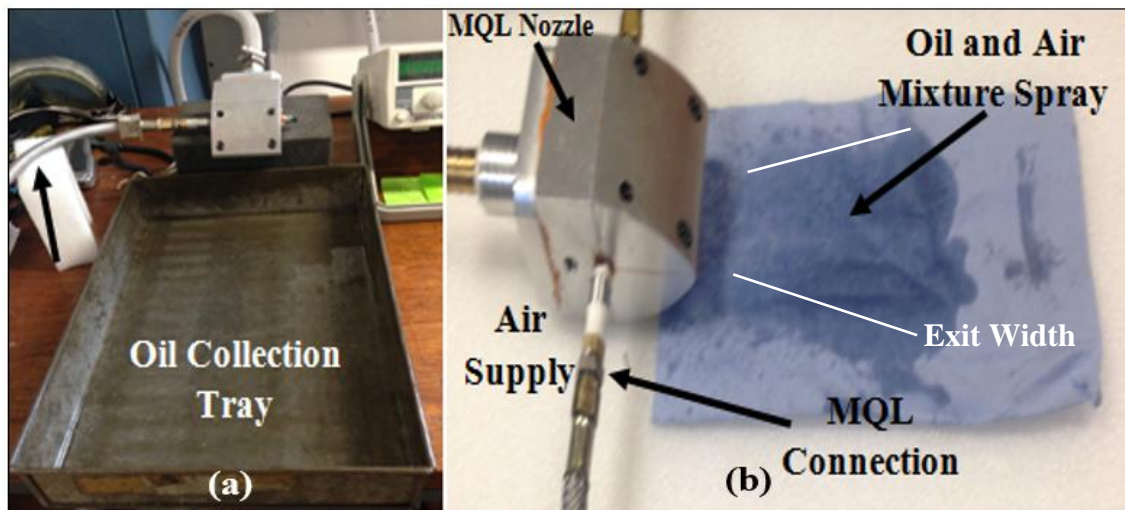


**Figure 7.11: Sampling of a MQL Spray Droplets on Paper**

The second test is using oil and air as a fluid media, to test the droplet formation (spray). The main objective of this experimental work is focussed on the MQL and conventional nozzles. Firstly the nozzle characterization tests were conducted on the nozzle with cone. The air pressure was set to be 4 and 6-bars and the oil flow rate delivery was set to be 50 ml/hour, the MQL inlet is connected from side face of the nozzle into the pressure cone where it pumps only minute amount of oil. The above Fig.7.11 (a) depicts MQL nozzle sampling of air and oil mist spray formation. The spray is collected in a tray to observe the quantity of the oil to be delivered and Fig 7.11 (b) depicts a paper is used to test the droplets coverage area for wheel-workpiece contact zone to supply adequate lubrication effect. It is observed that the mist spray is covering entire nozzle exit length (40-mm) this can be able to cover the wheel width and contact zone at certain distance. This investigation has given a basic idea into the concept of ‘optimal lubrication effect’ in MQL application. The main MQL components presented in appendix A-3.1.

## 7.12 LabVIEW Data Acquisition

LabVIEW is a general purpose programming system specially designed for data acquisition and instrument control. The data acquisition system capture the data from the three different sources, to do this an 8-channel 9215 input NI DAQ assistant was used. The sensor connected to the DAQ assistant requiring external power supply of 10V excitation signal. The sensor is a piezo-electric resistive differential transducer with range of 0-100 PSI and a full-scale output of 0-225 mV. This gave a sensitivity of 2.25 mV/PSI at a recommended excitation voltage of 10V. The sensitivity for the readings is 0.2%.

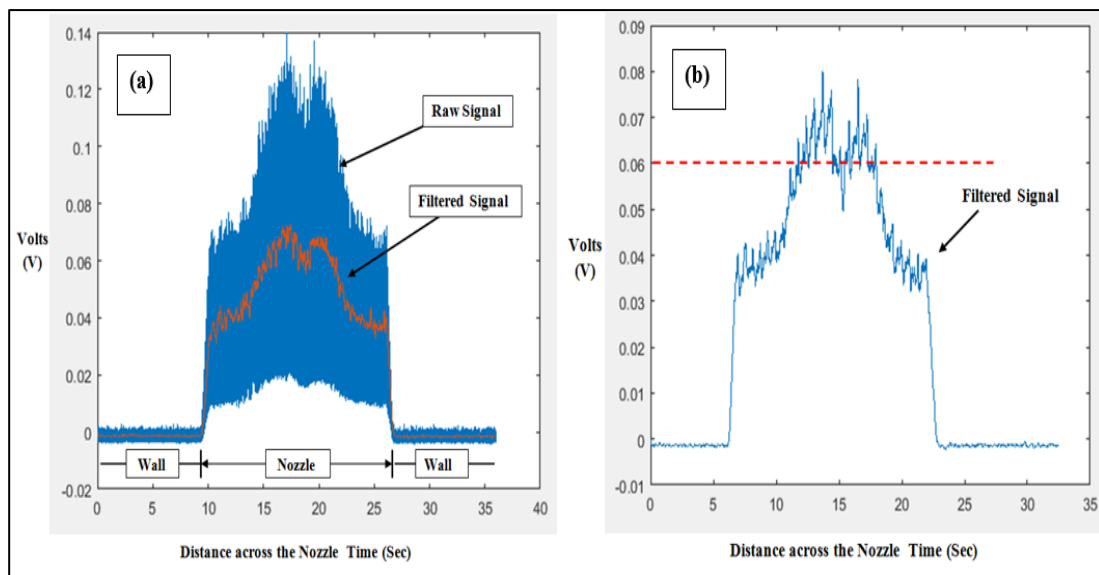


**Figure 7.12: Signal Acquired across Nozzle Exit (a) Raw Signal and (b) Filtered Signal**

This type of pressure transducer has a small inlet hole in which the Pitot tube is inserted, making suitable for the exit flow velocity measurement. It also has its own static pressure tap to give total pressure measurements. A LabVIEW tool is used to record the measurements of flow jet velocities and the input parameters was set to 50 Hz cut-off frequency and sampling rate were set to 500 K. The above Fig.7.12 (a) illustrates a signal recorded during a test to identify adequate time and conditions for jet

velocity measurement shows a raw signal where the cut-off frequency is  $CF=50$  Hz. Here, the actual signal lies in between its centre indicated by red curve this is mainly due to high electrical noise. Batako *et al*, (2005) investigated an experiment on several techniques of using thermocouple to measure over a large temperature field in high efficiency deep grinding (HEDG). Using thermocouple technique it is shown that the shape and size of the junction have a strong effect both on the reliability of the signal and on the accuracy of the signal. Other problems discussed that electrical noise require zero-shift filtering also include improvement of the signal to noise ratio, Signal filtering. The sensor signal is vulnerable to environmental electrical noise and interference. Noise is undesirable data added to the measurement signal. Noise can exist in many forms of interference from external electrical or magnetic fields with measurement system and random motion of electrons and other charge carriers from components within the system. Noise is also affected by main power supply system also multiple earths can cause noise. It clearly shows a high level of noise when other machinery is operated nearby. This reflects the importance of noise and defining optimal conditions to minimize the noise level. In order to draw the actual signal the raw signal was filtered and the jet velocity profile is illustrated in above Fig.7.12 (b). The work of developing block diagram and coding is shown in Appendix-4.1 to A-4.3.

It is observed that the supply of 1-bar input air flow pressure is increased after immediate exit of the nozzle with output of 1.82 bars which is 80% of increase. The experimental results and 3-D plots of all the nozzle characterisation tests are presented in chapter-8.

### 7.13 Summary

In this chapter nozzle with cone and no-cone fluid delivery and jet stream measurement techniques were presented and discussed. Implementation of fluid delivery system, pitot tube measurement system with pressure transducer (sensor) and testing methods were presented. Conducted experiments of both flood and MQL (air and oil) tested. Discussion on experimental work, nozzle angle positioning, Labview block diagram and procedure were presented.

### Key Observations

- Nozzle exit should overlap with probe during measurement.
- The air in the probe must be clear off before conducting experiment to record accurate readings.
- Minimization of electrical noise can give accurate results during the jet velocity measurements.
- Avoid any bends, elbows and leakages from supply pipe to the nozzle.
- The debris in the coolant can obstruct the nozzle exit and can led to fluctuate and unable to record the signals. Using filter cap is necessary for the pump.

## **Chapter-8**

### **Experimental procedure and Results**

## **Chapter-8 Experimental Procedure and Results**

This section presents the experimental procedure that was conducted to analyse the nozzle characteristics and performance. Three types of nozzle experiments were conducted i.e., 1, Nozzle with pressure cone (Nested) both air and coolant 2, Nozzle without pressure cone only coolant and 3, Nozzle with cone with exit aperture of 0.4 mm and 0.5 mm. Within each set of nozzle tests, only one variable was changed (Flow rate) to allow for comparison between the system and constants. Presented are results for each of the experiments with a discussion of the main findings in these experiments.

The importance of these experimental results lies in the overall trend of coherence length to a variety of flow conditions and test parameters. Hence, selections of results are brought forward into this chapter, with references made to individual figures presented in this section. Each graph has only one variable parameter, requiring the remaining parameters to be fixed. This allows a close comparison between the simulation and experimental findings.

### **8.1 Nozzle Flow Tests**

The experimental work on nozzle flow test was designed to test the effect of flow on nozzle exit jet and coherence length. The nozzle experimental tests took place using the flow inspection chamber and fluid delivery mechanisms. The test was aimed to measure fluid velocity profiles at several points, starting at the immediate nozzle exit, in the centreline across the nozzle aperture and then along the jet stream. A traversing Pitot tube measurement system was used to draw the jet stream velocity profiles. This required the calibration of the differential type pressure transducer to reference fluid velocities to the output of the sensor in (mV). Calibration of the pressure transducer involved setting the flow to a given velocity. To achieve this, a given flow rate was constant during this experiment the flow rate and the nozzle exit size; the fluid velocity obtained using the following expression given below:

$$\dot{Q} = V \times A \quad (8.1)$$

Where;  $\dot{Q}$  = Volumetric flowrate (L/min),

$V$  = Velocity (m/sec),

$A$  = Area (mm),

If the flowrate is 15 l/min through a circular diameter of 2.5 mm then the fluid velocity is given by

***For circular cross section:***

$$V = \frac{\dot{Q}}{A}$$

$$V = \frac{0.00025}{\pi \times 0.00125^2}$$

$$V = 50.9 \text{ m/sec}$$

***For Rectangular cross-section:***

If the flowrate is 10 L/min through a rectangular cross-section of 40 mm x 0.3 mm then the fluid velocity is given by

$$V = \frac{0.00016}{0.04 \times 0.0003}$$

$$V = \frac{0.00016}{1.2 \times 10^{-5}}$$

$$V = 13.3 \text{ m/sec}$$

For each different flow rate, a reading from the pressure transducer was recorded. This is shown in Fig.8.1. The recorded data were plotted, and a best-fit straight line gave the equation for the line, with an offset where the line crosses the x-axis. This allowed for the calibration of the sensor for any given flow rate.

The equation of the ‘best-fit’ line gives the correlation between sensor readings and the fluid velocity. This equation was used to calculate the velocities of the exit flow. The pressure gauge was supplied from OMEGA and the turbine flow-meter was calibrated and the accuracies these two are within 0.5 percent.



To build up the external fluid flow patterns, the readings were taken at several distances from the nozzle exit up to fluid jet breakup. The jet profile points were recorded at starting from 0, 5, 10, 15, 20, 25, 30, 35, 40, 45, 50, 75, 90, 100, 150, 200, 300, 400 and 500 mm. It was predicted that this would cover up to 50 to 100 mm jet coherence length and give a suitable range for analysis.

## 8.2 Nozzle & Pitot tube Measurement System

The determination of the nozzle jet coherence length is performed under a series of steps which includes nozzle position and exit opening adjustments for accuracy of the profile. The nozzle exit orifice is divided into 3-layers to study the fluid behaviour pattern within the 0.3 mm aperture illustrated in below Fig.8.1. A Pitot tube system was designed and implanted to investigate the jet coherence for grinding interface. In addition, the system allowed for measurement of the flow after it passed through nozzle conditions (with Cone and without Cone).

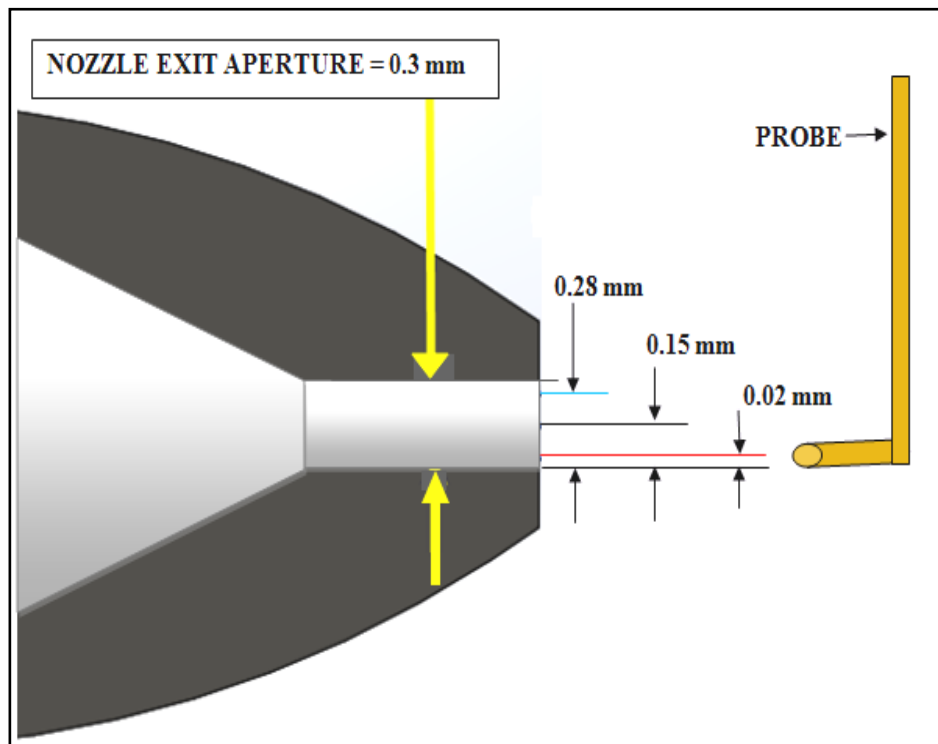
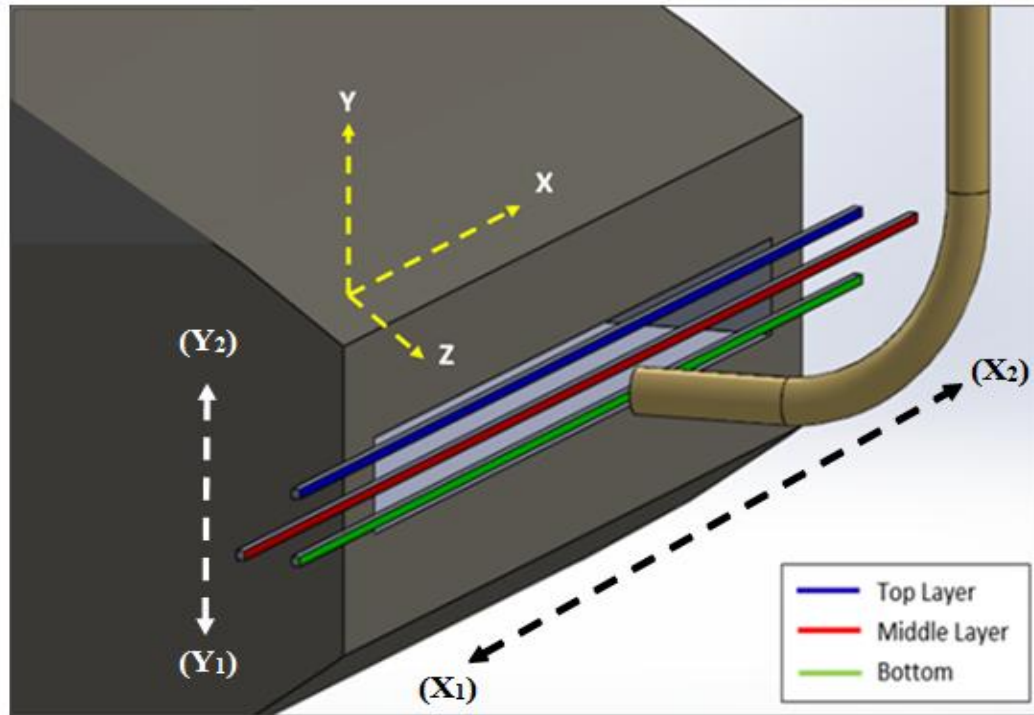


Figure 8.1: (a) Distance between Layers

A transverse measurement system, previously used for traversing the grinding wheel on the machine tool feeds into a linear scale mounted on top of the inspection chamber illustrated in below Fig 8.3.



**Figure 8.2: Close View of Nozzle Exit with 3-Layers**

Fig 8.2. A machine tool digital readout was used to measure the pitot tubes movement in both X and Y directions ( $X_1$  to  $X_2$ ) and ( $Y_1$  to  $Y_2$ ) with a resolution of 0.1 mm. The Pitot tube was fixed to the traverse measurement device with the use of two rigid bars with adjustable locking connections for accurate and repeatable positioning. For repeatability of the position, each set of results was calculated three times and then averaged.

The coherence length of the jet was measured by traversing the Pitot tube (probe) across the fluid jet stream area with overlap on either side and away from the nozzle where the jet breakup starts. The actual fluid jet velocity is measured by taking the first point at which the velocity profile starts to increase as a direct result of fluid entering the Pitot tube.

## Nozzle Investigation with Air

### 8.2.1 Nozzle with Pressure cone

A pressure sensor with traverse Pitot tube measurement system permitted the determination of the jet profiles and thickness. The sensor probe was positioned parallel to the nozzle exit and, moved whilst recording the output pressure readings in the x-direction. The collected data at nozzle exit are shown in table 8-1. The data acquisition system had to capture data from the three different sources; to do this an 8-channel input NI DAQ assistant with LabVIEW tool was used. The sensor was connected to the DAQ assistant requiring external power supply of 10V excitation signal.

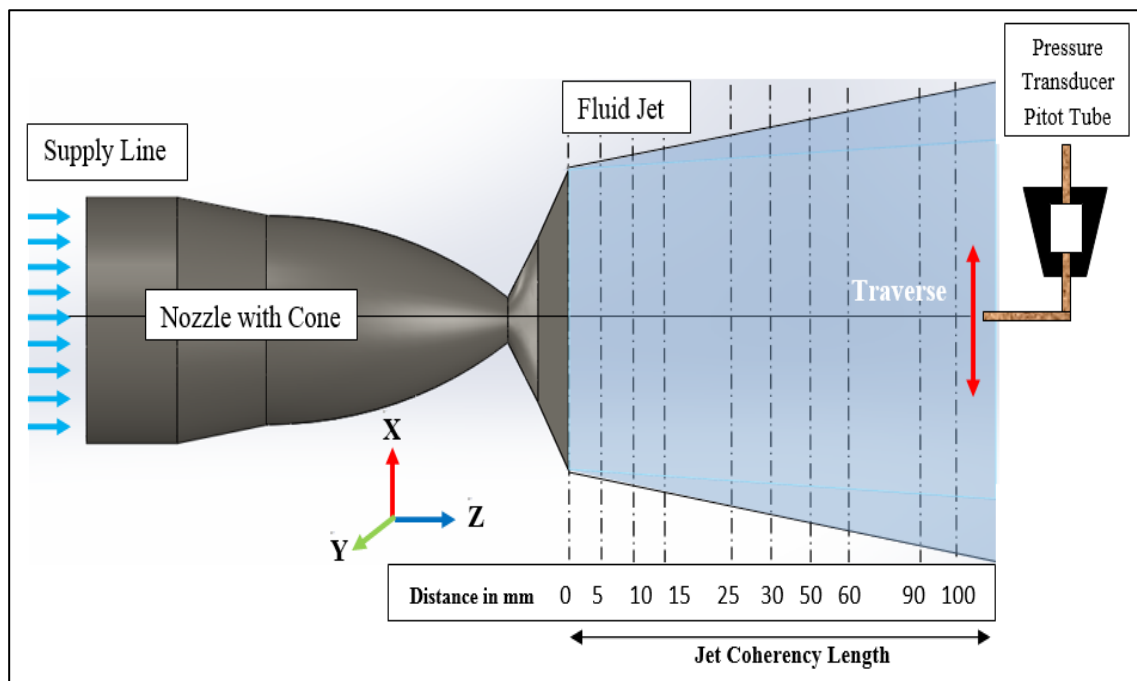


**Figure 8.3: Measurement System**

To measure the pressure within the exit flow, a differential type pressure transducer was used. The sensor is a piezo-electric resistive pressure transducer with a range of 0-100 PSI and a full-scale output of 0-225 mV. This gave a sensitivity of 2.25 mV/Psi at a recommended excitation voltage of 10V. The sensitivity for the readings is 0.2%. This type of pressure transducer has a small inlet hole in which the Pitot tube is inserted,

making it suitable for the exit flow velocity measurement. It also has its own static pressure tap to give total pressure measurements.

The testing of nozzle with cone on the exit jet thickness used a rouse-shape internal profile cavity with an exit opening of 0.3 mm is as shown in the above Fig.8.3. At the initial stage, to test the performance and influence of the egg-shaped pressure cone, air is used for MQL delivery. The pre-delivery arrangement and nozzle type varied. The air pressure was set to 1, 3 and 6 bars and data were recorded in 3-layers along the fluid jet. The nozzle exit aperture of 0.3 mm was divided into 3-layers starting from 0.02 to 0.15 to 0.28, as illustrated in Fig.8.1.

<b>INPUT (Bars)</b>	<b>(mV)</b>	<b>Output (Bars)</b>	<b>Jet Velocity (m/sec)</b>
<b>1.</b>	200	1.82	6.8
<b>2.</b>	310	9.4	10.5
<b>3.</b>	380	11.6	12.9
<b>4.</b>	400	12.2	13.5
<b>5.</b>	420	12.8	14.2
<b>6.</b>	430	13.1	14.6

**Table 8.1: Air pressure reading for Nozzle with Pressure Cone**

Two types of plots were produced for initial comparison of the coherence length and jet profiles under the influence of the egg shape pressure cone flow conditioner. The velocity profile obtained exactly at the immediate exit of nozzle in the middle layer is shown in below Fig.8.4.

By these surface plots it is concluded that output air jet velocity is increasing gradually which almost twice the supplied input air pressure and this is shown in below Fig.8.5 & 8.6. The Fig.8.5 depicts the surface plot of air in the range from 1 bar to 6 bars with an increase of air jet velocity profiles.

### 8.3 Nozzle with Cone Air Jet Velocity Profiles

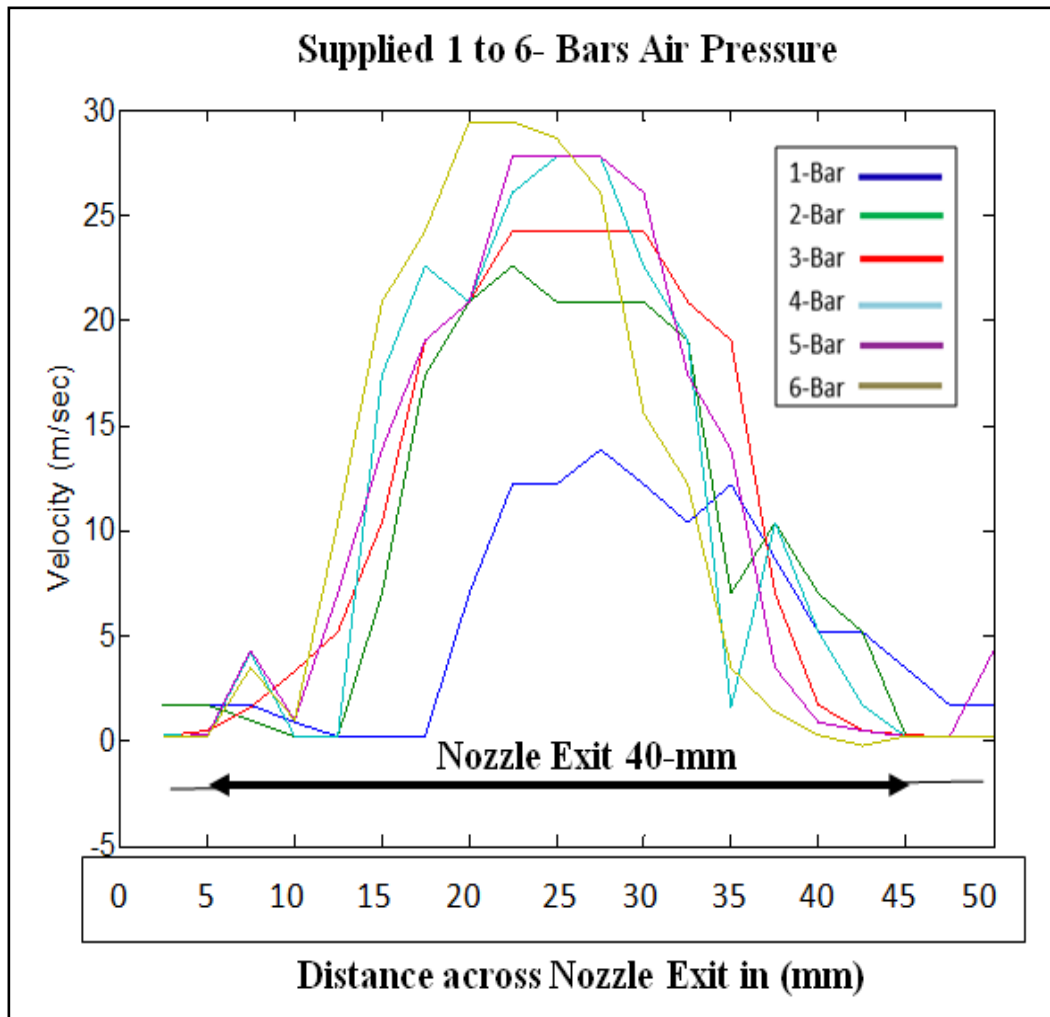


**Figure 8.4: Velocity Profiles of Nozzle with Cone**

The above Fig 8.4 illustrates the velocity profile obtained exactly at the immediate exit of nozzle in the middle layer. All the velocity profiles were drawn on nozzle aperture middle layer, it is indicated by colour code 1 bars to 6 bars. The above velocity profile plot gives a good insight into that increasing input air pressure is directly proportional to exit jet velocity. Also it was observed with these profiles that all jet velocity profiles are formed like a curved shape in the centre region. Using these data, a 3D surface plot was drawn to visualize the gradual increment of these velocity profiles in a systematic manner, as illustrated in below Fig 8.5 and 8.6.

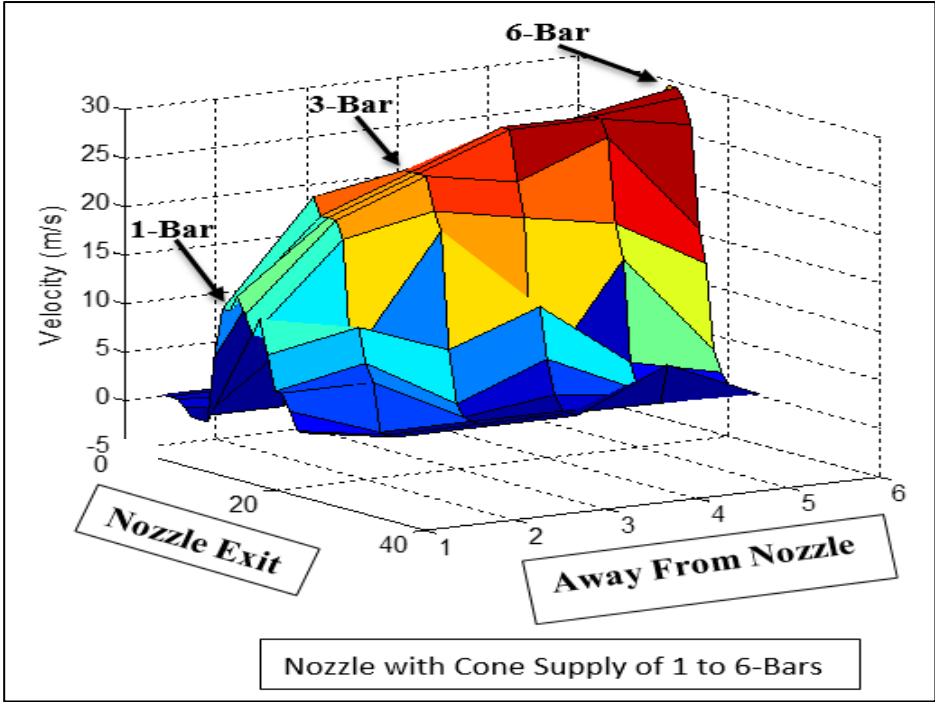


Figure 8.5: Velocity Surface Plot (1-6 Bars) on Nozzle Exit

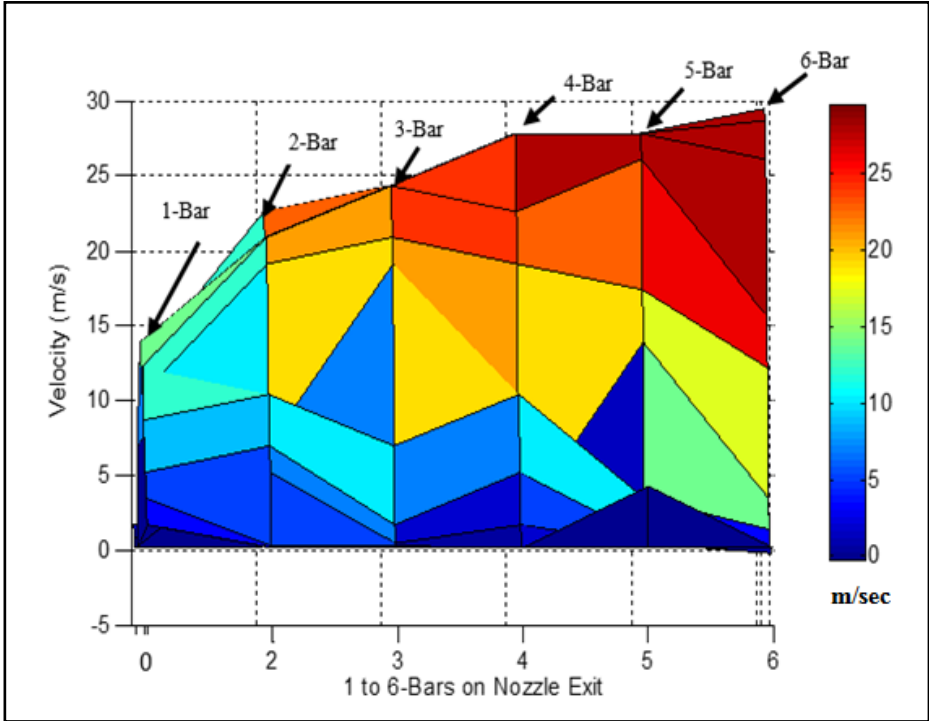


Figure 8.6: Surface plot of Increasing Air Velocity

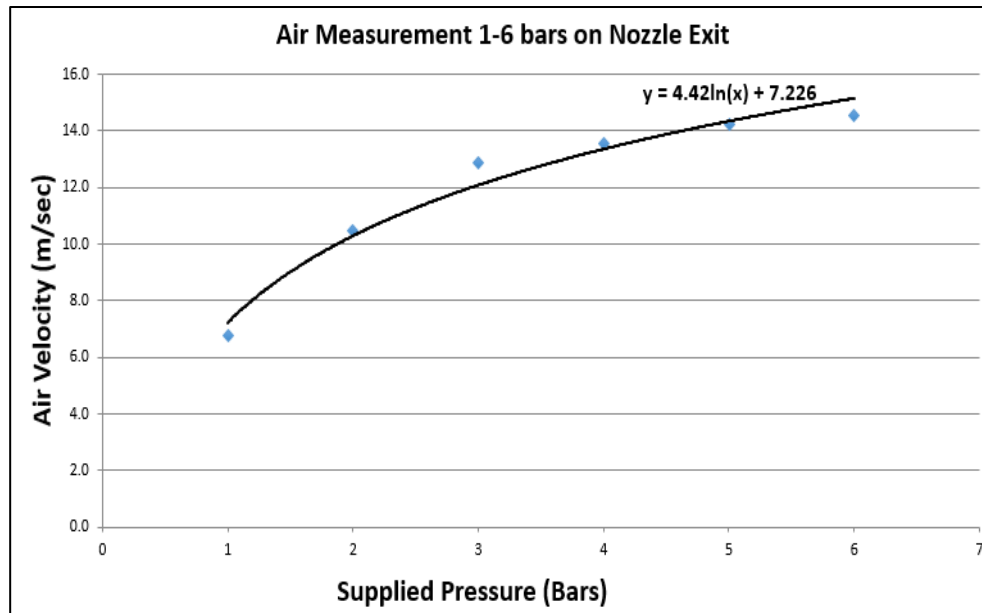


Figure 8.7: Graph- Input Supply (Bars) Vs Output Air Velocity (m/sec)

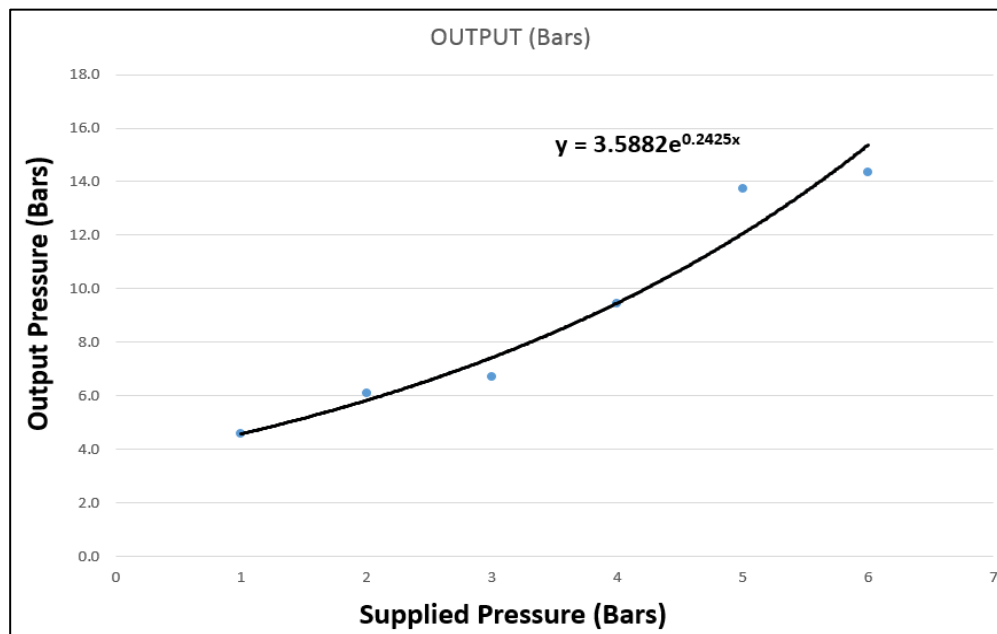
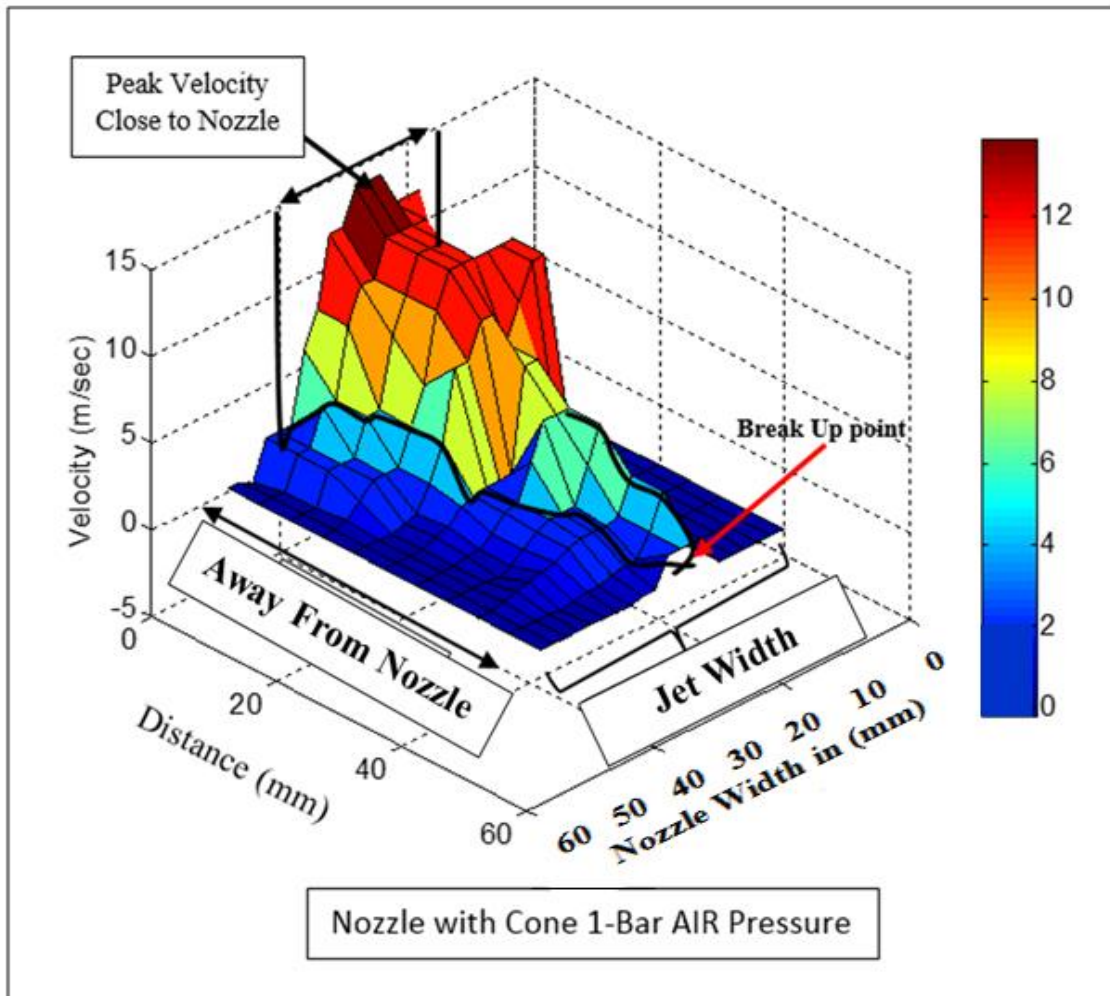


Figure 8.8: Graph- Input & Output Air Pressure in Bars

The above graphs presented Fig 8.7 are input supply of air verses jet velocity was shown gradual increase in jet velocity and Fig 8.8 depicts input and output comparison of air supply. In this graph reveals that supply of air pressure from 1-bar to 6-bars are plotted after immediate exit of the nozzle was shown increase in output jet velocity.

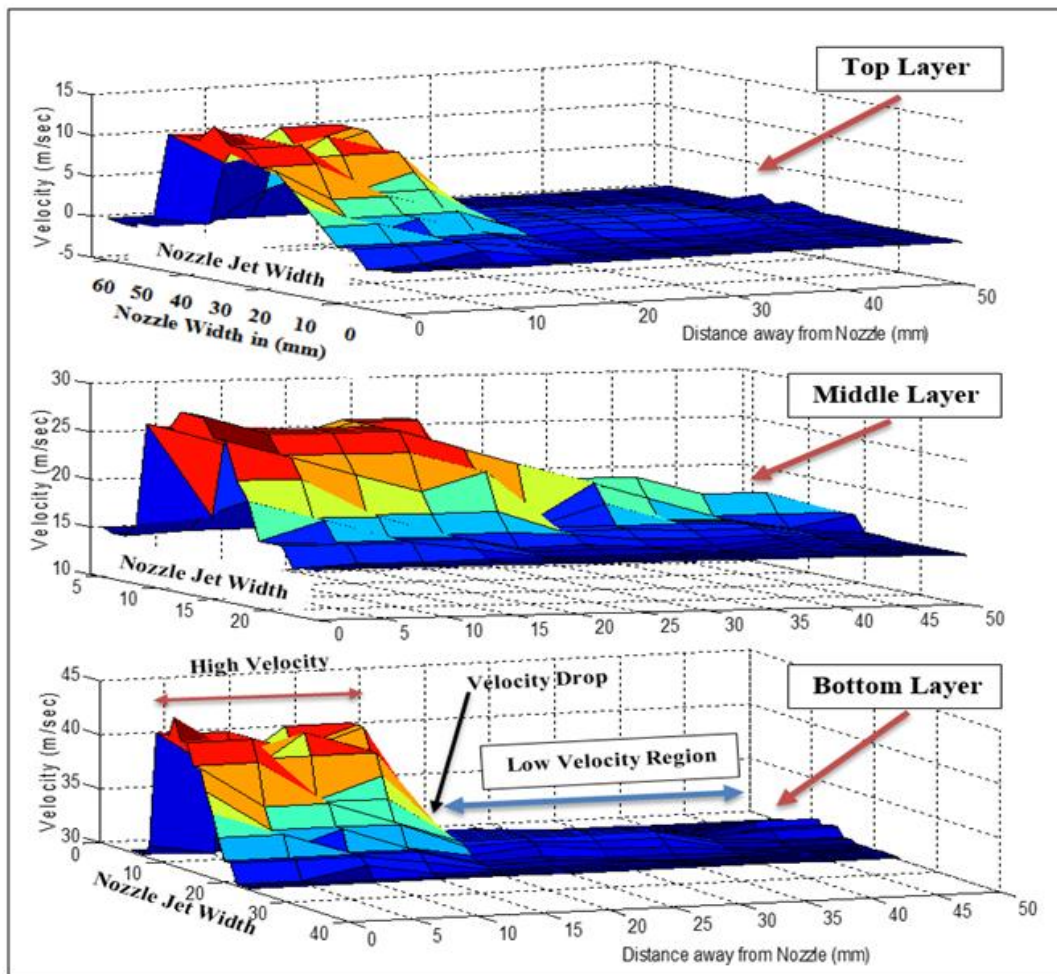
#### 8.4 Nozzle with Pressure Cone Velocity Surface plot (1-Bar Air Pressure)

The nozzle with pressure cone, the jet width increases rapidly from the nozzle exit and peak velocity is achieved at the top centre and gradually reduces with increasing in distance away from the nozzle orifice. Fig.8.9 is the middle layer surface plot representing the behaviour of external air flow velocity.



**Figure 8.9: Nozzle with Cone Middle Layer Surface Plot-(Input 1-Bar)**

The velocities at the bottom sides of the jet appears low are the velocities of the spray at the edges of the nozzle after the air exits from the aperture. It is observed that the peak velocity appears in centre of the profile and showing lower velocity at the jet break up as indicated in Fig.8.9.



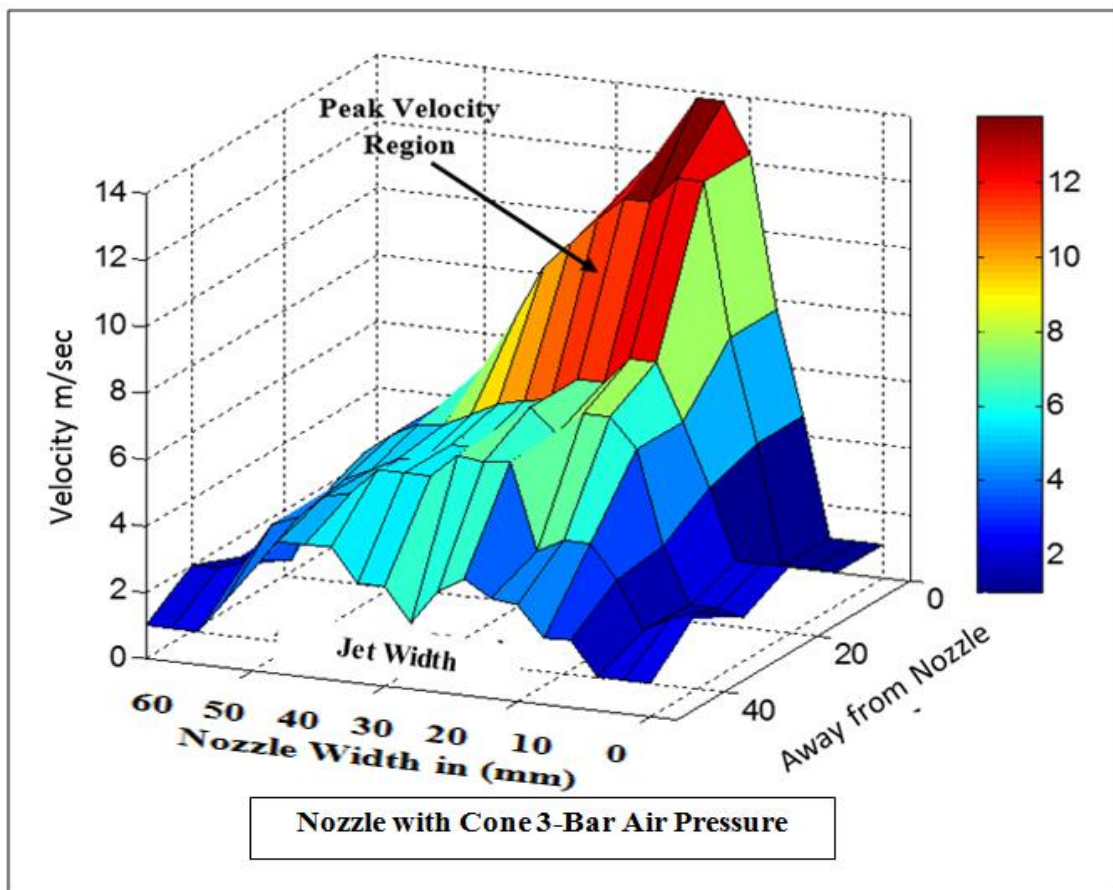
**Figure 8.10: Nozzle with Cone Multi-Layer Surface Plot (Input 1-Bar)**

Fig.8.10 illustrates the multi-layer surface plot, of nozzle with cone for an aperture of 0.3 mm. As schematically shown in Fig.8.2, the exit orifice is divided into 3-layers to visualize the actual outflow of air velocity behaviour of the nozzle. The multi-layer profiles are presented exactly after immediate exit of nozzle exit in 3-layer form namely top, middle and bottom layer. The dimensions of each layer are of 0.1 mm height and 40-mm in width illustrated in Fig.8.10. It is observed that the maximum air jet velocity is maintained up to a coherency length of 50-mm distance from the nozzle orifice and then the velocity is gradually reduced up to a distance of 60-mm which is jet break up. This surface plot reveals that due to lower input flowrate the jet profile breakup formed earlier than predicted i.e. supply of input air pressure 1-bar length maintained only 50-

mm. This gave a good idea and better understanding of that the nozzle with cone with low input that fluid break up reached at a distance of 50-mm length. By considering this, in the case of MQL delivery the minimum air input supply to the nozzle for grinding is 3-bar. Fig.8.12 presents the output of various input flowrates.

### 8.5 Nozzle with Pressure Cone (Input Supply 3-Bar Velocity Surface Plot) Results

The pre-delivery arrangement system is the same for all the air testing; only supply of air input was varied. Here, the nozzle is supplied with 3-bar air pressure, in this case the outflow of air velocity exhibits some improvements compared to 1-Bar.



**Figure 8.11: Nozzle with Cone Middle Layer Surface Plot (Input 3-Bar)**

The velocities at the centre and corners of the jet some improvement due to increase in air flowrate as shown in Fig.8.11. The increase of air input develops increased pressure

due to the inserted cone inside the nozzle cavity which results in an increase of outflow velocity. The velocity profile in this case diverged in shape with sharp edge at the top. This indicates that the peak velocity is projecting in centre of the flow.

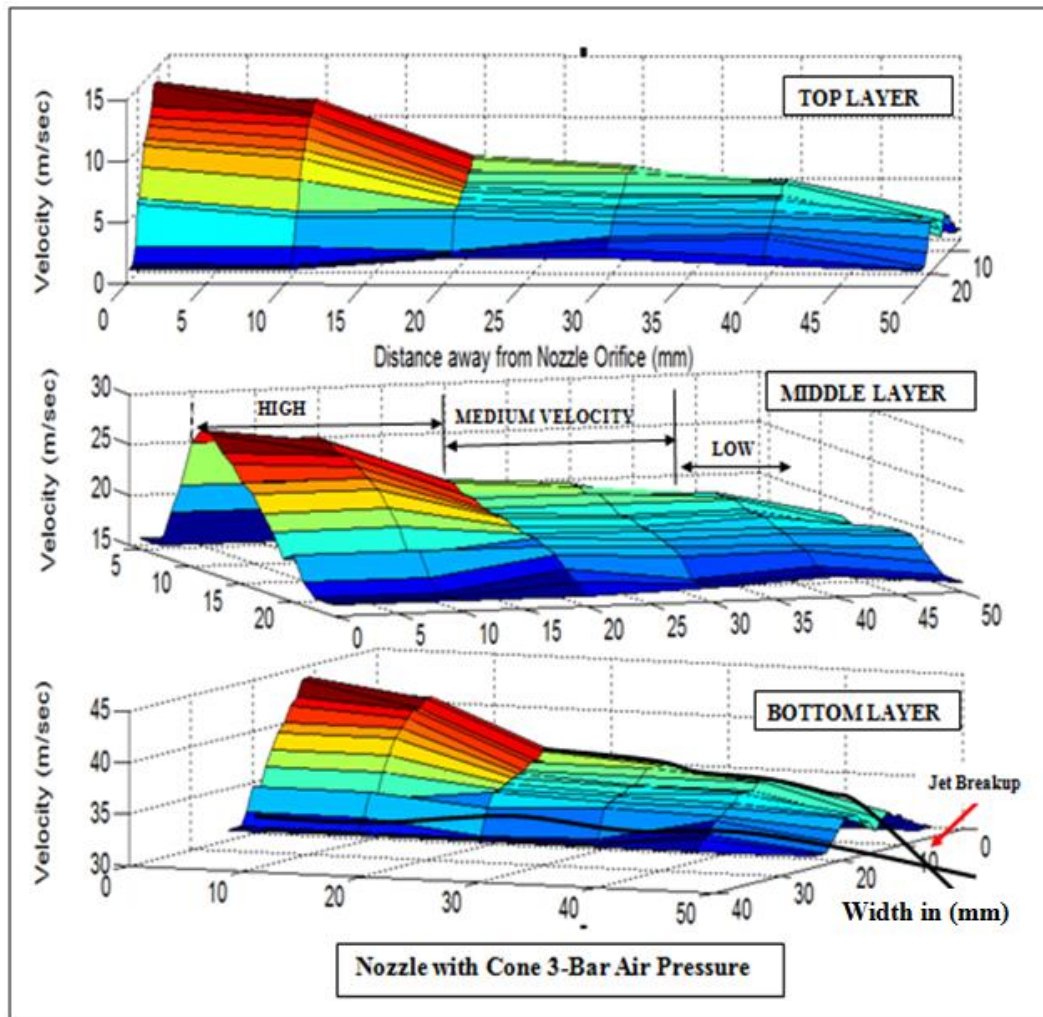


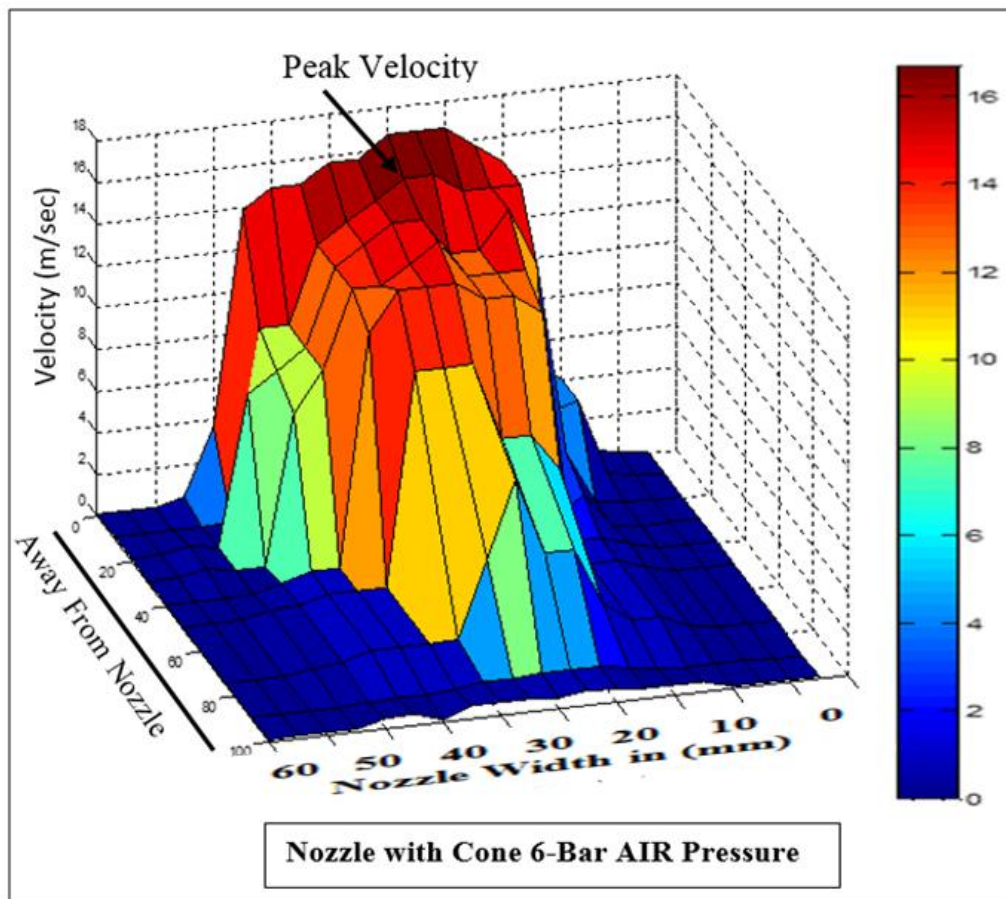
**Figure 8.12: Nozzle with Cone Multi-Layer Surface Plot (Input 3-Bar)**

The maximum jet velocity in this case is maintained with increase of 10 mm up to a coherency length of over 50-mm distance from the nozzle orifice. Fig.8.12 gives detail flow behaviour of air pattern in three-layer. The nozzle with 3-bar showed some improvement, where peak velocity is observed up to 20-mm then a uniform profile from 20 to 40-mm. Beyond 40mm the velocity drops and the jet breaks up at a distance exceeding 50-mm. In the test with 1-bar the peak velocity covered up to 15-mm and

started falling. Comparing both results it is revealed that the influence of cone has a strong effect showing better performance with the increase of inlet flowrate.

### 8.6 Nozzle with Pressure Cone (Input 6-Bar Velocity Surface Plot) Results

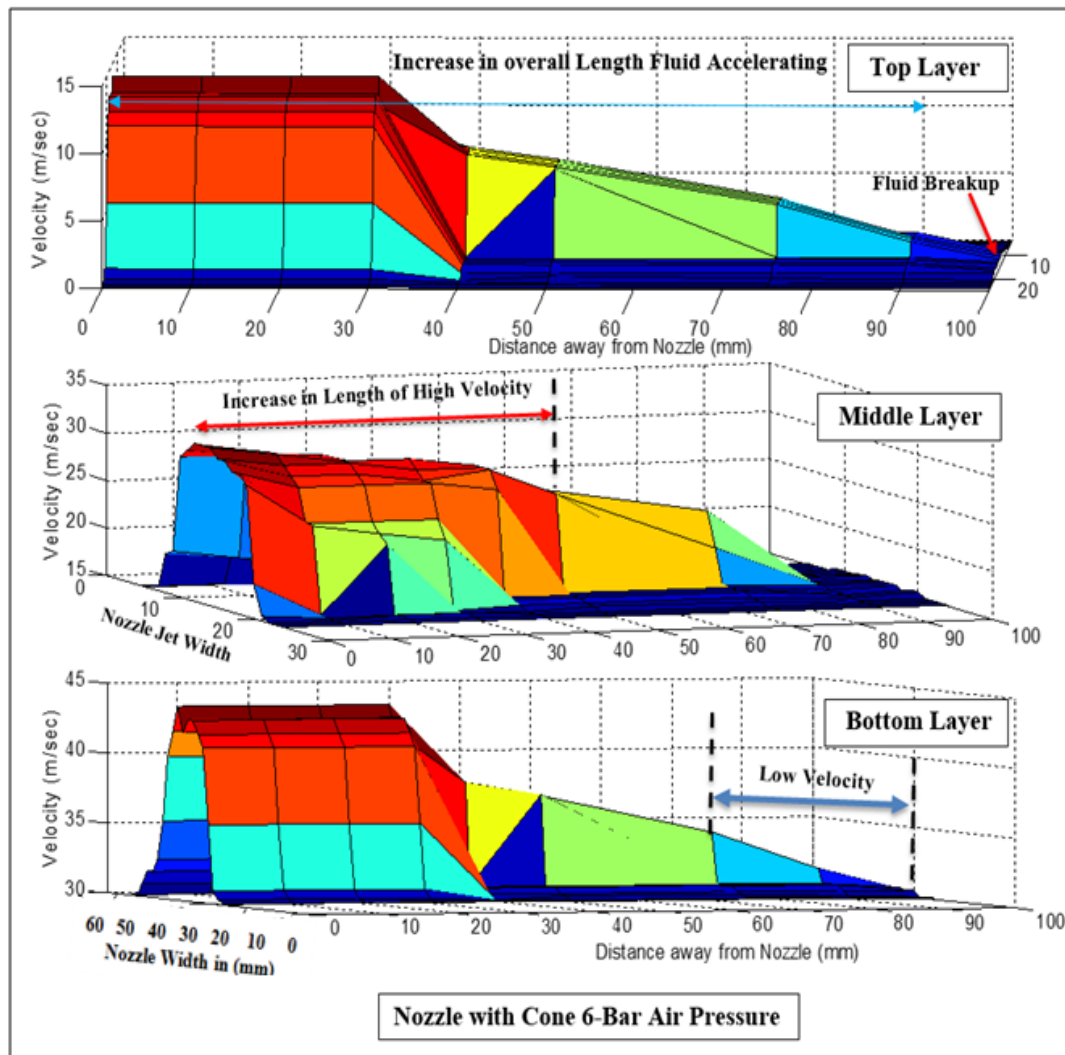
Here air is supplied at 6-bar pressure to the nozzle inlet and the velocity is recorded in the middle layer of the orifice. Fig.8.13 shows a parabolic profile of high peak velocity that is maintained almost to a distance of 100 mm.



**Figure 8.13: Nozzle with Cone Velocity Surface Plot (Input 6-Bar)**

The nozzle with cone of 6-bar input air pressure, in these case the outflow of air velocity achieved peak velocity with curved profile on top edges. The velocities at the centre and corners of the jet appear more improved due to further increase in air input pressure. The tests with 1, 3, and 6-bars shows that the effect of cone performance with

an increase of 35%. The jet thickness reduces at the far down the jet stream. The jet maintains a higher peak velocity profile until approximately 100 mm from the nozzle orifice.



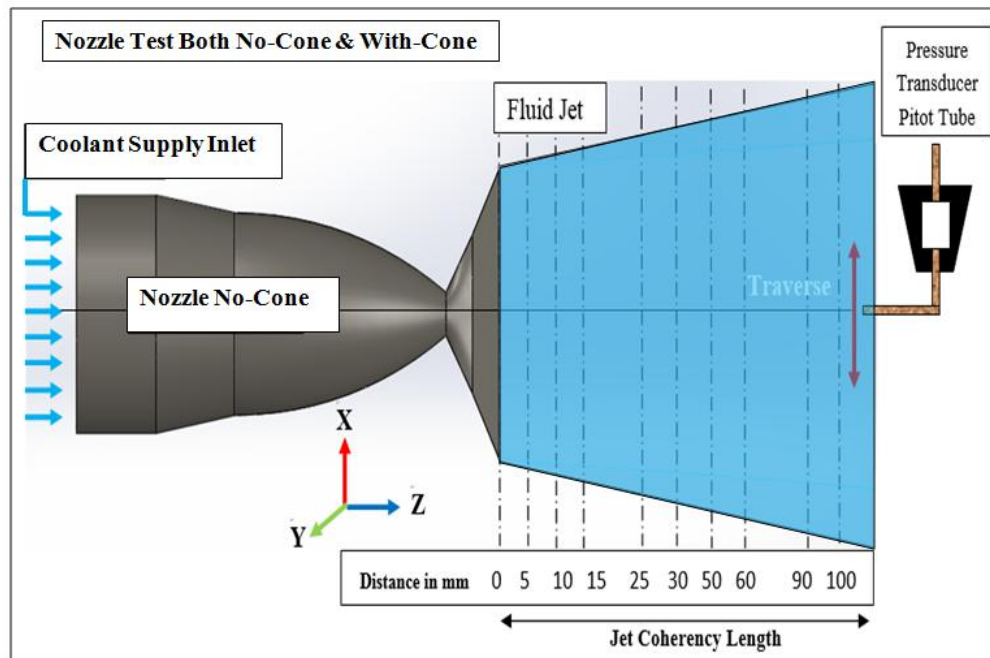
**Figure 8.14: Multi-Layer Velocity Surface Plot (Input 6-Bars)**

Fig.8.14 depicts, the multi-layer surface plot depicting an optimistic profile for delivery of MQL in the grinding applications. Investigating the external profile of the jet in this case shows that from 0 to 40-mm the profile maintained a peak velocity, however it started to narrow at its centre. This nozzle with 6-bar input air pressure proved that the insertion of cone leads to a better performance.

## Nozzle Investigation with water (Coolant)

### 8.7 Performance of Nozzle without Cone and With-Pressure Cone

In this experimentation the nozzle is tested both without pressure cone and with-pressure cone using coolant. This test is mainly to focus the effect of both cone and no-cone performance Fig.8.15 illustrates nozzle with coolant no-cone is conducted first with supplied flowrate of 10-l/min which is controlled by a rotary type flowmeter and valve for accurate measurement see (chapter-7 Fig.7.5 coolant supply system). Then the nozzle is conducted with-Cone of same flowrate, the results presented of these two experiments was shown and discussed detailed in below sections.



**Figure 8.15: Nozzle without Cone**

The coolant used in this experiment was delivered from a coolant supply pump system. To control the supplied pressure and coolant flowrate, two control valves were installed and a coolant return-circulating system was also used on a movable platform. The coolant pump supply system consists of a filter cap under the suction pipe to avoid any debris or particles which can obstruct the nozzle aperture. All the equipments were well installed for collecting the measurement data in order to eliminate any errors.

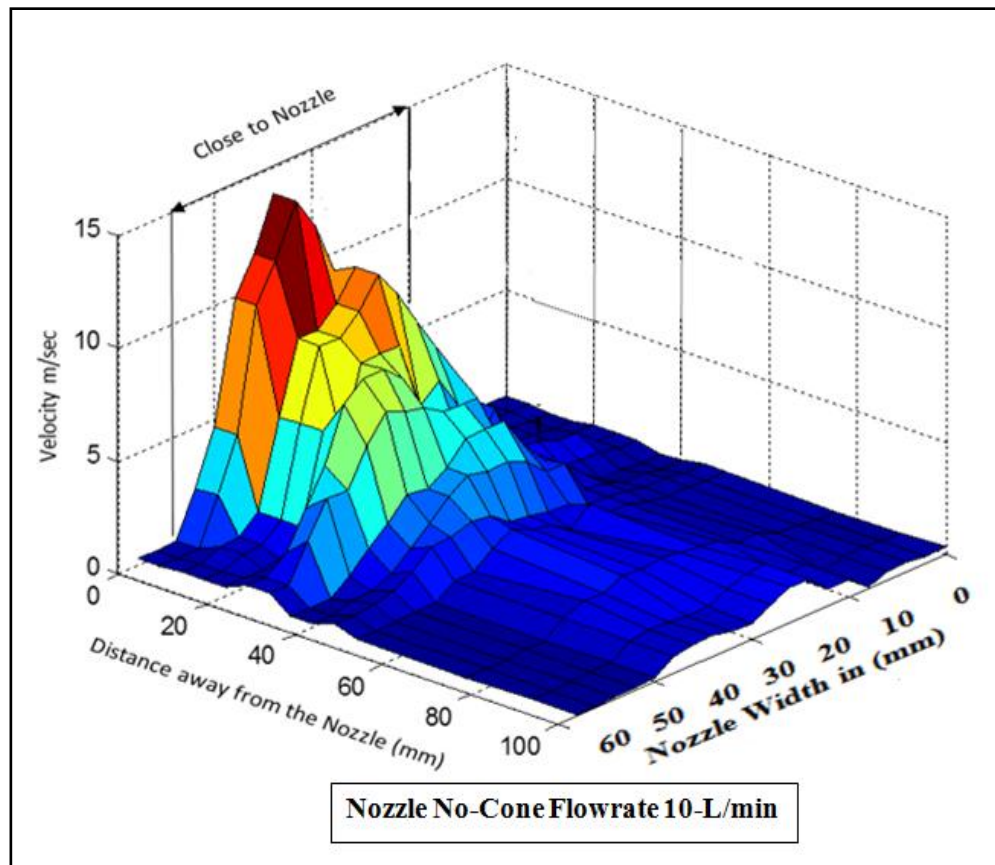


**Figure 8.16: Jet Velocity Profile of Nozzle without Cone at 10-L/min**

The above Fig.8.16 illustrates the velocity profile of the nozzle without cone of supply flowrate of 10- lit/min. Here, using water as coolant, the velocity profile appeared completely different compared to the nozzle with air as a fluid. Due to the mass of the coolant water, the jet profile formed like a diverged shape and the middle layer registered peak velocities at the centre region of the nozzle aperture. The diverged shape is formed due to the pressure developed inside the cavity profile. In this experimentation the jet is maintained up to a peak velocity of 15 m/sec and distance covered away from the nozzle is 40-mm later the fluid jet gradually decreased has a low speed up to the jet break up. The experimentation is measured and continued with three layers top, middle and bottom layers to visualize the actual fluid flow behaviour. The nozzle jet stream is schematically represented by multi-layered 3-D surface plot in below section see Fig.8.17.

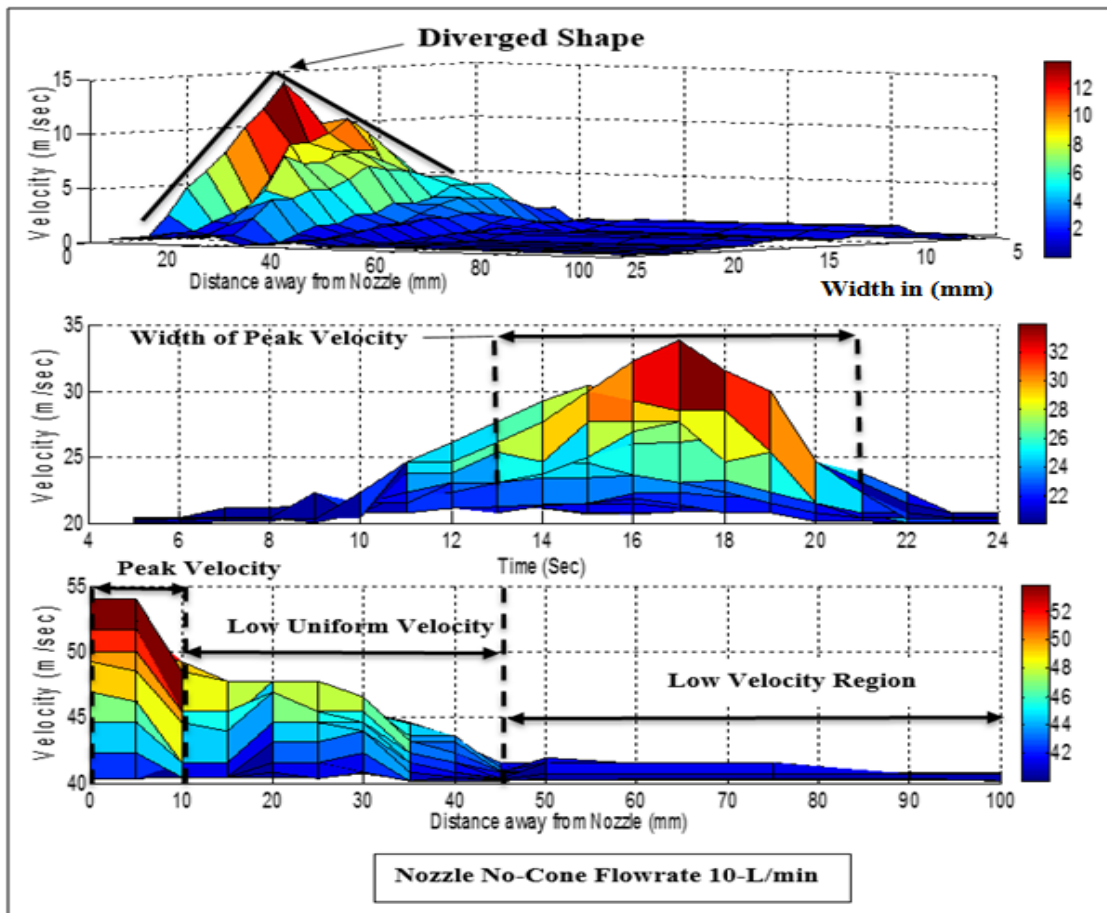


**Figure 8.17: Multi-Layer Velocity Surface Plot (No-Cone Flowrate 10-L/min)**

The above Fig.8.17 illustrates a multi-layered 3-D surface plot represented by top, middle and bottom layers, in this experiment using coolant of 10-lit/min flowrate, the fluid is varying from top to bottom layers. In the top layer it is seen that peak velocity profile maintained up to 15 m/sec however, the fluid maintained an average velocity up to a distance of 45-50 mm beyond this the fluid velocity drops gradually down the stream, the maximum distance measured was 0 to 100 mm.

### 8.8 Nozzle with Cone (Flowrate 10-L/min water)

In this test the nozzle with -cone is conducted with 10 l/min of water was supplied to the nozzle with the pressure cone. Fig.8.18 depicts the corresponding, and it is seen that the insertion of the cone lead to an increase in the exit velocity compared to the

previous nozzle no-cone. In Fig.8.17 where the nozzle was plain without pressure cone, the peak velocity was achieved 15 m/sec), and in Fig.8.18 where the nozzle is fitted with cone with the same flow rate was supplied, the exit velocity is 32 m/sec). This shows clearly using cone has some effect on internal flow which tends to speed up the fluid and by comparing both with-cone and no-cone using surface plots the jet velocity was increased doubled with peak velocity of 34 m/sec.

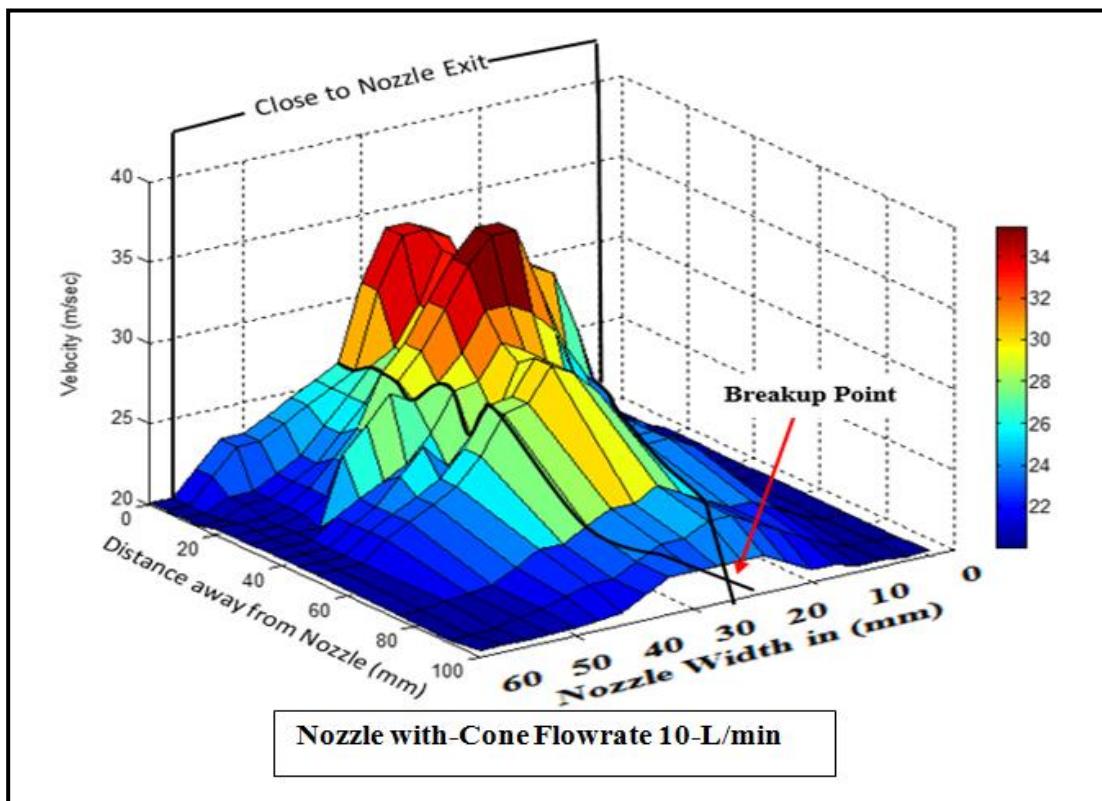


**Figure 8.18: Nozzle with Cone Middle Layer Surface Plot**

From the inspection of the above Fig.8.18, a clear trend of the jet thickness increasing with distance is apparent. The velocity profiles relax and become increasingly centred showing the peak velocity and increasing jet width. The surface plot shows after the coherent region general decreasing trend visualising the effect of jet break up starting point downstream of the nozzle exit. The insertion of pressure cone, at the length covered by high jet velocity is almost doubled (up to 80 mm) away from the nozzle exit. Theoretically the jet break up length is approximately 100 mm from the nozzle exit.

### 8.9 Multi-layer Surface Plot (Nozzle with Cone 10 L/min Flowrate)

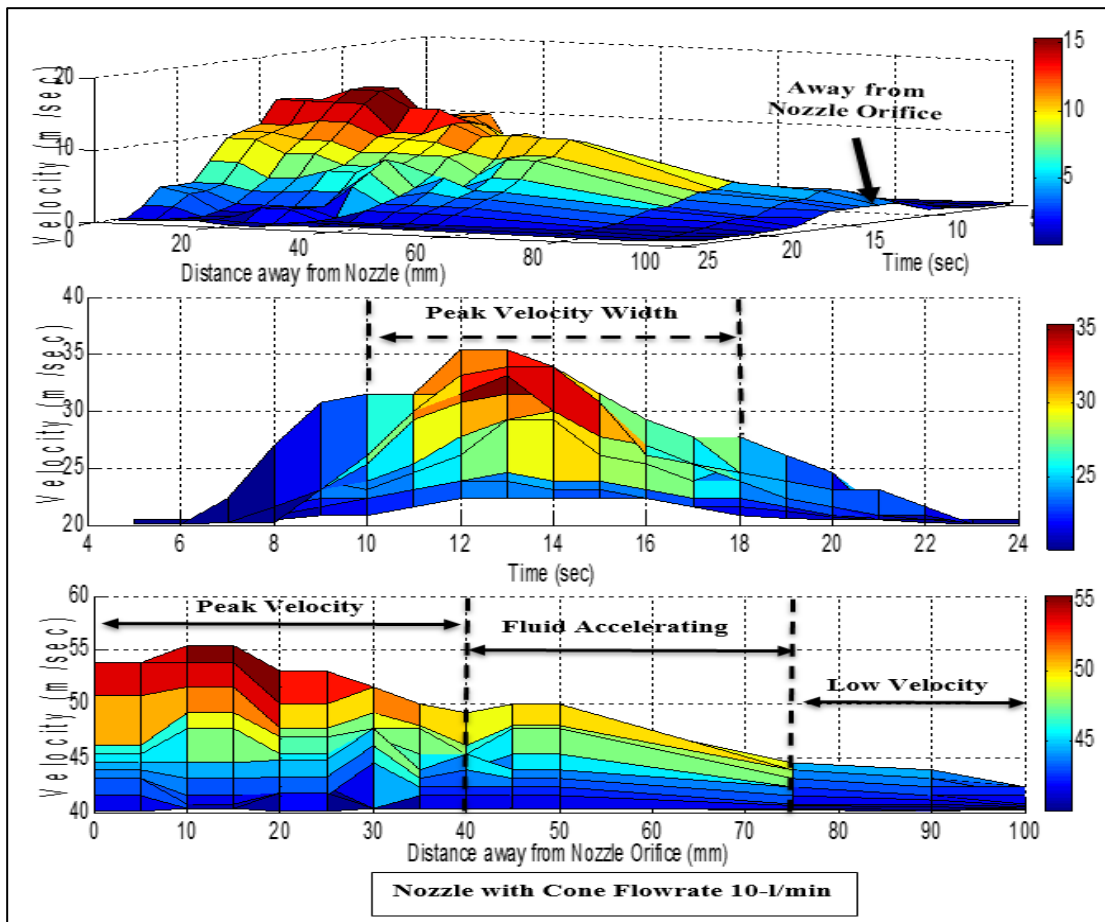


**Figure 8.19: Multi-Layer Surface Plot (Nozzle with Cone 10 L/min)**

The triple-layer plots presented in Fig.8.17 and Fig.8.19 reveal a new finding in the jet behaviour. It is observed that the three layers display different peak velocities. In Fig.8.19 the top layer has a peak velocity of about 15 m/s, the middle one show 35 m/s whereas the bottom layer secures up to 55 m/s. This interesting behaviour of the jet has never been shown before neither experimentally or theoretically. One would assume that the middle layer would have the average kinetic energy. However, it has been discovered here that the bottom layer gives the highest jet velocity. This can be explained by the effect of gravitational forces acting on the jet, thus bringing the bulk of the fluid to the bottom part of the jet illustrated in Fig.8.20 this discovery might change the perception of nozzle positioning in machining application. Here with a nozzle

aperture of 0.3 mm, it is now shown that one must take in consideration that the lower layer provides high jet velocities compared to any other part of jet. Therefore the nozzle must be positioned in a way that the lower third of the jet hits the cutting zone or the acute angle (wedge) between the workpiece and the grinding wheel.

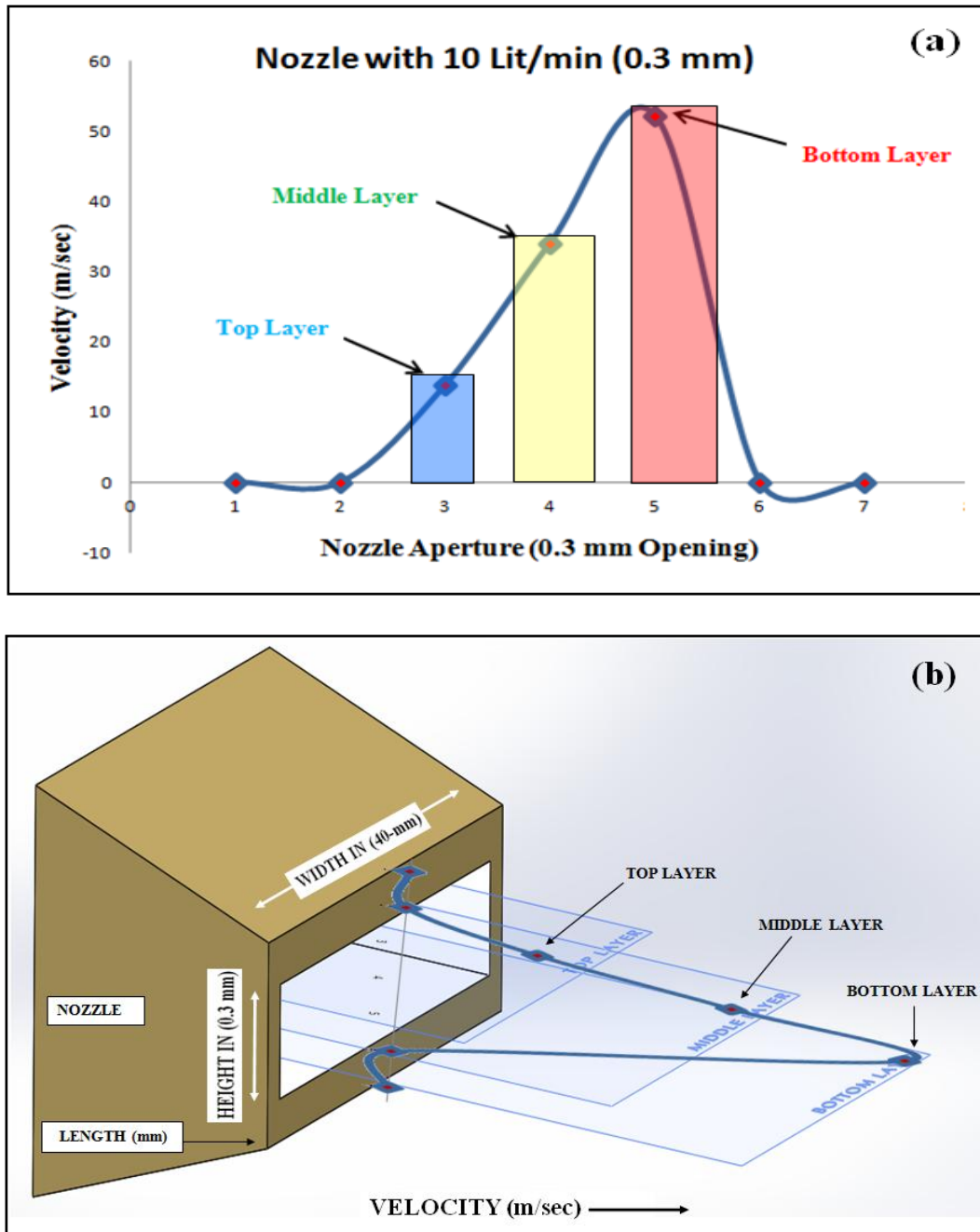


**Figure 8.20: (a) Velocity Profile (b) Visualization of 3-Layers in Vertical Direction**

The above Fig.8.20 illustrates the nozzle with 0.3 x 40 mm aperture with a supply flow rate of 10 lit/min. A velocity profile is drawn in a vertical plane at the centre of the fluid jet to visualize the variations within jet stream to illustrate that the fluid velocities increases from top to bottom layer. The graph is plotted by using average readings at each layer (see Figure 8.20a) across the nozzle vertical height that is 0.3 mm. It is observed here that the peak velocity is recorded at the bottom layer which shows varying velocities illustrated in Fig.8.20 (a). This plot reveals clearly that fluid velocity is gradually rising from the top to the bottom layers is schematically represented in actual fluid flow direction of 2-D velocity profile after immediate exit of the nozzle at 0-mm see Fig8.20 (b) in centre area vertical direction. This variation in jet velocities is due to the one of the main reason that masses of the coolant, gravity pulls downwards resulting in peak velocity.

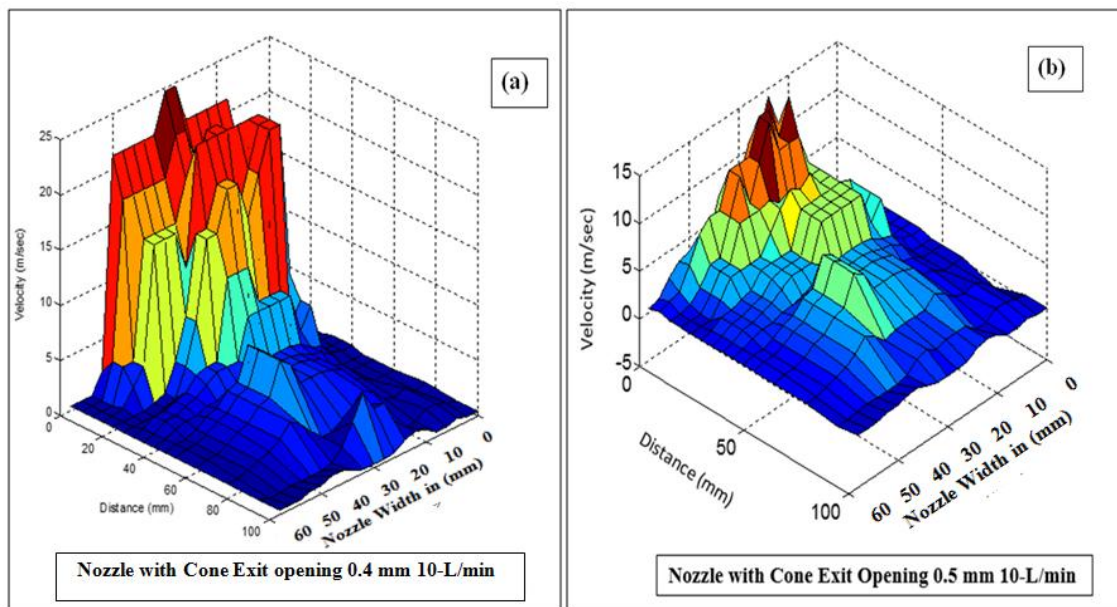


**Figure 8.21: Nozzle with Cone aperture (a) 0.4 and (b) 0.5 mm**

Fig.8.21 shows the nozzle performance with increased exit apertures of 0.4 and 0.5 mm. Here, it is seen that the increase of the aperture by 0.1 mm lead to a drop in pick velocity by 10 m/s, from 35 m/s (see Fig.8.18) to 25 m/s in Fig.8.21a (0.4 mm aperture). Similarly increasing the exit aperture by 0.2 mm, i.e. 0.5 mm dropped the

peak velocity by 20 m/s (15 m/s, Fig.8.21 (b)) with reference to 0.3 mm Fig. 8.18, or by 10 m/s reference to Fig.8.21 (a). As the increase in nozzle exit aperture brings a drop in peak velocities, it consequently, reduces the overall length covered by high jet velocities. It was also observed that in the same way the jet stream velocity distance away from the nozzle is also showed difference which is covered by a shorter length coverage up to 40-50 mm of both 0.4 & 0.5 mm aperture compare to over 80 mm for 0.3mm aperture. This is equally observed in below Fig.8.22 where additionally, one could see the eddy modulation of jet thickness profile. The multi-layer visualization of nozzle aperture with 0.4-mm has a profile of straight line formation after immediate exit see Fig.8.22 bottom layer. This is due to the fluid has enough space to exit from the nozzle aperture with increase in jet thickness.

### 8.10 Multi-layer Plot nozzle with cone Exit Opening 0.4 mm

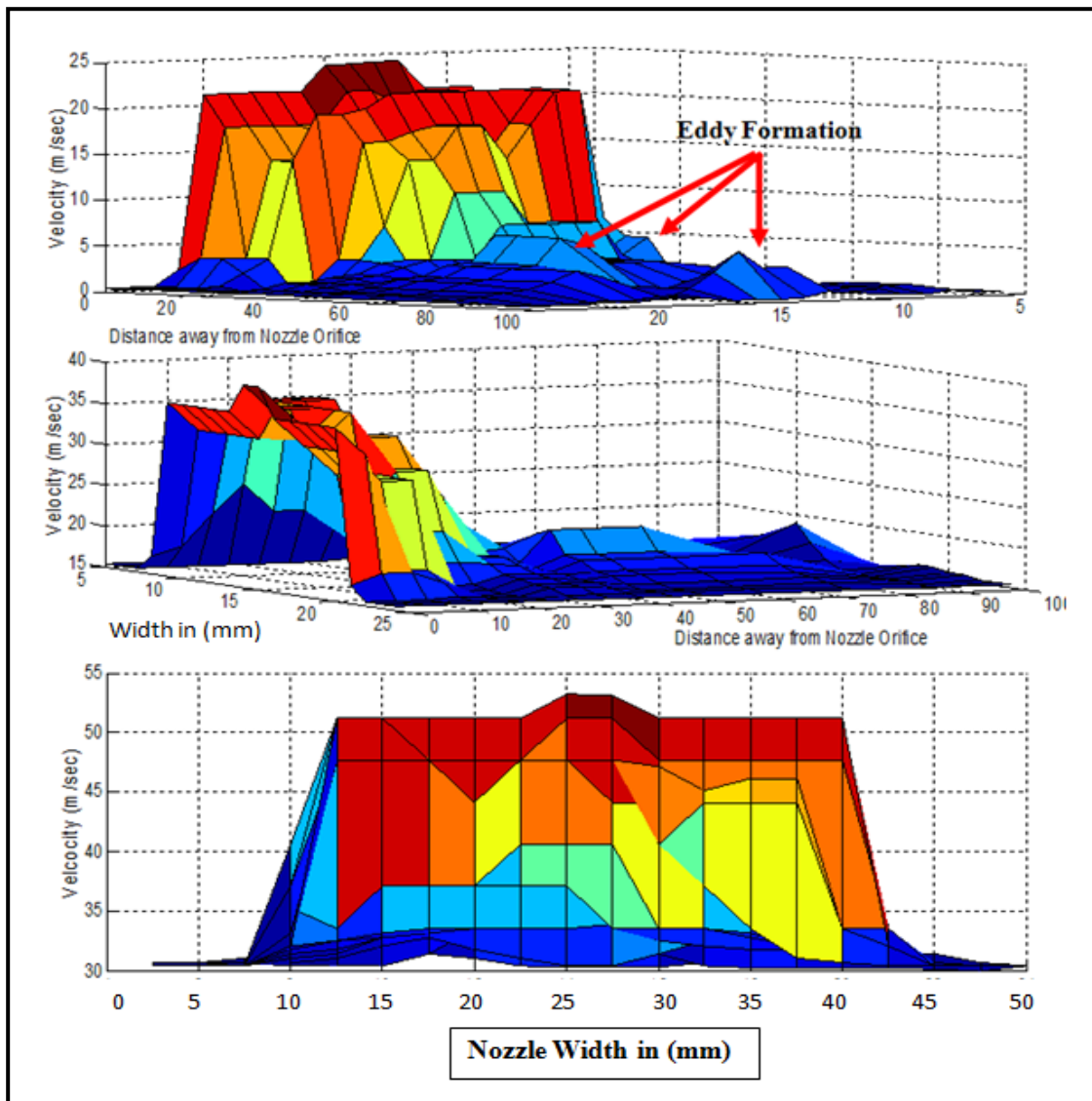


**Figure 8.22: Multi-Layer-Nozzle with Cone Exit Opening 0.4 mm**

Here, the multi-layered 3-D surface plot results of nozzle with cone of exit opening 0.4 mm is presented in above Fig.8.22. This 3-D surface plots reveals that increasing nozzle exit aperture has some great effect on the jet stream as well as in coherence length away from the nozzle also in jet stream a eddies formation is observed this is due the increase in opening couldn't able to creating the fluid speed inside the nozzle cavity, still can use with this 0.4 mm for bulk coolant application by increasing the supply flow rate.

### 8.11 Nozzle Coherence Length Tests

The nozzle tests focus on finding the coherence length of nozzle jet stream in order to position the nozzle to the grinding contact zone. The nozzle with cone was used with different input supply. A noticeable difference in the jet stream regions of peak velocity is observed. For 6-bar of air input pressure, the jet velocity is maintained up to 60 mm. and for 10 l/min of coolant supply, and the length covered by high velocity is about 75 mm. The below Fig.8.23 highlight this point further. Although the overall jet velocity is increasing but covering less distance up to 100 mm this is due to low flowrate. Increase of input flowrate will increase the nozzle exit jet velocity and coherence length furthermore. This is ideal for grinding situation as the nozzle with cone (flow conditioner) may be placed within the peak velocity region

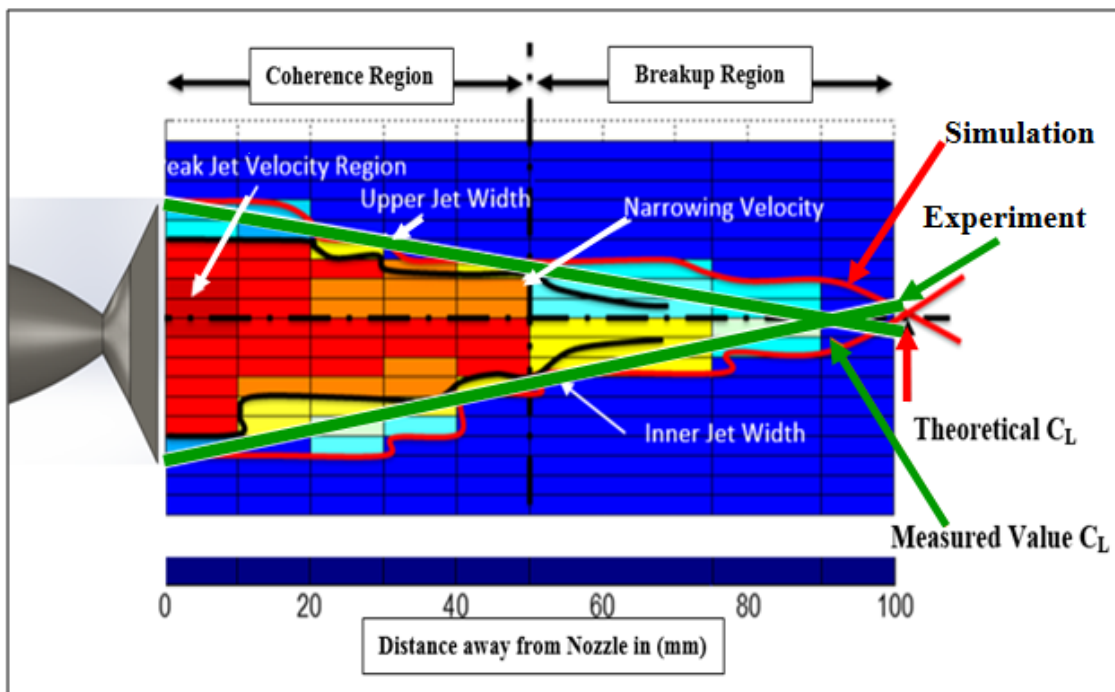


**Figure 8.23: Coherence Length of Nozzle with for 6 bar air pressure**

The above Fig.8.23 depicts the detailed concept of the nozzle coherence length, fluid jet breakup point and jet width. The external flow of the jet fluid is divided into two regions of either side of the centre area coherent region and fluid dispersion region of low velocity in blue. Focusing on the stream it is observed that the jet formed a

triangular core where the fluid holds together. As the fluid move away from the nozzle the dispersion are increases leaving only a narrow and eventually the dispersion covers the entire jet stream. It seems that this is the first time that this kind of velocity map of fluid jet illustrates clearly the behaviour of the external fluid flow, with jet breakup point and dispersion area.

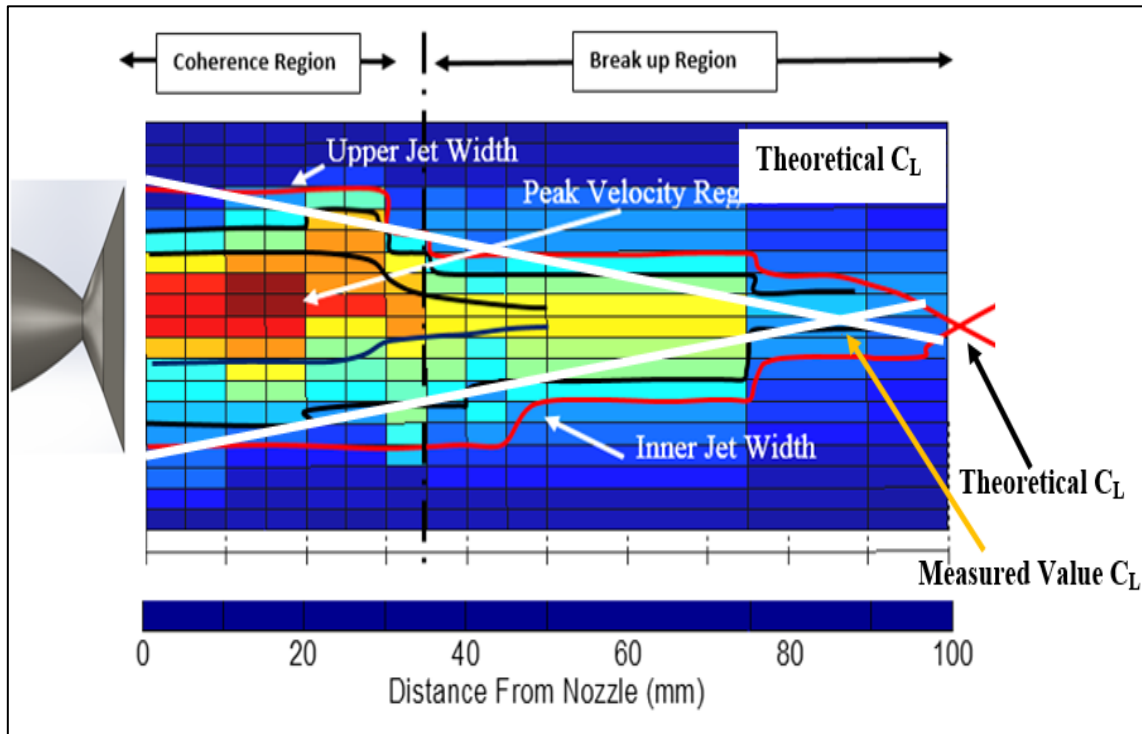


**Figure 8.24: Coherence length of Nozzle with Cone for 10 L/min (water)**

The nozzle coherence length and its usefulness in the grinding environment is based on the width of the actual jet and its velocity. Here only 10 l/min of supply flow was used due to technical limitation of the supply pump. Consequently the flowrate was limited to 10 l/min. As in the case of air, here in Fig.8.24, the same triangular profile of the jet core is observed sitting at the centre of the stream. However, with the water, the dispersed area gradually creeps into the core without abrupt end as observed in the Fig.8.23. Another problem encountered with water (emulsion) was the quality of the filtration process. With 0.3 mm aperture, swarf particle periodically obstructed the exit of the nozzle, causing misreading of the pressures.

### 8.12 Verification and Comparison of Simulation Results

The actual flow measurements are very complicate to perform and not all situations possible to measure. ‘CFD’ computational fluid dynamics modelling results are validated here with experimental results. For a flowrate of 5 L/min, Fig.8.25 represents the jet velocity profiles and the jet velocity achieved 21.1 m/sec without cone, however, with the insertion of the cone the jet exit velocity achieved was 25.75 m/sec, the difference was 4.45 m/sec which is an increase of 17.28%.

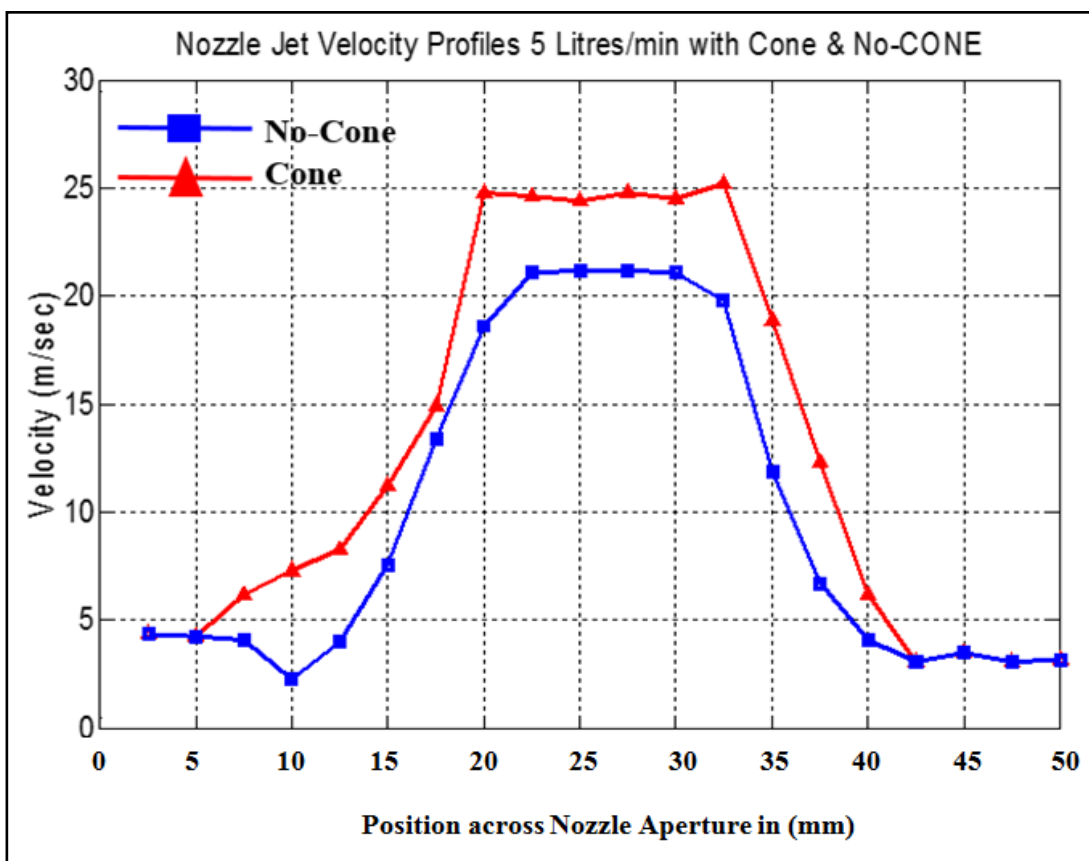


**Figure 8.25: Jet Velocity Profiles for 5-l/min with/out cone**

The below Fig.8.26 illustrates, the exit jet velocity profile of nozzle with cone and without cone. This plot reveals the effect of cone on the performance of both nozzles. The profile of 10-l/min no-cone represented by blue line with a maximum achieved the exit velocity of 25.1 m/sec. For the same flowrate with pressure cone inserted in the

nozzle output jet velocity jumps to 35.3 m/sec; this provides a step up of 10.2 m/sec which is an increase of 28.7%.

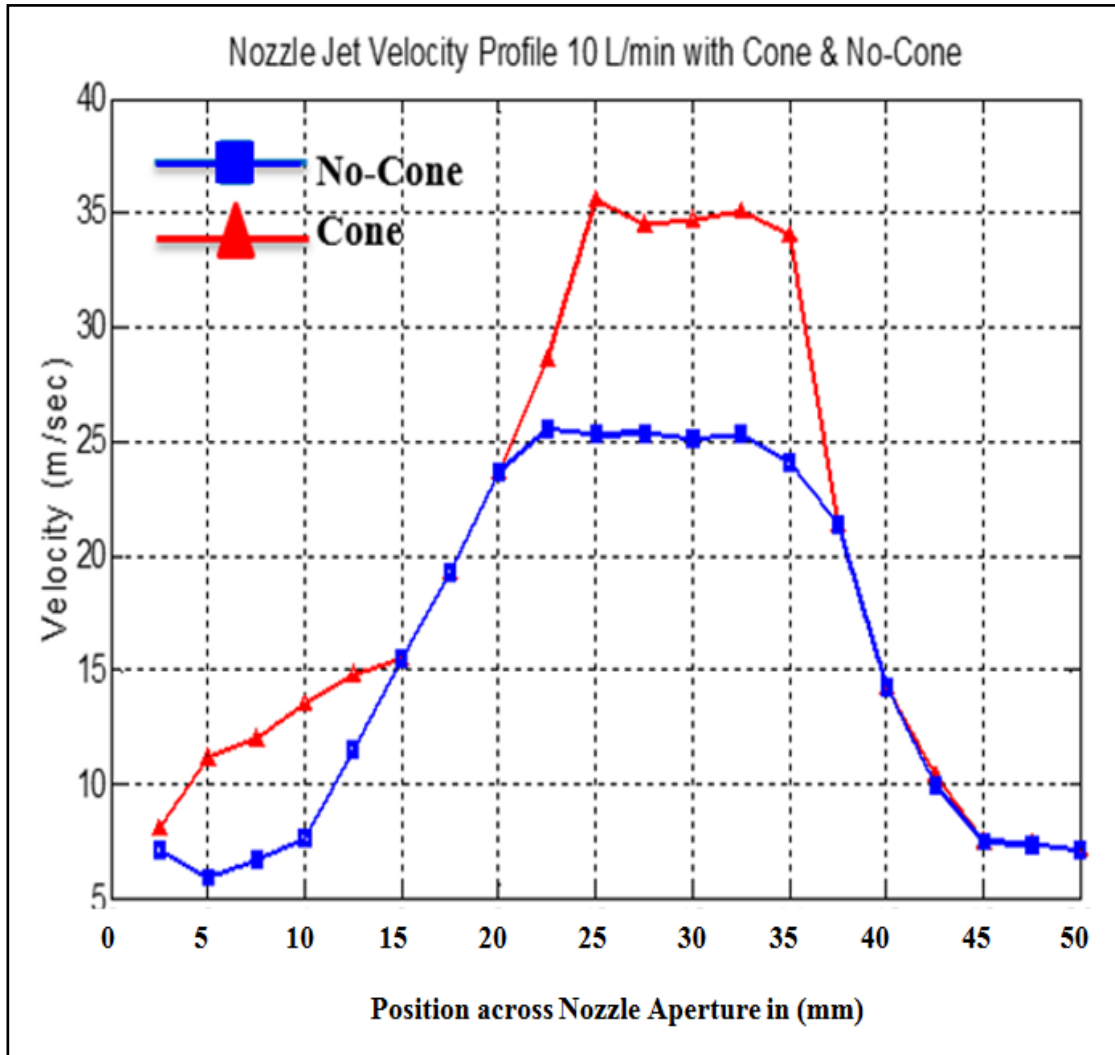


**Figure 8.26: Jet Velocity Profiles of Flowrate 10-L/min with cone & without Cone**

### 8.13 Comparative studies of MQL Nozzle performance

In this section a comparative study is undertaken to characterize the performance of the MQL part of this universal nozzle. Here the simulated results are put side by side with the actual measurement data recorded in experimental work is presented below.

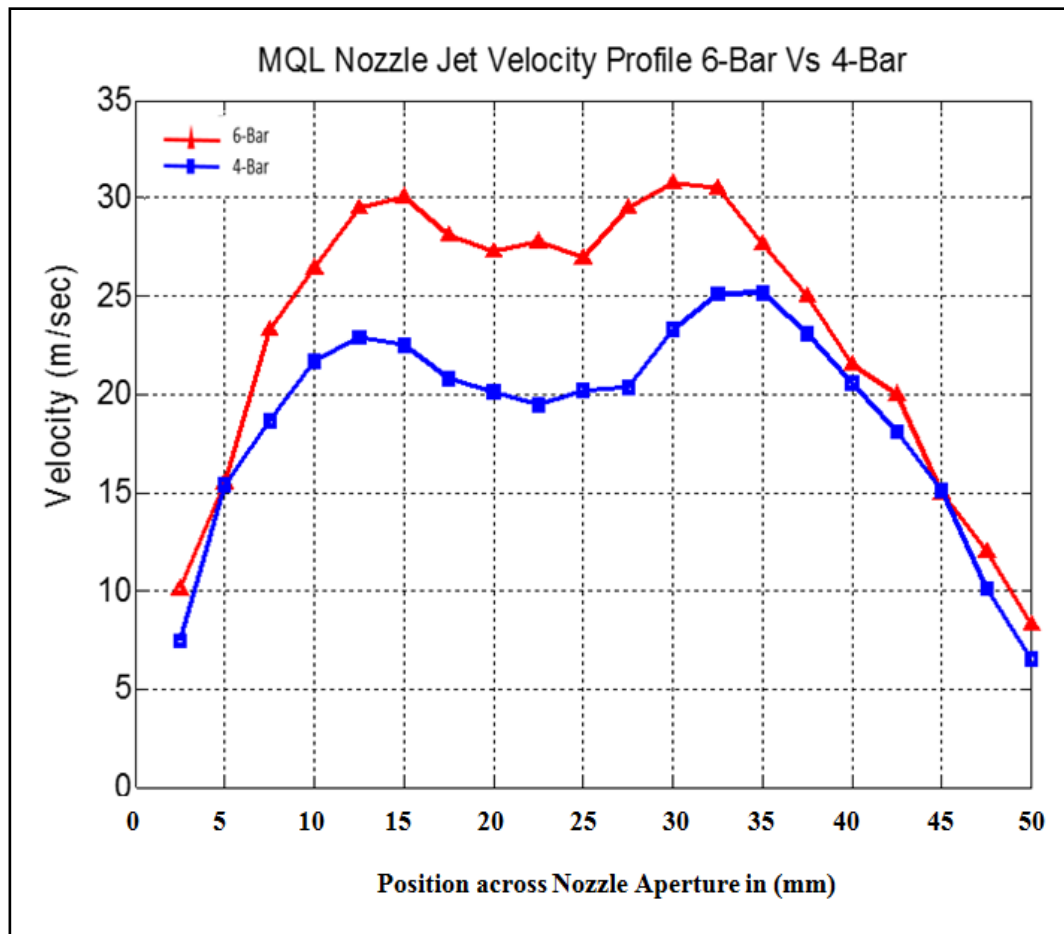


**Figure 8.27: MQL Nozzle with Cone (6-Bar & 4-Bar, Nested flow 100 ml/hr)**

Fig.8.27 illustrates the exit velocity profiles of 4 and 6 bars air pressure, in comparison the velocity profile of 4-bar has large drop in the middle this is due to the pressure cone outlet tip delivers fluid in a droplet formation (low velocity) and has turbulence when mixing of air and oil at the pressure cone tip. This small turbulence is desired here for thorough mixing of the so little amount of oil with air. As seen in this above figure, the higher the input pressure, the drop in the centre region is decreasing gradually with increase in exit velocity profile, 22 m/s and 30 m/s for 4 and 6 bar respectively.

In comparison with coolant, the air velocity profile of all 1, 3, 4 and 6 bars has various formations due to the amount of supply flow rate and mass of the air depicts in below Fig.8.28 and 8.29.

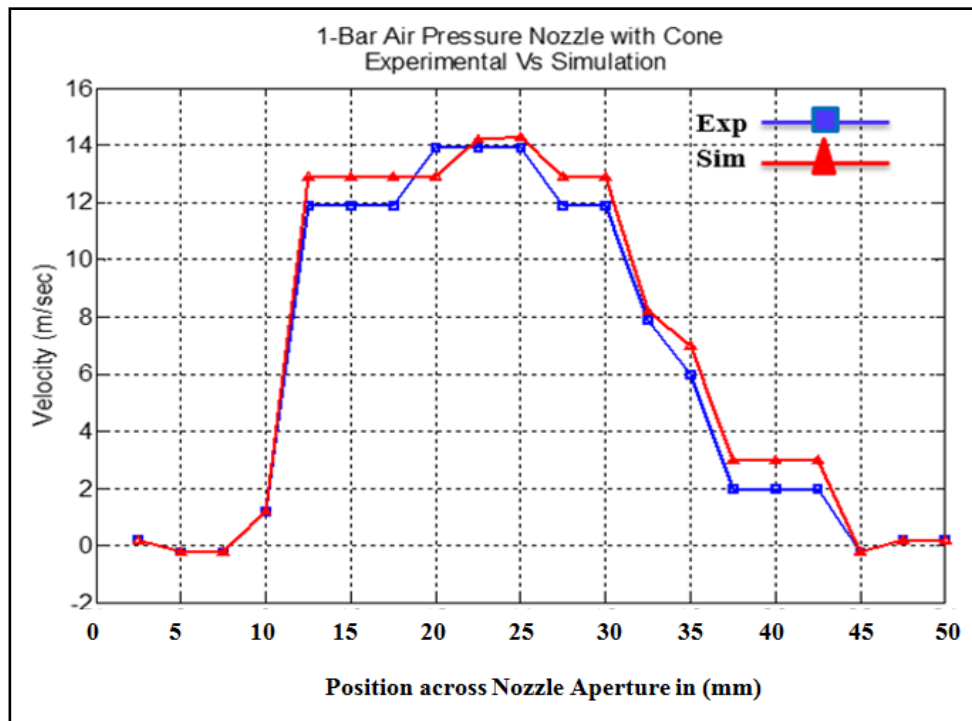


Figure 8.28: 1-Bar Air Nozzle with Cone Experimental Vs Simulation

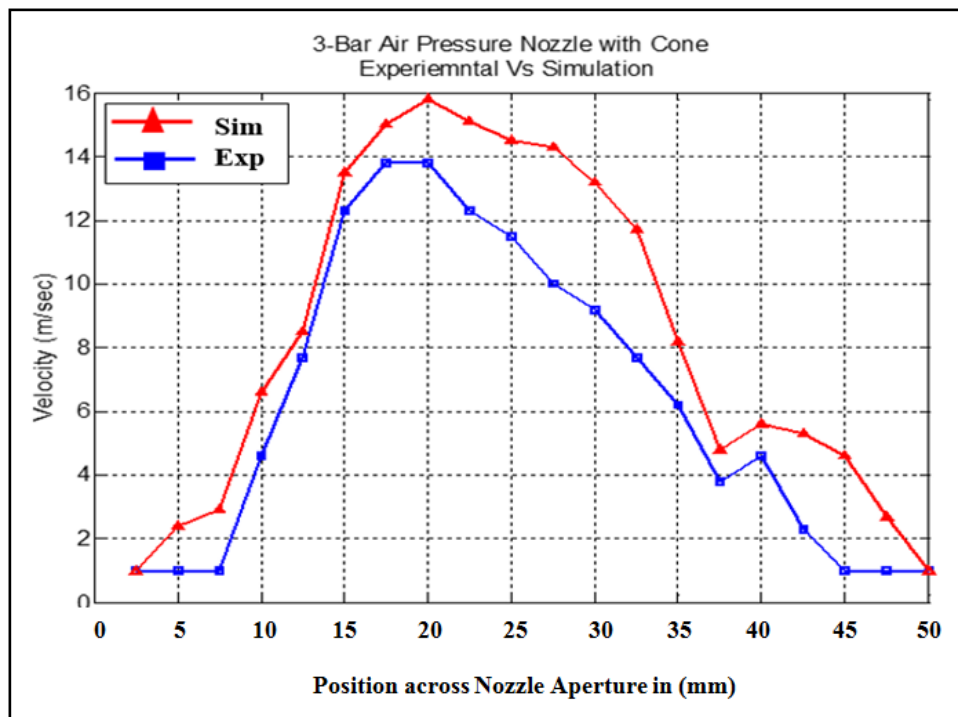


Figure 8.29: 3-Bar Air Nozzle with Cone Experimental Vs Simulation

In figures 8.28 and 8.29 it is observed that at low input supply flow rate of air pressure, the simulation results and the experimental results of velocity profiles are shown almost in exact match. However, with the increase in input air pressure, the discrepancy between the simulation and measurement increase, as the simulation overestimate the jet velocities.

It is observed that both simulation and experimental depicts similar velocity profiles. However, the simulation overestimated the velocities, whereas the measured values are nearly close to the predicted value. This is explained by the fact that in simulation the conditions were ideal, whereas in actual measurement there were a number of issues that affected the results. These issues were, the losses in the supply pipes, the fluid filtration, the particle blocking the nozzle exit and the size of the Pitot tube. In addition the results presented here are taken from the middle layer; however, it is shown the bottom layer has higher velocity, this mean that if the velocities of bottom layer were to be used the discrepancy would be less.

#### **8.14 Key Findings**

1. The bottom layer has higher velocity compared to top and middle, this mean that if the velocities of bottom layer were to be used the discrepancy would be less.
2. With the help of 3D multi-layer surface plots the Eddies formation are observed for the first time in actual measurement, though it is well defined theoretically in many textbooks.
3. The peak velocity profiles are observed in centre region of the jet stream; this can be used for effective positioning of the nozzle.
4. The visualization of multi-layers top, middle and bottom has variations in velocities is represented by 2-D velocity profiles drawn in vertical position. This shows a clear understanding of fluid behaviour that the third bottom layer acting downwards due to gravitation.
5. A 2-D velocity profile is drawn vertically in the centre region of the nozzle after immediate exit of the nozzle at 0-mm represents step by step increase in velocity.

# **Chapter-9**

## **Discussion**

## Chapter-9 Discussion

The main study of this research work is based on the design and development of a parametric multi-purpose nozzle system with intent to reduce the volume of cutting fluid and used to deliver a low volume, high pressure flow for both conventional and MQL fluid in grinding application. The work focused and analysed a solution for the large reduction in grinding fluids. Providing a deeper understanding of coolants, would allow savings to be made in manufacturing industries regarding the amount of coolant required for the grinding process. This would in turn have implications for the environmental and ecological impact on the manufacturing industry. As discussed earlier even small savings in volume of coolant delivery can result in significant savings when scaled up to multiple machines in many industries.

However, grinding which accounts for 25% of manufacturing processes, cannot be performed dry, hence fluids are applied at high pressure and high flow rates. Imagine the gain if all metal machining could go dry, or even a 5% cut off, or employing minimum quantity lubricant as low as 30 ml/hour for grinding? Minimum quantity lubrication (MQL) is a prime example of the attempts to advance coolant delivery, consumption and efficacy. Both flood and MQL have specialised fields of application and lead to the focus of this investigation. This project is an attempt to solve the above mentioned problem by developing a system of supply of coolant accurately to the grinding contact zone (Targeted area).

The importance of cutting fluid and nozzle performance during the grinding process is well documented in the literature. In a highly competitive world, where manufacturing processes are constantly under scrutiny for further optimization it is important to exploit any new developments and theories proposed through research. By studying the different mechanisms of the grinding process, fluid application in contact zone, nozzle position, MQL application, air boundary effect, useful flow, fluid penetration into pores



of the wheel, a new concept was proposed and developed for cutting fluid delivery where benefits of each mechanism are harnessed.

### 9.1 Development of the Nozzle Design

The novelty in this work presented here reflects the need of high performance nozzles. A concept of novel modular adaptive nozzle design with nested flow nozzle (Secondary Nozzle) was designed and implemented, this give birth to a new generation of nozzles that deliver '*Dual/triple Fluid*' delivery system. This concept was studied using 3D solid modelling, CFD flow simulation with design and simulation iterations before actual implementation. During optimisation process the nozzle internal cavity and nested nozzle structures of the model were modified in a series of steps from initial design stage to final design stage. Here the '*Nested Nozzle*' acting as a flow conditioner allows to straightening the fluid flow in the main nozzle cavity. In this work the performance of various types of nested nozzles (Flow Conditioners) designs were tested in simulation.

Another aspect of the novelty is the '*MQL flow*' delivery, which intends to reduce further the quantity of fluid used. Here a special mechanism was designed to pressurise the flow in the nozzle. The nozzles which exist traditionally are in the form of the click-fit nozzle. These types of nozzles are not efficient in grinding application because the grinding wheels are wider in width so these spot nozzles are not fit for the purpose.

Combining these two new approaches to nozzle design; a new optimized MQL nozzle was derived. Therefore, this optimized design allows for cleaning, flood and MQL coolant applications.

According to the results of the simulation a better performance is achieved by introducing a concept of pressure cone. During the optimization process different pressure cone designs were simulated but, some of them showed a poor performance. However, after a series of designs alterations and investigations, an Egg shaped pressure cone design provided a better performance therefore it was implemented. the Egg



shaped pressure cone had an internal flow conduits for fluid inlet whilst placed within the main nozzle chamber. The relationship between the flows and the pressures in the main and nested nozzles was investigated and the design was optimized in the attempt to reduce the amount of coolant used with reference to traditional flood cooling.

## 9.2 Development of the Simulation

As in the first stage, preliminary simulation was conducted on previous nozzle designs to examine any losses or recirculations for acquiring knowledge of internal flow patterns. A novel modular adaptable nozzle was designed and tested, All the CAD 3D solid modelling were carried in solidworks CFD for initial studies and later the optimised nozzle design was transferred to ANSYS CFX for detailed study, refining of the simulations. These packages allow to simulating liquid, gas or their mixture using various working conditions. The chapter-5 and 6 shows that the simulation results have real physical interpretations of the internal fluid flow pattern and external flows and peak velocity distribution

All the nozzle simulations were conducted with various exit profiles as presented in chapter-5. According to these results it was noticed that a better performance was obtained by introduced a concept of pressure cone. For this a basic MQL nozzle in a shape of a pressure cone was introduced and during this optimization process different pressure cone designs have been made and simulated. However, some of them showed a poor performance, subsequently, an Egg shaped pressure cone which consists of internal flow conduits was placed within the chamber of the main nozzle. the latter nozzle produced better results when compared to previous designs. This design was thoroughly simulated under different nozzle exit profiles which helped selecting the better performing nozzle. A modular structured nozzle emerged and was studied using up to 6-bars air and 150 ml/hour of oil as MQL fluid. The jet of the droplet spray (air & oil mixture) was able to cover the entire wheel width which is not possible with commercial spot nozzle. It has been found that the nozzle with 0.3mm exit aperture with

a dove tail exit profile had an increased velocity compared to other designs (whale tail and flat exits).

### **9.3 Limitations of the Simulation**

It is important to inspect the solution output from a simulation before applying any post-processing operations. If the simulation data contain any significant differences with the expected results such as unexpected output higher velocity, then a suitable adaption and refining of the mesh quality is required. A high quality mesh is considered a mesh that does not suffer from large increases in cell sizes high aspect ratio cells, local mesh clustering and low orthogonal cells. The tetrahedral mesh is applied for accuracy of the model with skewed mesh quality. The latter cannot be controlled during adaption process since it is entirely dependent on the initial mesh and hence necessitates the development of an accurate mesh base to begin with. A problem was identified with the coherence length due to increased entrainment of air at the free surface boundary. This was a difficulty in the work presented here since predictions of effective coherence length which had to be based on initial calculations from the simulation and consequently these results could only be partly validated experimentally. When an improved mesh was used at the free surface boundary, the error between simulation and the experimental results was reduced. However, there is some increasing percentage of errors in some region in the velocity profile at distances away from the nozzle orifice. This mainly affected in the centre of core region and hence had an effect on the peak velocity distribution. The change in overall coherence length however, was found to be of the same order for both the simulation and experimental work for MQL.

A significant proportion of the work concentrated on the development of the simulation method and a high degree of success was achieved. Considerable effort was spent in trying to ensure correct break up region and interaction between the two phases at the free surface interface. There is an inevitable loss of velocity when momentum of coolant passed from the orifice region of high water concentration to the region of high air concentration and this is significant even in models where velocities are low. The



adaption technique was used to increase the mesh resolution in regions where these significant changes were present and to move imperfect numerical boundaries away from the region of interest.

A uniform mesh is used instead of a multigrid mesh without the need for mesh adaption if sufficient process power and space were available. However, to produce simulations of the free surface, with detailed mesh running to thousands the number of nodes and elements already in use, the computation stations used within the laboratory would need several weeks to complete a single simulation. The method will only be practical when required storage and memory are available.

#### **9.4 Experimental Methods**

One of the key developments required for this project was the experimental rig and traverse pitot tube measurement system. Without such system and device the analytical testing would not have been possible to validate the nozzle characteristics. As shown in chapter-7, a fully developed and thoroughly tested system was arranged and implemented on 'Jakobsen surface grinding machine'. This arrangement allowed manipulating the measurement device in 3-axis (X, Y, Z) directions. Further the traverse pitot tube system was fixed to the machine head which moved in Z-direction away from the nozzle to measure the velocities across the nozzle exit.

The first problem tackled using pitot tube measuring method was the ability of the sensor to withstand the input pressures. Identifying the actual pressure that the free jet exerted on the sensor was a challenge that limited the range of measurement and data recorded for during the experiment with water. Therefore, experiments were limited to 6 bars for air and 10 l/min for water. It was observed at later stage during data graphical representation that, the results of measurements had noticeable discrepancy with reference to the simulation results. However, the measurements with air were in good agreement with the modelling results. This brought in a reassurance that the modelling was correct and fit for the purpose. An initial attempt was to re-run the experiment with



water at high flow rate, yet re-ordering expensive sensors and the lead time for delivery meant more time and the experiment with high flow rate was not done. The discrepancy between simulation and experimental results is attributed to the sensor imperfection and its inability to perform at high pressures. However, the good agreement of the simulations and experimental results with air up to 6 bars shows the adequacy and value added of the work done.

The sensor performance might have affected all results including the coherency length; however, the data recorded allowed revealing for the first time to the research community in 3D plots the layered behaviour of the fluid as it flows from the nozzle to full dispersion. The observation focussed on the nozzle exit dividing it into multiple layers to study the flow behaviour after the immediate exit of the nozzle aperture all the way down the stream till complete dispersion. The inspection of the velocity profiles shows that peak velocity region is maintained up to 80-90mm max, in addition, eddies oscillation (modulation) that are used to define the coherency length in theory was visualised in these measurements. Here it was shown that the jet does not keep the theoretical exit velocity across the nozzle width, only a central core in the form of a triangle keeps the exit velocity over a given period. The finding of this triangle of fluid carrying the desired jet is critical for matching wheel velocity with jet velocity. If one assumes that the exit jet has a homogeneous velocity across the nozzle, thus placing the cutting zone an arbitrary length, this would lead under-cooling edges as the boundary air layer would deflect low velocity jet at both side of the jet presented in below Fig 9.1 and Fig 9.2.



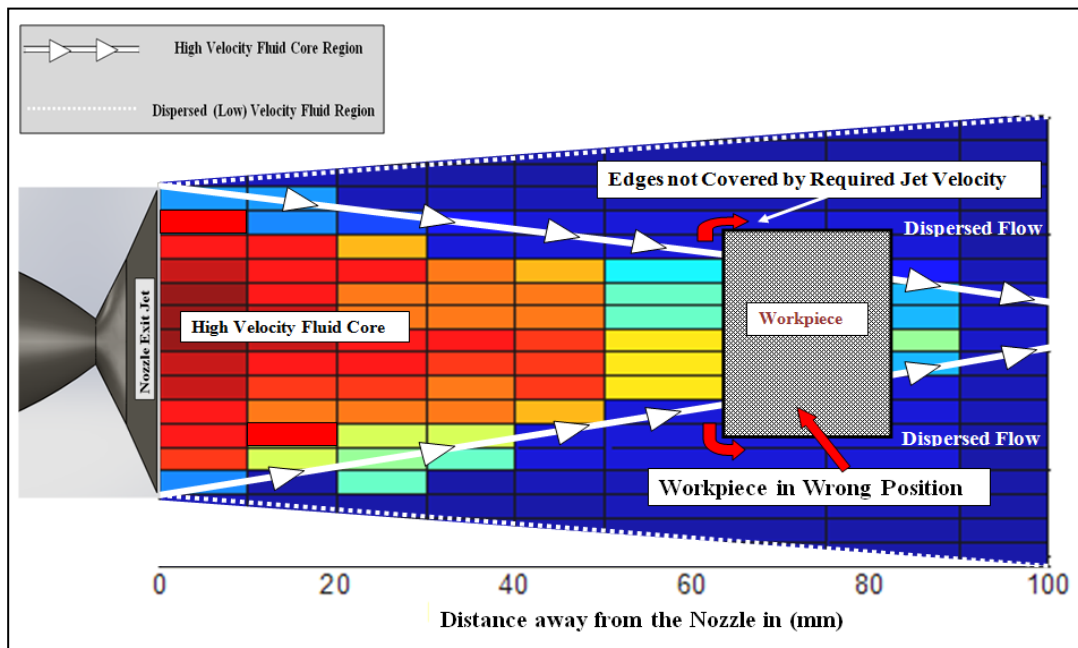


Figure 9.1: Workpiece in wrong position

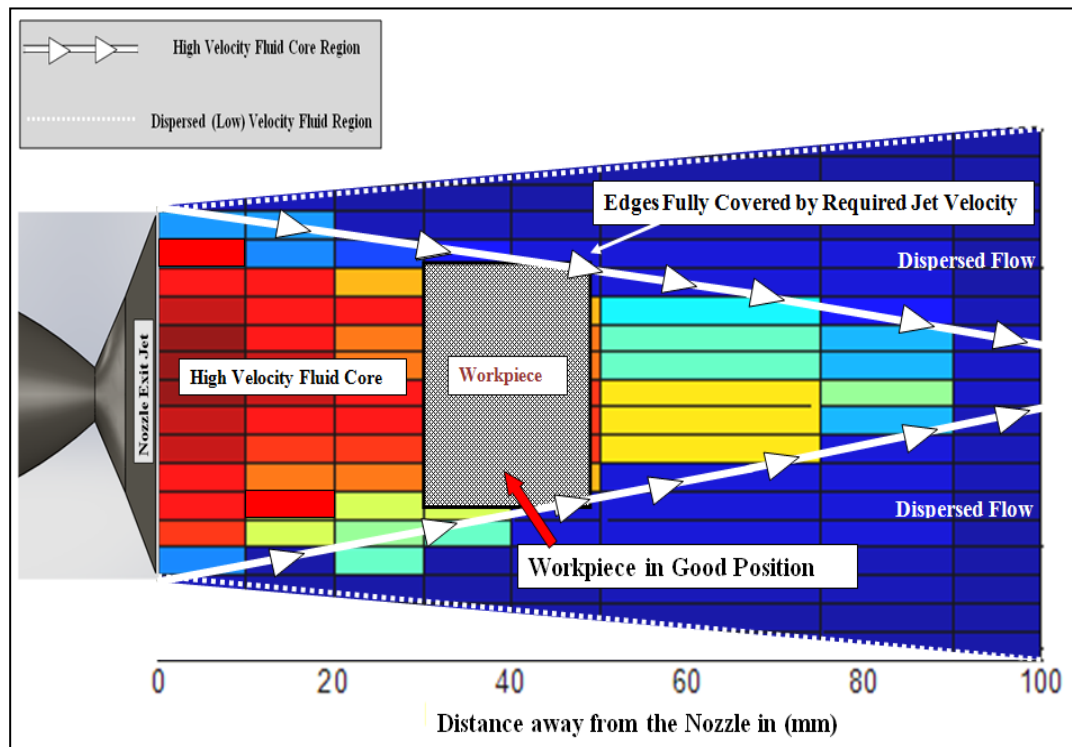
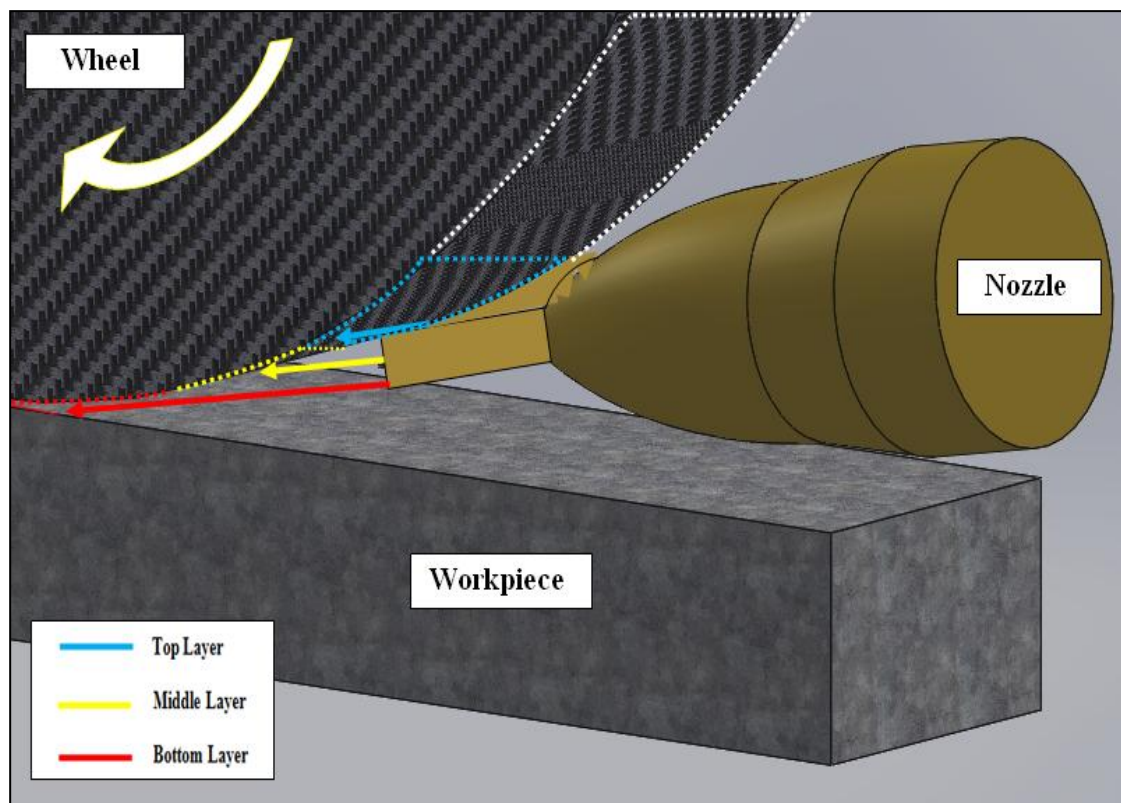


Figure 9.2: Workpiece in good position

#### 9.4 Summary

The experimental work showed that variations within the nozzle exit have significant effects on the overall length of the jet stream and peak velocity distribution within jet stream. The satisfactory results achieved by using the rouse based internal profile of this nozzle allows less coolant to be used to achieve desired results and optimise the grinding process. To achieve sufficient supply of coolant into the wheel/workpiece contact zone, it is necessary to adopt the schematic presented above Fig.9.2 and to position the nozzle in such a way that the bottom third of the fluid is targeted at the nip between the wheel and the workpiece. This suggestion is supported by the multi-layered measurement results showed that the jet velocity increases from the top layer to bottom layer. Therefore positioning the bottom third layer of the fluid directly to the contact zone would exploit the high jet velocity required to push the fluid into the zone.



**Figure 9.3: Position of Nozzle Exit Bottom Layer Targeted to Contact Zone**

The above Fig.9.3 illustrates the positioning of nozzle in such a way that high jet velocity exit matches to the wheel width also to cover the workpiece. As previously presented the grinding wheel surface is divided into four zones i.e., mixing zone, entrance zone, grinding zone and open zone. Here, within the grinding contact zone is again divided into 3-layers according to the nozzle design exit the one should position the nozzle that bottom third of the jet is targeted to the zone with the upper two third contouring the wheel surface which depicts in below Fig.9.4 in detail.

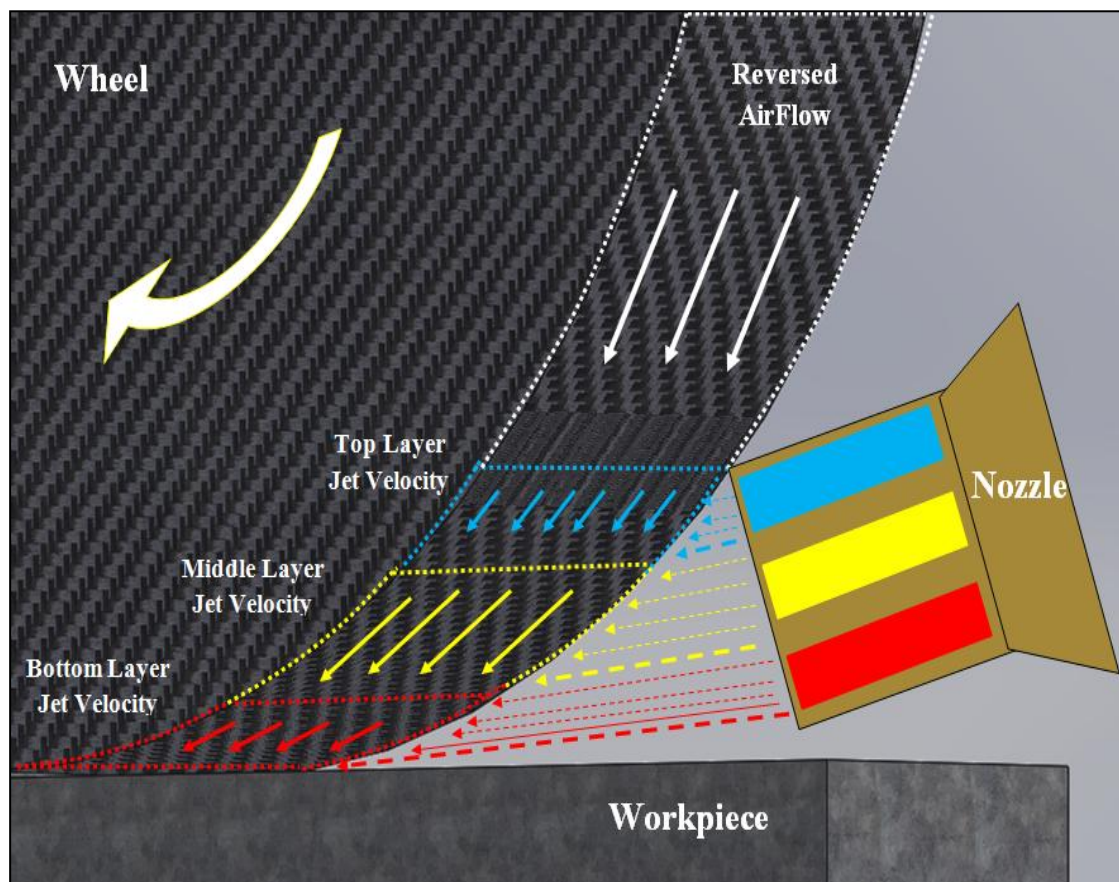


**Figure 9.4: Close View of 3-Layers Matching to Targeted Contact Zone**

The above figures represent the clear understanding of wheel-workpiece-nozzle system matching of multi-layers of jet velocity targeted to the contact zone for adequate cooling and lubrication in grinding process.

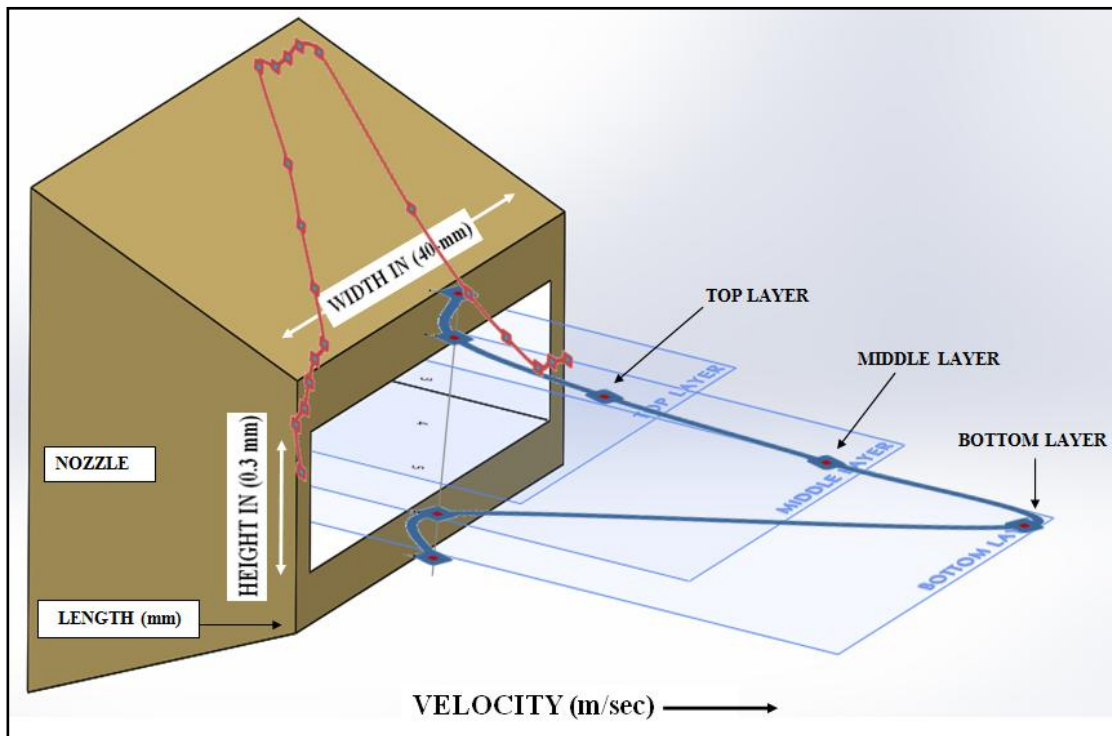


**Figure 9.5 Triple-Layer Velocity Profiles in Vertical and Horizontal Planes**

Figure 9.5 illustrates 2-D Velocity profiles in horizontal and vertical planes. Here in the vertical plane the jet velocity profile is given in the centre of the nozzle which depicts that the velocities in three layers gradually increase from top to the bottom. It is seen that the top layer has the minimum velocity, whereas the bottom layer registered the highest velocity. Similarly, a velocity profile is drawn in the horizontal plane representing the flow profile as illustrated in above Figure 9.5. Here velocity is distributed symmetrically across the nozzle aperture. It is seen thus that in the horizontal plane the jet velocity is symmetrical whereas in the vertical plane the jet high velocities as skewed towards the bottom layer.

- The design and optimisation process were critical for the success of this work. Coupled with numerous design iterations with Cosmos Flow-works and ANSYS CFX the work presented here shows for the first time the effects, the performance and the advantage of a nested nozzle.

- To the knowledge of the author, there is no previous work on nested nozzle and pressure cone in form of internal nozzle system. However, it is to mention that flow straighteners (conditioners) have been in use to straighten the flow before exit. In many cases these straighteners cause turbulence if wrongly placed in the flow.
- The design of the pressure cone in form of a nozzle that performs a flow straightening function is a novelty in itself and this cannot be found in the literature.
- The simulations in CFD and CFX have been an indispensable tool that helped visualising internal and external flow patterns of this new concept of dual flow.
- The new nozzle allows achieving high exit jet velocities with low flow rates, reducing fluid requirement and pumping power. This in its own has positive impact on environment and cost saving in cutting fluid purchase and management.
- The experimental work has shown a new fluid behaviour that was not recorded in any previous research. This is because conventionally all measurements are made in the middle of the nozzle and in the horizontal plane. There has never been any work on multi-layer measurements jet profile. Here it was shown for the first time by measuring the jet profile in three layers that the lower layer carries more momentum thus higher velocity. One can stipulate that this is cause by the force of gravity dragging more fluid mass towards the lower part of the fluid hence high momentum and high velocity.
- It was shown that the fluid has a central core that hold the original exit velocity, and that this core has a triangle shape the tip of which defines the coherency length.
- It was shown here that, with this novel nozzle one can apply conventional fluid cooling in flood mode or in MQL regime, without changing the set up. This can be achieved by a simple switch of coolant with air supply and MQL oil.
- An optimum nozzle position was suggested based on the finding from the triple layer measurement.

## **Chapter-10**

### **Conclusions and Recommendations of Future Works**

## Chapter-10 Conclusions and Recommendations of Future Works

### 10.1 Conclusion

This project brought up an advanced understanding of the fundamental of research and development of a multipurpose nozzle system that could be used for both flood and MQL coolants application. With the current legislations putting pressures on industries to energy efficient and environmentally friendly, this new development, if adopted and adequately applied would bring needed cost saving in coolant usage and impact on environment.

The major study of this research work is based on the design and development of a grinding fluid nozzle and to investigate into coolant flow delivery system in order to develop a radically new generation of nozzles which incorporate a dual flow coupled to deliver a low volume, high pressure flow for both conventional and MQL systems.

In this investigation SolidWorks and ANSYS CFX software packages were used for design and simulation iterations. It has been found that the nozzle with 0.3mm exit opening of a dove tail exit profile where an increased velocity is observed compared to other designs whale tail and flat exits. A comparative study of the performance of the manufactured nozzles was undertaken and correlated the experimental findings with the simulation. From these investigations the following conclusions had been drawn.

1. Throughout the design, simulations and optimizing iterations, a bespoke dual/triple flow nozzles was manufactured and characterised. However, the third inlet was not used in this study but was included in the design for further exploration of triple flow.
2. For the first time a dual flow nested nozzle is presented to the manufacturing communities to exploit the advantage of this multipurpose nozzle as it offers the use of one, two or three fluids either alone or in combination.



3. This design is modular and allows for a range of nozzle exit apertures to set depending on the application. However, smaller apertures say below 0.3mm for a blade jet, one must secure fine filtration as dirt and swarf particles begin to clog the narrow (film) exit.
4. For the first a secondary nozzle is used as flow conditioner to create laminar flow, and at the same time the flow through this nested nozzle is used to accelerate the primary, low flow which was supplied at a bare minimum pressure of 2-4 bar. It was shown that with this design it is possible to exert a 15 to 28 percent increase in outlet pressure with respective increase in jet velocity.

Using three distinct configuration of nozzle i.e., nozzle with cone (Nested), nozzle without cone and nozzle with cone with exit aperture of 0.4 mm and 0.5 mm, the conducted experiments reveal underpinning behaviour of the fluid which to the knowledge of the author has not been explored early by other researchers.

5. The fluid flow behaviour inside the engineered nozzle cavity was studied in details using slicing planes vertically and horizontally depicting critical paths and responses of the fluid to the surrounding nozzle wall. The jet behaviour was scrutinised as the fluid exited the nozzle all the down the stream, providing invaluable knowledge that has not been recorded before. Using specially designed test rig, the study of the jet was undertaken similarly to the study inside the nozzle cavity. Here, the jet was sliced using the measurement system to portray the fluid dynamic behaviour in three horizontal planes drawn along the nozzle aperture width. The 3D plots of the layers elucidated the performance of the fluid at the top, middle and bottom layer.
6. To the knowledge of the author up to date, it was shown as never before that the jet velocity increases from the top layer to the bottom, with the latter having the highest peak velocity is illustrated in Fig.8.20 & Fig.9.6 with two velocity profiles in horizontal and vertical planes. From these graphs, it is concluded that for optimum fluid delivery to the cutting zone with the expected jet velocity, one should position the nozzle in such a way that the bottom third of the jet is targeted to the grinding zone with the upper two third contouring the wheel surface.



7. It was shown in simulation that with 40-50 l/min this bespoke nozzle secured jet velocities of 120-160 m/s (see Figure 6.24) which are about some high-end wheel velocities used in current industrial application. This shows that it is possible to use low inlet flow rates and achieve higher velocities with this novel nozzle design. However, at flow rates greater than 60 l/min the exit jet velocity became sonic still it can be used at close distance between the nozzle exit and contact zone and for wheel cleaning purpose.
8. In MQL application, the maximum air pressure available in the workshop was 6 bars, which secured and exit mist jet velocity of 32 m/s which is applicable for conventional grinding. As the exit jet velocity increases with the increase in inlet pressure, it is possible to achieve high MQL jet speed with industrial high pressure air supply. This was proved with experimental and simulation work illustrated in Fig.8.27.

This work provides an advanced understanding of MQL performance and provides evidence that MQL can be effective to cover the wheel width. The most notable result achieved from the present work is the concept of pressure cone method improved jet velocity and it was proven that variations is observed in nozzle external jet velocity this was shown by 3-D multi-layer surface plots experimentally in chapter-8.

Based on the principles of coherence length tests and considerations of nozzle geometry, simulations for grinding fluid nozzle were established and the part (nozzle model) validated through experimentation to provide understanding of the mechanisms of coolant behaviour on both external and internal of MQL and conventional fluid nozzles grinding applications.

## **10.2 Recommendations of Future Works**

The present work focused on the design and characterization of a bespoke nested triple flow nozzle and two-phase flow model using air and oil as fluid media was studied. However, this work simply opened the door for further work and development. Therefore, the following areas are suggested for further work for a better understanding:



- The actual nozzle was designed with three inlets (3-inlets) which allows to deliver three-phase flow for future investigations where air, oil and water/coolant and their combinations can be used for better lubricating effect. Further investigation is needed to characterise triple-phase flow i.e. water-oil-air, in order to define the ratio of these media and their effect on cooling and lubrication efficiency.
- Investigation should be conducted into the simulating the entire grinding process i.e. wheel/workpiece/coolant. The model should include the effect of fluid structure interactions with grinding mechanisms in an attempt to explain the optimum triple-fluid supply into the contact region.
- Undertake an industrial test of the nozzle for MQL with higher pressures greater than 10 bars to create a jet blade with very high velocities that would allow for wheel cleaning, debris removal and effective cooling. Here triple-fluid supply would of great interest in terms of their ratio to increase the momentum of the air mist jet blade.
- Explore other exit profiles including concave, swivel and adjustable exits
- Investigates into thermal profile numerically and during actual grinding.
- Undertake a wide range of experimental in order to produce a machining map and user guidance for the application of triple-fluid supply with this new nozzle.
- It is of interest to investigate into oscillatory fluid supply with the intent to cut further the volume of cutting fluid employed.
- Characterise quantitatively the amount of coolant and pressure reduction using this triple-flow nested nozzle, and to quantify possible cost saving for the industries and the impact accrued to the environment.

# **Appendixes**

## Appendix-1 Optimisation of Nozzle Exits

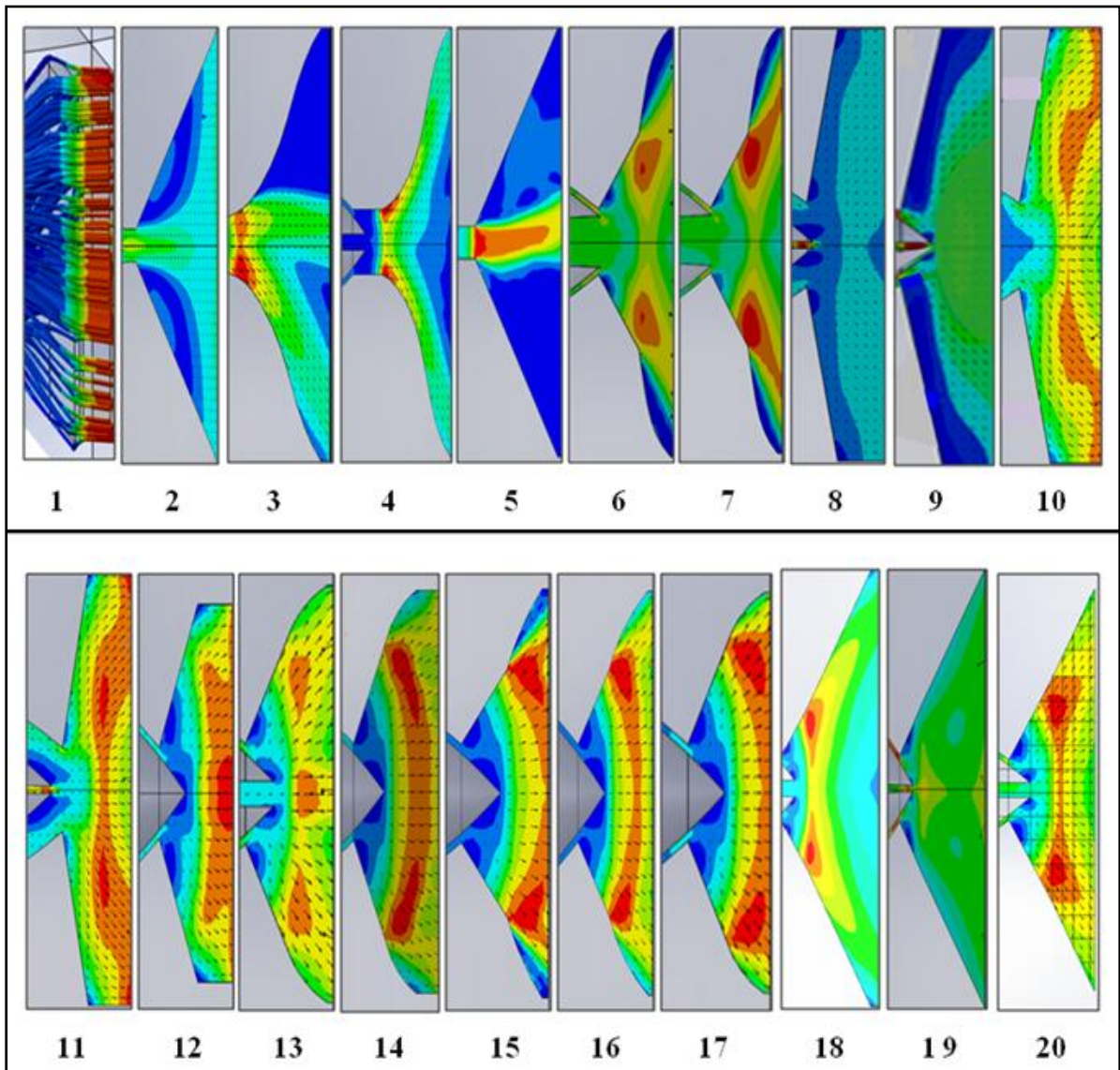


**Figure A-1.1: Optimisation of Nozzle Exits**

The above Fig A-1 illustrates the various modifications of nozzle exits during optimisation process is performed for a required jet velocity; in this a series of more than twenty exits was designed and modified. The nozzle exits are indicated by numbering system that Fig A-1 (1) depicts the exit flow is fully developed but the flow rate is high. Fig A-1 (2) to (9) are not fully developed and not performed well due to its internal profile. Fig A-1 (10) to (17) these

exits are fully developed, given good results and idea to further modifications for final output of the nozzle exit but little bit falls in exit velocity. Fig A-1 (18) to (20) these modifications reached high exit velocity air blade type jet due to their narrow exit opening 0.3 mm.

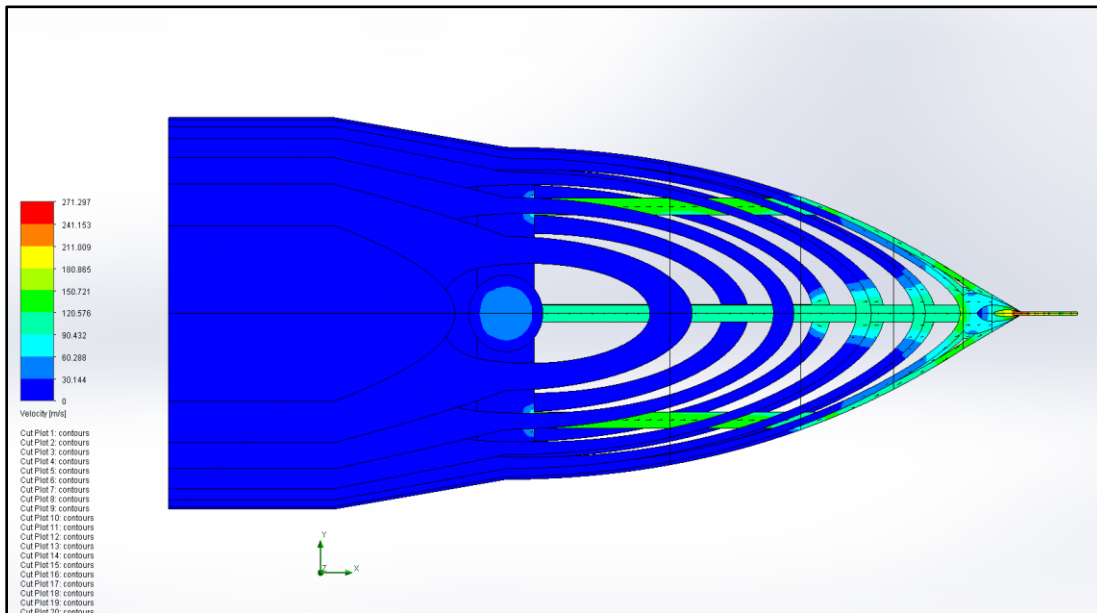


**Figure A-1.2: Vertical and Horizontal Velocity Cut-plot Slices**

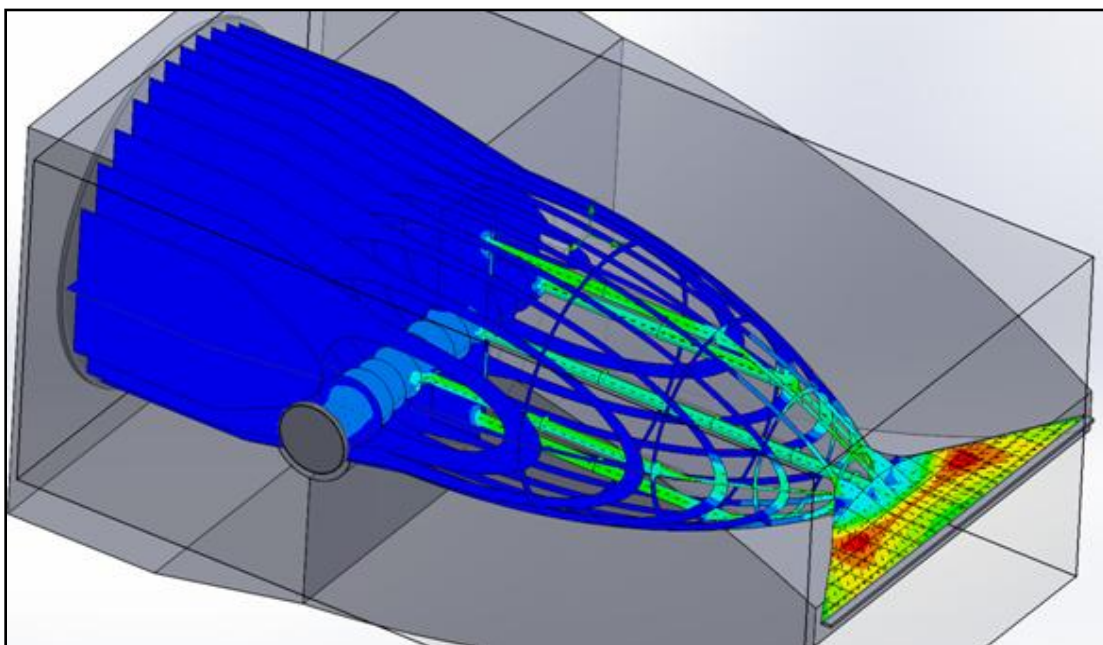


**Figure A-1.3: primary and secondary cross cuts**

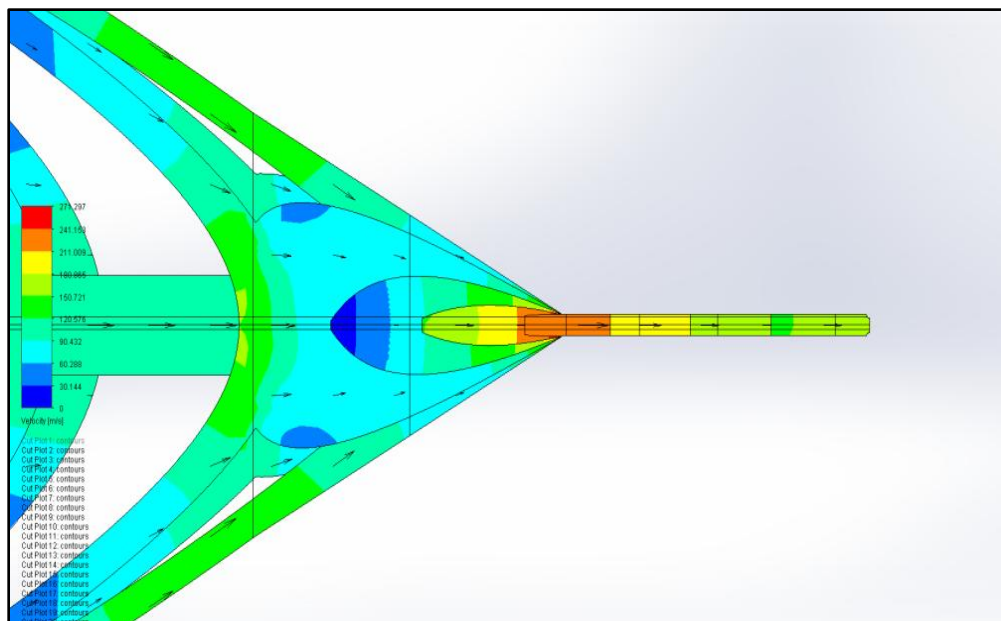


Figure A-1.4: Close View of Nozzle Exit Velocity Distribution

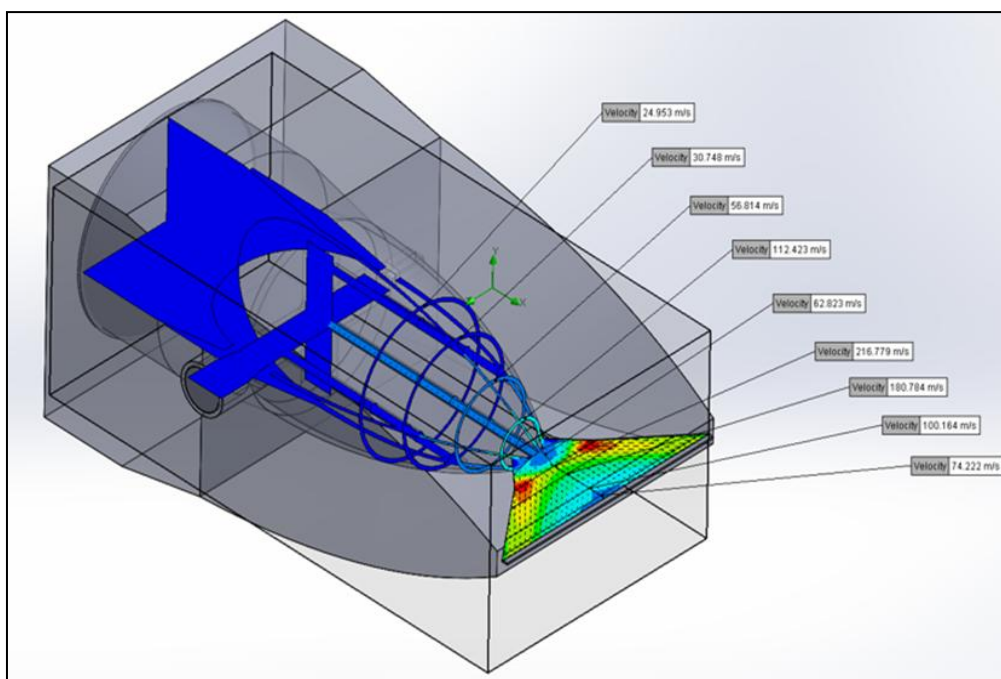
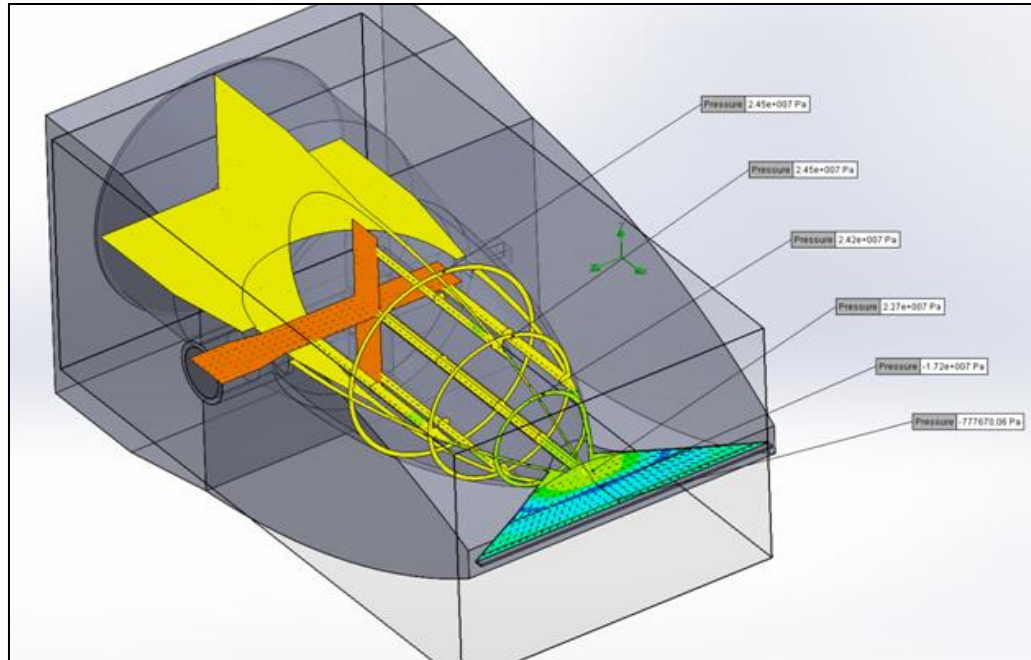
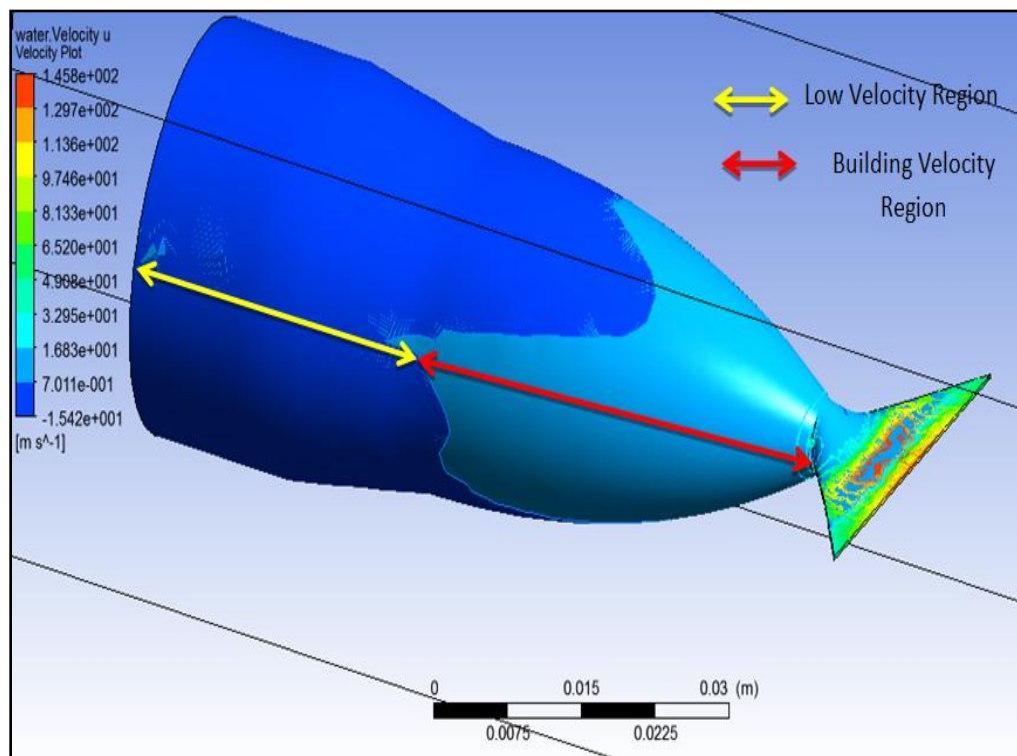


Figure A-1.5: Velocity Measurement on Cone surface (1-mm gap)



**Figure A-1.6: Pressure Measurement on Cone surface (1-mm gap)**

## Appendix-2 Refining of Nozzles



**Figure A-2.1 Nozzle surface water velocity plot ( Isometric View )**

- Plane nozzle without cone
- Inlet flow ( mass flow rate-kg/sec )= 50 Lit/min = (0.85 kg/sec)
- Outlet = set to opening (Domain air = 25 ° C)
- Peak velocity achieved = 144.9 m/sec
- Domain dimension = 500 mm x 50 mm x 40 mm

The Fig A-2.1 depicts nozzle internal surface velocity plot represents the flow behaviour inside the nozzle cavity. The fluid from main inlet to centre of the nozzle which has the same no increase in velocity indicated by yellow arrow after this point due to the curved profile the fluid velocity starts building and highest velocity is reached at the exit end.

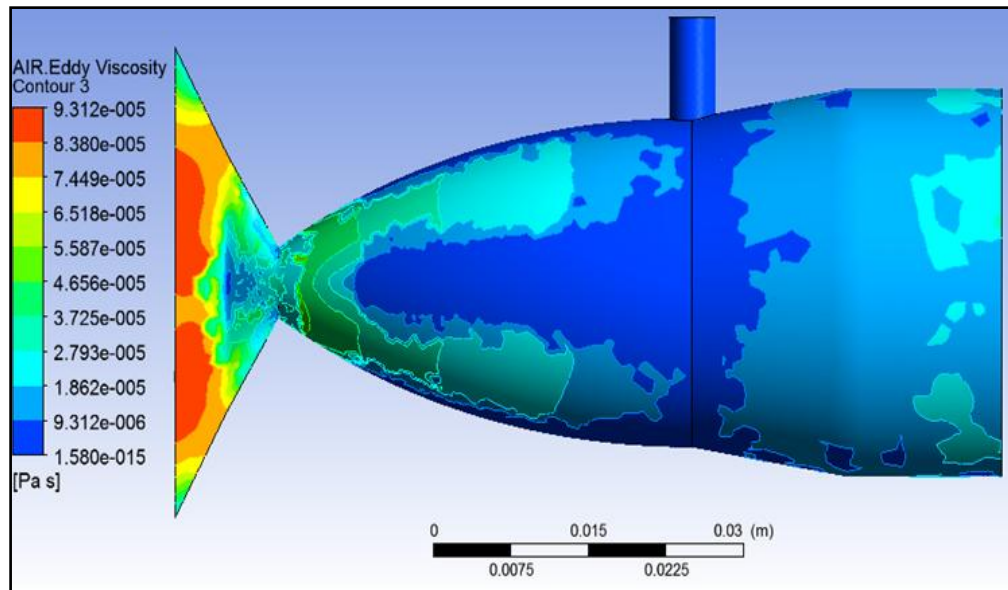


Figure A-2.2 MQL Nozzle Air eddy viscosity surface plot

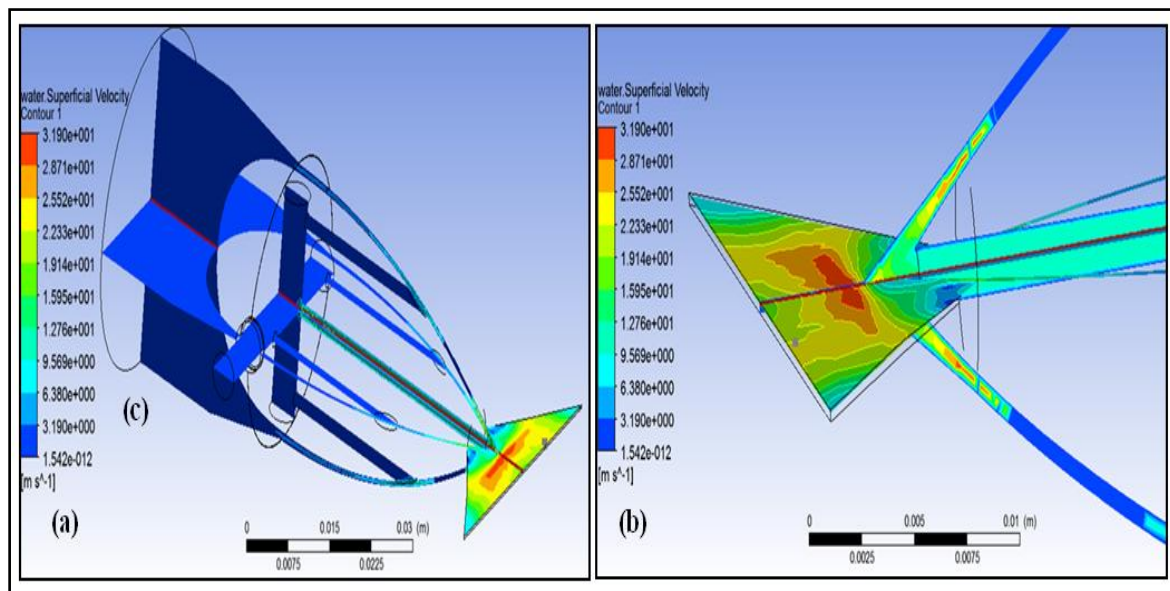
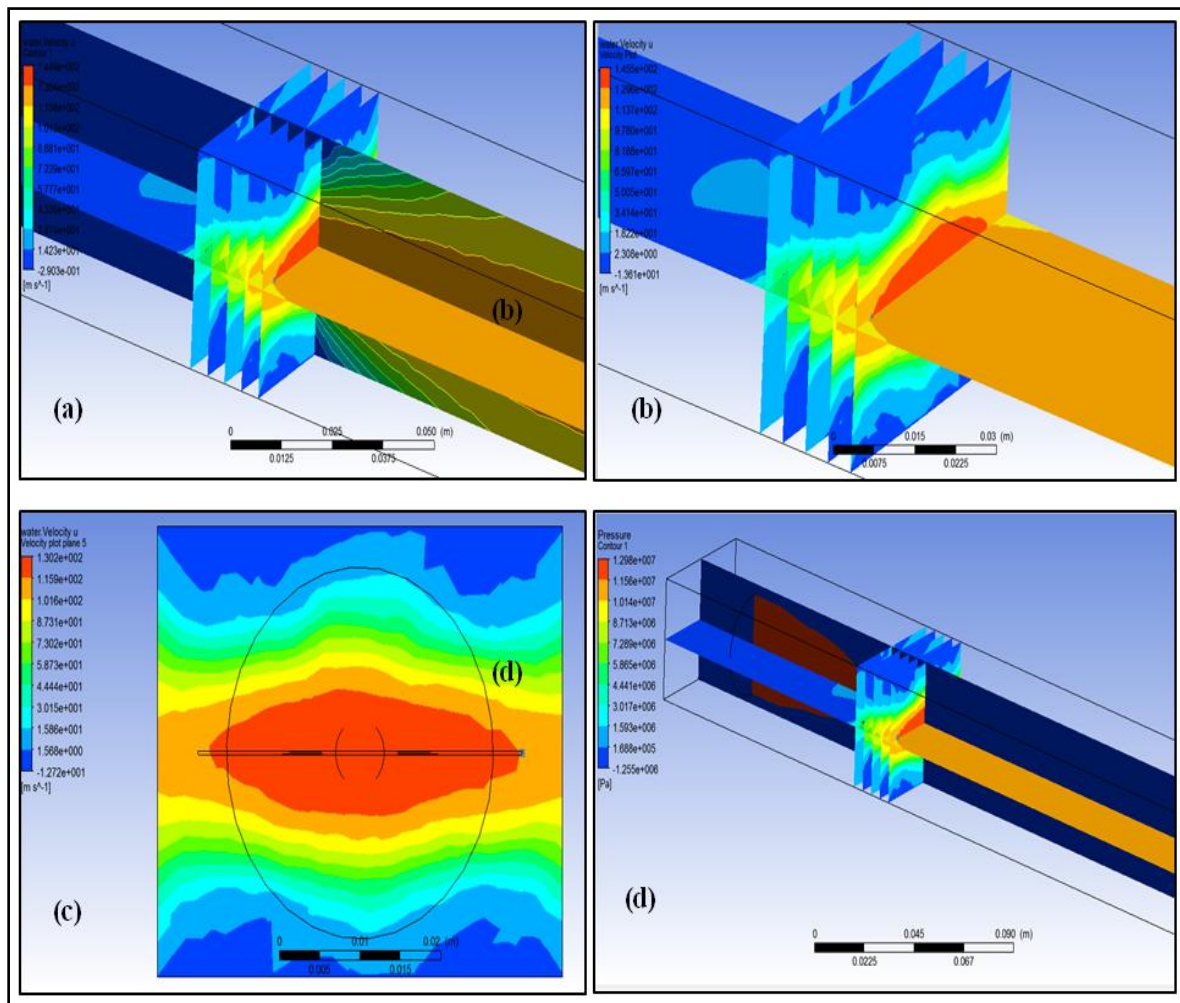


Figure A-2.3 MQL Simulation



**Figure A-2.4 Coherence Length measurement using slices with different intervals**

- (a) Vertical and horizontal velocity cut plot with slices.
- (b) Close view of horizontal cut plot with slices.
- (c) Velocity distribution slice drawn on nozzle exit.
- (d) Combined Pressure and velocity plot with slices.

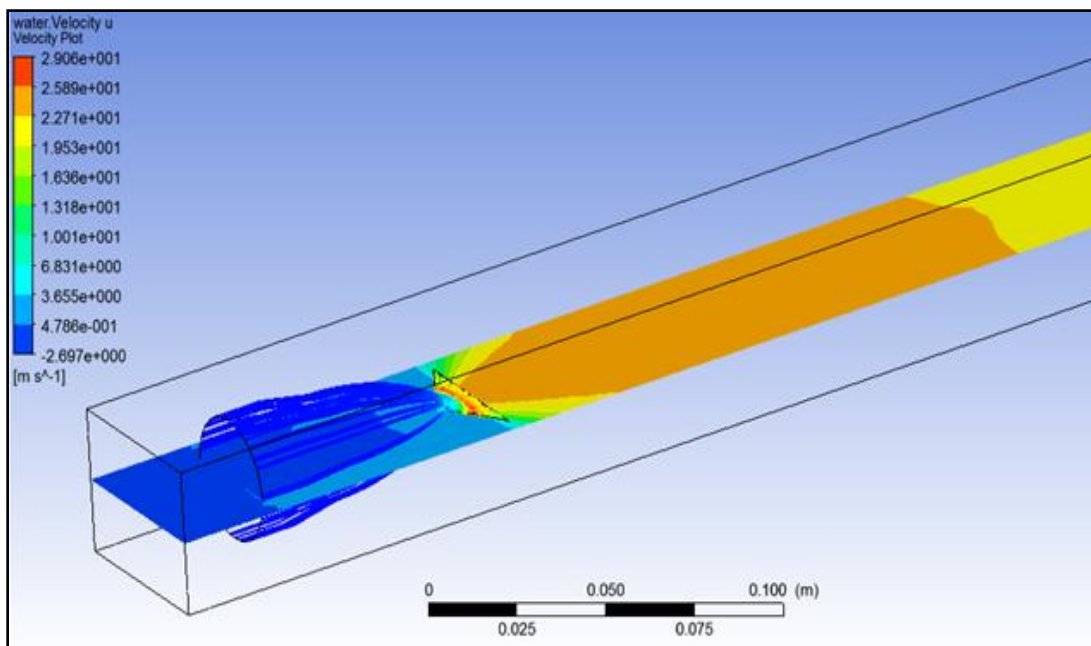


Figure A-2.5 Velocity Cutplot drawn middle of the nozzle exit

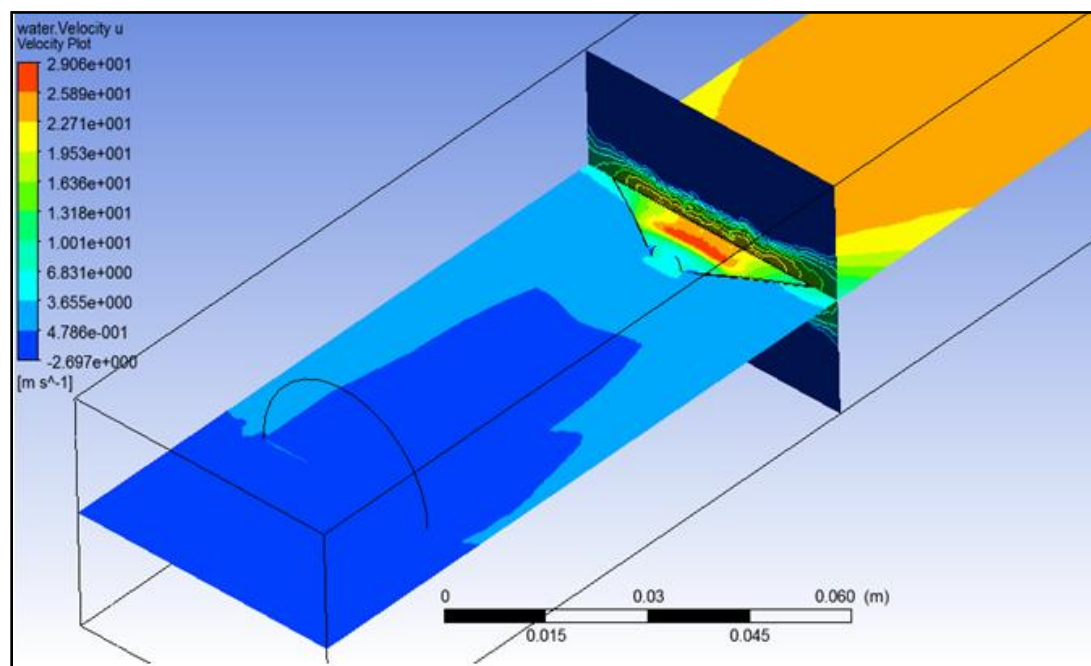


Figure A-2.6 Coherence Length measurement using slices with different intervals

### Appendix-3 MQL System and Equipments

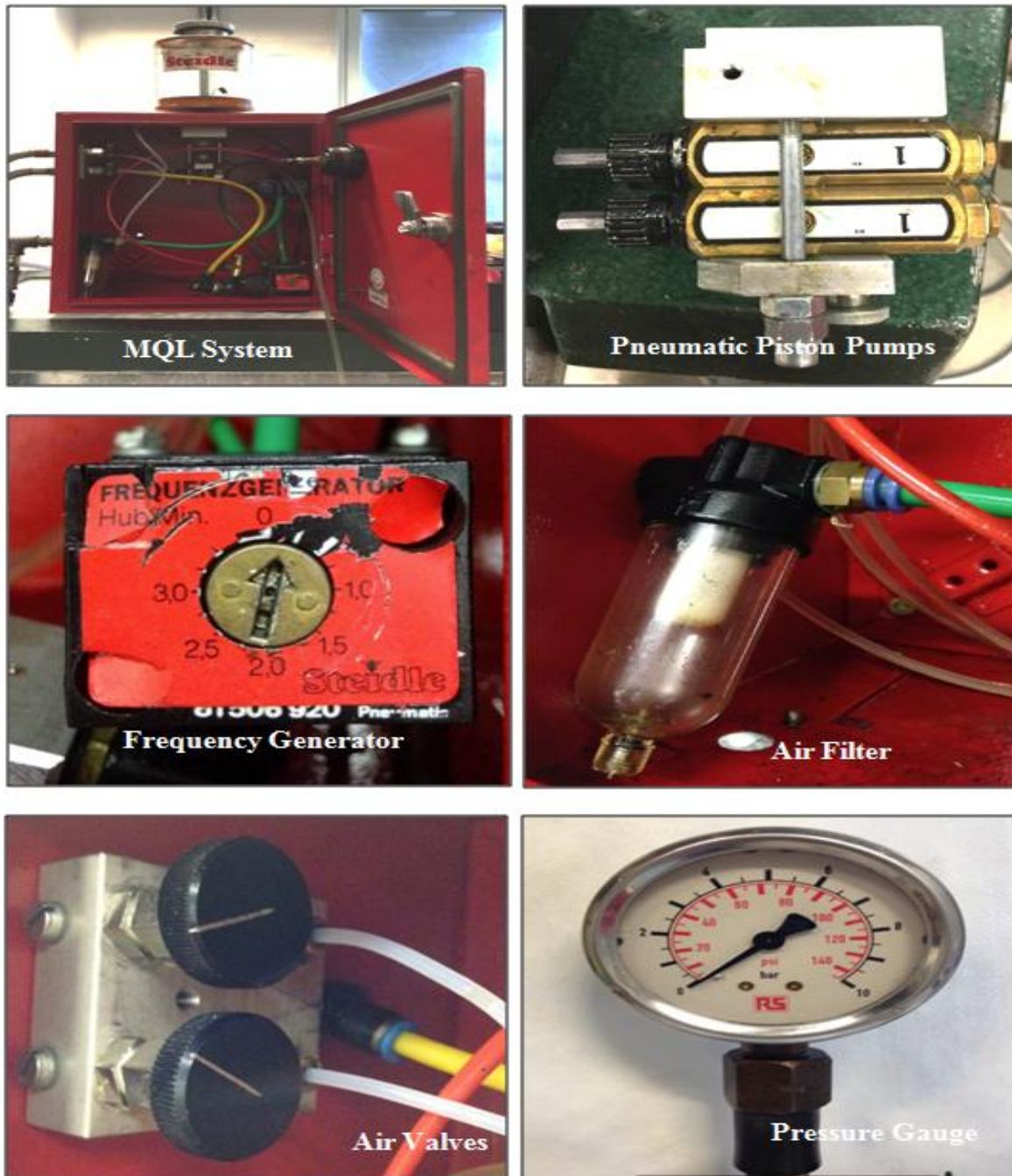


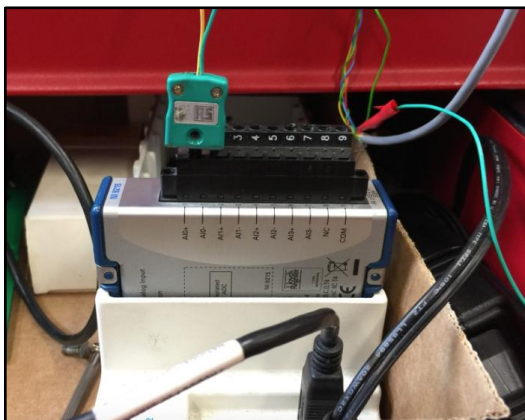
Figure A-3.1 MQL System Main Components



(a) Digital Flow meter



(b) Digital Readout



(c) NI DAQ Assistant Connection



(d) Flow Measurement with Probe



(e) Digital Flow meter and Pressure meter

Figure A-3.2 Equipment Used in Experiment

## Appendix-4 LabVIEW Program

### Nozzle Calibration Experiment

No.	Nozzle specifications	Type	Units
1.	Test Type:	Nozzle Calibration Test external flow	Psi
2.	Nozzle Type:	Nozzle with Pressure Cone	
3.	Fluid Type:	Only Air	Bar
4.	Input pressure:	1-Bar	
5.	Measurements:	Nozzle exit Face	
	<b>Sensor specifications</b>	<b>Piezo Resistive Sensor</b>	
1.	Pressure sensor:	Differential Pressure sensor	Psi
2.	Excitation Voltage:	10 Volts	10 VDC
3.	Max. Over Pressure:	200	Psi
4.	Output range:	0-100	Psi
5.	Output Type:	Uncompensated, Unamplified	-
6.	Power Supply Input:	10 V	Volts (V)
7.	Input Resistance Ohms:	5 K	Ohms
8.	Full Scale Output:	225	mV
9.	Sensitivity:	2.25	Psi/mV
10.	Response Time:	1	milli second (ms)
11.	Accuracy:	0.2 %	%
12.	Linearity:	P2>P1, BFSL min = +/-0.25;max = +/-1.0 =%span	%
13.	Null Offset:	Min= -30; Max= +30	mV
14.	Span error:		%
15.	Scale Type:	Linear scale	Volts/Time

**Table A-4.1: Specification of Differential Pressure Gauge**

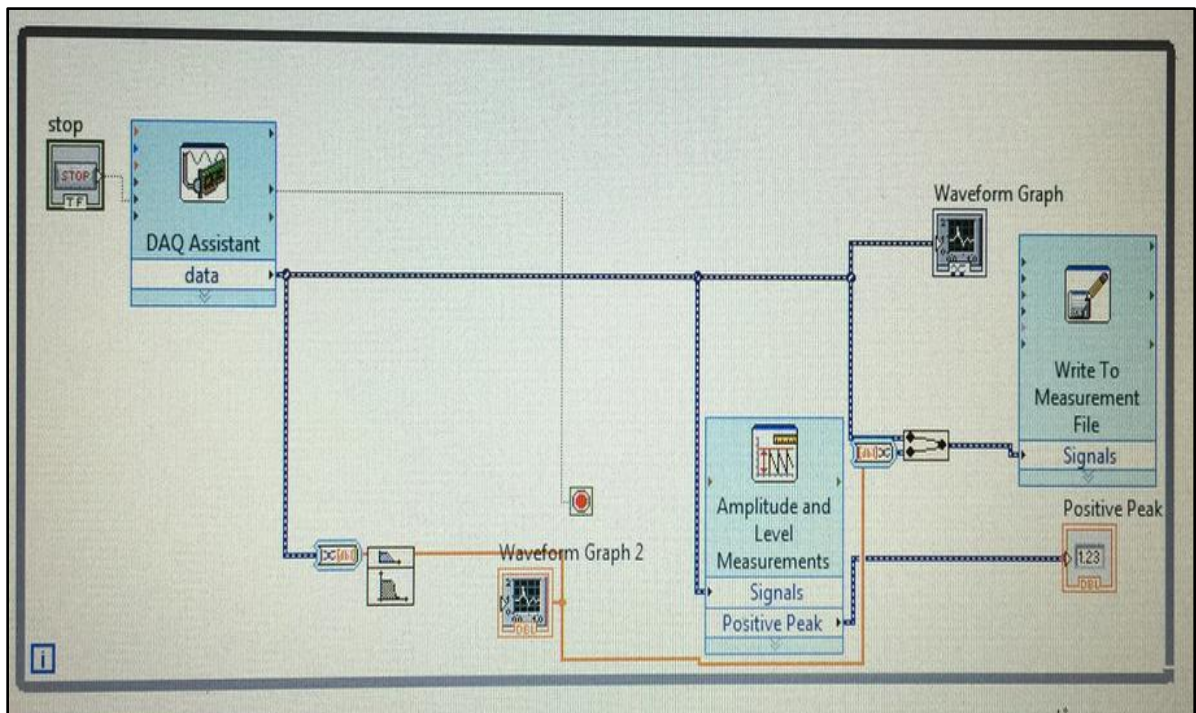


Figure A-4.2 LabView Block Diagram (With Filter)

### A-3.8 3-D Surface plot MATLAB sample Code

$D_s = [0,5,10,15,20,25,30,35,40,45,50,75,90,100];$

$T_s = [5,6,7,8,9,10,11,12,13,14,15,16,17,18,19,20,21,22,23,24];$

$V_s = [0.08,0.08,0.15,0.15,3.08,6.16,10.02,13.10,13.87,13.87,10.79,6.16,5.39,4.62,3.85,3.08,3.08,1.54,0.08,0.08;$   
 $0.08,0.08,0.15,1.54,3.08,6.16,10.02,13.10,13.87,13.87,10.79,6.16,5.39,4.62,3.85,3.08,3.08,1.54,0.08,0.08;$

$0.08,0.08,2.31,6.93,10.79,11.56,11.56,11.56,13.10,10.02,7.70,6.93,5.39,3.85,2.31,1.54,0.77,0.77,0.08,0.08;$

$0.08,0.08,2.31,6.93,10.79,11.56,11.56,11.56,13.10,10.02,7.70,6.93,5.39,3.85,2.31,1.54,0.77,0.77,0.08,0.08;$   
 $0.39,0.39,0.39,3.85,5.39,7.70,11.56,15.41,15.41,13.87,11.56,9.24,7.70,4.62,3.08,1.54,0.77,0.39,0.39,0.39;$   
 $0.39,0.39,0.39,3.85,5.39,7.70,11.56,15.41,15.41,13.87,11.56,9.24,7.70,4.62,3.08,1.54,0.77,0.39,0.39,0.39;$   
 $0.39,0.39,0.39,2.31,3.08,5.39,9.24,10.79,11.56,11.56,9.24,7.70,6.93,7.70,6.16,4.62,0.39,0.39,0.39,0.39;$   
 $0.31,0.39,0.39,3.08,3.85,3.85,5.39,7.70,9.24,10.02,8.00,7.70,5.39,3.85,3.08,2.31,1.54,0.39,0.39,0.39;$   
 $0.31,0.31,0.69,2.31,3.85,3.08,4.62,6.16,9.24,9.24,6.16,5.39,3.85,5.39,3.85,2.31,1.54,0.39,0.39,0.39;$   
 $0.31,0.39,0.39,3.08,3.85,3.85,5.39,7.70,9.24,10.02,8.00,7.70,5.39,3.85,3.08,2.31,1.54,0.39,0.39,0.39;$   
 $0.31,0.39,0.39,3.08,3.85,3.85,5.39,7.70,9.24,10.02,8.00,7.70,5.39,3.85,3.08,2.31,1.54,0.39,0.39,0.39;$   
 $0.23,0.23,0.77,1.54,2.31,2.31,3.08,3.85,4.62,3.85,3.85,3.08,2.31,2.31,1.54,0.77,0.54,0.39,0.23,0.23;$   
 $0.23,0.31,0.31,0.77,1.54,2.31,3.08,3.85,3.85,3.08,3.08,2.31,1.54,1.54,1.16,0.69,0.46,0.15,0.08,0.08;$   
 $0.31,0.23,0.39,0.39,0.77,0.77,1.54,2.31,2.31,2.31,2.31,2.31,2.31,1.54,0.77,0.62,0.46,0.39,0.39,0.39,0.39];$

$\text{surf}(T_s, D_s, V_s)$



**A-3.10 Multi-Layer Surface Plot Code (10 l/m-NC-exit = 0.3 mm)**

```

gap = 20;
Ds = [0,5,10,15,20,25,30,35,40,45,50,75,90,100];
Ts = [5,6,7,8,9,10,11,12,13,14,15,16,17,18,19,20,21,22,23,24];
Vs = [0.31,0.31,0.31,2.31,4.62,4.62,6.16,7.70,10.02,12.33,13.87,11.56,10.02,7.70,6.16,4.62,2.31,0.31,0.31,0.31;
      0.23,0.39,2.31,0.39,4.62,6.16,7.70,9.24,10.48,9.24,8.47,8.47,5.39,3.08,2.31,1.54,0.77,0.77,0.39,0.39;
      0.39,0.39,0.39,1.54,3.85,3.85,5.39,4.62,7.70,7.70,7.70,4.62,5.39,3.85,1.54,1.54,0.39,0.39,0.39,0.39;
      0.39,1.16,1.54,1.54,2.31,3.08,3.08,3.77,5.01,6.93,7.70,7.70,6.93,6.93,7.70,4.62,3.08,1.54,0.77,0.77;
      0.39,0.62,0.77,1.54,1.54,3.08,3.08,5.39,5.39,6.01,6.16,6.55,5.39,4.62,4.62,3.85,3.85,2.31,0.77,0.77;
      0.08,0.15,0.77,1.54,2.08,3.08,4.62,4.62,4.55,3.62,3.08,3.24,2.31,2.31,1.54,1.54,0.77,0.08,0.08,0.08;
      0.15,0.31,0.62,0.77,2.31,2.31,3.08,3.47,3.47,3.62,3.08,2.31,1.54,1.54,0.77,0.77,0.39,0.39,0.08,0.08;
      0.31,0.46,0.62,0.77,0.77,1.16,1.23,1.46,1.54,2.23,2.31,2.00,2.00,1.54,1.54,1.23,0.77,0.54,0.39,0.39;
      0.31,0.39,0.46,0.77,0.77,1.54,0.77,1.31,1.54,1.93,1.46,0.77,0.77,0.39,0.38,0.15,0.15,0.08,0.08,0.08;
      0.23,0.39,0.77,0.77,1.23,1.31,1.46,1.54,1.39,1.54,1.16,1.16,0.77,0.92,0.77,0.15,0.15,0.08,0.08,0.08;
      0.31,0.39,0.08,0.77,0.77,1.54,1.54,1.16,0.77,0.77,0.92,0.92,0.77,0.31,0.31,0.23,0.15,0.08,0.08,0.08;
      0.31,0.39,0.08,0.77,0.77,1.54,1.54,1.16,0.71,0.71,0.92,0.92,0.77,0.31,0.31,0.23,0.15,0.08,0.08,0.08;
      0.31,0.39,0.08,0.77,0.77,1.54,1.54,1.16,0.65,0.65,0.92,0.92,0.77,0.31,0.31,0.23,0.15,0.08,0.08,0.08;
      0.31,0.39,0.08,0.77,0.77,1.54,1.54,1.16,0.60,0.60,0.92,0.92,0.77,0.31,0.31,0.23,0.15,0.08,0.08,0.08];
surf(Ts,Ds,Vs)
hold on;
Vs1 =
[0.31,0.31,0.31,0.31,0.31,2.31,4.62,4.62,6.16,7.70,10.02,12.33,13.87,11.56,10.02,4.62,2.31,0.31,0.31,0.31;

0.31,0.31,0.31,0.31,0.31,2.31,4.62,4.62,6.16,7.70,10.02,12.33,13.87,11.56,10.02,4.62,2.31,0.31,0.31,0.31;
      0.23,0.23,0.39,0.39,2.31,0.39,4.62,6.16,7.70,9.24,10.48,9.24,8.47,8.47,5.39,1.54,0.77,0.77,0.39,0.39;
      0.23,0.23,0.39,0.39,2.31,0.39,4.62,6.16,7.70,9.24,10.48,9.24,8.47,8.47,5.39,1.54,0.77,0.77,0.39,0.39;
      0.39,0.39,0.39,0.39,0.39,1.54,3.85,3.85,5.39,4.62,7.70,7.70,7.70,4.62,5.39,1.54,0.39,0.39,0.39,0.39;
      0.39,0.39,1.16,1.16,1.54,1.54,2.31,3.08,3.08,3.77,5.01,6.93,7.70,7.70,6.93,4.62,3.08,1.54,0.77,0.77;
      0.39,0.39,0.62,0.62,0.77,1.54,1.54,3.08,3.08,5.39,5.39,6.01,6.16,6.55,5.39,3.85,3.85,2.31,0.77,0.77;
      0.08,0.08,0.15,0.15,0.77,1.54,2.08,3.08,4.62,4.62,4.55,3.62,3.08,3.24,2.31,1.54,0.77,0.08,0.08,0.08;
      0.15,0.15,0.31,0.31,0.62,0.77,2.31,2.31,3.08,3.47,3.47,3.62,3.08,2.31,1.54,0.77,0.39,0.39,0.08,0.08;
      0.31,0.31,0.46,0.46,0.62,0.77,0.77,1.16,1.23,1.46,1.54,2.23,2.31,2.00,2.00,1.23,0.77,0.54,0.39,0.39;
      0.31,0.31,0.39,0.39,0.46,0.77,0.77,1.54,0.77,1.31,1.54,1.93,1.46,0.77,0.77,0.15,0.15,0.08,0.08,0.08;
      0.23,0.23,0.39,0.39,0.77,0.77,1.23,1.31,1.46,1.54,1.39,1.54,1.16,1.16,0.77,0.15,0.15,0.08,0.08,0.08;
      0.31,0.31,0.39,0.39,0.08,0.77,0.77,1.54,1.54,1.16,0.77,0.77,0.92,0.92,0.77,0.23,0.15,0.08,0.08,0.08;
      0.31,0.31,0.39,0.39,0.08,0.77,0.77,1.54,1.54,1.16,0.71,0.71,0.92,0.92,0.77,0.23,0.15,0.08,0.08,0.08];
Vs1 = Vs1+gap;
surf(Ts,Ds,Vs1)
hold on;
gap1 = 40;
Vs2 = [0.3,0.3,0.3,2.3,4.6,4.6,6.2,13.1,13.1,13.1,13.9,11.6,10.0,9.2,6.9,4.6,2.3,0.3,0.3,0.3;
      0.3,0.3,0.3,2.3,4.6,4.6,6.2,12.3,10.0,12.3,13.9,11.6,10.0,8.5,6.2,4.6,2.3,0.3,0.3,0.3;
      0.4,0.4,0.4,1.5,3.9,3.9,5.4,4.6,9.2,8.5,8.5,4.6,5.4,4.6,1.5,1.5,0.4,0.4,0.4,0.4;
      0.4,0.4,0.4,1.5,3.9,3.9,5.4,4.6,7.7,7.7,7.7,4.6,5.4,3.9,1.5,1.5,0.4,0.4,0.4,0.4;
      0.4,1.2,1.5,1.5,2.3,3.1,3.1,3.8,5.0,6.9,7.7,7.7,6.9,6.9,4.6,4.6,3.1,1.5,0.8,0.8;
      0.4,0.4,1.5,1.5,2.3,3.1,3.1,3.9,4.6,6.9,7.7,7.7,5.4,5.4,4.6,4.6,3.1,1.5,0.3,0.3;
      0.8,0.7,0.8,1.5,1.5,3.1,3.1,5.4,5.4,6.0,6.2,6.5,5.4,4.6,4.6,3.9,3.9,2.3,0.8,0.8;
      0.1,0.2,0.8,1.5,2.1,3.1,4.6,4.6,4.5,3.6,3.1,3.2,2.3,2.3,1.5,1.5,0.8,0.1,0.1,0.1;
      0.2,0.3,0.6,0.8,2.3,2.3,3.1,3.5,3.5,3.6,3.1,2.3,1.5,1.5,0.8,0.8,0.4,0.4,0.1,0.1;

0.3,0.4,0.1,0.8,0.8,1.5,1.5,1.2,0.8,0.8,0.9,0.9,0.8,0.3,0.3,0.2,0.2,0.1,0.1,0.1;

```



0.2,0.3,0.4,0.7,0.6,1.5,0.8,1.3,1.5,1.9,1.5,0.8,0.8,0.8,1.5,0.7,0.7,0.3,0.2,0.2;  
 0.2,0.3,0.4,0.7,0.6,0.8,0.8,0.8,0.8,0.8,0.8,0.8,0.8,0.8,1.5,0.7,0.7,0.3,0.2,0.2;  
 0.2,0.3,0.4,0.7,0.6,0.6,0.6,0.6,0.8,0.8,0.8,0.8,0.6,0.6,0.6,0.7,0.7,0.3,0.2,0.2;  
 0.1,0.1,0.1,0.7,0.6,0.5,0.5,0.5,0.8,0.8,0.8,0.8,0.5,0.5,0.5,0.7,0.7,0.1,0.1,0.1];

Vs2 = Vs2+gap1;  
 surf(Ts,Ds,Vs2)

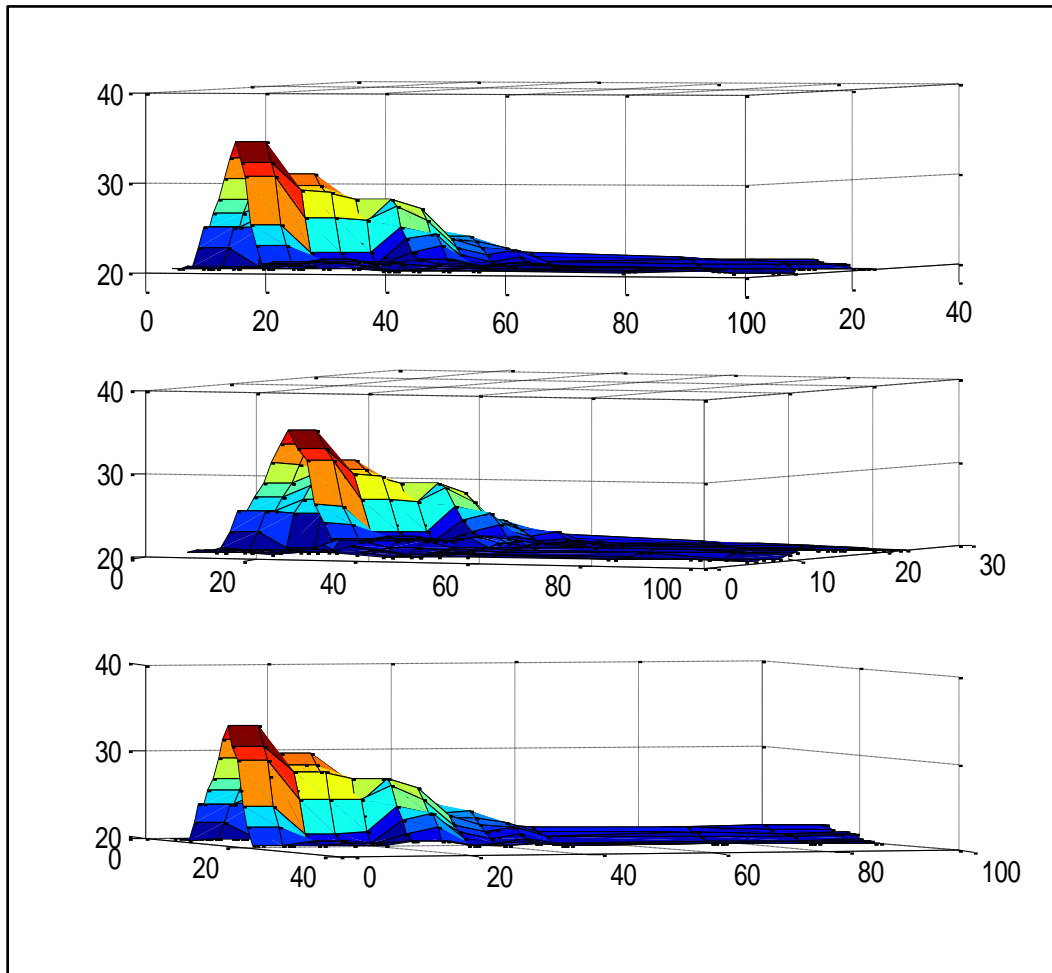


Figure A-4.3 Multi-Layer Surface Plot (10 l/m-NC-exit = 0.3 mm)

## Appendix-5 Nozzle External Jet 3-D Surface Plots

### 10 L/min 0.4 mm Exit Middle Layer Plot

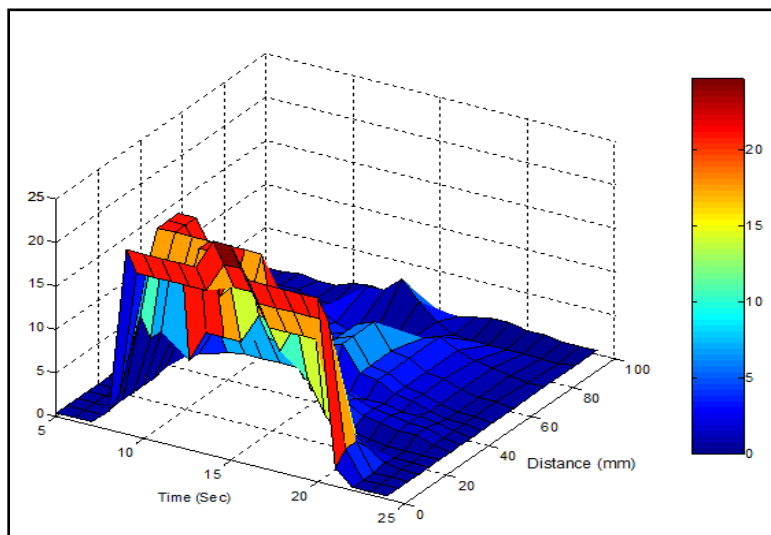


Figure A-5.1 Nozzle exit 0.4 mm opening

### 10 L/min 0.5 mm Exit Middle Layer Plot

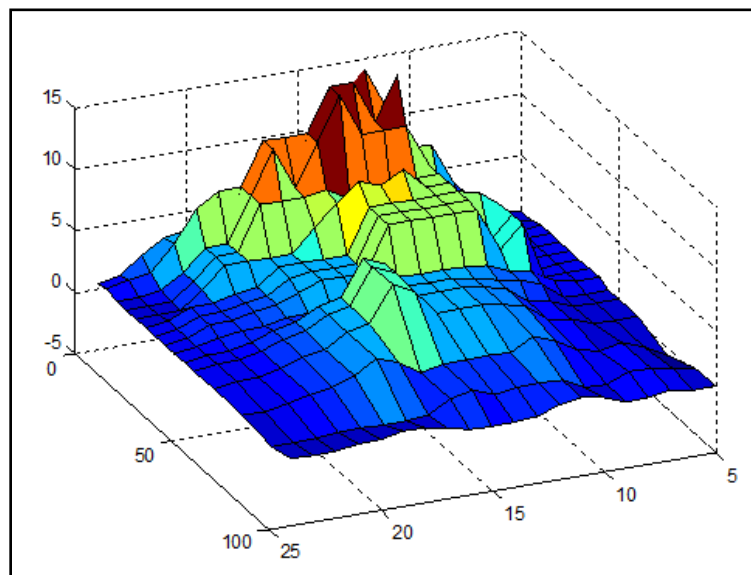


Figure A-5.2 Nozzle exit 0.5 mm opening

## 10 L/min 0.5 mm Exit Middle Layer Plot

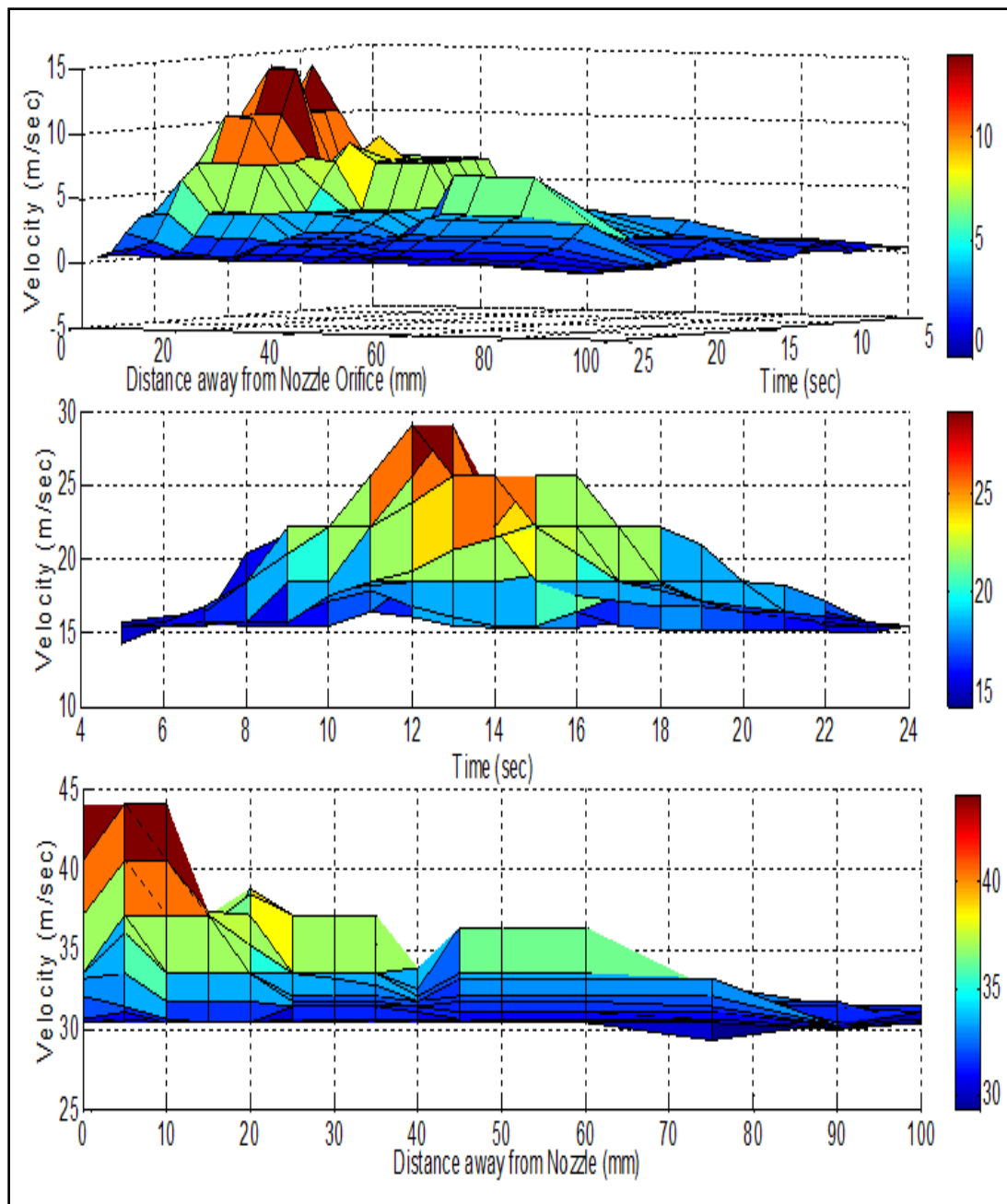


Figure A-5.3 Nozzle with Cone exit opening = 0.5 mm 10 Litres/min

## References

1. Alberdi R., Sanchez J.A., Pombo I., Ortega N., Izquierdo B., Plaza S., Barrenetxea., (2011), Strategies for Optimal Use of Fluids in Grinding, Ideko Technological Center, Arriaga Kalea, Elgoibar , Spain.
2. Alberto Lopez-Arraiza, German Castillo, Hom N.Dhakal, Raul Alberdi, High performance composite nozzle for the improvement of cooling in grinding machine tools, 2013, university of the Basque country, Portugalete-Bizkaia, Spain.
3. Alves M.C.S., Bianchi E.C., Aguiar P.R., Canarim R.C., (2011), Influence of optimised lubrication-cooling and minimum quantity lubrication on the cutting forces, on the geometric quality of the surfaces and on the micro-structural integrity of hardened steel parts, Sao Paulo state university, faculty of industrial wood engineering.
4. Amir Masoud Tahvilian, Zhaoheng Liu, Henri Champlaud, Bruce Hazel, (2013), Experimental and Finite Element Analysis of Temperature and Energy Partition to the Workpiece While Grinding with a Flexible Robot, Journal of Materials Processing Technology, 213, 2292-2303.
5. ANSYS Introduction to CFX, Training Manual, 2009.
6. Attanasio A., Gelfi M., Giardini C., Remino C. (2005), Minimum Quantity Lubrication in Turning. Wear, 260, 333-338.
7. Babic D., Murray D.B., Torrance A.A., (2005), Mist Jet Cooling of Grinding processes, Department of Mechanical and Manufacturing Engineering, Trinity College, Dublin, Ireland.
8. Badger, S., (2004), “Abrasive, Belt Grinders, Belt grinder, Grinding, Belt grinding, belt polishing, Belt Centreless, finishing, belt Finishing,
9. Baines-Jones V., Batako, A.D.L, Morgan, M.N., (2007), Computational Fluid Dynamics Analysis of grinding Fluid Nozzles, 3rd GERI Annual Research Symposium GARS-2007, GERI, Liverpool John Moores University.
10. Baines-Jones V., Morgan M.N., Allanson D.R., Batako A.D.L, (2005), Grinding Fluid Delivery System Design-Nozzle Optimisation. AMTRel, GERI, Liverpool John Moores University.

11. Batako A.D.L., Tsiakoumis V., Grigor'ev S. and Kuzin V., (2012), Grinding Wheel Wear in Vibration Assisted Grinding of Steel. *Proc. ICMR 2012, Advanced in Manuf. Technol.XXVI*, 517-522.
12. Batako Andre D.L. and Tsiakoumis Vaios., (2014), An Experimental Investigation into Resonance Grinding of Hardened Steel and Nickel Alloys with MQL, *Int. J Adv Manuf Technol* 77(1-4), 27-41.
13. Batako, A.D., Morgan, M.N., Rowe, W.B., (2012), High-efficiency deep Grinding with very High Removal rates. Proceedings of the Institute of Mechanical Engineers, *Int.J.Adv.Manuf.Technology*. 66, 1367-1377, Pulished by Springer and also online.
14. Batako, A.D., Rowe, W.B., Morgan, M.N., (2005) 'Temperature Measurement in High Efficiency Deep Grinding' *International journal of machine tools & manufacture*, 45 pp 1231-1245.
15. BijoyMandal, Rajender Singh., Santanu Das., Simul Banerjee., (2011), Improving Grinding Performance by Controlling Air Flow Around a Grinding Wheel. Department of Mechanical Engineering, Jadavpur University, India.
16. Brinksmeier E., Heinzl C., Wittmann M., (1999), Friction, Cooling and Lubrication in grinding, Division of Production Technology and Manufacturing Technologies, Bremen University, Germany.
17. Brinksmeier, E., Brockhoff, T., Walter, A. (1997) Minimum Quantity Lubrication in Grinding. In Proceedigs of 2nd International Machining and Grinding Conference, Dearborn, Michigan.
18. Brinksmeier, E., Meyer, D., Huesmann-Cordes, A.G., Hermann, C. (2015) Metalworking Fluids-Mechanisms and performance. *CIRP Annals-Manufacturing Technology* 64 605-628.
19. Brinksmeier, E., Walter, A., Jassen, R., Diersen, P. (1999), Aspects of Cooling Lubrication Reduction in machining Advanced Materials. Proceedings of the Instituttion of Mechanical Engineers, 213, Part-B, 769-778.
20. Brinksmeier, E., Heinzl, C., Wittman, M., 1999. Friction, cooling and lubrication in grinding. *Annals of the CIRP*, 48 (2), p.581-598.
21. Cambell, J.D., (1995), "Optimised Coolant Application", in 1st Int.machining and Grinding Conf., Michigan, USA, 12-14 Sept. Society of Manufacturing engineers.

22. CFD Training Manual, 2013.
23. Chang Chong-Ching., (1997), An Application of Lubrication Theory to predict Useful flow rate of Coolants on Grinding Porous Media, Department of Mechanical Engineering, Kung-Shan University of Technology, Taiwan, Tribology International.Vol.30, No.8, pp.575-581.
24. Chang, C.C., (1994), An Analysis of Coolant Flow and heat transfer in Grinding, PhD. Thesis, University of Pittsburgh.
25. Cui,C., (1995), Experiemntal Investigation of Thermofluids in the grinding Zone, PhD. Thesis, University of Connecticut.
26. Dhar N.R., Islam M.W., Islam S., Mithu M.A.H. (2006), The Influence of Minimum Quantity of Lubrication (MQL) on Cutting Temperature, Chip and Dimensional Accuracy in Turning AISI-1040 Steel. Journal of Materials Processing Technology, 171, 93-99.
27. Ebbrell, S., Woolley, N.H., Tridimas, Y.D., Allanson, D.R., Rowe, EW.B. (2000), The effects of cutting fluid application methods on the grinding process. International Journal of Machine Tools & Manufacture, 40,209-223.
28. Elin Stenmark., On Multiphase Flow Models in ANSYS CFD Software, (2013), Department of Applied Mechanics, Division of Fluid Dynamics, Chalmers University of Technology, Goteborg, Sweden.
29. Emami M., Sadeghi M.H., Ahmed A.D. Sarhan. (2013), Investigating the Effects of Liquid Atomization and Delivery Parameters of Minimum Quantity Lubrication on the Grinding Process of AL2O3 Engineering Ceramics. Journal of Manufacturing Processes, 15, 374-388.
30. Euler, L., "Principes generaux de l'etat d'equilibre des fluids;" "Principies generaux du movement des fluids;" "Continuation des recherches sur la theorie du movement des fluids". Historie de l'Acadernie de berlin (1755).
31. Gaitonade V.N., Karnik S.R., Paulo Davim J. (2008) Selection of Optimal MQL and Cutting Conditions for Enhancing Machinability in Turning of Brass. Journal of Materials Processing Technology, 204, 459-464.
32. Gu, D.Y., and Wager, J.G., (1988), New Evidance on the Contact Zone in Grinding- Contact Length, Sliding and Cutting Regions, University of Western Australia.

33. Guo, C and Malkin, S., 1992, Analysis of Fluid Flow through the Grinding Zone, *Journal of Engineering for Industry-Transactions of the ASME*, Vol.114 (4), Nov, pp 427-434.
34. Gviniashvili V.K., Woolley N.H., Rowe W.B., (2004), Useful Coolant Flow Rate in Grinding, *International journal of machine tools & manufacture*, Vol. 44, May 2004, pp 629-636.
35. Gviniashvili, V.K., (2003), Fluid Application System Optimization for High Speed Grinding, PhD. Thesis, Liverpool John Moores University.
36. Hadad M.J., Tawakoli T., Sadeghi M.H., Sadeghi B. (2012), Temperature and Energy Partition in Minimum Quantity Lubrication-MQL Grinding Process. *International Journal of Machine Tools & Manufacture*, 54-55, 10-17.
37. Han, Z.L and Li, C.H., 2013, "Theoretical Modeling and Simulation of Airflow Field near Grinding Wheel", *International Journal of Control and Automation*, Vol.6. No.4, School of Mechanical Engineering, Qingdao Technology University, China.
38. Howes, T. (1990) assessment of the Cooling and Lubricative properties of Grinding Fluids. *CIRP Annals-Manufacturing Technology*, 39/1, 313-316.
39. Hryniewicz P., 1998, Coolant Flow in Surface Grinding with non-porous wheel, Department of Mechanical Engineering, University of Delaware, Newark, USA. Available Online 11 July 2000. Received 9 Feb 1999, Accepted 8 June 1999, Available Online 7 Oct 1999.
40. Irani R.A., Bauer R.J., Warkentin, A., (2005), A Review of Cutting Fluid Application in the Grinding Process, Mechanical Engineering Department, Dalhousie University, Canada.
41. Inasaki, I., (1998), Fluid Film in the grinding Arc of Contact, Contribution on January CIRP Meeting, Paris, 27-31. Jan.
42. Itoigawa F., Childs T.H.C., Nakamura T., Belluco W., "Effects and mechanisms in Minimal quantity lubrication machining of an aluminium alloy", (2005), Department of mechanical engineering, Nagoya Institute of Technology, Gokiso, Nagoya 466-8555, Japan.
43. Jackson, A., (2008). An Investigation of Useful Fluid Flow in Grinding, PhD Thesis. Liverpool John Moores University, Liverpool, UK.

44. Jackson, A., Batako, A.D., Morgan, M.N., (2005), "Fluid Delivery in Grinding-A Review of the Term Useful Flow", Submitted to GARS-2005, LJMU, UK, 22 June.
45. Jyothirishwar Kumar, S. Saha., (2015), laminar Modeling and Simulation of Cutting Fluid Flow through Sudden Contraction Nozzle, Internal journal of Engineering Research and General Science Volume 3, Issue 3, Kolkata, West Bengal, India.
46. Kamata Y., Obikawa T., "High Speed MQL finish-turning of Inconel 718 with different coated tools". (2007), Institute of Industrial science, The University of Tokyo, 4-6-1 komaba, meguro-ku, Tokyo 153-8505, Japan, Journal of Materials processing Technolgy, 192-193 (2007) 281-286.
47. Kedare, S.B., Borse D.R., and Shahane P.T. (2014), Effect of Minimum Quantity Lubrication (MQL) on Surface Roughness of Mild steel of 15HRC on universal milling machine, 3rd International Conference on Materials Processing and characterisatrion (ICMPC), Department of Mechanical & Industrial Engineering, Indian Institute of Technology, Roorkee, Department of Mechanical engineering, Veermata Jijabai Technological, Mumbai, India.
48. Khan M.M.A., Mithu M.A.H., Dhar N.R. (2009), Effects of Minimum Quantity Lubrication on Turning AISI 9310 Alloy Steel Vegetable Oil-Based Cutting Fluid. Journal of Material Processing Technology, 209, 5573-5583.
49. Kim, N.K., Guo, C., Malkon, S., (1997), Heat Flux Distribution and Energy Partition in Creep-feed Grinding, Chinju national University, Korea; University of Massachusetts, USA.
50. Klocke, F., Beck, T., Eisenblatter, G., Lung, D. (2000) Minimal Quantity of Lubrication (MQL)-Motivation, Fundamental vistas. 12<sup>th</sup> International Colloquium, 929-942.
51. Kuriyagawa Tsunemoto., Katsuo Syoji., Hideo Ohshita., (2002), Grinding Temperature within Contact Arc Between Wheel and Work piece in High-Efficiency Grinding of Ultra Hard Cutting Tool Materials, Department of Mechatronics and Precision Engineering, Tohoku University, Aramaki, Japan.
52. Kuroda, (2013) Jena Tec Holdings LTD, Kuroda precision Industries ltd of japan, ME Plant and Maintenance (Jena-tec.co.uk).

53. Kyung-Hee Park., Jorge Olortegui-Yume., Moon-Chul Yoon., Patrick Kwon., (2010), A Study on Droplets and Their Distribution for Minimum Quantity Lubrication (MQL), Department of Mechanical Engineering, Michigan State University, East Lansing, USA.
54. Le Coz G., Marinescu M., Devillez A., Dudzinski D., Velnom I. (2012), Measuring Temperature of Rotating Cutting Tools: Application to MQL Drilling and Dry Milling of Aerospace Alloys. *Applied Thermal Engineering*, 36, 434-441.
55. Lukasz Barczak, (2010), “Application of Minimum Quantity Lubrication (MQL) in Plane Surface Grinding”, Liverpool John Moores University.
56. Malkin S., (1989) *Grinding Technology: Theory and Applications of Machining with Abrasives*, Wiley, New York.
57. Malkin, S., & Guo, C., (2008) ‘Grinding Technology-Theory and applications of Machining with Abrasives’ Second Edition, industrial Press Inc., New York.
58. Malkin, S., Guo, C., (2007), *Thermal Analysis of Grinding*, University of Massachusetts, Amherst, Massachusetts, USA., United Technologies research Center, East Hartford, Connecticut, USA.
59. Marinescu, I., Rowe, W.B., Dimitrov, B., & Ohmori, H., (2013) *Tribology of Abrasive machining Processes*, second edition, Elsevier.
60. Marinescu, I.D., Rowe, W.B., Dimitrov, B., Inasaki, I. (2004) *Tribology of Abrasive Machining Process*. William Andrew Publishing.
61. McCarthy, M.J., Molloy, N.A., (1974), review of stability of liquid jets and the influence of nozzle design, *Chem.Eng.J.* 7-1.
62. Meena A., Mansori M, El., “Study of dry and minimum quantity lubrication drilling of novel austempered ductile iron (ADI) for automotive applications”, 2011, Elsevier.
63. Morgan M.N., Jackson A.R, Wu. H., Baines V.A., Batako A., Rowe W.B., (2008), Optimisation of fluid application in grinding, AMTReL, Liverpool John Moores University, UK.
64. Morgan, M.N., Rowe, W.B., Black, S.C.E& Allanson, D.R., (1998), Effective thermal properties of grinding wheels and grains, *Proceedings of the Institution of Mechanical Engineers, Part B: Journal of Engineering Manufacture*, Vol212, n B8, pp 661-669.
65. Mortimer, J., (2005), Less Coolant can be More, *Machinery*, 5, 25-28.

66. Murphy, Brian., David Pottle., Andrew Rockwell., Kyle Ryan., (2006), Coolant Delivery System for Creep-Feed Grinding, Mechanical Engineering Department, Dalhousie University.
67. Nadolny K., Wojtewicz., Sienicki W., Herman D. (2014), An Analysis of Centrifugal MQL Supply System Potential in the Internal Cylindrical Grinding Process.
68. Najiha M.S., Rahman M.M., Yusoff A.R. (2016), Environmental Impacts and Hazards associated with metal working fluids and recent advances in the Sustainable Systems: A Review. *Renewable and Sustainable Energy Reviews*, 60, 1008-1031.
69. Najiha M.S., Rahman M.M., Yusoff A.R., Kadirgama K., (2012), Investigation of flow behaviour in minimum quantity lubrication nozzle for end milling processes, *International journal of automotive and mechanical engineering*, university of Malaysia Pahang.
70. Nguyen T., Zhang L.C., (2005); The coolant penetration in grinding with segmented wheels-part1: mechanism and comparison with conventional wheels, school of Aerospace, mechanical and mechatronics engineering, the University of Sydney, NSW, Australia.
71. Nourredine Boubekri., Vasim Shaikh., (2012), Machining Using Minimum Quantity Lubrication: A Technology for Sustainability, Department of Engineering & Technology, University of North Texas Discovery Park, USA.
72. Okuyama S., Nakmura Y., Kawamura S., 1993, Cooling Action of Grinding Fluid in Shallow Grinding, *Int. Mach. Tools Manufact.* Vol. 33, No.1, pp.13-23.
73. Peter Dybdahl Hede., Poul Bach., Anker D., Jensen. (2008), Two-Fluid Spray Atomisation and Pneumatic Nozzles for Fluid Bed Coating/Agglomeration Purposes: A Review. *Chemical Engineering Science* 63, 3821-3842.
74. Qi H.S., 1995, A Contact Length Model for Grinding Wheel Workpiece Contact, PhD Thesis. Liverpool John Moores University, Liverpool.
75. Qi, H.S., Mills, B., and Xu, X.P., (1995), Applications of Contact Length Models in Grinding Processes, University of Bradford, Uk.
76. Qi, H.S., Rowe, W.B., and Mills, B., (1997), Experimental Investigation of Contact Behaviour in Grinding, *tribology International* Vol.30, No.4. pp. 283-294.

77. Rabiei F., Rahimi A.R., Hadad M.J., Ashrafi Jou M., "Performance improvement of minimum quantity Lubrication (MQL) technique in surface grinding by modelling and optimization". (2014).
78. Rafael de Mello Belentani, Hamilton Funes Junior, Rubens Chinali Canarim, Anselmo Eduardo Diniz, Amauri Hassu, Paulo Roberto Aguiar, Eduardo Carlos Bianchi, (2013), Utilization of Minimum quantity lubrication (MQL) with water in CBN grinding of steel, Department of mechanical engineering, University of Estadual Paulista-UNESP.
79. Rahim, E.A., Ibrahim, M.R., Rahim, A.A., Aziz, S., Mohid, Z., 2015, "Experimental investigation of Minimum Quantity lubrication (MQI) as a Sustainable Cooling Technique", advanced machining reserch group, faculty of Mechanical and manufacuring engineering, universiti Tun hussein Onn, batupahat, Johor, Malaysia.
80. Rakurthy C.S., Varela P.I., Balaji A.K. (2013), Effects of Targeted Minimum Quantity Fluid (MQF) application on Surface Integrity. 14<sup>th</sup> CIRP Conference on Modeling of Machining Operations. Procedia CIRP 8, 462-468.
81. Rodrigo E.Catai., Bianchi E.C., Silva L.R., Aguiar P.R., (2006), Global Analysis of Aerodynamics Deflectors Efficiency in the Grinding Process, Vol.XXVIII, No.2.
82. Rowe, W.B. (2014) Principles of Modern Grinding Technology. Norwich, NY: William Andrew, Second edition.
83. Rowe, W.B., Ebbrell, S., Morgan, M.N., (2004), Process requirements for Cost Effective Precision Grinding. CIRP Annals-Manufacturing Technology, 53/1, 255-258.
84. Rowe, W.B., Morgan, M.N., Batako, A., and Jin, T., (2003) Energy and Temperature Analysis in Grinding, School of Engineering, Liverpool John Moores University, UK.
85. Rowe, W.B., Morgan, M.N., Liverpool John Moores University/England; Qi, H.S., Zheng, W.H., North East University of Technology/China. (1993), The Effect of Deformation on the Contact Area in Grinding.
86. Rowe, W.B., Pettit, J.A., Boyle, A., and Moruzzi, J.L., (1988), Avoidance of Thermal Damage in Grinding and Prediction of the Damage Threshold, Annals of the CIRP, Vol. 37/1.

87. Schumack, M.R., Chung, J.B., Schultz, W.W. and Kannatey-Asibu Jnr, E., 1991, Analysis of Fluid Flow Under a Grinding Wheel, *Journal of Engineering for Industry Transactions of the ASME*, Vol.113 (2), May, pp 190-197.
88. Shibata J., Goto T., Yamamoto M., (1982), Characteristics of Air Flow Around a Grinding Wheel and Their Availability for Assessing the Wheel Wear, *Shibaura Institute of Technology, Saitama, Japan*.
89. Silva L.R., Bianchi E.C., Catai R.E., Fusse R.Y., Franca T.V., Aguiar P.R. (2005) Study on the Behaviour of the Minimum Quantity Lubrication-MQL Technique under different Lubricating and Cooling Conditions when Grinding ABNT 4340 Steel. *Journal of the Brazilian Society of Mechanical Science & Engineering*, 2, 192-199.
90. SKF Vogel Aerosol Process.
91. SKF Vogel MQL System.
92. Somasundaram, S., Thiagarajan, C., (2013), Experiemntal Evaulation of a Chip Thickness Model Based on the Fracture Toughness of Abrasive and Work Material in Grinding of Alumina Ceramics, *Internataional Journal of Modern Engineering rsearch (IJMER)*, Vol. 3, Issue. 6, pp-3825-3829.
93. Sourav Ray., Sujoy Saha., (2015), Simulation on Flow of Cutting Fluid Having Laminar Characteristics through a Sudden Contraction Nozzle. Department of mechanical Engineering, *International Journal of Modern Engineering Research (IJMER)*, India.
94. Stefan Mihic., CFD Investigation of Metalworking Fluid and Heat Transfer in Grinding, (2011), PhD Thesis, University of Toledo.
95. Tan Jin., Rowe, W.B., David McCormack, (2001), Temperatures in Deep Grinding of Finite Workpieces, School of Engineering, Liverpool John Moores University, *International Journal of Machine Tools & Manufacture*, 42, 53-59.
96. Tasdelen B., Thordenberg H., Olofsson D., (2007) An experimental investigation on contact length during minimum quantity lubrication (MQL) machining, *Materials and manufacturing technology department, Chalmers university of technology*, 41296, Gothenberg, Sweden.
97. Tawakoli T., Hadad M.J., Sadeghi M.H, (2010), Influence of Oil Mist Parameters on Minimum Quantity Lubrication-MQL Grinding Process, *Institute of Grinding and*

- Precision Technology (KSF), Furtwangen University, Germany.
98. Tawakoli, T., 1990, Hochleistungs-Flachschleifen: Technologie, Verfahrensplanung und Wirtschaftlicher Einsatz, Dr.-Ing. Diss., TU Berlin.
  99. Theobald C., (1981), The Effect of Nozzle Design on the Stability and Performance of Turbulent Water Jets, Fire Safety Journal, Great Britain.
  100. Tonshoff, H.K., Friemuth, T., Becker, J.C., (2002) Process Monitoring in Grinding, Institute of Production Engineering and Machine Tools, University of Hannover, Germany.
  101. Toshiyuki Obikawa., Yasuhiro kamata., jun Shinozuka., (2006), "High-Speed Grooving with Applying MQL", Internal journal of Machine Tools & manufacture 46 (2006) 1854-1861.
  102. Tsiakoumis V, 2012, Vibration-Assisted Machining- Application to Surface Grinding, PhD, LJMU.
  103. Tsiakoumis V., Batako A., 2012, Vibration Assisted Grinding Of Mild And Hardened Steel: A Novel Design Vibrating Jig And Process Performance, *ASME, Volume 4 - 141-146; Nantes 2-4th July 2012.*
  104. W.Brian Rowe, 'Principles of modern grinding Technology', (2014), William Andrew, second edition, Elsevier.
  105. W.Brian Rowe, 'Principles of modern grinding Technology', William Andrew, (2009).
  106. Webster J.A., Cui C., Mindek Jr R.B., (1995), Grinding Fluid Application System Design. Centre for grinding research and development, University of Connecticut, USA.
  107. Webster, J.A., Brinksmeier, E., Heinzl, C., Wittman, M., Thoens, K., Assessment of grinding fluid effectiveness in continuous-dress creep feed grinding, *Annals of the CIRP, Vol. 48/2, (2002), pp. 581-598.*
  108. Webster, J.A., Cui, C., Mindek Jr., R.B. Grinding fluid application System design, *Annals of the CIRP, Vol. 44/1, (1995), pp. 333-338.*
  109. Weinert k., Inasaki I., Sutherland J.W., Wakabayashi T. (200), Dry Machining and Minimum Quantity Lubrication. *CIRP Annals-Manufacturing Technology, 53/2, 511-537.*

110. Wu, H., (2009), Investigation of Fluid Flow in Grinding using LDA Techniques and CFD Simulation. PhD Thesis, LJMU.
111. Xun Chen and Rowe, W.B., (1995), Analysis and Simulation of the Grinding Process, Part II: Mechanics of Grinding, Int.J.Mech.Tools Manufact.Vol.36, No.8, pp. 883-896.
112. Xun Chen, Rowe, W.B., Mills, B., and Allanson, D.R., (1996), Analysis and Simulation of the Grinding Process. Part III: Comparison with experiment, Int.J.Mech.Tools Manufact. Vol.36, No. 8, pp. 897-906.
113. Xun Chen, Rowe, W.B., Mills, B., and Allanson, D.R., (1997), Analysis and Simulation of the Grinding Process. Part IV: Effects of Wheel Wear, Int.J.Mech.Tools Manufact. Vol.38, No. 1-2, pp. 41-49.
114. Yan Lutao., YUAN Songmei., And LIU Qiang. (2011), Influence of Minimum Quantity Lubrication Parameters on Tool wear and Surface Roughness in Milling of Forged Steel. Chinese Journal of Mechanical Engineering.
115. Yumusak M., Eyi S., (2012), Design Optimisation of Rocket Nozzles in Chemically Reacting Flows, Roketsan Missile Industries, Middle East Technical University, Ankara, Turkey.
116. Zhou, Z.X., Van Lutterwelt, C.A., (1992), The Real Contact Length Between Grinding Wheel and Workpiece-A New Concept and a New Measuring Method, Laboratory for Flexible Production Automation, Technical University Delft/Netherlands.

## Bibliography

1. <https://www.gov.uk/topic/environmental-management/waste>.
2. <http://www.ni.com/white-paper/13034/en/>
3. <http://sensing.honeywell.com/white-paper-effectivelyusingpressureloadandtorquesensorswithtodaysdataacquisitionsystems-008883-2-en.pdf>
4. <http://www.sensormag.com/sensors/pressure/pressure-measurement-principles-and-practice-969>
5. <https://www.grc.nasa.gov/www/k-12/airplane/dragosphere.html>
6. Coolgrind technologies.com.
7. NI Instruments.com.
8. Mathworks.com.

